NASA CR-134894

SINGLE STAGE, LOW NOISE, ADVANCED TECHNOLOGY FAN

VOLUME V FAN ACOUSTICS

Section 1: Results and Analysis

BY: R.R. JUTRAS

ADVANCED ENGINEERING AND TECHNOLOGY
PROGRAMS DEPARTMENT
GENERAL ELECTRIC COMPANY
CINCINNATI, OHIO

PREPARED FOR

NATIONAL AERONAUTICS AND SPACE ADMINISTRATION

NASA LEWIS RESEARCH CENTER
CONTRACT NAS 3-16813

1. Report No.	2. Government Accession No.	3. Recipient's Catalog No.
NASA CR-134894		

4. Title and Subtitle	5. Report Date
Single Stage, Low Noise, Advanced Technology Fan, Volume V - Fan Acoustics, Section 1 - Results and Analysis	May 1976
	6. Performing Organization Code
7. Author(s)	8. Performing Organization Report No.
R.R. Jutras	
	10. Work Unit No.
9. Performing Organization Name and Address	11. Contract or Grant No.
General Electric Company Aircraft Engine Group Advanced Engineering and Technology Programs Department Evendale, Ohio 45215	NAS3-16813
	13. Type of Report and Period Covered
12. Sponsoring Agency Name and Address	Contractor Report
National Aeronautics and Space Administration Washington, D.C. 20546	14. Sponsoring Agency Code

15. Supplementary Notes

Acoustic Design Report. Project Manager, T.F. Gelder, Fluid System Components Division. Technical Advisor, M.F. Heidmann, V/STOL and Noise Division, NASA-Lewis Research Center. Cleveland, Ohio 44135.

16. Abstract

The acoustic tests and data analysis for a 0.508-scale fan vehicle of a 111,300 newton (25,000 pound) thrust, full-size engine, which would have application on an advanced transport aircraft, is described. The single-stage advanced technology fan was designed to a pressure ratio of 1.8 at a tip speed of 503 m/sec (1650 ft/sec) to achieve the desired pressure ratio in a single-stage fan with low radius ratio (0.38), and to maintain adequate stall margin. The fan has 44 tip-shrouded rotor blades and 90 outlet guide vanes. The two basic approaches taken in the acoustic design were: 1) minimization of noise at the source, and 2) suppression of the generated noise in the inlet and bypass exhaust duct. Suppression of the generated noise was accomplished in the inlet through use of the "hybrid" concept (wall acoustic treatment plus airflow acceleration suppression) and in the exhaust duct with extensive acoustic treatment including a splitter. The goal of the design was attainment of twenty effective perceived noise decibels (20 EPNdB) below current Federal Air Regulation noise standards for a full-scale fan at the takeoff, cutback, and approach conditions. The suppression goal of FAR 36-20 was not reached, but improvements in the technology of both front and aft fan-noise suppression were realized. The total fan noise resulted in EPNL suppression below FAR 36 of 10.6 ΔEPNdB for takeoff, 6.7 ΔEPNdB for cutback and 7.1 ΔEPNdB for approach.

The suppressed fan noise was shown to be consistent with the proposed federal regulation on aircraft noise (FAR 36 - XYZ).

This report entitled "Volume V - Fan Acoustics," is one of two in a series of final analysis reports. The other report is entitled "Volume IV - Fan Aerodynamics."

Volume V is bound in two covers:

Section 1 - Results and Analysis
Section 2 - Tabulations and Selected Narrowband Traces

Three design reports precede this series of final analysis reports. They are: Volume I - Aerodynamic Design, Volume II - Structural Design, and Volume III - Acoustic Design.

17. Key Words (Suggested by Author(s))	18. Distribution Statement
Engine acoustics High speed fan Acoustic design Hybrid inlet	Unclassified - Unlimited

19. Security Classif. (of this report)	20. Security Classif. (of this page)	21. No. of Pages	22. Price*
Unclassified	Unclassified	210	

*For sale by the National Technical Information Service, Springfield, Virginia 22151

NASA-C-168 (Rev. 6-71)

TABLE OF CONTENTS

LIST OF ILLUSTRATIONS

LIST OF ILLUSTRATIONS (Cont'd)

LIST OF ILLUSTRATIONS (Cont'd)

LIST OF ILLUSTRATIONS (Cont'd)

LIST OF ILLUSTRATIONS (Cont'd)

LIST OF ILLUSTRATIONS (Cont'd)

LIST OF ILLUSTRATIONS (Cont'd)

LIST OF ILLUSTRATIONS (Cont'd)

LIST OF ILLUSTRATIONS (Cont'd)

LIST OF ILLUSTRATIONS (Cont'd)

LIST OF ILLUSTRATIONS (Cont'd)

LIST OF ILLUSTRATIONS (Cont'd)

LIST OF ILLUSTRATIONS (Cont'd)

LIST OF ILLUSTRATIONS (Cont'd)

LIST OF ILLUSTRATIONS (Cont'd)

LIST OF ILLUSTRATIONS (Cont'd)

LIST OF ILLUSTRATIONS (Cont'd)

LIST OF ILLUSTRATIONS (Cont'd)

LIST OF TABLES

SECTION I

SUMMARY

A high speed, low noise, high bypass ratio, single-stage research fan with a variable-geometry inlet was designed, fabricated and tested by the General Electric Company under the sponsorship of NASA (Contract No. NAS3-16813). This report, entitled Volume V - Fan Acoustics, is one of two in a series of final analysis reports. Three design reports precede the series of final analysis reports. They are: Volume I - Aerodynamic Design, Volume II - Structural Design and Volume III - Acoustic Design, which are references 1, 2 and 3 respectively. The other final analysis report in the series, Volume IV - Fan Aerodynamics is reference 4. The present volume is bound in two separate covers:

Section 1 - Results and Analysis

Section 2 - One-Third Octave Data Tabulations and Selected Narrow-Band Traces

The 90.37 cm (35.58 in.) diameter tip-shrouded fan was designed to a bypass pressure ratio of 1.8, and a corrected airflow of 117.9 kg/sec (259.9 lbm/sec) at a tip speed of 503 m/sec (1650 ft/sec). The fan was designed to a stall margin goal at constant speed of 13% and an objective adiabatic efficiency of 84.0%, with a peak efficiency objective of 85%. Several low fan source noise features were included in the design, such as a vane/blade ratio of 2.05, a rotor/stator spacing of 2.06 (rotor tip chords) and a fan blade designed for a swallowed shock at takeoff conditions.

Two separate series of tests were conducted on the advanced technology fan vehicle at General Electric's, Peebles, Ohio, Site IV-B outdoor facility. The rear-shaft drive test series provided the evaluation of front-quadrant acoustic performance, as well as fan and inlet aerodynamic performance. The inlet configurations tested are shown in the schematic on Page 2. The major portion of the fan and inlet aerodynamic performance tests were conducted with a long (L/D_F = 2.3) bellmouth inlet which contained an extra instrumentation section (not shown) ahead of the fan. This was followed by a brief diagnostic test with a shorter (L/D_F = 1.4) bellmouth inlet, which also served as the reference, or baseline, acoustic inlet. The inlet noise suppression system employed a hybrid inlet, which combined an adjustable-geometry cowl, capable of generating high throat Mach numbers (design M_{TH} = 0.79) at all critical noise operating points, with wall acoustic treatment. The wall treatment panels were replaceable with hardwall panels so that the effects of the treatment on noise suppression and inlet aerodynamic performance could be isolated.

The second series of tests involved driving the fan vehicle from a front shaft for the evaluation of aft-propagating fan noise and bypass duct aerodynamic performance. The configurations tested included a hardwall bypass duct without a splitter and a fully treated duct with a midstream acoustic splitter. They are shown schematically on page 3.

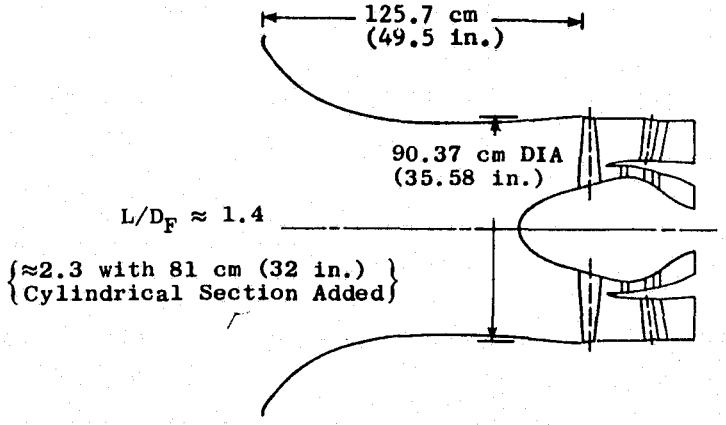

BELLMOUTH INLET, ACOUSTIC BASELINE

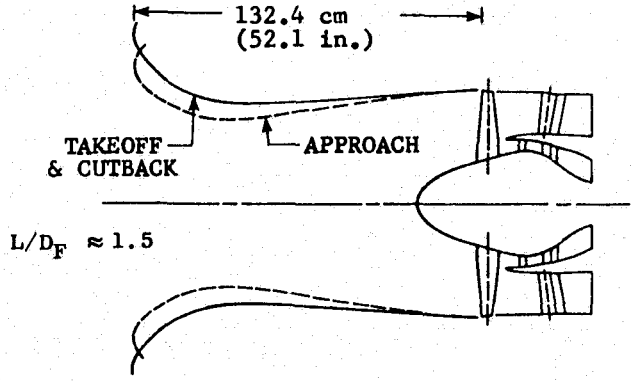

ACCELERATING INLET

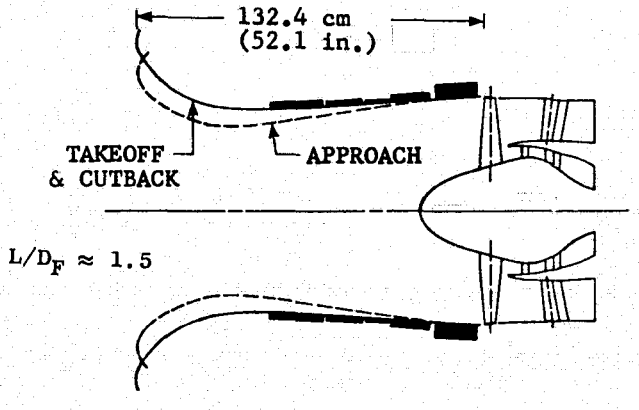

HYBRID INLET
(ACCELERATING INLET + WALL TREATMENT)

FAN INLET CONFIGURATIONS FOR REAR-DRIVE TESTS

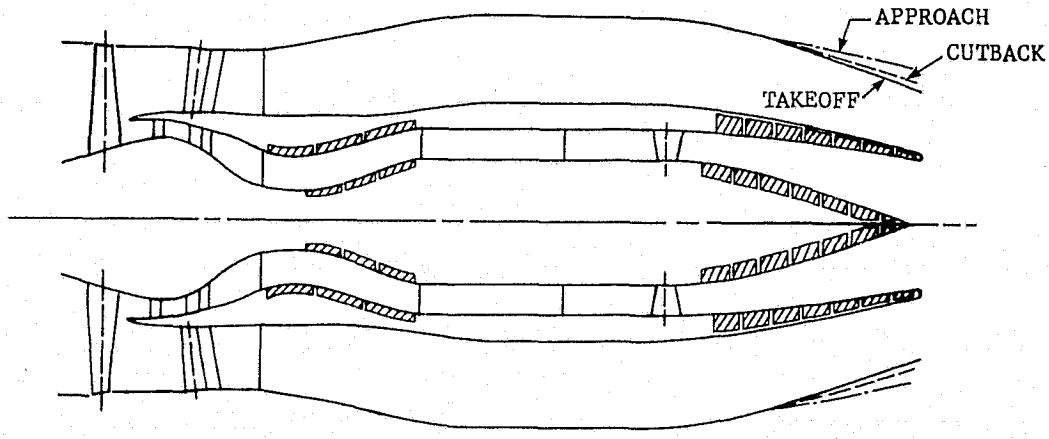

HARDWALL DUCT WITHOUT SPLITTER

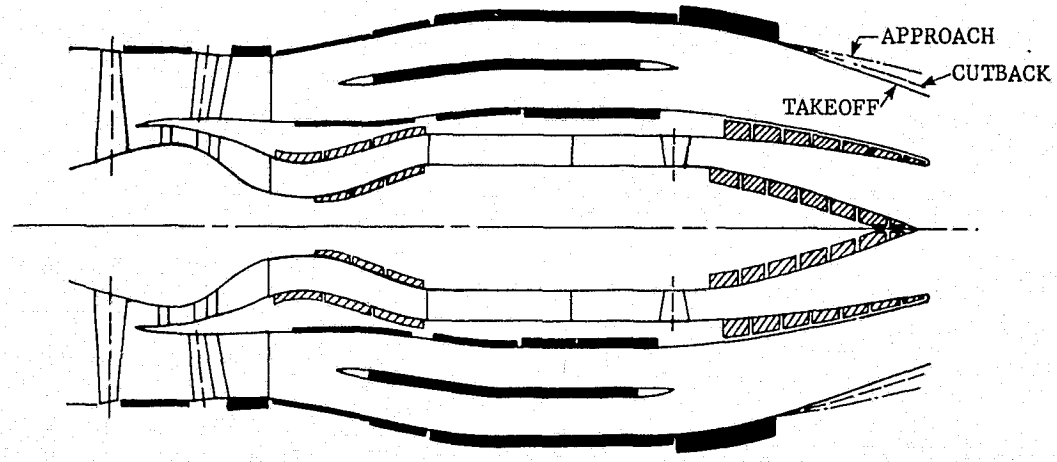

TREATED DUCT WITH SPLITTER

FAN DUCT CONFIGURATIONS FOR FRONT-DRIVE TESTS

The design point static acoustic results from the individual spectra of both front-drive (aft noise) and rear-drive (front noise) tests were scaled and extrapolated to the projected takeoff, cutback, and approach flight conditions for a Boeing 767-640 trijet with a takeoff gross weight of 137,892 kg. (The preliminary design of this $0.85 \leq M_O \leq 0.90$ Boeing airplane was the basis for earlier engine cycle-selection studies used to determine the fan design parameters and overall system noise goals.)

A. Front-Quadrant Acoustic Performance

The isolated forward fan noise with the hybrid inlet at an average throat Mach number of 0.79 was 16.3 ΔEPNdB at takeoff, 9.6 ΔEPNdB at cutback, and 9.1 ΔEPNdB at approach below the current FAR 36 aircraft noise regulation level. This was accomplished with a static total pressure recovery in the inlet of 98.9% at the takeoff and cutback conditions and 98.2% at approach, and with steady-state total pressure distortion levels below 10%. Further noise reductions could be obtained by increasing the throat Mach number to 0.84 at takeoff and cutback and 0.81 at approach without exceeding 10% pressure distortion, and without significant reductions in pressure recovery.

B. Aft-Quadrant Acoustic Performance

Aft fan noise for the fully suppressed exhaust duct configuration was below FAR 36 by 12.1 ΔEPNdB at takeoff, 9.4 ΔEPNdB at cutback, and 12.2 ΔEPNdB at approach. This was accomplished with increased bypass duct pressure losses (relative to the hardwall duct without a splitter) of 0.56, 1.96, and 2.05% at takeoff, cutback, and approach respectively. A penalty of 0.68% in cruise specific fuel consumption was estimated to result from the wall treatment and splitter in the exhaust duct.

C. Total Fan System Noise

The combined front and aft fan noise, extrapolated to flight, resulted in EPNL's of 10.6 ΔEPNdB at takeoff, 6.7 ΔEPNdB at cutback, and 7.1 ΔEPNdB at approach below FAR 36.

Although the suppression goal of FAR 36 - 20 EPNdB was not reached, improvements in the technology of both front and aft fan noise suppression were realized. Comparisons with results from the Quiet Engine Program (QEP) indicated improved suppression efficiency of the hybrid inlet relative to the Fan "C" splitter inlet, and improved suppression in the bypass duct relative to that of Engine "C". In addition, the suppressed advanced technology fan was shown to be compatible with the proposed FAR 36-XYZ regulation. Specifically, the total fan-noise levels were 1.6, 0.7, and 3.1 EPNdB below the proposed new levels (per the draft of the FAA Environmental Impact Statement dated July 9, 1975) at takeoff, cutback, and approach, respectively.

SECTION II

INTRODUCTION

Low noise and exhaust emissions and economical operation are the primary requirements for advanced transport aircraft. The successful development and acceptance of a subsonic, long-range transport for the next generation are greatly dependent upon technological improvements in the areas of fan aerodynamics and acoustic suppression. To help provide this fan technology, the General Electric Company was contracted to design, build and test a high speed, low noise, single-stage research fan (hereafter referred to as an advanced technology fan), a variable-geometry inlet with high throat Mach number capability, and an acoustically treated fan exit duct, all applicable for an advanced high bypass, low noise engine. To utilize existing hardware and facilities, the subject fan was designed to be half scale.

Under a separate and earlier contract with NASA (Contract NAS3-15544, References 5 and 6), parametric studies were performed to optimize the engine cycle for a typical advanced transport aircraft. Based on these studies, plus the current contract Statement of Work, an engine cycle was selected for an advanced transport designed to cruise between 0.85 and 0.90 Mach number. A fan pressure ratio of 1.8 to 1.9 and a bypass ratio of approximately 6:1 were desirable. Furthermore, it is desirable to raise the pressure ratio of the flow entering the core compressor to about 2.5 to 3.0 by the addition of booster stages. This then provides an overall cycle pressure ratio of 30:1 or greater and still uses only a single-stage turbine to drive the high pressure compressor. Fan tip speeds of 488 to 518 m/sec (1600 to 1700 ft/sec) are required to achieve the desired pressure ratio in a single, low radius-ratio stage with adequate stall margin. A high specific flow rate of 215 kg/sec m^2 (44.0 lbm/sec ft^2) was chosen to minimize the fan diameter.

The aerodynamic and acoustic performance of the fan vehicle was evaluated in two separate series of tests conducted at General Electric, Peebles, Ohio outdoor sound-field facility. In the first series of tests, the fan was driven by a rear shaft and detailed fan and inlet aerodynamic performance information was obtained. A long bellmouth inlet (L/D_F = 2.3) was used for the majority of the fan aerodynamic performance tests, because it contained an additional instrumentation section ahead of the fan. Unsuppressed and suppressed forward-propagating fan noise was evaluated with the shorter bellmouth inlet, with aft-propagating noise virtually eliminated from the system by a massive exhaust suppressor. In the second series of tests, the fan was shaft driven from the front and the inlet system was enclosed in a large "silencer box" to eliminate forward-propagating fan noise. This test program was used to evaluate bypass duct aerodynamic performance and aft-radiating fan noise, both suppressed and unsuppressed. An abbreviated description of the complete test program follows; the acoustic portions are boxed-in for easy identification.

ADVANCED TECHNOLOGY FAN TEST PROGRAM OUTLINE

REAR-DRIVE TESTS

Fan Aerodynamic Performance Tests

1. Long Bellmouth Inlet
   - Inlet L/D_F = 2.3
   - Full instrumentation
   - Bypass Ratio Migration

2. Short Bellmouth Inlet
   - Inlet L/D_F = 1.4
   - Tip Clearance Tightened Initially
   - Limited Aerodynamic Instrumentation

3. Hybrid Inlet
   - Inlet L/D_F = 1.5
   - Limited Aerodynamic Instrumentation
   - Takeoff/Cutback and Approach Configurations

Inlet Aerodynamic Performance Tests

3. Hybrid Inlet
   - Inlet L/D_F = 1.5
   - Takeoff/Cutback and Approach Configurations

4. Accelerating Inlet
   - Inlet L/D_F = 1.5
   - Hybrid Inlet without Wall Treatment
   - Takeoff/Cutback and Approach Configurations

Inlet Acoustics Tests

2. Short Bellmouth Inlet (Baseline)
   - Takeoff, Cutback, and Approach Operating Lines

3. Hybrid Inlet
   - Takeoff, Cutback, and Approach Operating Lines

4. Accelerating Inlet
   - Takeoff, Cutback, and Approach Operating Lines

FRONT-DRIVE TESTS

Bypass Duct Aerodynamic Performance Tests

5. Fully Treated Duct with Splitter
   - Takeoff, Cutback, and Approach Nozzles

6. Hardwall Duct without Splitter
   - Takeoff, Cutback, and Approach Nozzles

Aft-Noise Acoustic Tests

5. Fully Treated Duct with Splitter
   - Takeoff, Cutback, and Approach Nozzles

6. Hardwall Duct without Splitter (Baseline)
   - Takeoff, Cutback, and Approach Nozzles

The advanced technology fan, in combination with the inlet and bypass duct system, was designed to the very challenging noise goal of 20 EPNdB below FAR-36. As a result, the fan design incorporated many low noise features such as a vane/blade ratio of 2.05, a rotor/stator spacing of 2.06 (rotor tip chords) and a blade designed for a swallowed shock at takeoff. The inlet noise suppression system employed a "hybrid" inlet with an adjustable-geometry cowl (two position) capable of generating high throat Mach numbers (design M_{TH} = 0.79) at all critical noise conditions [takeoff (sideline), cutback, and approach]. The high Mach number, variable-geometry inlet concept was designed to operate in conjunction with a variable-area fan exhaust nozzle, which was already determined to be necessary for reducing exhaust velocity at the cutback position. This combination reduces the range of area change required of the inlet. At takeoff the exhaust area was assumed to be at the nominal value (necessary to reach takeoff rated thrust), and the inlet throat was adjusted to obtain M_{TH} = 0.79. Throat area at cutback (0.457 m^2) was maintained at the takeoff setting for operational simplicity, and the cycle was matched to the proper weight flow by selecting the appropriate combination of throttle setting and exhaust nozzle area. The nozzle was opened during the cutback setting tests 25% above nominal, compared to pretest design estimates of 15%. The difference was due to variation in vehicle performance relative to design. At approach the exhaust nozzle was opened to an area 35% greater than nominal (design estimate was 40%) and the inlet throat was reduced to 0.339 m^2 in order to achieve M_{TH} = 0.79 at the low thrust level required at approach. During rear-drive tests, these nozzle positions were simulated with core and bypass stream discharge valves, while during the front-drive tests, three separate nozzles were employed and trimmed to duplicate the appropriate operating lines.

Four segments of acoustic-treatment panels, which were tuned to the predicted dominant noise frequencies, were combined with airflow acceleration to form the hybrid inlet. The wall treatment panels were replaceable with hardwall panels so that suppression due to flow acceleration and suppression due to treatment could be isolated, and the effect of wall treatment on inlet aerodynamic performance could be evaluated. The exhaust duct suppression system consisted of a full compliment of wall acoustic treatment and a mid-duct splitter. The hardwall duct without splitter served as the acoustic baseline and as the reference in determining the aerodynamic performance penalty associated with the suppressed configuration.

The present volume first describes the test vehicle design and the test specifications and procedures, followed by acoustic performance results and discussion from all tests. Section 2 of this volume (under separate cover) contains 1/3-octave data tabulations and selected narrow-band traces. Other reports of work performed under this contract include: Volume I - Aerodynamic Design, Volume II - Structural Design, Volume III - Acoustic Design and Volume IV - Fan Aerodynamics, which are References 1, 2, 3 and 4 respectively.

A visual representation of the overall program and report organization is shown on the following page.

DESCRIPTION OF ADVANCED TECHNOLOGY FAN REPORTS

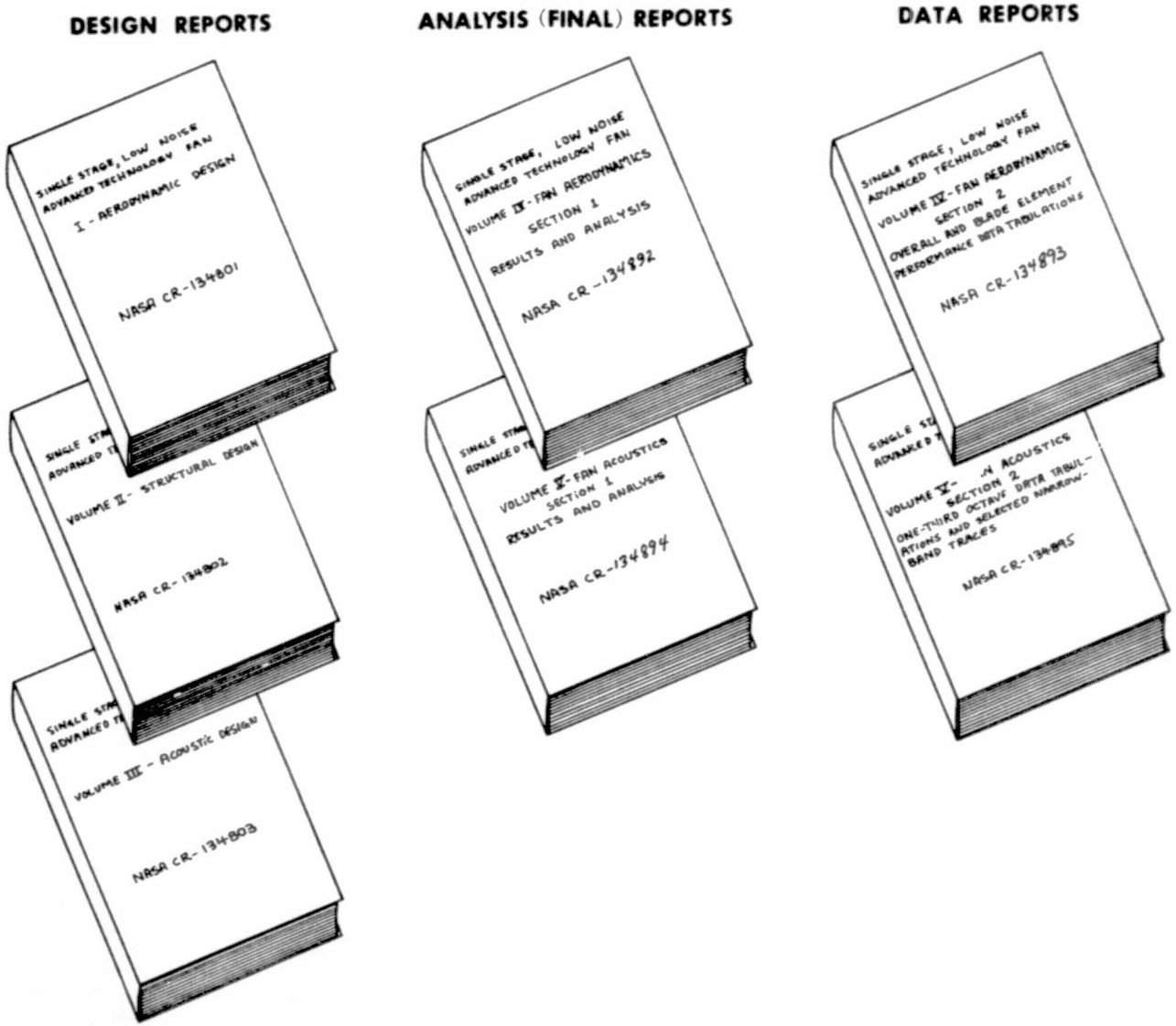

SECTION III

FAN VEHICLE ACOUSTIC DESCRIPTION

A. Fan Acoustic Design

The design of this single-stage, high tip speed fan for advanced conventional takeoff and landing (CTOL) application was guided by the objective of attaining the goal of FAR 36 minus 20 EPNdB for three full-scale fans on a 137,892 kg (304,000 lb) gross weight airplane at the takeoff, cutback, and approach operating points. A full-size engine with this fan would produce 111,300 newtons (25,000 lbs) of thrust as determined in the cycle studies, References 5 and 6.

The pertinent aerodynamic design parameters for the fan are summarized and compared to actual measured values in Table I.

Table I. Comparison of Actual Fan Aerodynamic Parameters with Design Values.

Fan Aerodynamic Parameters	Design	Actual
Pressure Ratio (100% $N/\sqrt{\theta}$)	1.8	1.73
Corrected Speed (100% $N/\sqrt{\theta}$) rpm	10620	10620
Fan Diameter, cm (inches)	90.37 (35.38)	90.37 (35.38)
Corrected Tip Speed (100% $N/\sqrt{\theta}$), m/sec (ft/sec)	503 (1650)	503 (1650)
Hub/Tip Ratio (Inlet)	0.38	0.38
Airflow (100% $N/\sqrt{\theta}$), (lb/sec)	117.9 (259.9)	114.5 (252)
Number of Rotor Blades	44	44
Number of OGV's	90	90
Rotor/OGV Spacing (Rotor Tip Chords)	2.06	2.06
Number of Core OGV's	82	82
Rotor/Core OGV Spacing (Hub Chords)	0.90	0.90

The pressure ratio for the fan was essentially set by the cycle selection study conducted under a separate Contract (NAS3-15544) and is reported in Reference 5. The low radius ratio (0.38) was selected on the basis of minimizing the overall diameter. A lower than average tip pressure ratio was employed to help reduce the blade tip loading and thus the stage-generated noise. The design radial pressure distribution is shown in Figure 1. Selection of a large number of blades was consistent with the theoretical hypothesis that the attenuation of the multiple pure tones (MPT) as they propagate forward in the inlet duct is greater for large blade-number fans.

A tip-shrouded blade design was chosen for both aerodynamic and acoustic performance benefits. The blades were designed to have a "swallowed" shock at takeoff (~92% $N/\sqrt{\theta}$). The intent was to reduce the MPT noise level at this critical operating point. This approach to reducing MPT's had been successfully demonstrated in the Quiet Engine Fan "C" Scale Model Program (Contract NAS3-12430) and is reported in Reference 7.

The generally accepted criteria of high vane/blade ratio and wide rotor/stator spacing were incorporated in order to reduce fan source noise. The number of bypass outlet guide vanes (OGV) was set at 90 for a vane/blade ratio of 2.045. The rotor/OGV spacing was set at 2.06 true rotor tip chords. In the booster, the number of first-stage stators was set at 82 for a vane/blade ratio of 1.86 and the spacing between the fan rotor and booster first-stage stator was set at 0.90 rotor hub chords, which is untypically large for this parameter. The fan vehicle flowpath is shown in Figure 2. Although the booster rotors are shown in this figure, they were not fabricated and were not present in the scale-model tests.

B. Inlet Acoustic Design

System studies of aero-acoustic inlet designs for this CTOL system were completed under Contract NAS3-15544 and are reported in Reference 8. Preliminary designs were completed on several variable-throat concepts, establishing a tradeoff between the acoustic requirements, mechanical considerations such as weight and complexity, and the aerodynamic performance aspects such as recovery, distortion, drag, and boundary layer separation potential. The variable-geometry inlet design configuration selected is shown in Figure 3. The inlet consists of a circumferential series of hinged, radially variable flowpath wedged panels (see Figure 4). The variable panels provide the capability of selecting the desired throat Mach number (M_{TH} = 0.79 at takeoff, cutback, and approach, for acoustic suppression, and selecting a larger throat geometry for the cruise and maximum climb conditions where engine corrected airflow is higher but inlet throat Mach number is desired lower.

The term "accelerating inlet" has been applied to the concept which obtains acoustic suppression by increased average Mach number at the inlet throat (i.e., sonic-type inlet with partial choking). The term "hybrid inlet" refers to the concept where acoustic wall treatment is incorporated into an accelerating inlet to obtain suppression levels that are greater than that possible with either concept alone, for a given inlet length.

For this fan, a contracting cowl with contoured inner walls was designed to obtain an average throat Mach number of 0.79 at the three important operating points: takeoff, cutback, and approach. The takeoff and cutback operating points had the same inlet throat position. A lower bypass pressure ratio required for the cutback point to reduce jet noise was obtained by opening the bypass discharge valve for rear-drive testing and properly trimming the cutback nozzle for front-drive testing. At the takeoff/cutback inlet position, the throat area was 4565 cm^2 (708.5 $in.^2$) while at approach (more closed to obtain an average throat Mach number of 0.79 at lower flow)

the throat area was 3385 cm^2 (525.6 $in.^2$). The contracting cowl inlet had an overall length-to-fan diameter ratio (L/D_F) of ~1.5 with the acoustic wall treatment L/D_F of 0.85 for the hybrid inlet. This overall length would be reduced to an L/D_F of 1.4 if a flight-type lip were employed. The conventional cylindrical bellmouth used for the acoustic baseline test had an L/D_F of 1.4. A schematic of the three inlet test configurations is shown in Figure 5. The treatment in the hybrid inlet was initiated aft of the throat at a point where the wall Mach number was less than or equal to 0.70 at the design point. This was done in order to minimize the adverse performance effect of high Mach number flow over the relatively rough acoustic treatment, and to help maintain the acoustic suppression characteristics . Historically, an adverse effect on suppression of high Mach number flow over the treatment has been witnessed. See Section V-A, 2.

The inlet acoustic treatment consisted of four (4) optimized single degree of freedom (SDOF) designs tuned to the dominant frequencies at the three important acoustic operating points of takeoff, cutback, and approach. Five panels are shown in Figures 3 and 5, but two of the panels have the same design parameters. The details of the acoustic treatment design for the scale-model inlet are shown in Figure 6. With a goal of FAR 36 - 20 EPNdB, cutback was predicted to be the most critical operating point. Thus, the design was based on achieving the maximum treatment suppression at cutback with minimum sacrifice at takeoff and approach.

C. Exhaust Duct Acoustic Design

The exhaust duct system for this vehicle was designed and configured to accommodate a treated acoustic splitter. The addition of a splitter reduced the duct height parameter, H/λ (height of duct to wavelength ratio) and provided for additional treated area as shown in Figure 7. The inner duct wall treatment was terminated sooner than that on the outer wall to allow for placement of a core stream mixer nozzle in an actual engine. The exhaust duct acoustic treatment consisted of four (4) SDOF acoustic liners tuned to the dominant frequencies at the three important acoustic operating points. The exhaust nozzles schematically indicated in Figure 8 were sized and trimmed so as to obtain acoustic data on the three nominal operating lines passing through the critical operating points; (takeoff -2948 cm^2, cutback -3677 cm^2, and approach -3980 cm^2) during front-drive testing. The baseline hardwall configuration was designed to have Mach number distributions similar to conventional long-duct engines and match those on the splitter configuration. This was accomplished by decreasing the outer wall contour for the hardwall duct. In this way, changes in bypass duct performance (pressure drop) were due only to the addition of the wall treatment and splitter, and not because of duct Mach number changes. Both configurations are shown schematically in Figure 8. The figure also includes the core duct acoustic treatment used to suppress fan noise passing through the core. The core duct acoustic treatment consisted of the Scottfelt Type 3-900 bulk absorber. The treatment aft of the core struts was 1.27 cm (0.50 in.) thick on both inner and outer walls while the treatment in the core nozzle was as thick as possible within the constraints imposed by the physical size of the structure.

SECTION IV

TEST DESCRIPTION AND PROCEDURES

A. Test Facility

Testing of the scale-model fan vehicle was performed at the Peebles Test Operation, General Electric's outdoor test site, using a General Electric LM1500 stationary gas turbine as the drive system. The same fan vehicle was driven through the exhaust (rear drive) for inlet-radiated noise and through the inlet (front drive) for fan exhaust noise. The gear box and the LM1500 gas turbine are contained within acoustically absorbing housings. For the isolation of front-end noise, and for more accurate flow measurements, the facility was equipped with a collection system, four standard airflow-measuring venturies, and a suppressor exhaust stack. A schematic of the scale-model vehicle facility is shown in Figure 9 for rear drive.

With the vehicle in the rear-drive configuration, throttling the fan was accomplished with a variable discharge valve located in the fan exhaust duct and the core duct. The discharge valve in the fan duct (bypass discharge valve) was used to vary the fan pressure ratio while the core duct discharge valve was used to control the bypass ratio.

For the aft fan-noise evaluation, the facility was equipped with a massive inlet suppressor (Figure 10) with the vehicle in a front-drive position. A schematic of the scale-model facility with the vehicle in the front-drive position is shown in Figure 11. Critical operating points on three operating lines with the vehicle in front drive were obtained by the use of three fixed (bypass fan duct), trimmable exhaust nozzles. The bypass ratio, as in rear drive, was controlled by a variable discharge valve in the core duct.

B. Test Program and Instrumentation

Acoustic data were taken on five different configurations with the vehicle in the rear-drive position; i.e., a baseline cylindrical bellmouth with an inlet-length-to-fan diameter ratio (L/D_F) of 1.4, the accelerating inlet (no treatment) in the takeoff and approach positions, and the hybrid inlet (treated accelerating inlet) in the takeoff and approach positions (see Figure 5). The baseline bellmouth (cylindrical) inlet with a throat area of 5765 cm^2 (893 $in.^2$) had throat Mach numbers consideratly lower than that of the contoured accelerating and hybrid inlets. Therefore, the baseline acoustic data were obtained at the same corrected tip speeds at which the accelerating and hybrid inlet data were measured. A photograph of the test vehicle with the hybrid inlet (takeoff configuration) is shown in Figure 4. In the rear-drive position, acoustic

data were obtained on three operating lines for each of the three critical operating points; takeoff, cutback, and approach. A summary of the baseline acoustic-data points for the rear-drive configuration is shown in Figure 12 for takeoff and cutback and Figure 13 for approach. Acoustic data points on the accelerating and hybrid inlets were set by one-dimensional average inlet throat Mach number, while the baseline data points were set at specific corrected speeds. The speeds chosen for the baseline inlet were matched with that of the accelerating and hybrid inlets at specific average throat Mach numbers so as to obtain comparable data. Additional acoustic data were taken from 50 to 106% corrected speed with the baseline configuration to get a complete definition of the basic acoustic signature of the fan.

With the vehicle in front drive, acoustic data were taken for two exhaust configurations, i.e., hardwall duct without splitter and treated duct with splitter. (see Figure 8). Three fixed fan exhaust nozzles were tested for each configuration. The standard baseline bellmouth inlet (L/D_F = 1.4) was used inside the inlet noise suppressor housing.

Acoustic instrumentation for these tests consisted of farfield microphones located on a 31 m (100 ft) arc positioned at 10 degree increments from 0 to 150° as measured from the inlet axis for front drive. The microphones were set at the height of the fan centerline, 4.57 m (15 ft) above the asphalt sound-field surface. For rear drive, acoustic data were taken with eight (8) inlet wall-mounted high pressure transducers (Kulites) and three (3) traversing probes; one at the inlet face, one directly ahead of the fan rotor, and one in the fan discharge aft of the fan frame struts. Locations of these Kulites and probes are shown in Figure 14. For front drive, acoustic data were taken with ten (10) exhaust duct outer wall-mounted Kulitites and three (3) traversing acoustic probes; one directly ahead of the fan rotor, one at the fan discharge aft of the fan frame struts, and one aft of the splitter as shown in Figure 15.

Restrictions were imposed on acoustic testing to assure reliable data. These included steady winds of less than 8.03 km/hr (5 mph) and gusts of no more than 4.82 km/hr (3 mph) above the maximum steady wind from any direction. In addition, data were not taken when the field was wet or covered with snow, the relative humidity was less than 30% or in excess of 90%, or temperatures less than 266.7° K (20° F). Also, all instrumentation protruding into the flowpath was removed prior to farfield acoustic data acquisition.

For all farfield acoustic testing, two separate sets of data were taken at each point. Between each set of data a change in fan speed was made. A summary of the acoustic data operating conditions for the front-drive configuration is shown in Figure 16 for the takeoff, cutback and approach operating lines.

C. Data Analysis Procedures

The acoustic data-reduction system, schematically illustrated in Figure 17, was designed specifically to perform time-averaged spectral analysis using a 32 second averaging time with a General Radio 1/3-octave bandwidth parallel filter system. Data was recorded on FM analog magnetic tape and played back through an amplifier/attenuator to provide the optimum signal input level to utilize the 50 dB dynamic range of the 1/3-octave filter system. The FM signal has a flat response through 20 kHz at a tape speed of 152.4 cm/sec (60 in./sec). The data was then processed through the analog-to-digital converter. The digital signal was then input to the GEPAC 30 computer which provides a digital magnetic tape used for further computations and "quick look" printout of sound pressure level spectra.

The acoustic data were analyzed in two ways. Most of the analysis was in 1/3-octave bands. All 1/3-octave band data were corrected to a standard day of 288.5° K (59° F) and 70% relative humidity according to the SAE method described in ARP 866 (Reference 9). The other method of data analysis was through narrowband filtering in 20 Hz bandwidths. For these analyses, a UA-6A Federal Scientific Ubiquitous spectrum analyzer and a high resolution digital averager were used with a 12.8 second averaging time. This method of analysis, particularly, provides a more definitive look at the spectrum than does 1/3-octave analysis. The 1/3-octave data were also scaled to full size (178.5 cm, 70.2 in. diameter) and extrapolated to 61.0 m (200 ft) and 152 m (500 ft) sidelines with extra ground attenuation (EGA) effects applied according to the SAE report AIR 923 (Reference 10). Scale-model and full-scale design parameters are summarized in Table II.

Table II. Scale-Model and Full-Scale Fan Design Parameters.

	Scale Model	Full-Scale
Diameter cm (in.)	90.37 (35.58)	178.5 (70.2)
Design rpm	10628	5391
Number of Blades	44	44
Tip Speed at Design rpm m/sec (ft/sec)	503 (1650)	503 (1650)
Weight Flow Ratio to Scale Model	1.0	3.9
Blade Passing Frequency, Hz at Design rpm	7790	3960
Inlet Hub-Tip Radius Ratio	0.38	0.38

The data to be presented have been scaled to reflect a full-scale fan design for a 111,300 newton (25,000 lb) thrust engine except where noted. The linear scale factor was 0.508 based on the full-scale fan which is 178.5 cm (70.2 in.) in diameter. The effect of adjusting the data to full scale is to lower the frequency spectrum, since for a given tip speed a larger fan turns at a lower rotational speed than a smaller fan. For the case being considered, the scaling requires a downward shift of three 1/3-octave bands or one octave band. In addition to the frequency shift, the noise levels were increased by 10 times the logarithm of the weight flow ratio. By employing the scaling process, a more realistic evaluation of the extrapolation of the noise data to distances far from the vehicle can be obtained. This is true because of the difference in attenuation of various frequency noises in air. With the spectral compoments of noise in their proper bands, this attenuation is applied in a more realistic manner. Perceived noise levels were calculated from these extrapolated spectra according to SAE procedures in ARP 865 A (Reference 11).

Scale-model acoustic data (1/3-octave bands corrected to standard day) are tabulated in Section 2 of Volume V, NASA CR-134895, along with selected narrowband traces.

The noise characteristics produced at a ground measurement point by an aircraft flyover along a given flight path were also calculated. The calculation procedure solved the complex geometry of an aircraft traversing a selected path with varying engine angles and frequencies (from static spectrum) and resulted in a flight noise spectrum. The spectrum was then projected over the appropriate acoustic range with the necessary corrections for preparation of a spectrum at the ground position desired. From this predicted spectrum, the flight PNL and PNLT values were calculated. This information was then used to calculate an Effective Perceived Noise Level (EPNL) value for the flyover event as specified in FAR 36 (Reference 12). However, the 90 EPNdB floor of the current regulation was not used in this study since the noise goal for this program was lower than the floor.

There are two direct effects of aircraft flight velocity which alter the noise spectra, in this case, fan-only noise spectra. (Fan jet noise removal is discussed in a following part of this report.) First, the velocity results in Doppler shifting of the spectrum. The Doppler shift is made according to the value of the Doppler factor, defined as $1/(1 + M_o)$ where M_o is the component of flight Mach number in the direction from the airplane to the microphone. This factor is multiplied by the 1/3-octave center frequencies. If the result is a frequency in a neighboring band, a shift is made. Thus, if the factor exceeds 1.12, a 1/3-octave band shift is made to a higher frequency (source moving toward the observer), if the factor is less than 0.89, a 1/3-octave band shift is made to a lower frequency (source moving away from the observer).

A second effect of flight velocity is that of acoustic-wave expansion and compression known as "dynamic effect" and depends on the position of the observer relative to the source (Reference 13). The acoustic-wave compression that occurs as the aircraft approaches an observer is

characterized by an increase in acoustic pressure. Similarly, as the aircraft moves away from the observer the acoustic pressure is decreased due to an effective wave expansion. At 90 degrees from the inlet axis, the farfield acoustic pressure is the same as when the source is at rest. The equation used was:

$$\Delta dB \text{ (dynamic effect)} = \pm 40 \log (1 - M_o \cos \theta)$$

where

M_o = Flight Mach Number

θ = Angle of Observer from Inlet Axis (+ is used for $\theta > 90°$, - for $\theta > 90°$)

Other correction factors were applied to the static data depending on the separation distance and aircraft velocity. These correction factors were spherical divergence, atmospheric absorption as specified in SAE Specification ARP 866 (Reference 9), and a ground boundary attenuation as specified in SAE Specification AIR 923 (Reference 10). The ground boundary layer or EGA factor was further modified by General Electric with the assumption that it applies only in a layer below 30.48 m (100 ft) altitude. Noise transmission above this altitude was not attenuated with EGA.

For rear drive, data comparisons between the baseline bellmouth and accelerating hardwall inlets were intended to define the flow acceleration suppression, while comparisons between the accelerating and the hybrid (treated accelerating) inlets defined the treatment effectiveness. With the vehicle in front drive a comparison was made between the hardwall and the treated duct with splitter to evaluate the suppression characteristics of the wall and splitter treatment.

To evaluate the overall noise characterisitcs of this fan at the three critical operating conditions, the acoustic data from front drive (aft-end noise) was adjusted by removing the jet noise and the fan noise leakage through the core duct (see Appendix C). The forward- and aft-end acoustic spectra were then separately averaged between the run and repeat point at each farfield angle. The resultant spectra (average of two readings) from front and rear drive at a given farfield angle were then combined logarithmically to give the representative spectra at each angle for this fan. The static acoustic data was then extrapolated to the flight conditions of interest per the procedures previously stated.

In the frequency ranges where possible, the acoustic-probe narrowband spectra data and the farfield (30.5 m scale model) narrowband spectra data were separated into three components: broadband noise, multiple pure

tones (MPT's), and blade passing frequency tones and its harmonics. These noise components were resolved as follows: a broadband base or substratum was faired below each maximum resulting from a blade passing tone or its harmonics, and the maximum was corrected for broadband base level to obtain the amplitude of the blade passing frequency tone or harmonic alone. A similar procedure was applied to the subharmonic maxima which represent the MPT's. After subtracting these two components from the sound pressure level, the remainder was designated as broadband noise. Sound power levels for each of these noise components as well as total sound power level was obtained by integrating the intensity calculated at each of the radial traverse positions for the probes and at each microphone angle for the farfield acoustic data. These data are presented in Appendices A and B.

SECTION V

ACOUSTIC RESULTS AND DISCUSSION

A. Fan Inlet Noise - Rear Drive

1. Baseline Bellmouth Inlet

The acoustic baseline bellmouth inlet was used for part of the aerodynamic tests with the cylindrical aerodynamic measuring section removed (Figure 5). The baseline inlet was tested primarily to define the unsuppressed fan noise characteristics and as a baseline for evaluating the accelerating and hybrid contoured inlets. The basic acoustic signature of this single-stage, high tip-speed fan was obtained on the takeoff nominal operating line at corrected speeds from 50 to 106%. Full-scale 152.4 m (500 ft) sideline front maximum PNL variations with corrected tip speed for the bellmouth inlet are shown in Figure 18 for takeoff, cutback, and approach nominal operating lines. At takeoff and cutback, the noise peaks at about 440 m/sec (1445 ft/sec) and a gradual decrease occurs with increasing speed. Acoustic data were taken up to 550 m/sec (1800 ft/sec) physical tip speed. On the takeoff operating line, the noise level decreased by about 8.5 PNdB from the peak. The continual decrease in noise with increasing tip speed above 440 m/sec is probably due to the development of a more stable swallowed shock system covering more of the blade span as the speed is increased past the initial tip-shock swallowing speed. As a result of this, a significant reduction in multiple pure tone is witnessed, which provides the PNL noise reduction. As previously mentioned, this fan was designed to have a swallowed shock system at the takeoff operating condition which is at about 92% speed. The acoustic data at cutback, which is on a lower operating line (lower pressure ratio), shows a similar trend. At a tip speed corresponding to a throat Mach number of 0.79 (on the contoured inlets), the pressure ratio on the takeoff operating line was about 1.58, while on the cutback operating line it was about 1.38. At the same tip speed, cutback has a lower noise (than takeoff) as would be expected with the lower pressure ratio, although, the change is not very large. The approach operating line shows the noise to be slightly higher than the takeoff operating line for the same tip speeds. This might be caused by the fan operating so far off design (i.e. the approach operating line is well below the nominal, takeoff, operating line, see Figure 16).

The directivity patterns at selected tip speeds on the takeoff nominal operating line are shown in Figure 19 for the bellmouth inlet. The 152.4 m (500 ft) sideline unsuppressed noise peaks at 50° from the inlet axis at all speeds. A decrease in noise throughout the arc due to a swallowed shock system is evident at a corrected tip speed of 534.9 m/sec (1755 ft/sec) relative to 424 m/sec (1390 ft/sec). The increased PNL's at the aft angles (110° and 120°) for 423.7 m/sec (1390 ft/sec) are caused by an increase in rear radiation of low frequency MPT's as seen in Figure 20. The 1/3-octave, full-scale spectra at 152.4 m (500 ft) sideline for the peak forward angle

are shown at four different tip speeds in Figure 21. Although the spectra at corrected tip speeds of 349.9 m/sec (1148 ft/sec) and 534.9 m/sec (1755 ft/sec) are considerably different, the PNL's are of the same magnitude. At 534.9 m/sec (1755 ft/sec) there is a significant increase in MPT amplitudes throughout the frequency range and a BPF amplitude reduction and shift relative to the 349.9 m/sec (1148 ft/sec) spectra. This can be seen more clearly from the narrowband comparison (scale model) shown in Figure 22. In this figure, the onset of MPT's is noticed at 349.9 m (1148 ft/sec) where they start dominating the PNL. This can be observed in Figure 18 as a slope change at this speed. The fact that the BPF and the higher amplitude MPT's are now in a lower noy-weighted region and that the broadband noise is considerably lower at 534.9 m/sec (1755 ft/sec) than at 349.9 m/sec (1148 ft/sec) caused both tip speeds to have the same maximum forward PNL levels. Ground reflection effects can be observed in the low frequency range and possibly effects of cutoff for the 423.7 m/sec (1390 ft/sec) narrowband spectra.

2. Accelerating and Hybrid Inlets

The as-measured 31.0 m (100 ft) arc scale-model data for the takeoff operating point were corrected to standard day conditions and are shown in Figure 23 for the three inlet configurations; baseline, accelerating, and hybrid inlets. The noise from the baseline (cylindrical) inlet peaks at 40° from the inlet axis while the contoured (accelerating and hybrid) inlets show the peak to be at a more forward angle. The major difference between these inlets which may cause a change in peak angle is contouring, since the L/D_F's are approximately the same (1.4 for the baseline and 1.5 for the contoured inlets). The aft noise is considerably lower than the front-end noise due to the massive aft suppressor.

The full-scale 152 m (500 ft) sideline maximum forward PNL variations with average throat Mach number (and corrected tip speed) are shown in Figure 24 for the three inlets: baseline bellmouth (L/D_F = 1.4), accelerating, and hybrid inlets (L/D_F = 1.5, treated L/D_F = 0.85). These data were taken on the nominal operating line passing through the takeoff operating point. The takeoff operating point was defined at 100% of engine thrust (per Reference 5) with an average throat Mach number of 0.79 in the accelerating and hybrid inlets. As expected, there was essentially no noise suppression due to flow acceleration in the low Mach number region. At the defined takeoff operating point of M_{TH} = 0.79 (V_T = 466 m/sec) the noise reduction due to flow acceleration was about 13.5 PNdB which was approximately 4.0 PNdB more suppression than predicted, as seen in Figure 25.

At low average throat Mach numbers, about 6.0 PNdB noise reduction was obtained due to wall acoustic treatment on the takeoff operating line with the hybrid inlet (Figure 24). As the average throat Mach number was increased, the apparent treatment effectiveness decreased with the onset of flow acceleration suppression. This phenomenon is consistent with previous results. At the design average throat Mach number 0.79, about 1.0 PNdB can be attributed to treatment effectiveness which gives a total inlet suppression

of 14.5 PNdB at the takeoff operating point. The apparent reduction of treatment suppression may actually be a reduction in acceleration suppression for the hybrid inlet relative to the accelerating inlet. That is, in the hybrid inlet, the noise has been reduced by the wall treatment prior to reaching the high Mach number throat region of the inlet. With less acoustic energy going into the throat region, less net suppression due to flow acceleration may take place. In any case, it is obvious that the acceleration and treatment suppressions are not directly additive. The overall sound power level variations with average throat Mach number are similar to that of perceived noise level as shown in Figure 26.

The full-scale 152 m (500 ft) sideline directivity pattern at the takeoff operating point (M_{TH} = 0.79) is shown in Figure 27 for the baseline, accelerating, and hybrid inlets. The baseline inlet shows a maximum PNL at 50° with a relatively steep slope up to 80° from the inlet axis, while the PNL's for the accelerating and hybrid inlets flatten out considerably at the forward angles. A similar distribution for the overall sound pressure level is seen in Figure 28. The slope between 50 and 80° for the baseline inlet is probably steeper than normally observed, due to the lack of rear-noise contribution to front-end noise. The low level at 110° for the baseline configuration was caused by a bad microphone and the data are not valid. The hybrid and accelerating inlets did suppress the MPT's and caused a reduction in rear-propagating noise. Full-scale spectral comparisons at the takeoff operating point are shown in Figures 29 through 43 for inlet angles of 10 to 150° respectively. All of the baseline spectra are MPT dominated (at this supersonic tip speed) and the BPF level is not discernible above the broadband noise. The hybrid and accelerating inlet spectra, in contrast, contain mostly broadband noise and a few low frequency MPT's that were not fully suppressed. The peaks at 80 and 160 Hz are the drive shaft's one and two per-rev signals and have essentially no effect on the PNL. At the maximum forward angle of 50°, Figure 33, a considerable decrease in high frequency noise due to flow acceleration is observed with the hybrid and accelerating inlets. In general, the spectra at the takeoff operating point (M_{TH} = 0.79) show that the accelerating inlet did provide a substantial decrease in SPL's throughout the frequency range. The treatment effectiveness of the hybrid inlet, however, fell short of expectations. Comparisons of measured results relative to prediction and design goals are included in Section V-D.

Figures 44 through 50 show the 1/3-octave sound power level spectral comparisons for the three inlet configurations; baseline, accelerating and hybrid inlets. The data shown are from the takeoff nominal operating line for a range of average throat Mach numbers of 0.47 to 0.88. At the higher one-dimensional Mach numbers of 0.87 and 0.88, the hybrid and accelerating inlets are choked and a facility noise floor is reached.

The scale-model 31 m (100 ft) arc data for the cutback operating point are shown in Figure 51 for the three inlet configurations. As at takeoff, the baseline noise peaks at 50° while the contoured inlets shows the peak to be further forward. The aft noise is lower than the forward noise due to the massive aft suppressor.

The full-scale 152 m (500 ft) sideline maximum PNL variations with average throat Mach number on the cutback operating line are shown in Figure 52. The cutback operating point was defined at about 80% of the takeoff engine thrust with an average throat Mach number of 0.79 in the inlet. On the fan aerodynamic performance map, this would appear on a lower operating line relative to the takeoff condition and at a lower speed but with the same corrected weight flow (see Section V-C). Treatment effectiveness at low average throat Mach number is somewhat less than expected. Suppression due to flow acceleration at an M_{TH} of 0.79 is about 11.0 PNdB. Approximately 2.5 PNdb suppression is attributed to treatment at the 0.79 throat Mach number, which gives a total inlet suppression of 13.5 PNdB at the cutback operating point. The noise trend with increasing throat Mach numbers beyond 0.79 is similar to that of the takeoff condition.

The tip speed for the defined cutback point is about 30.5 m/sec (100 ft/sec) lower than the takeoff point at an average throat Mach number of 0.79. Despite the lower tip speed and pressure ratio, the peak forward fan noise at cutback is slightly higher than at takeoff for the M_{TH} = 0.79 operating point. This is because, at takeoff, the shock is probably more swallowed and the stable shock region covers more blade span, resulting in lower MPT levels relative to cutback. The overall sound power level variation with average throat Mach number for the cutback point is shown in Figure 53. The directivity pattern, Figure 54, shows the baseline, accelerating, and hybrid inlets to have the same directivity as takeoff (see Figure 27) for the same average throat Mach number. An overlay of the hybrid inlet directivities is provided in Figure 55 for the takeoff and cutback operating points. This indicates that fan pressure ratio has little effect on forward-radiated fan noise directivity at supersonic tip speeds for the highly suppressed case. The overall sound pressure level directivities for cutback, Figure 56, are also consistent with that of takeoff. Full-scale 152 m (500 ft) sideline spectral comparisons at M_{TH} of 0.79 for the cutback operating condition are shown in Figures 57 through 71 for inlet angles of 10 to 150° from the inlet axis. At the maximum forward angle of 50°, Figure 61, a substantial decrease in high frequency noise due to flow acceleration is obtained with both the accelerating and hybrid inlets. More treatment suppression was obtained at the cutback point than at takeoff.

1/3-octave sound power level spectra from the cutback operating line are shown in Figures 72 through 78 for a range of throat Mach numbers for 0.52 to 0.94. A noise floor was reached at throat Mach numbers of 0.90 and 0.94 with the hybrid and accelerating inlets.

The 31 m (100 ft) arc scale-model data at the approach operating condition is shown in Figure 79. The change in peak forward angle is somewhat more pronounced than that of the takeoff and cutback operating points. This is most likely an inlet contour effect caused by the higher diffusion angle when the inlet is at the approach position (smaller throat area).

Figure 80 shows the full-scale, 152 m (500 ft) sideline maximum PNL variation with average throat Mach number and tip speed at the approach operating point for the baseline, accelerating, and hybrid inlets. The

approach point was defined at 26% of the engine takeoff thrust with an average inlet throat Mach number of 0.79. At low average throat Mach numbers (~0.68), about 2.0 PNdB was obtained due to flow acceleration and about 5.5 PNdB due to treatment effectiveness. At the approach inlet design throat Mach number of 0.79 the noise suppression due to flow acceleration was about 8.0 PNdB. The treatment (hybrid inlet) was responsible for 3.0 PNdB suppression for a total of 11.0 PNdB reduction at the approach design point. On an overall sound power level basis, Figure 81, the trends are the same but the delta suppression is slightly less than on a perceived noise basis. Figures 82 and 83 show the directivity of the PNL and overall sound pressure level at the approach design point. A slight shift rearward in maximum forward PNL is observed with the hybrid and accelerating inlets. An examination of the spectral data, Figures 84 through 98, shows that the PNL shift is due to slight changes in BPF and high frequency noise suppression. The spectra at the approach operating point have no MPT's since the relative Mach number is subsonic. The tone at approach should have been suppressed by about 18.0 dB based on the treatment design (Reference 3). The lower than expected tone suppression at approach may be due to the increased diffuser angle (area ratio of 1.89) and the larger boundary layer, which increases fan interaction noise. This could cause the approach suppression to be less, or more likely cause a source noise increase (see probe data in Appendix A). Although the suppression was not as expected, there was an increase in treatment suppression relative to takeoff and cutback at the design point.

The 1/3-octave sound power level spectra for the approach operating point are shown in Figures 99 through 104 for a throat Mach number range of 0.68 to 0.90. As the Mach number increases above 0.79 a facility noise floor is reached and little or no suppression is obtained.

A summary of the inferred acoustic treatment suppression versus average throat Mach number is shown in Figure 105 for the takeoff, cutback, and approach inlet positions. The largest inferred suppression is obtained at low throat Mach numbers and decreases with increasing throat Mach numbers. This trend is consistent with previous experience on both low and high tip speed fans. The apparent reduction of treatment suppression may actually be a reduction in acceleration suppression for the hybrid inlet relative to the accelerating inlet. That is, in the hybrid inlet, the noise has been reduced by the wall treatment prior to reaching the high Mach number throat region of the inlet. With less acoustic energy going into the throat region, less net suppression due to flow acceleration may take place. Figure 106 shows the total suppression, i.e., flow acceleration plus treatment, versus average throat Mach number. Noise suppression at $M_{TH} < 0.55$ is due to acoustic treatment only since there is no flow acceleration in the inlet below this throat Mach number. At throat Mach numbers above 0.70, flow acceleration becomes the dominant noise-suppression mechanism, while the treatment effectiveness continually decreases, as seen in Figure 105.

In summary, the results of acoustic testing of the single-stage fan operated in rear drive reaffirms that a swallowed shock system in the fan blade row has a favorable effect in reducing high tip speed fan multiple pure tone (buzzsaw) noise. The total suppression obtained with the hybrid inlet

at the design point was 11.0 to 14.5 PNdB on a 152 m (500 ft) sideline for the maximum forward angle at the three critical operating points. Treatment effectiveness at low Mach number conditions was lower than expected based on prediction. At the design average throat Mach numbers of 0.79, the major noise suppression mechanism was flow acceleration which resulted in a reduction of 13.5 PNdB at takeoff, 11.0 PNdB at cutback, and 8.0 PNdB at approach. There is an apparent loss in acoustic treatment effectiveness with increasing inlet throat Mach number. This is consistent with previous results from hybrid inlet tests; but in actuality, the loss might be acceleration suppression. Further investigation is required in order to separate the suppression mechanisms. At any rate, the two are not directly additive in hybrid inlets.

B. Fan Exhaust Noise - Front Drive

The acoustic data for aft noise were obtained with the vehicle in the front-drive position. The inlet had the baseline bellmouth inlet and a massive inlet suppressor for the isolation of aft noise. Acoustic data were taken with two fan exhaust-duct configurations, a hardwall without splitter and treated walls with splitter. The choice of data points was based on matching corrected tip speed with that of the rear-drive configurations so as to have comparable acoustic data. This allows for the summation of front and aft noise to get the total noise for the fan.

The as-measured 31.0 (100 ft) arc scale-model data for the takeoff operating point were corrected to standard day conditions and are shown in Figure 107 for the two exhaust configurations; hardwall and treated with splitter. At the maximum angle, about 4.5 PNdB suppression is obtained with the treated configuration.

Full scale 152 m (500 ft) sideline aft maximum PNL variations with corrected tip speed for both hardwall and treated configurations are shown in Figure 108 for the takeoff nominal operating line. A monotonic increase in maximum aft noise with tip speed is observed for both the treated and hardwall configurations. At the takeoff operating point, 466 m/sec (1530 ft/sec) a reduction of about 8.0 PNdB is obtained with the treated aft fan duct with a splitter. Slightly more suppression, about 2.0 PNdB, is obtained at tip speeds lower than takeoff. The probable reason is that at low speed the unsuppressed spectra is tone dominated and the treatment is more effective than at high speed, which has considerably more high frequency broadband noise. This will be examined in greater detail in the succeeding discussion. Maximum aft-noise variations with fan pressure ratio are shown in Figure 109 on the takeoff operating line for both hardwall and treated configurations. The overall sound power level variations with tip speed, shown in Figure 110, are similar to that of preceived noise level, although the delta between the treated and hardwall configurations is slightly lower.

The full-scale 152 m (500 ft) sideline directivity pattern at the takeoff operating point is shown in Figure 111 for the hardwall duct and treated duct with a splitter. There is a slight shift of the maximum aft angle from 110 to 120° for the treated configuration. As previously noted, there is an 8.0 PNdB suppression due to treatment at the maximum angle (peak-to-peak). A

similar distribution for the overall sound pressure level is seen in Figure 112. Full-scale spectral comparisons are shown in Figures 113 through 128 for 30 to 160° from the inlet axis. At the maximum aft angle of 110° for the unsuppressed spectra, Figure 121, about 13.0 dB suppression is obtained at the BPF (4000 Hz) while at the maximum angle for the suppressed spectra, 120° (Figure 122), the suppression at BPF is about 10 dB. This results from a slightly lower unsuppressed tone at 120° as indicated in the narrow-band spectra of Figures 123 and 124. It is also interesting to note there appears to be some low frequency MPT's propagating through the fan duct and into the farfield for the hardwall configuration. The BPF haystacking is a modulation of the BPF as it propagates down the core and fan duct and through both turbulent exhaust regions to the farfield microphones. A more detailed investigation of the haystacking phenomenon is presented in Appendix C.

In general, the aft spectra at the takeoff operating point (V_T = 466) m/sec) shows that the treatment in the aft fan duct did provide a substantial decrease in SPL's in the 800 Hz to 10,000 Hz frequency range. There was little or no suppression at frequencies below 800 Hz because the acoustic treatment was not tuned for those frequencies and the jet noise is controlling some of these levels.

Figures 129 through 133 show the 1/3-octave sound power level (PWL) spectral comparisons for the two exhaust configurations; hardwall and treated with splitter exhaust ducts. The data shown are from the nominal takeoff operating line for a range of corrected tip speeds of 268 m/sec (880 ft/sec) to 507 m/sec (1665 ft/sec). The suppression characteristics seem to be better at the lower speeds. This may be caused by the lower wall Mach numbers (≈0.4) resulting in a decrease in acoustic treatment resistance and subsequently more suppression with this configuration.

The scale-model 31.0 m (100 ft) arc data for the cutback operating point is shown in Figure 134 for the two exhaust configurations. About 11.0 PNdB suppression is obtained at the maximum aft angle of 130° with good suppression throughout the arc.

The 152 m (500 ft) sideline full-scale aft maximum PNL variations with corrected tip speed are shown in Figure 135 for the hardwall and treated aft-duct configurations on the nominal cutback operating line. The treated aft duct with a splitter caused a noise reduction of about 13.0 PNdB at the cutback operating point, 439 m/sec (1440 ft/sec). On this operating line, the suppression at the maximum aft angle is fairly constant throughout the speed range except at the lowest speed tested where the suppression increased to about 15.0 PNdB. Spectral comparisons at 120° for 351 m/sec (1152 ft/sec), Figure 136, and 402 m/sec (1318 ft/sec), Figure 137 show that the amount of suppression is similar for the two speeds except in the vicinity of the BPF where the suppressed BPF tone is higher for the higher tip speed. The remaining BPF tone noise for the suppressed configuration is not believed due to treatment ineffectiveness but rather to the tone leakage through the core flowpath (see Figure 15). As the tone energy passes through the exhaust wakes, the energy is redistributed in the side bands

of the tone and appears as a haystack. (A more detailed explanation is given in Appendix C.) On a 1/3-octave basis, this appears as a higher tone due to the broadband energy within the 1/3-octave bandwidth. On the engine, there would be a core (compressor, turbines, and combustor), therefore, this tone noise would not propagate through the core duct.

The cutback operating line maximum aft PNL is shown versus fan pressure ratio in Figure 138. The overall sound power level variation with tip speed for the cutback operating line is shown in Figure 139. The trends are similar to the PNL variations with tip speed but the delta between the treated and hardwall configurations is lower.

The directivity pattern at the cutback operating point, Figure 140, shows a 13.0 PNdB reduction in maximum aft noise with the treated duct. The unsuppressed directivity at cutback is about the same as that of takeoff, (see Figure 111), although at cutback, the pressure ratio and tip speed are lower. A comparison of the takeoff and cutback suppressed directivity shows that the aft-duct treatment was more effective at the lower design operating point (cutback). This is a result of better suppression characteristics throughout the fan-noise frequency range for the cutback (lower) operating point. The improved treatment suppression for the cutback condition relative to takeoff is probably because the cutback condition, known to be the most challenging with respect to meeting the suppression level goals, was given particular attention when selecting the treatment design (see Reference 3). The overall sound pressure level directivity for the cutback operating point is shown in Figure 141 and is consistent with that of takeoff except for the lower suppressed levels (Figure 112). Full-scale 152 m (500 ft) sideline spectral comparisons for the cutback operating point are shown in Figures 142 through 155 for angles of 30 to 160° from the inlet axis. At the maximum aft angle of 120°, Figure 151, a substantial decrease in noise was obtained in the frequency range of 1000 Hz to 10,000 Hz.

1/3-octave sound power level spectra from the cutback operating line are shown in Figures 156 through 160 for tip speeds ranging from 351 m/sec (1150 ft/sec) to 503 m/sec (1650 ft/sec). It is evident that there is fan noise propagating through the core from examining the delta power at the BPF (hardwall treated) and comparing it to the nozzle probe results shown in Appendix A for the cutback operating condition. The probe data shows a 25 dB reduction with the treated configuration while the 1/3-octave data shows a reduction of about 18 dB, Figure 158 (see Appendix C).

The 31.0 m (100 ft) arc scale-model data at the approach operating condition is shown in Figure 161. At the maximum aft angle, there is an 11.0 PNdB suppression with the treated configuration. The peak angle on the 31.0 m arc occurs at 140° from the inlet axis. When extrapolated to a sideline the peak angle moves forward to 120°. Good data repeatability was obtained for both configurations.

Figure 162 shows the full-scale, 152 m (500 ft) sideline maximum PNL variation with corrected tip speed on the approach operating line for the hardwall and treated aft-duct configurations. Only slight variations in aft noise were expected since the ranges of tip speeds and pressure ratios were small. At the approach operating point, 316 m/sec (1036 ft/sec), the amount

of suppression obtained with the treated duct was about 13.5 PNdB. All speeds on the approach operating line showed similar suppression characteristics. This can also be observed on a pressure ratio basis as shown in Figure 163. On an overall sound power level basis, Figure 164, the trends with the tip speed are the same but the delta suppression is slightly less than on a perceived noise basis. Figures 165 and 166 show the PNL and overall sound pressure level directivity comparisons of the two exhaust duct configurations at the approach operating point. The spectral comparisons at the approach condition are shown in Figure 167 through 182 for angles of 30 to 160° from the inlet axis. At the maximum angle of 120°, Figure 176, the treated configuration shows that a definite tone stands out at the blade passing frequency of 2500 Hz. By examining the farfield narrowbands, Figure 177, it can be seen that this is a result of a haystacking phenomenon. From the nature of the haystack, that is, its presence in the farfield but not at the nozzle probe, (see Figure 178 and Appendix A), it is believed that the noise is coming through the core duct and contributing to the farfield results. (See Appendix C for a more detailed discussion of noise leakage through the core). The 1/3-octave sound power level spectra for the approach operating line are shown in Figures 183 through 187 for corrected tip speeds of 296 m/sec (970 ft/sec) to 328 m/sec (1075 ft/sec). At the approach operating point, Figure 185, the delta power suppression at the BPF is considerably less, by about 10 dB on the average, when compared to the nozzle probe delta power shown in Appendix A. This discrepancy occurs to some degree at all speeds on the approach operating line. It is also suspected that there is some high frequency broadband noise (above BPF) coming through the core.

As with the other operating conditions, this specific haystack noise should not appear on an actual engine due to the presence of a core engine compressor, combustor, and turbines.

In summary, the total suppression obtained with the treated fan exhaust duct with splitter was about 8.0 PNdB at takeoff and about 13.0 PNdB at cutback and approach for the maximum aft angle on a 152 m (500 ft) sideline. In reality, the measured suppression was not truly indicative of the treatment effectiveness since there was some apparent leakage of fan noise through the facility core flowpath.

In Section V-D, an effort was made to apply corrections to the spectra so as to obtain more realistic suppression results.

C. Aerodynamic Performance Results

Detailed fan aerodynamic performance data were taken and are discussed in Reference 4. Inlet and bypass duct aerodynamic data were taken for several acoustic test points for the three inlet and two exhaust configurations. These data are summarized in Figures 188 through 196. For rear drive, the inlet throat area for approach with the hybrid and accelerating inlets was smaller than at takeoff and cutback, in order to obtain the required average throat Mach number of 0.79. This resulted in a slightly lower stall line than that obtained with the cylindrical baseline bellmouth inlet (Figure 190). This presented no problems since the approach operating

lines were considerably lower than the established stall line (Figure 191). Throttling was accomplished with a variable discharge valve in the fan exhaust duct (for rear drive) while the bypass ratio was maintained with a core discharge valve which was also variable.

With the vehicle in front drive (for the isolation of aft-end noise) both hardwall and treated configurations were tested with the baseline bellmouth (fixed geometry) inlet. For these configurations, three fixed fan-duct exhaust nozzles were used to obtain the appropriate operating lines for the three critical operating points; takeoff, cutback and approach. The bypass ratio was maintained, as in rear drive, with the core discharge valve. The fan did not make the design goals of 1.8 pressure ratio at 100% corrected speed with 117.9 kg/sec (259.9 lb/sec) flow. At 100% corrected speed the pressure ratio was actually 1.73, about 3.3% low, at a flow of 114.5 kg/sec (252 lb/sec), which was about 3.5% below the predicted level. The fact that the fan operated slightly off design did not have a significant effect on the acoustic results.

Generally, the inlet aerodynamic performance was as expected (see Reference 4). The hybrid inlet performed well at the design throat Mach number (0.79) with little chance of separation in either mode; i.e. approach or takeoff. If anything, the hybrid inlet tended to retard separation relative to the accelerating inlet; an effect of the greater surface roughness of the acoustic treatment leading to greater shear stresses at the wall. The inlet total pressure recoveries were encouragingly high (see Figures 194 and 195) in spite of the long inlet, high area ratios, and high average throat Mach numbers. The spread in trend lines indicate the accuracy of the area-weighted total pressures when attempting to account for wedge blockage and loss effects. At the design point, the recoveries were 98.9 and 98.2% for takeoff and approach conditions, respectively. In the takeoff position, where most of the wedge is exposed (see Figure 4), recovery can be determined within a 1/2% band. At approach, where very little wedge is exposed, recovery can be more accurately determined. Figure 196 shows that the hybrid inlet may be expected to have less than 10% distortion in either mode over the entire operating range under static condtions.

From an inlet aerodynamic standpoint, the penalty for increasing the inlet throat Mach number to about 0.84 at takeoff and cutback and to 0.81 at approach would be very small in terms of inlet recovery or distortion under static conditions. The inlet recoveries would be above 0.98 and the inlet distortion would be about 10%. The increase in throat Mach number would provide additional acoustic suppression (see Figure 25).

Total pressure losses of the acoustically treated splitter duct were in general agreement with the original predictions. A comparison of these losses with those of the hardwall duct without splitter is provided in Table III.

In high bypass ratio engines, the change in specific fuel consumption (SFC) associated with a change in duct pressure loss can be translated through an influence coefficient of about 1.1 at cruise conditions. Thus the acoustically treated duct results in a penalty of about 0.68% in cruise SFC.

This is not a large penalty, considering the extensiveness of the treatment applied, including the splitter.

Table III. Duct Pressure Losses.

	Takeoff	Cutback	Cruise*	Approach
Treated Duct with Splitter $[\Delta P_T/P_T]_{28}(\%)$	1.35	3.24	1.41	2.05
Hardwall Duct without Splitter $[\Delta P_T/P_T]_{28}(\%)$	0.79	1.28	0.79	0
$\Delta[\Delta P_T/P_T]_{28}(\%)$	0.56	1.96	0.62	2.05

*Estimated, based on measured results.

D. Static Data Projected to Flight

One of the goals of this program was to demonstrate, through extrapolation of ground static data, the fan noise levels that would be anticipated in flight for takeoff, cutback, and approach operating points relative to FAR 36 (Reference 12) requirements. The host vehicle used to define the flight conditions for noise evaluation during cycle selection studies was the Boeing 767-640 trijet with a Takeoff Gross Weight (TOGW) of 137,892 kg (304,000 lbs) as described in Reference 5. The trijet had two wing-mounted and one tail-mounted engines.

The static acoustic data used for flight extrapolation were a combination of the individual spectra of both front drive (aft noise) and rear drive (front noise) for the three critical operating points. Since the noise goal of FAR 36 - 20 EPNdB was based on "fan only" noise, the front-drive acoustic data (aft noise) were adjusted by removing jet noise from each spectra from 80 to 160° from the inlet axis. The procedure used to predict and remove the jet noise from the measured spectra is given in Appendix C. Another factor that contributed to the static noise levels which is not representative of a real engine is the leakage of fan noise through the core duct. When the BPF tone energy propagates via the core duct and passes through the turbulent wake of the exhaust nozzle, the energy of the tone is scattered into sidebands and appears as a haystack in the farfield. On an actual engine, there would be a core compressor, combustor, and turbines through which the fan tone would be attenuated. The method of isolating and removing the core tone noise leakage from the static spectra is explained in Appendix C.

The full-scale 152 m (500 ft) sideline PNL directivity of the combined front- and aft-noise static spectra for the takeoff operating point is shown in Figure 197. The resultant PNL directivity was obtained by logarithmically

adding the average (of two points) sound pressure levels at each angle for both front and rear drive. This was done for the hardwall and treated configurations after the removal of the jet noise and fan tone leakage through the core from the aft noise. At takeoff, the PNL directivity shows this fan to be rear dominant by about 1.5 PNdB for the treated configuration. The treated configuration consists of a treated aft fan duct with splitter and the hybrid inlet. The front-radiated, aft-generated noise is actually controlling the front PNL's for both hardwall and treated configurations. This indicates that further noise reduction in the inlet would not decrease the front or aft noise. For additional reductions in fan noise at the takeoff operating condition, it would first be necessary to provide for additional noise reduction in the exhaust fan duct before additional inlet noise suppression would have a payoff.

The suppressed directivity at takeoff shows the PNL distribution to be almost flat, which indicates a balanced suppression design. This also occurs at the other operating points of cutback and approach.

Spectral comparisons at the maximum forward and aft angles are shown in Figures 198 and 200. The tone at 400 Hz at the maximum forward angle for the unsuppressed spectra, Figure 198, is a low frequency MPT not attenuated with the hardwall (accelerating) inlet (from rear-drive spectra, see Figure 35). An example of how the front- and rear-generated noise are combined on a spectral basis is shown in Figure 199 at the maximum forward angle for the unsuppressed configuration. At the maximum aft angle (110°), Figure 200, the fully suppressed configuration shows high frequency noise dominating the PNL. It is possible that some of this high frequency noise may be leaking through the core duct as did the tone, see Appendix C. Figure 201 illustrates how the individual front- and rear-generated noise are combined on a spectral basis at the maximum aft angle for the suppressed configuration.

The resultant directivities for the cutback operating condition were obtained in a similar manner as that described for takeoff and are shown in Figure 202. As a takeoff, the PNL directivity shows the fan to be rear dominant for both hardwall and treated configurations. Similarly, the suppressed forward noise has a contribution from front-radiated, aft-generated fan noise.

The total suppression for the combined spectra is about 12.5 PNdB at the maximum forward angle and 13.0 PNdB at the maximum aft angle. A decrease in suppression of 1.5 PNdB results at the maximum forward angle due to the contribution of aft fan noise. Maximum aft PNL decreased by about 0.5 PNdB due to the absence of jet noise and tone leakage through the core. For the aft angles, the corrected directivity is the same as the uncorrected directivity since the aft noise from the rear-drive configuration does not contribute to the front-drive aft PNL's. A peak-to-peak spectral comparison of the forward and aft angles is shown in Figures 203 and 204 for the cutback operating point. As with the takeoff operating point, the aft spectra at cutback show considerable high frequency noise for the treated configuration which possibly leaked through the core duct.

At the approach operating point, the resultant 152 m (500 ft) sideline PNL distributions for the hardwall and completely suppressed configurations are shown in Figure 205. Since the front noise, at this point, is not

controlled by aft fan noise, the delta suppression remained unchanged (10.5 PNdB) relative to measured front-end noise. The resultant maximum aft noise at approach does show a decrease in PNL of about 1.5 PNdB, not because of front contribution, but because of the contribution of jet noise and fan tone leakage through the core for the as-measured aft noise. Spectral comparisons at the maximum forward and aft angles are shown in Figures 206 and 207 respectively. As with the takeoff and cutback operating points, the aft suppressed spectra at approach shows high frequency noise which possibly radiated from the core duct.

The resultant static spectra for takeoff, cutback, and approach were extrapolated to their respective flight conditions to determine the EPNL's for each mode of operation. Table IV describes the three flight conditions. There are some differences between the design predicted and the measured parameters. These include higher speeds at the three operating conditions for the measured data required to obtain the flow necessary for an inlet throat Mach number of 0.79. Flight noise calculations were done according to the procedures described in Section IV-C.

Table IV. Flight Conditions for EPNL Calculations (M_{TH} = 0.79).

Condition	Actual % Fan Speed	Predicted (design) % Fan Speed	Tip Speed		Altitude		Measuring Point	Front Max PNL Angle	Acoustic Range		Rear Max PNL Angle	Acoustic Range	
			m/sec	ft/sec	m	ft			m	ft		m	ft
Takeoff	92.7	92.0	466	1530	248	800	457 m (1500 ft) S.L.	50°	676	2219	110°	551	1809
Cutback	87.4	85.0	439	1440	390	1280	6.48 km (3.5 n. mi.)	50°	492	1617	120°	450	1478
Approach	626	58.0	316	1036	113	370	1.852 km (1.0 n. mi.)	50°	147	483	120°	130	427

At takeoff, Figure 208, the flight PNL directivity indicates the fan noise to be front dominant for the suppressed configuration. It was previously illustrated on a static basis that the front-radiated, aft-generated noise actually is controlling the front noise. Additional noise suppression in the inlet would not contribute significantly to the reduction of front noise. The takeoff flight spectra at the maximum forward and aft angles are shown in Figures 209 and 210 for the hardwall and treated configurations. At the maximum forward angle, Figure 209, the suppressed spectra is actually aft noise radiated to the front angle and not inlet noise. At the maximum aft angle, Figure 210, the suppressed spectra is dominated by rear noise.

The flight PNL directivity for the power cutback point is shown in Figure 211. As at takeoff, the fan noise is front dominant due to dynamic effect. Spectral comparisons of the hardwall and suppressed configurations at the maximum forward and aft angles are shown in Figures 212 and 213

respectively. The unsuppressed spectra at cutback are slightly higher than at takeoff due to slightly higher source noise (see Section V-B) and to the shorter acoustic range as shown in Table IV. However, as previously noted (Section V-B) for the static data, better acoustic suppression was obtained at cutback relative to takeoff. For their designated acoustic range (takeoff and cutback), the suppressed levels at the maximum forward and aft angles are about the same.

Flight PNL's and spectral comparisons at the maximum forward and aft angles for the approach operating point are shown in Figures 214 through 216. The suppressed PNL directivity at approach is front dominant with no contribution from aft fan noise. Front noise at approach is controlled by the BPF which was not completely suppressed with the hybrid inlet. As previously explained for the static results, the lower than expected tone suppression at approach may be due to the increased diffuser angle (area ratio of 1.89) causing a larger fan inlet boundary layer, which increases fan interaction noise. Although the suppression was not as expected, there was an increase in treatment suppression relative to the takeoff and cutback operating points.

The tone-corrected perceived noise levels (PNLT) were calculated for both hardwall and treated configurations for all three modes of operation. These are shown in Figures 217, 218, and 219 for takeoff, cutback, and approach respectively. The unsuppressed PNLT's show a considerable difference in directivity when compared with the static PNL directivities (Figures 197, 202, and 205), especially at the forward angles. This is due to the tone-controlled spectra for the unsuppressed configurations and to dynamic effect for both suppressed and unsuppressed configurations. An example of the PNLT directivity without dynamic effect is shown in Figure 217 for the suppressed configuration. Without dynamic effect, a decrease in PNLT of about 2.0 PNdB is obtained at the maximum forward angle and an increase of about 2.0 PNdB at the maximum aft angle.

A summary of the projected EPNL's for the hardwall and treated configurations at the three critical operating points, are presented in Table V.

Table V. Projected EPNLs for Hardwall and Treated Configuration.

3 Engines
(level flyover)

Condition	Front Unsupp	Front Supp	Δ Front	Back Unsupp	Back Supp	Δ Back	Total Unsupp	Total Supp	Δ Total
Takeoff	104.5	89.7	14.8	100.0	93.9	6.1	105.8	95.4	10.4
Cutback	104.5	93.4	11.1	104.8	93.6	11.2	108.7	96.3	12.4
Approach	105.7	96.9	8.8	108.2	93.8	14.4	110.2	98.9	11.3

The effective perceived noise levels shown are for a level flyover of a three-engine aircraft. The total EPNL suppressions were 10.4 EPNdB at takeoff, 12.4 EPNdB at cutback, and 11.3 EPNdB at approach. The total suppression for the front and aft components were arrived at by flying the adjusted static spectra for both front and aft individually. At takeoff and cutback, the suppressed EPNL is dominated by rear fan noise. At approach, a decrease in EPNL may be realized by operating either at a lower tip speed to avoid the sharp controlling tone indicated at this point, or at a higher throat Mach number. A higher throat Mach number at approach (with increased airflow and larger exhaust area) appears practical from an inlet performance standpoint.

Table VI summarizes the EPNL's for the forward, aft, and total fan noise relative to FAR 36 at the three critical points. The EPNL for the total (front and back) unsuppressed fan noise at takeoff was slightly lower than FAR 36 while at cutback and approach, they were higher by 5.7 EPNdB and 4.2 EPNdB respectively.

The hybrid inlet, at a throat Mach number of 0.79, resulted in forward fan-noise suppressions ranging from 9.1 to 16.3 ΔEPNdB relative to FAR 36. Additional suppressions could be obtained by increasing the throat Mach number to 0.84 at the takeoff/cutback and 0.81 at approach. Furthermore, additional fan-inlet noise reductions could possibly result from inlet flight effects (cleanup) which have been observed between ground static data extrapolated to flight and actual measured flight noise. The reduced noise levels in flight are generally attributed to reduced flight turbulence levels relative to the static test case, which results in reduced rotor-turbulence interaction noise from the fan source.

The fully treated exhaust duct with splitter provided aft fan-noise suppressions ranging from 9.4 to 12.2 ΔEPNdB relative to FAR 36. It is considered that additional suppressions beyond these values might have been obtained, depending on whether or not the farfield noise measurements during testing contained a significant amount of high frequency noise leaked from the core stream flowpath. There was no quantitative method to determine this with the test instrumemtation available.

Combining the front and aft suppressed fan noise in flight, EPNL suppressions ranging from 6.7 to 10.6 ΔEPNdB relative to FAR 36 resulted. As was suspected early in the design phase, the cutback condition emerged the most critical, (regarding the design goal suppression of FAR 36 minus 20 EPNdB) with the approach point close behind (see Reference 3). As discussed above, greater suppressions than those measured might be possible with this same vehicle and suppression system. As a point of interest, the suppressed fan noise level relative to the proposed new regulation (ΔEPNdB), as defined in the draft of the FAA Environmental Impact Statement dated July 9, 1975, is included on Table VI. This comparison shows that the single-stage advanced technology fan noise is less than the proposed new regulation levels at all conditions. Thus, use of this fan on an engine would be compatible with the new regulation, if the same suppression devices were employed.

Table VI. Projected EPNL Levels Compared to FAR 36.

UNSUPPRESSED COMPARISONS

Conditions	FAR 36[1)]	Front Unsuppressed	Δ Front Unsuppressed	Back Unsuppressed	Δ Back Unsuppressed	Total Unsuppressed	Δ Total Unsuppressed
Takeoff	106.0	104.5	-1.5	100.0	-6.0	105.8	-0.2
Cutback	103.0	104.5	+1.5	104.8	+1.8	108.7	+5.7
Approach	106.0	105.7	-0.3	108.2	+2.2	110.2	+4.2

SUPPRESSED COMPARISONS

Condition	FAR 36	Front Suppressed	Δ Front Suppressed	Back Suppressed	Δ Back Suppressed	Total Suppressed	Δ Total Suppressed	Δ[2)]
Takeoff	106.0	89.7	-16.3	93.9	-12.1	95.4	-10.6	-1.6 (Y)
Cutback	103.0	93.4	-9.6	93.6	-9.4	96.3	-6.7	-0.7 (X)
Approach	106.0	96.9	-9.1	93.8	-12.2	98.9	-7.1	-3.1 (Z)

Notes: 1) Reference 12.

2) Δ's are relative to the proposed change to FAR 36 as defined by the Draft of the FAA Environment Impact Statement dated July 9, 1975.

Though the contract goal noise levels were not reached for this high tip speed single-stage fan, some improvement in the technology of both front and aft fan-noise suppression was realized. To illustrate this, a comparison of acoustic performance with inlet aerodynamic performance was made between the advanced technology fan hybrid inlet and the Fan "C" scale-model splitter inlet tested during the Quiet Engine Program (Reference 14). These vehicles were tested at the same facility (Peebles Site IVB) and in the same size (93 cm), so the comparison should be a valid one. Figure 220 shows the trend of noise suppression in 61 meter sideline PNdB versus inlet total pressure recovery in percent lost (from the clean inlet low throat Mach number reference value of 0.998). The treated wall scale model Fan "C" inlet gives 11 PNdB suppression with practically no change in recovery over the hardwall inlet. As splitters are added to the inlet, the suppression gets even greater, but the recovery loss is also greater. In the hybrid inlet, the parameter which increases the recovery loss is the inlet throat Mach number. It is seen that 15 PNdB suppression is obtained before a significant loss in recovery occurs. The aforementioned data of Figure 220 were obtained under sea level static takeoff conditions. At cruise, the splitters are still present and the recovery loss translates into a significant loss in specific fuel consumption (roughly a one-to-one trade on a percentage basis relative to the sea level static recoveries). For the variable-geometry hybrid inlet, the throat is set at the optimum position for cruise and essentially no penalty in performance results. Of course, the variable geometry has its inherent penalties of weight and cost, but not necessarily much greater than the weight and cost of a splitter inlet, requiring anti-icing on the splitter. Thus, the advantages and basic concept of the hybrid inlet for front fan-noise suppression are realized.

In Figure 221 a comparison of PNL suppression at the aft maximum noise angle is compared between the advanced technology fan and Engine "C" tested in the Quiet Engine Program (Reference 15). The bypass duct treatment configurations were quite similar (treated walls plus a midduct splitter) except that the Engine "C" overall treated length to fan diameter was 0.923, versus 0.819 for the advanced technology fan. It is noted that Engine "C" was never tested without aft frame treatment. To account for this, the PNL maximum aft angle suppression due to frame treatment was obtained from NASA-Lewis test data on full-scale Fan "C" and added to the suppression obtained on Engine "C" between the frame-treated and fully treated aft duct configurations. It is seen in the figure that, at low pressure ratios typical of the approach flight condition, the advanced technology fan bypass duct treatment resulted in slightly better suppression, while at higher pressure ratios typical of takeoff, Engine "C" suppression was slightly better. However, when compared in terms of the efficiency of suppression, using the $\Delta PNL/L/D_F$ parameter, the advanced technology fan was somewhat better. That is, at approach, the PNL suppression per unit L/D_F for the advanced technology fan was 1.34 PNdB, while for Engine "C" it was 1.03; i.e., there was a 30% improvement with the advanced technology fan. At takeoff, the ratios were equal at 1.23 ΔPNdB per unit L/D_F of the treatment. These comparisons, then, show some improvement in both inlet and aft fan-noise suppression technology.

In summary, for a payoff in additional inlet noise suppression at takeoff and cutback, it would first be necessary to provide for additional noise reduction in the exhaust fan duct, because the aft fan noise radiated to the forward angles is higher than the inlet fan noise.

Forward fan-noise suppression with the hybrid inlet at a throat Mach number of 0.79 ranges from 9.1 to 16.3 ΔEPNdB relative to FAR 36. Further reductions could be obtained by increasing the average throat Mach number to 0.84 at takeoff and cutback and 0.81 at approach without exceeding aerodynamic performance limitations. Additional fan-inlet noise reduction could possibly result from inlet flight effects (inlet "clean-up"). The reduced noise levels in flight are generally attributed to reduced flight turbulence levels relative to the static test case, which results in reduced rotor-turbulence interaction noise from the fan source.

Aft fan-noise suppression in the fully treated fan exhaust duct ranged from 9.4 to 12.2 ΔEPNdB relative to FAR 36. Additional noise suppression might have been obtained had it been possible to determine the amount of high frequency noise leaking through the core stream flowpath.

The combined front and aft suppressed fan noise, for a full-scale flight application, resulted in EPNL suppressions ranging from 6.7 to 10.6 ΔEPNdB relative to FAR 36. Although the suppression goal of FAR 36-20 EPNdB was not reached, improvements in the technology of both front and aft fan-noise suppression were realized. Also, the suppressed fan was shown to be consistent with proposed new federal noise regulations (FAR 36-XYZ) for subsonic transports. Specifically, the total fan noise levels were 1.6, 0.7, and 3.1 EPNdB below the proposed new levels (per the draft of the FAA Environmental Impact Statement dated July 9, 1975) at takeoff, cutback, and approach, respectively.

SECTION VI

SUMMARY OF RESULTS

The following summarizes the results of acoustic testing of the single-stage, low noise, advanced technology fan:

- The combined front and aft suppressed fan noise, for a full-scale flight application, resulted in EPNL suppressions ranging from 6.7 to 10.6 ΔEPNdB relative to FAR 36. Although the suppression goal of FAR 36-20 EPNdB was not reached, improvements in the technology of both front and aft fan-noise suppression were realized.

- Increasing speed above the design shock swallowing speed of $92\%N/\sqrt{\theta}$ resulted in continued reductions in perceived noise level for the unsuppressed fan. This effect was the result of reduced multiple pure tone noise, which was caused by the more stable swallowed shock system covering more of the blade span as the speed was increased.

- Flow acceleration suppression for the full-scale fan on a 152 m sideline was 13.5 PNdB; about 4.0 PNdB more than predicted.

- Suppressions due to flow acceleration and acoustic treatment are not directly additive in hybrid inlets. Further investigation is required to determine if acceleration suppression or treatment suppression or both are reduced when they are combined.

- There was an effect on noise directly resulting from the contouring of the hybrid inlet relative to the cylindrical hardwall inlet (baseline). Directivity patterns were less peaked and the maximum noise angle moved toward the inlet axis (on an arc) with the hybrid inlet.

- A variable-geometry hybrid inlet is a viable fan-noise suppression device. Forward fan-noise suppressions ranging from 9.1 to 16.3 ΔEPNdB relative to FAR 36 were measured, depending on operating point, at the design throat Mach number condition of 0.79. This was accomplished with static inlet total pressure recoveries of 98.9% at takeoff/cutback and 98.2% at approach and with steady-state distortion levels well below 10%. The hybrid inlet was shown to have less performance penalty with the same suppression than a splitter inlet.

- Additional hybrid inlet fan-noise suppression could be obtained by increasing the average throat Mach numbers to 0.84 at takeoff/cutback and 0.81 at approach without exceeding acceptable static values of pressure recovery and inlet distortion.

- The aft fan-noise suppression obtained with a fully treated duct with a single midduct splitter was a viable approach, in that an estimated cruise specific fuel consumption penalty of only 0.68% resulted. Aft fan-noise suppressions ranged from 9.4 to 12.2 ΔEPNdB relative to FAR 36, depending on operating point. Some improvement in bypass duct treatment design technology was determined by comparision with Engine "C" results for the same configuration.

- The fan-noise suppression at takeoff and cutback was limited in terms of EPNL by the bypass duct suppression obtained. Aft fan noise propagating to the front provided a floor and added noise to the forward angles at these operating points. There was evidence that fan noise leakage through the core stream provided a floor on aft fan noise and limited the amount of measureable suppression.

- The flat PNL directivity patterns for total fan noise at the three operating points indicated success in the attempt to provide a balanced suppression design for the advanced technology fan.

APPENDIX A

ACOUSTIC PROBE

An acoustic probe has been developed by General Electric and used extensively in fan and compressor acoustic tests to provide a means of determining noise source location and radiation paths within the flow stream.

The probe, shown in Figure A1, is basically a hollow tube, placed through the outer wall of the vehicle inlet or exhaust duct. The open end of the tube is in the flow passage and the opposite end of the tube is connected to a coiled tube which eliminates reflection and standing waves. A microphone is mounted outside the vehicle at the end of the probe tube and normal to the longitudinal axis of the probe. The entire assembly is actuator driven to permit sensing of sound levels at selected immersions depths across the flow passage. The nose cone shape and hole size and pattern are the results of extensive research to produce a probe with low self-noise characteristics.

The dynamic data are reduced through a narrowband analyzer. These data are used to reveal both the tone and broadband noise content passing the plane in which the probe is traversed. For absolute acoustic levels, the probe measurements must be corrected for the following:

- Probe loss, as defined through probe calibration for frequency response.
- Flow Mach number correction.
- Nonplane wave incidence on the probe.

The probe correction for viscous losses as measured without flow is shown in Figure A2.

Without flow, the acoustic pressure recorded by the probe in the duct is interpreted as the factor which determines acoustic energy flux, I, according to:

$$I = \frac{P^2}{\rho_o c} \text{ W/cm}^2 \qquad (1)$$

and the acoustic power, W, is defined as

$$PWL = IA \text{ watts} \qquad (2)$$

where

P = acoustic pressure

$\rho_o c$ = characteristic impedance of air

A = cross-sectional area of the duct at which the acoustic pressure was measured.

These relationships must be modified when there is airflow within the duct.

Based on the assumption that sound is a plane wave propagating perpendicular to the duct cross section, the sound pressure level amplitude is changed by the airflow according to

$$P = P_F \left[1 - M \cos \theta\right] \exp \left[\frac{-i\, k_o y M \cos \theta}{1 - M \cos \theta} \right] \tag{3}$$

where

P_F = measured sound pressure with flow

P = corrected sound pressure to be used for calculation of I and W

M = airflow Mach number at location of acoustic pressure measurements

θ = angle of the propagating wave front relative to the incoming airflow direction (0° at the inlet and 180° at the exhaust)

k_o = 2π[FREQ]/c

y = axial distance along the duct (for plane wave)

Only the amplitude correction need be considered, as the phase correction changes only the wavelength, not the level. The corrected acoustic pressure, when used in the expression for I and W, will yield the proper values of intensity and power for fan noise. The reason the corrected pressure is used in the formulas for I and W is that airflow is assumed to change the sound pressure level but not the energy flux of a plane wave traveling in the same or opposite direction as the airflow.

In the actual case, the direction of propagation usually is not a plane wave, but varies with time. For this reason, an average value for θ of 45° is used in the inlet and 135° in the exhaust. As can be seen, this has the effect of taking one-half the plane wave correction. Note that, in the inlet, the correction is negative (the probe measures too high) and, in the exhaust, it is positive (the probe measures too low). The correction is obtained from

$$\Delta SPL = 20 \log \left[1 - M \cos \theta\right]. \tag{4}$$

Finally, in correcting the calculated power level, an account must be made of the nonplane wave incidence on the probe. If the pressure and particle velocity are in phase, and if the particle velocity is normal to the measuring plane, then the power normal to the measuring plane is calculated properly from Equation (1) and (2). Taking into consideration the wavelengths usually involved in fan noise and the duct dimensions, the assumption of particle velocity and pressure being in phase is probably good. The only way that the

particle velocity would be normal to the plane of measurement is if there were only plane waves being propagated in the duct. In view of the geometry involved, as well as the scattering effects of the air stream, it is probable that many higher-order modes exist in the duct. In this case, the exact power is difficult to calculate. With the assumption that there are enough modes in the duct to consider the angle of the particle's velocity to be coming equally from all directions, the power flowing normal to the measuring plane (out of the duct) can be calculated. A factor, then, of 2 dB is subtracted from the calculated power using Equation (2). This results from the fact that if the sound pressure measured in the duct is used to calculate intensity, using a plane wave relationship, then this intensity is too high by a factor of the average value of the sine of the angle from 0 to 180°. In the power calculation this would appear as ten times the log of the value of the average sine, which is 2 dB.

The total power is the sum of the powers of each immersion minus 2 dB random-incidence correction. An average value of $\rho_o c$ is used.

$$PWL_{TOT} = 10 \log \frac{\frac{1}{\rho_o c} \int_{i=1}^{n} P_i^2 A_i}{10^{-13}} - 2 \qquad (5)$$

where n is the number of immersions

P_i is the acoustic pressure

A_i is the cross-sectional area of each immersion at which the acoustic pressure was measured.

Acoustic-probe data with the vehicle in rear drive were taken at the takeoff, cutback, and approach operating points for the three inlet configurations at the design average throat Mach number of 0.79. Three acoustic probes were traversed at five immersions to centers of equal area for the three operating points. The probes were located at the inlet lip, the fan face, and the fan discharge as shown in Figure 14. Probe data for the low Mach number inlet (baseline) were taken at tip speeds corresponding to that of the accelerating and hybrid inlets operating at average throat Mach number of 0.79. This provides the proper base for data comparison.

Plots of sound power level versus immersion are presented in Figures A3 through A17 with a breakdown, from narrowband-spectra data, of sound contributions from MPT's, broadband and BPF where possible. These noise components were resolved as follows: a broadband base or substratum was faired below each maximum resulting from a blade passing tone or its harmonics, and the maximum was corrected for broadband base level to obtain the amplitude of the blade passing frequency tone or harmonic alone. A similar procedure was applied to the subharmonic maxima which represent the MPT's. After subtracting these two components from the sound pressure level the remainder

was designated as broadband noise. Sound power levels for each of these noise components as well as total sound power level was obtained by integrating the intensity calculated at each of the radial traverse positions for the probes and at each microphone angle for the farfield acoustic data.

At takeoff, a considerable increase in BPF sound power levels is observed at the fan discharge probe, Figure A6, for the hybrid and accelerating inlets relative to the baseline inlet. This is probably due to the increased boundary layer in the contoured inlets which increases rotor/stator interaction noise. At the fan face and fan discharge, broadband and MPT power levels are about the same for the baseline and accelerating inlets with a slight increase with the hybrid inlet. This is also true at the cutback and approach operating points. From the bellmouth probe, Figures A4 and A5, it is evident that both accelerating and hybrid inlets show a considerable decrease in MPT's and broadband power. This reduction is primarily due to flow acceleration as observed in the farfield data presented in the text, Section V-A.

Sound power distributions for the cutback condition are shown in Figures A7 through A10. MPT's dominate, at the fan face, with little contribution from the BPF for the baseline configuration, as seen in Figure A11. This is why no baseline data appears in Figure A10. As at takeoff, a significant decrease in broadband and MPT power levels is observed at the bellmouth probe due to flow acceleration.

At approach, the total sound power for the bellmouth and fan discharge probes is essentially all broadband noise as shown in Figures A12 and A13. It can be seen from the bellmouth probe, Figures A14 and A15, that flow acceleration is the mechanism which contributes to the major reduction in average throat Mach number. This result agrees with farfield data and is consistent at the three critical operating points. At approach, the boundary layer is greater by about 3 cm (1.2 in.) relative to takeoff and cutback due to the increase in diffuser area ratio from about 1.21 to 1.89. All the data presented confirms the fact that there is an increase in broadband source noise level with the hybrid inlet and occasionally with the accelerating inlet. A probable cause is the increased turbulence/rotor interaction noise caused by the larger turbulent boundary layer.

Table A1 summarizes the overall sound power levels for each inlet at the three operating points.

With the vehicle in front drive, acoustic-probe data were taken at the three critical operating conditons; takeoff, cutback, and approach, for the hardwall and treated with splitter fan exhaust configurations. As with rear drive, three acoustic probes were traversed at 5 immersions to centers of equal areas. These probes were located at the fan face, fan discharge, and forward of the nozzle in the fan exhaust duct as shown in Figure 15. In front drive, the low Mach number inlet (baseline bellmouth) was used; therefore, probe data were taken at tip speeds corresponding to that of the accelerating and hybrid inlets operating at the design condition (M_{TH} = 0.79).

Table A1. Probe Overall Power Levels.

Nominal Operating Line

Rear-Drive Configuration	OAPWL @ Takeoff			OAPWL @ Cutback			OAPWL @ Approach		
	Bellmouth	Fan Face	Fan Discharge	Bellmouth	Fan Face	Fan Discharge	Bellmouth	Fan Face	Fan Discharge
Baseline Bellmouth	158.1	166.1	164.2	158.9	168.0	164.5	150.1	155.8	154.5
Accelerating Inlet	146.6	165.6	163.6	148.1	167.2	165.5	144.3	156.2	156.3
Hybrid Inlet	147.0	165.9	166.7	147.1	166.2	166.0	142.8	153.6	157.9
Front-Drive Configuration	**Fan Face**	**Fan Discharge**	**Nozzle**	**Fan Face**	**Fan Discharge**	**Nozzle**	**Fan Face**	**Fan Discharge**	**Nozzle**
Hardwall (Without Splitter)	167.3	162.8	161.4	169.1	165.3	162.4	158.3	153.9	155.1
Treated W/Splitter	166.7	161.6	155.0	169.3	160.7	159.1	159.6	154.3	146.6

Acoustic-probe sound power levels versus immersion are presented in Figures A18 through A29 for the hardwall and treated configuration. These plots also show a breakdown of sound power contribution from MPT's, broadband noise, and BPF tones where possible. As would be expected, the fan-face probe total power levels indicate no change in acoustic power between the hardwall and treated configuration, and the levels are similar, within a few dB, to that of the rear-drive configurations at all three operating points.

At takeoff, the fan-discharge probe indicates a decrease in BPF sound power level at the outer immersions, see Figure A21, when the treated exhaust is employed. This is probably due to the frame treatment between the rotor and the OGV's (see Figure 15). Similar results are observed at cutback and approach, Figures A27 and A31. At cutback, the fan discharge BPF power levels for the treated configuration show a decrease of about 4.0 dB relative to the hardwall. It may be that the frame treatment is more effective at this operating point.

The significant observation to be made from the nozzle probe data is that there was a BPF noise reduction (average for five immersions) of about 27 dB with the treated aft duct at takeoff (Figure A21). This tone suppression is considerably greater than the 13.9 dB (PWL) suppression obtained from 1/3-octave data (see Figure 132). The overlays of the farfield narrowband at the maximum aft angle (hardwall and treated) and a representative immersion (No. 3) from the nozzle probe (hardwall and treated) are shown in Figures A22 and A23. This comparison shows that for the treated configuration, a BPF tone exists in the farfield while the probe data indicates that the tone was completely suppressed. One conclusion that can be drawn from these comparisons is that the fan tone noise is leaking through the core. It could not have escaped through the inlet since the inlet had a massive inlet suppressor (Figure 10). Similar results occurred at the cutback operating point. At cutback, the tone energy in the farfield (from the core duct) was distributed into the sidebands forming a haystack around the tone as explained in Appendix C. Although there exists leakage through the core duct, the redistribution of the tone power to the sidebands results in relatively good agreement between the farfield and probe narrowband BPF power.

At approach, the average probe tone power suppression was about 23 dB while in the farfield (1/3-octave) approximately 19 dB suppression was obtained (see Figure 185). As previously discussed for the other operating points, indications are that the difference between the tone suppression in the fan duct and the farfield is caused by tone energy propagating through the core duct into the farfield.

A summary of overall sound power levels for each probe at the critical operating points is shown in Table A1.

APPENDIX B

FARFIELD DATA AND SOURCE-NOISE SEPARATION

Farfield acoustic data were taken for each of the five configurations tested, three inlet configurations (rear drive), and two exhaust configurations (front drive). Data analysis was done on a 1/3-octave basis for all the test points. In addition, farfield narrowband (20 Hz bandwidth) analysis was obtained at two speeds on each of the three operating lines for the five configurations. The speeds chosen on each nominal operating line included the critical operating point (M_{TH} = 0.79) and a low speed point. With the vehicle in a front-drive position, the critical operating point was chosen so as to match the tip speed of the rear-drive configuration with the accelerating or hybrid inlet operating at an average inlet throat Mach number of 0.79.

In the frequency ranges where possible, the scale-model farfield narrowband acoustic data were separated into three components: broadband noise, multiple pure tones (at rotor speed frequencies), and blade passing frequency tones and its harmonics. These noise components were resolved in the same manner as previously described under Data Analysis Procedures, Section IV-C, except that the total sound power levels were obtained from 1/3-octave data while the broadband and BPF power levels were calculated from narrowband results. The logarithmic subtraction of the broadband and BPF power from the 1/3-octave power resulted in the MPT power spectra.

Figures B1 through B6 show the rear-drive total and component sound power level spectra for the takeoff operating point (M_{TH} = 0.79) and at a lower operating condition (M_{TH} = 0.47) on the takeoff operating line. The data are consistent with that discussed in Section V-A of the report. Similar results are shown for the cutback and approach operating points in Figures B7 through B18.

A similar analysis was done for the data taken with the vehicle in front drive. Figures B19 through B24 show the component power spectra for two operating points on the takeoff operating line. The results of the cutback and approach operating points are shown in Figures B25 through B30 and Figures B31 through B36 respectively. As with the rear-drive data, these powers spectral components tend to reiterate data previously examined in Section VB.

APPENDIX C

SPECTRA CORRECTION PROCEDURES

Tone Power Leakage Through Core Duct

A factor that contributed to the measured static noise levels with the vehicle in front drive, which was not representative of aft fan noise propagating from a real engine, is the leakage of tone power through the core duct. In an actual engine the core duct would include a core compressor, a combustor, and turbines, which would attenuate all the fan noise propagating through the core duct. The leakage was identified by a comparison of BPF sound power levels from the nozzle probe and from farfield narrowbands. A summary of these power levels is shown in Table C1 below for the hardwall and treated with splitter configuration at the takeoff and approach operating points. At takeoff, the nozzle probe shows a tone power suppression of 27.7 dB while in the farfield, the tone power suppression was only 18.3 dB. Similar results are shown at approach with a 28.0 dB tone power reduction in the duct and a 22.8 dB reduction in the farfield. These results indicate the BPF tone energy in the farfield is not totally fan duct tone energy but a combination of tone energy propagating through the fan and core duct. Tone energy radiating from the inlet was eliminated as a possible cause because of the massive inlet suppressor and the observation that 1/3-octave data shows the tone energy to decrease at the more forward angles, indicating forward radiation of aft-generated tone energy (see spectra in Section V-B).

Table C1. BPF Sound Power Levels (Front Drive).

		Probe		Farfield Narrowband	1/3-Octave
		Fan Discharge	Nozzle		
Takeoff	Hardwall	149.6	147.6	144.4	153.1
	Treated	145.6	119.9	126.1	139.2
			27.7	18.3	13.9
Approach	Hardwall	136.8	134.6	137.9	146.5
	Treated	131.5	106.6	115.1	127.3
			28.0	22.8	19.2

The 1/3-octave sound power levels shown above indicate less suppression at the BPF than the farfield narrowbands. This is caused primarily by the core duct tone energy, passing through the turbulent exhaust wakes of the core and fan duct, being redistributed into the sidebands of the tone. The redistribution of tone energy appears as a haystack on the narrowbands but on a 1/3-octave basis, the haystack (broadband) energy within the 1/3-octave

band containing the tone appears as tone energy. Figures C1 and C2 show the difference in spectral content between the probe and farfield narrowbands for takeoff and approach, respectively.

The method of removing the core contribution from the measured data was to determine the broadband level from the farfield narrowbands by fairing a line through the broadband level to either side of the haystack as shown in Figures C1 and C2. This 20 Hz bandwidth broadband level was then converted to a 1/3-octave level by adding 10 log of the ratio of the tone bandwidth (1136 Hz for approach, Figure C2) to the narrowband filter bandwidth (20 Hz in this case). For the suppressed approach case, this provided an adder of 17.5 dB to the 55.5 dB broadband level faired on the narrowband, resulting in a level of 73.0 dB. This broadband level, when scaled to full size and extrapolated to the 152 m (500 ft) sideline, was 59.1 dB and occurred in the 2500 Hz 1/3-octave band. Figure C3 shows both the uncorrected and corrected tone SPL's for the treated configuration. Tone corrections for the unsuppressed configurations were not necessary since the fan duct contains most of the unsuppressed tone energy. This tone or haystacking correction was made on acoustic data obtained with the vehicle in front drive for each angle from 80 to 160° from the inlet axis at the three critical operating points. In most cases, the PNL's were only effected by 0.5 to 1.5 PNdB.

Jet Noise

Since the noise goal was based on "fan only" noise, the static acoustic data obtained with the vehicle in front drive (aft noise) were adjusted by removing the jet noise contribution from each spectra from 80 to 160° from the inlet axis. The correction for jet noise was done at the three critical operating points of takeoff, cutback, and approach.

The procedure used to determine the jet noise contribution to farfield results was to predict the general shape of the jet noise at each condition by the use of a General Electric conical nozzle prediction. The advanced technology fan exhaust configuration was actually a coannular-coplanar nozzle, but due to the high velocity ratios (V_{fan}/V_{core}) of 6.7, 9.5, and 4.1 for takeoff, cutback and approach respectively, it was considered that the jet noise would be adequately predicted using a conical jet prediction method with fan parameters as input.

An example of a step-by-step procedure used at each angle for the three operating points is explained below with the use of the 120° spectra at approach, see Figure C3.

As a first step, it was assumed that the low frequency fan noise has a slope of 3 dB per 1/3-octave beginning at a frequency for which no suppression was observed with the treated configuration. For this case, the transition point between low frequency fan noise and jet noise is at a frequency of 500 Hz. Since the predicted jet noise does not include ground reflections which exist at low frequency for the measured data, a mean line was drawn through the measured data up to the transition frequency of 500 Hz. The predicted jet noise spectra for this specific angle of 120° was then adjusted (up or

down) so as to match with the 3 dB per 1/3-octave projection. That is, the results of the logarithmic addition of the predicted jet and the 3 dB per 1/3-octave projection is the mean line through the measured low frequency data, at least in the vicinity of the crossover point of the two lines. The primary reason for this adjustment was to obtain a reasonable estimate of the jet noise level in the higher frequency range. The 3 dB per 1/3-octave line has little ($\leq$ 0.5 dB) effect on the PNL's due to the low noy weighting associated with the SPL's in the low frequency range. This combination of predicted jet noise and 3 dB per 1/3-octave projection was assumed to be representative of the actual jet noise for this vehicle. This jet noise spectra was then logarithmically subtracted from the measured suppressed spectra. The unsuppressed spectra is dominated by fan noise with no significant contribution from jet noise in the high frequency range. The resultant suppressed spectra were then considered to be representative of the aft-radiated "fan only" noise and were subsequently used to obtain extrapolated flight spectra and EPNL for the three critical operating points.

APPENDIX D

LIST OF SYMBOLS AND NOMENCLATURE

Symbol		Units
A	Area (Duct cross-sectional)	m^2 or cm^2
AMB	Ambient	-
APP	Approach	-
ARP	Aerospace Recommended Practice	-
AVG	Average	-
B/M	Bellmouth	-
BPF	Blade Passing Frequency	Hz
c	Speed of sound	m/sec
C/B	Cutback	-
CTOL	Conventional Takeoff and Landing	-
D	Diameter	cm
DEG	Degrees	-
DV	Discharge Valve	-
EPNdB	Effective Perceived Noise Decibels	dB
EPNL	Effective Perceived Noise Level	EPNdB
FAA	Federal Aviation Administration	-
FAR	Federal Aviation Regulation	-
FM	Frequency Modulation	-
FREQ	Frequency	Hz
GE	General Electric	-
H/λ	Duct Height Parameter: Height/Wavelength	-
I	Acoustic Energy Flux	watts/cm^2
L/D_F	Length to Fan Diameter Ratio	-
k_o	$2\pi(FREQ)/c$	m^{-1}
M	Mach Number	-
M_o	Freestream Mach Number	-
MPT	Multiple Pure Tone	-
M_{PTH}	Peak Wall Mach Number at the Throat	-
M_{TH}	One-Dimensional Average Throat Mach Number	-

LIST OF SYMBOLS AND NOMENCLATURE (CONTINUED)

Symbol		Units
M_{wall}	Mach Number along Wall	-
N	Fan Speed	rpm
n	Number of Immersions (of Acoustic Probe)	-
Noz.	Nozzle	-
OAPWL	Overall Sound Power Level	dB
OGV	Outlet Guide Vane	-
P	Acoustic Pressure	N/m^2
P_F	Measured Sound Pressure with Flow	N/m^2
PNdB	Perceived Noise Decibels	dB
PNL	Perceived Noise Level	PNdB
PNLT	Tone-Corrected Perceived Noise Level	PNdB
PPG	Peebles Proving Ground	-
P_{T_2}	Fan Inlet Total Pressure	N/m^2
$P_{T_{28}}$	Fan Bypass Exit Total Pressure	N/m^2
PWL	Sound Power Level; re: 10^{-13} watts	dB
QEP	Quiet Engine Program	-
R	Radius	cm
re:	Relative to	-
S	Acoustic-Treatment Cavity Depth	cm
SAE	Society of Automotive Engineers	-
SDOF	Single Degree of Freedom	-
SFC	Specific Fuel Consumption	kg/N
SLS	Sea Level Static	-
SPL	Sound Pressure Level	dB
STD	Standard Day	-
T	Temperature	° K
t	Acoustic Treatment Thickness	cm
T/O	Takeoff	-
V_{core}	Exhaust Velocity of Core Stream	m/sec
V_{fan}	Exhaust Velocity of Fan Stream	m/sec

LIST OF SYMBOLS AND NOMENCLATURE (CONCLUDED)

Symbol		Units
$W\sqrt{\theta}/\delta$	Total Corrected Fan Face Flow	kg/sec
$W\sqrt{\theta}/\delta_{TH}$	Weight Flow at Inlet Throat (Corrected to Standard Day)	kg/sec
Δ	Difference, or Change in	-
δ	Pressure Correction: P/P_{ref} where P_{ref} = Standard Sea Level Pressure	-
η	Efficiency	-
θ	Temperature Correction: T/T_{ref} where T_{ref} = Standard Sea Level Temperature	-
θ	Acoustic Wave Front Relative to the Incoming Air-Flow Direction, or Microphone or Observer Angle Relative to the Inlet Axis	degrees
ρ	Air Density	kg/m^3

REFERENCES

1. Sullivan, T.J., Younghans, J.L., and Little, D.R.; "Single Stage, Low Noise, Advanced Technology Fan, Volume I - Aerodynamic Design," NASA CR-134801.

2. Schoener, J.L., Black, G.R. and Roth, R.H., "Single Stage, Low Noise, Advanced Technology Fan, Volume II - Structural Design," NASA CR-134802, March 1976.

3. Kazin, S.B., and Mishler, R.B.; "Single Stage, Low Noise, Advanced Technology Fan, Volume III - Acoustic Design," NASA CR-134803.

4. Little, D.R., Silverman, I.A., and Sullivan, T.J.; "Single Stage, Low Noise, Advanced Technology Fan, Volume IV - Fan Aerodynamics, Section 1 - Results and Analysis," NASA CR-134892
Section 2 - Overall and Blade-Element Performance Data Tabulations," NASA CR-134893

5. Compagnon, M.A.; "Propulsion System Studies for an Advanced High Subsonic, Long Range Jet Commercial Transport Aircraft, NASA CR-121016, November, 1972.

6. "Studies for Determining the Optimum Propulsion System Characteristics for Use in a Long-Range Transport Aircraft - Comprehensive Data Report," NASA Contract NAS3-15544, June 1972.

7. Jutras, R.R., and Kazin, S.B.; "Acoustic Results of Supersonic Tip Speed Fan Blade Modifications," NASA CR-121233 (R73AEG407), September 14, 1973.

8. Compagnon, M.A.; "A Study of Engine Variable Geometry Systems for an Advanced High Subsonic Long Range Commercial Aircraft, NASA CR-134495 (R73AEG185), October, 1973.

9. "Standard Values of Atmospheric Absorption as a Function of Temperature and Humidity for Use in Evaluating Aircraft Flyover Noise," SAE Aerospace Recommended Practice 866, August 1964.

10. "Methods for Calculating the Attenuation of Aircraft Ground to Ground Noise Propagation During Takeoff and Landing," SAE Aerospace Information Report 923, August 1966.

11. "Definitions and Procedures for Computing the Perceived Noise Level of Aircraft Noise," SAE Aerospace Recommened Practice 865A, August 1969.

12. Noise Standards: "Aircraft Type Certification," Vol. III, Part 36, Federal Aviation Regulations, December 1, 1969.

13. Morse, P.M., Ingard, K.V.; "Theoretical Acoustics," pp. 716-726, 1968.

14. Kazin, S.B., "High Tip Speed Fan Inlet Noise Reduction Using Treated Inlet Splitters and Accelerating Inlets (Quiet Engine Program Fan C Scale Model)," NASA CR-121268, August 1973.

15. Kazin, S.B., Paas, J.E.; "NASA/GE Quiet Engine "C" Acoustic Test Results," NASA CR-121176 (R73AEG364), April 1974.

ILLUSTRATIONS

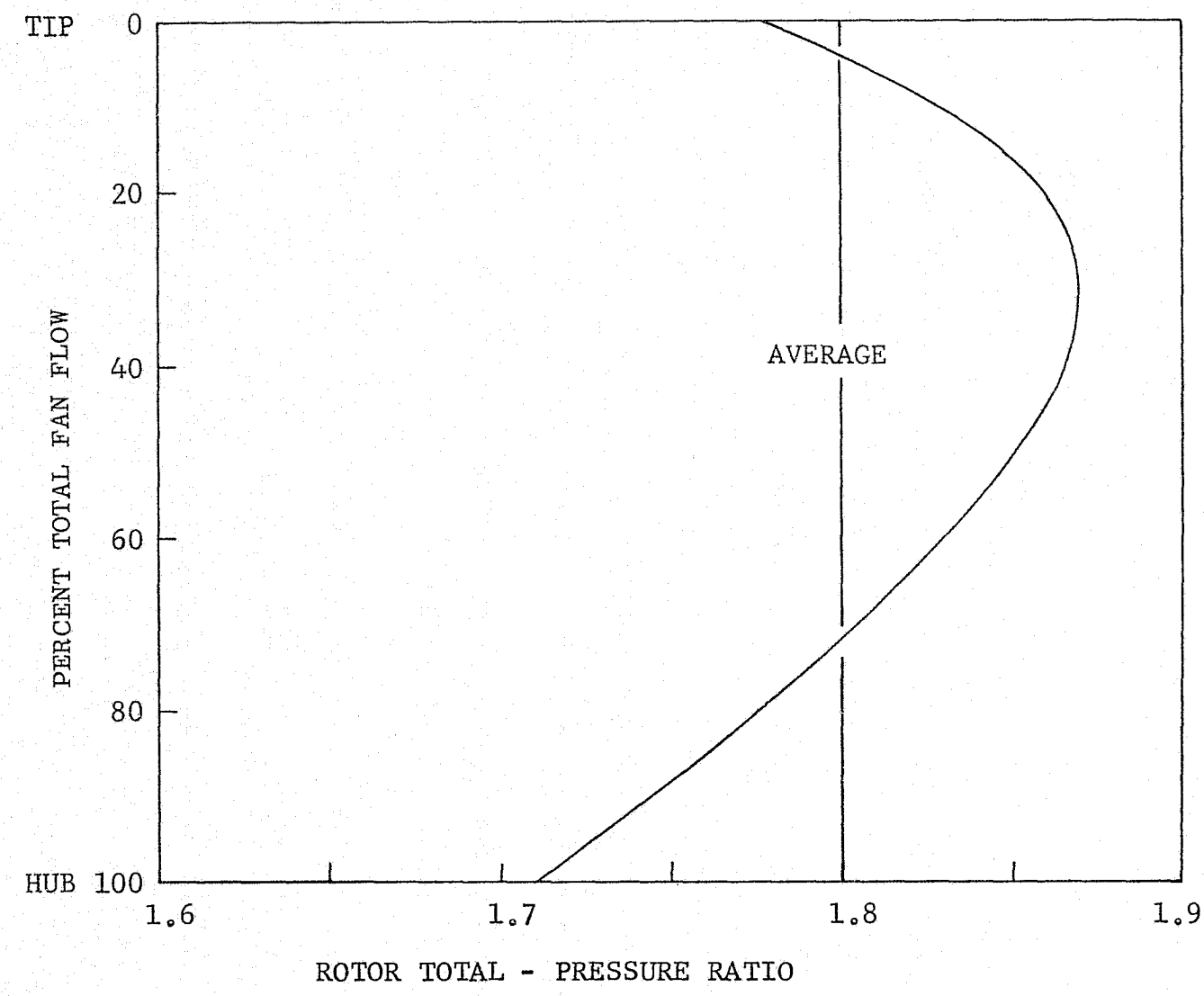

Figure 1. Advanced Technology Fan Design Pressure Ratio Distribution.

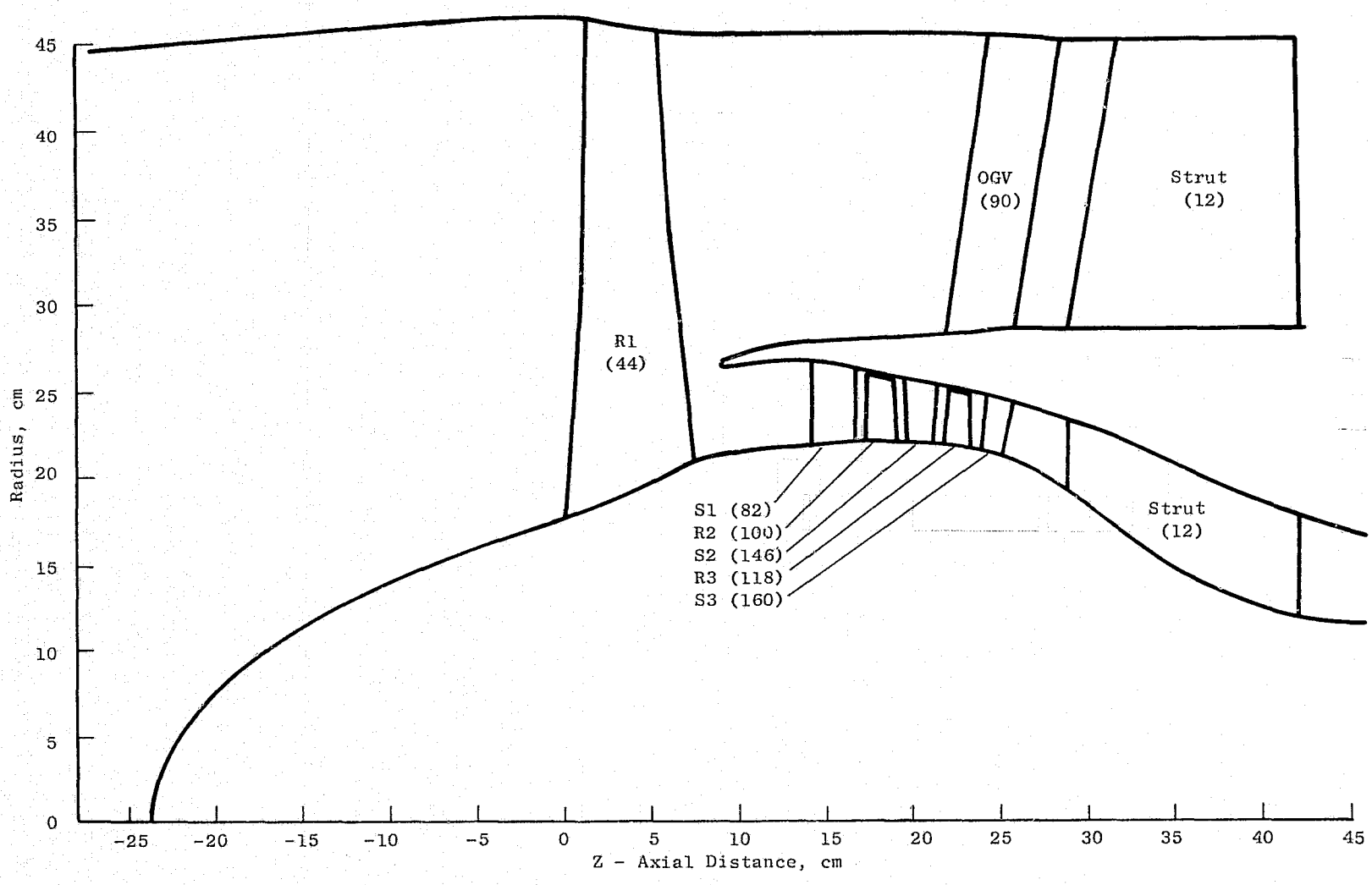

Figure 2. Advanced Technology Fan and Booster Flowpath.

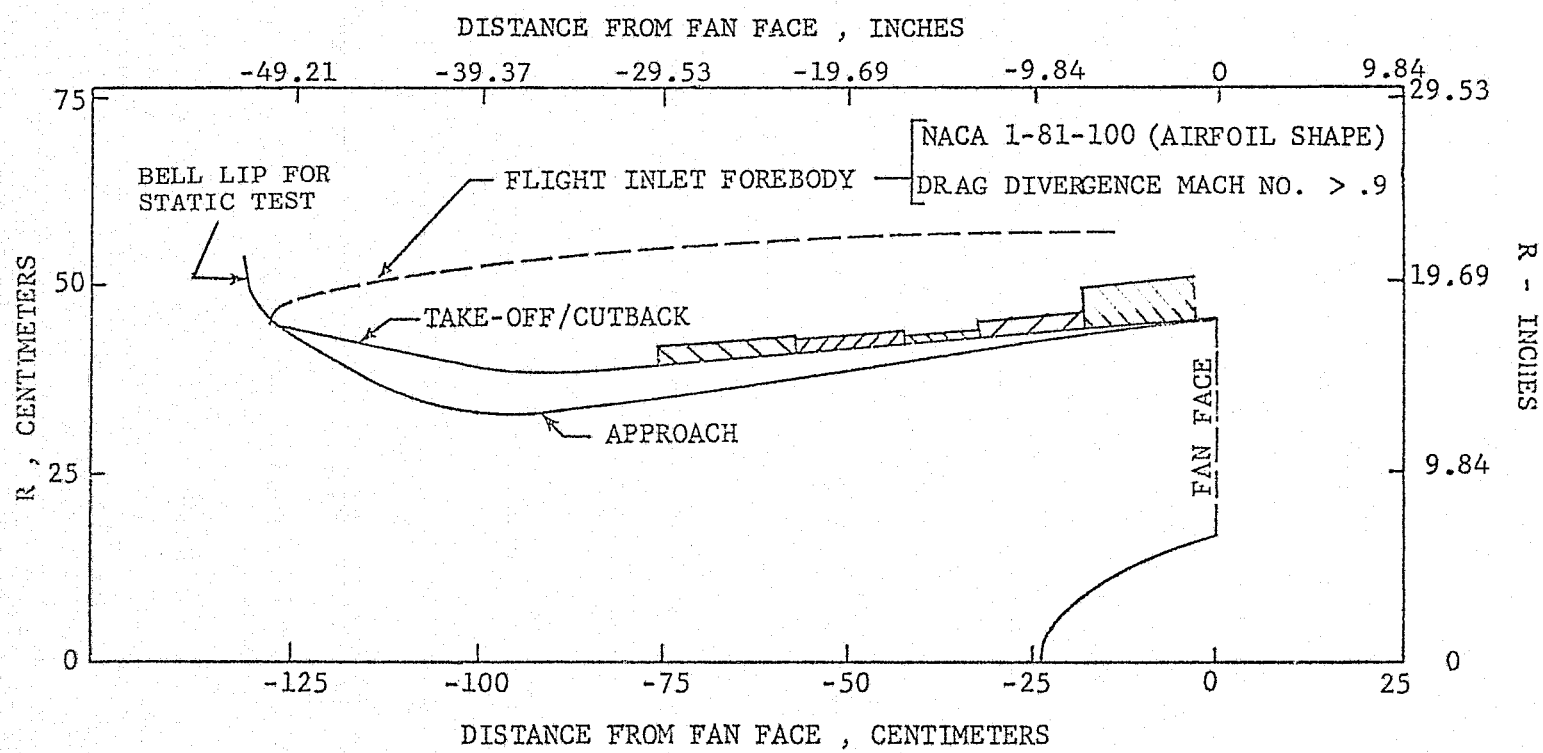

- TRANSLATING PANELS AND VARIABLE NOZZLE TO PROVIDE M_{TH}=0.79 AT ALL 3 OPERATING POINTS
- 5 SECTIONS OF TREATMENT TUNED TO DOMINANT FREQUENCIES.
- L/D_{INLET} = 1.5 (WITH BELL LIP) , L/D_{TREAT} = 0.85
- TREATMENT LOCATED WHERE $M_{WALL} \leq 0.70$

Figure 3. Hybrid Inlet Design.

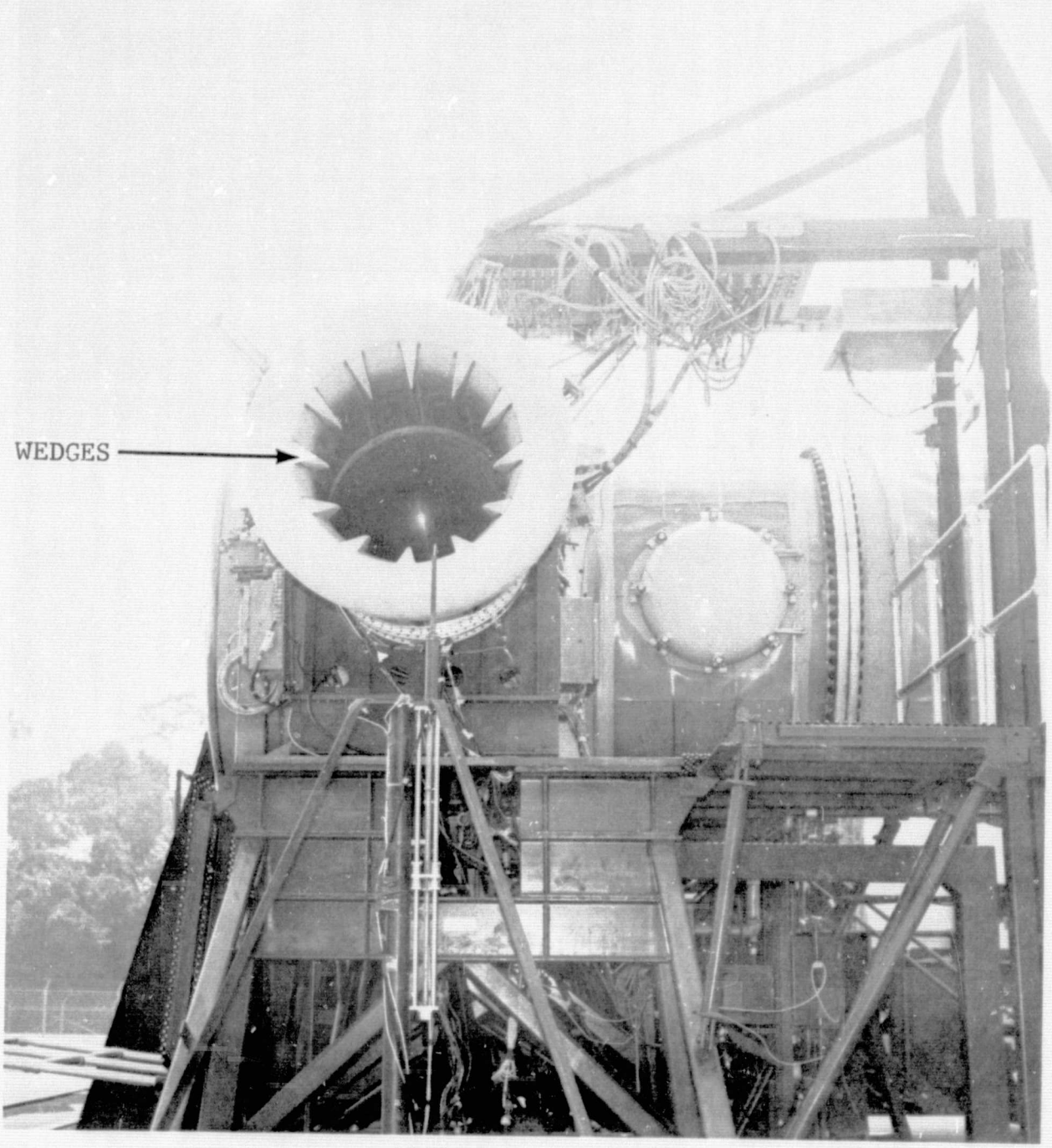

Figure 4. Hybrid Inlet on Test Stand.

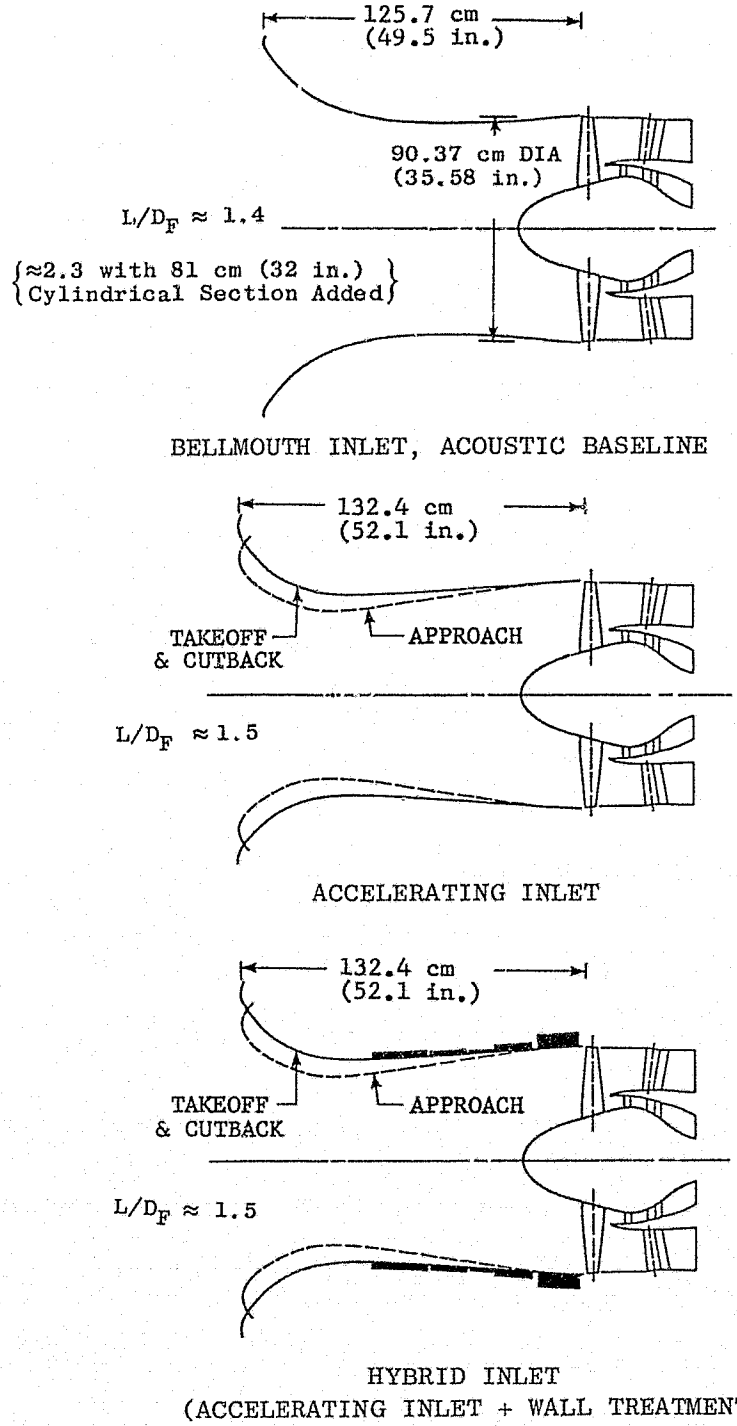

Figure 5. Fan Inlet Configurations for Rear-Drive Tests.

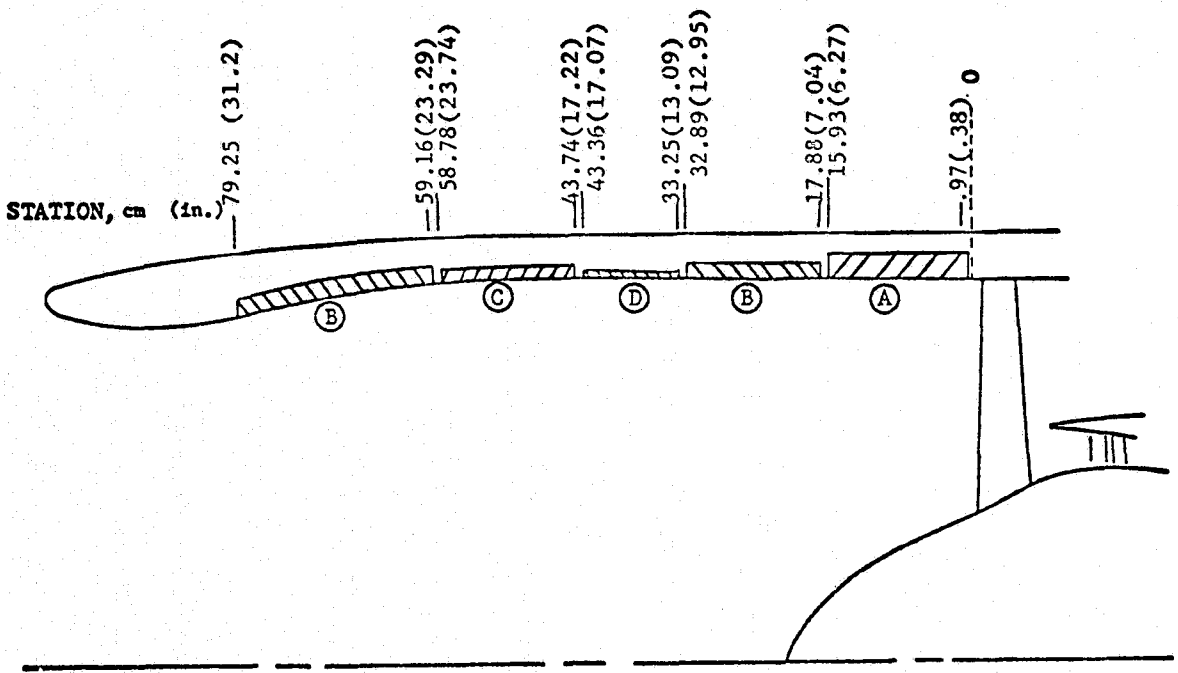

ACOUSTIC TREATMENT	t , cm (in)[a]	d, cm (in)[a]	OPEN AREA BEFORE BOND.	OPEN AREA AFTER BOND.	S , cm (in)[a]
A	0.036(.014)	0.058(.023)	6.7±0.2%	6.0±0.2%	2.29 (.90)
B	0.036(.014)	0.058(.023)	6.7±0.2%	6.0±0.2%	0.94 (.37)
C	0.036(.014)	0.058(.023)	6.7±0.2%	6.0±0.2%	0.71 (.28)
D	0.036(.014)	0.058(.023)	6.7±0.2%	6.0±0.2%	0.36 (.14)

a) t = face plate thickness, cm (in.)
d = hole diameter, cm (in.)
S = cavity depth, cm (in.)

Figure 6. Fan Inlet Treatment Design.

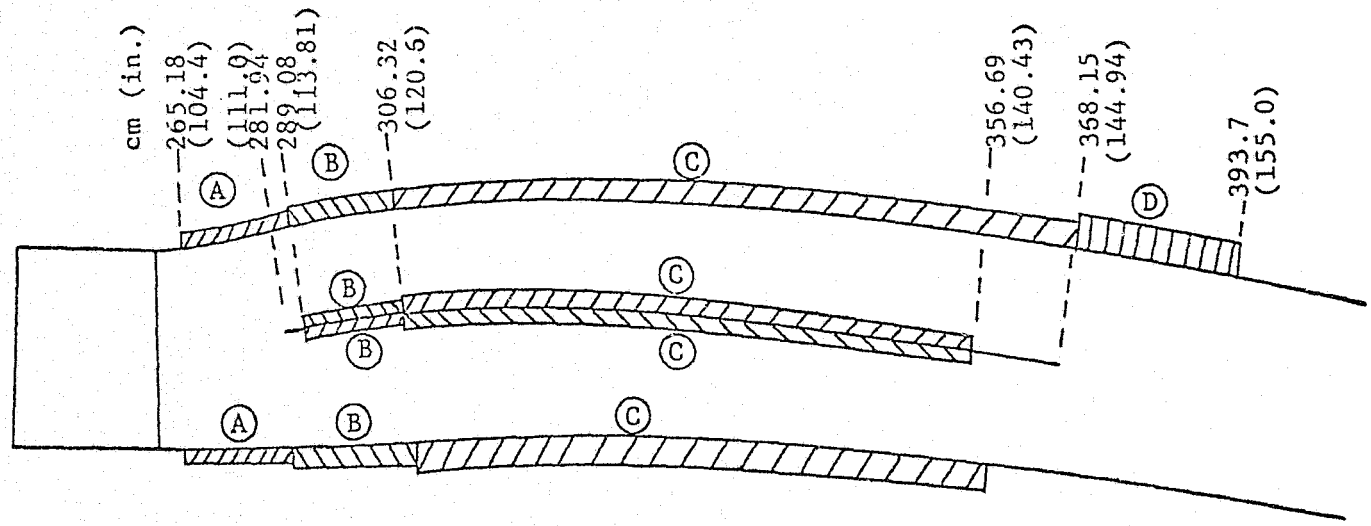

NOTE : Dimensions are Relative to Fan Blade Leading Edge at the Hub.

ACOUSTIC TREATMENT	t [a], cm (in.)	d [a], cm (in.)	OPEN AREA BEFORE BOND.	OPEN AREA AFTER BOND.	S [a], cm (in.)
A	0.046 (.018)	0.069 (.027)	17.0±2.0%	≥ 15.0%	0.24 (.09)
B	0.046 (.018)	0.069 (.027)	17.0±2.0%	≥ 15.0%	0.36 (.14)
C	0.046 (.018)	0.069 (.027)	17.0±2.0%	≥ 15.0%	0.97 (.38)
D	0.046 (.018)	0.152 (.060)	11.0±1.0%	≥ 10.0%	2.54 (1.0)

a) t = face plate thickness
d = hole diameter
S = cavity depth

Figure 7. Fan Scale-Model Exhaust Duct, Acoustic Treatment Design.

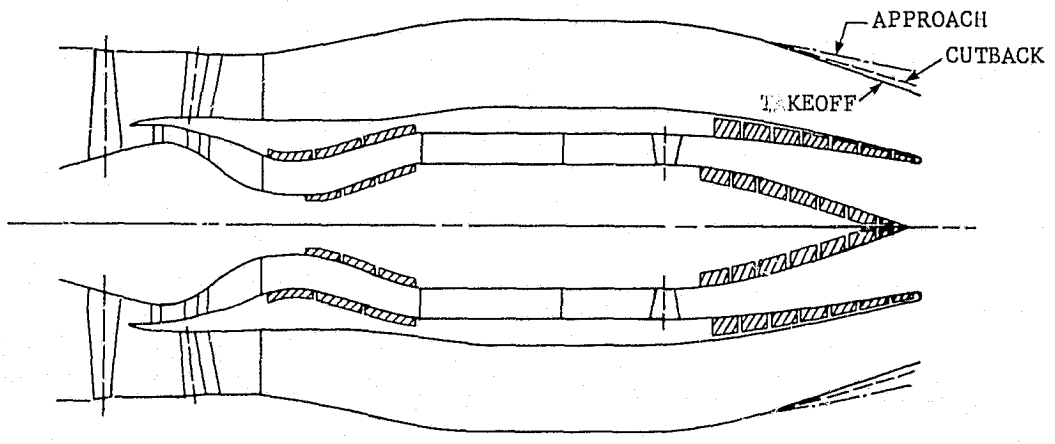

HARDWALL DUCT WITHOUT SPLITTER

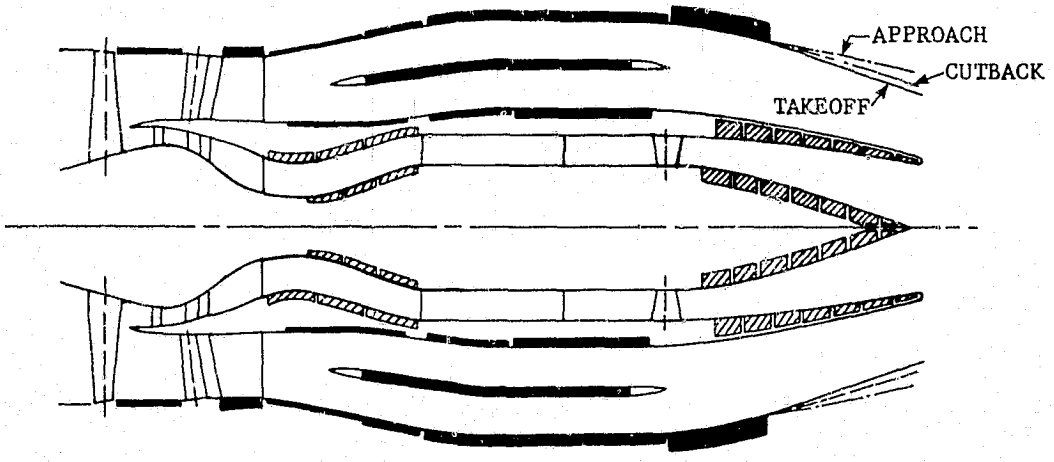

TREATED DUCT WITH SPLITTER

Figure 8. Fan Duct Configurations for Front-Drive Tests.

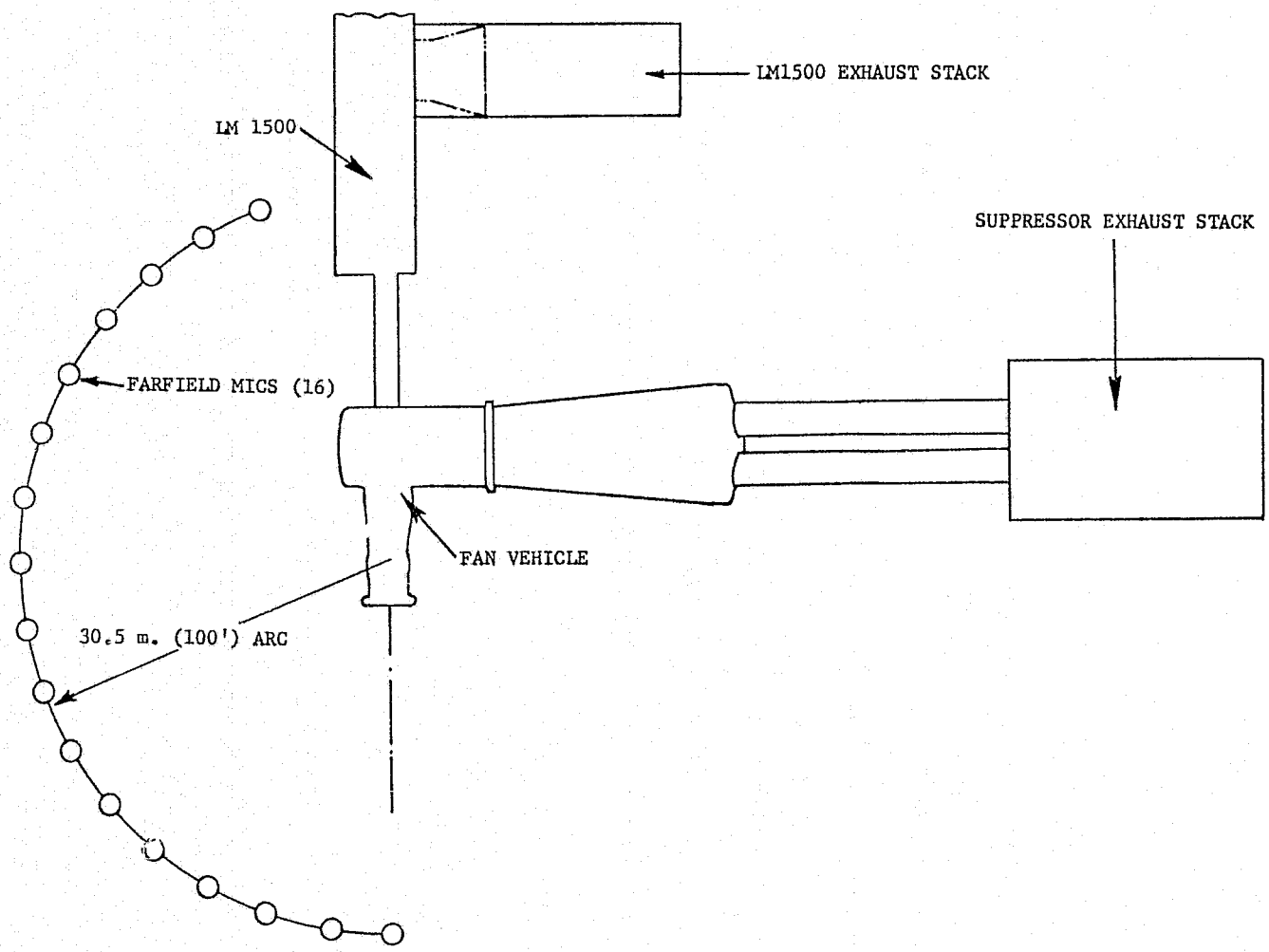

Figure 9. Rear-Drive Tests Sound Field, GE Peebles Site IV.

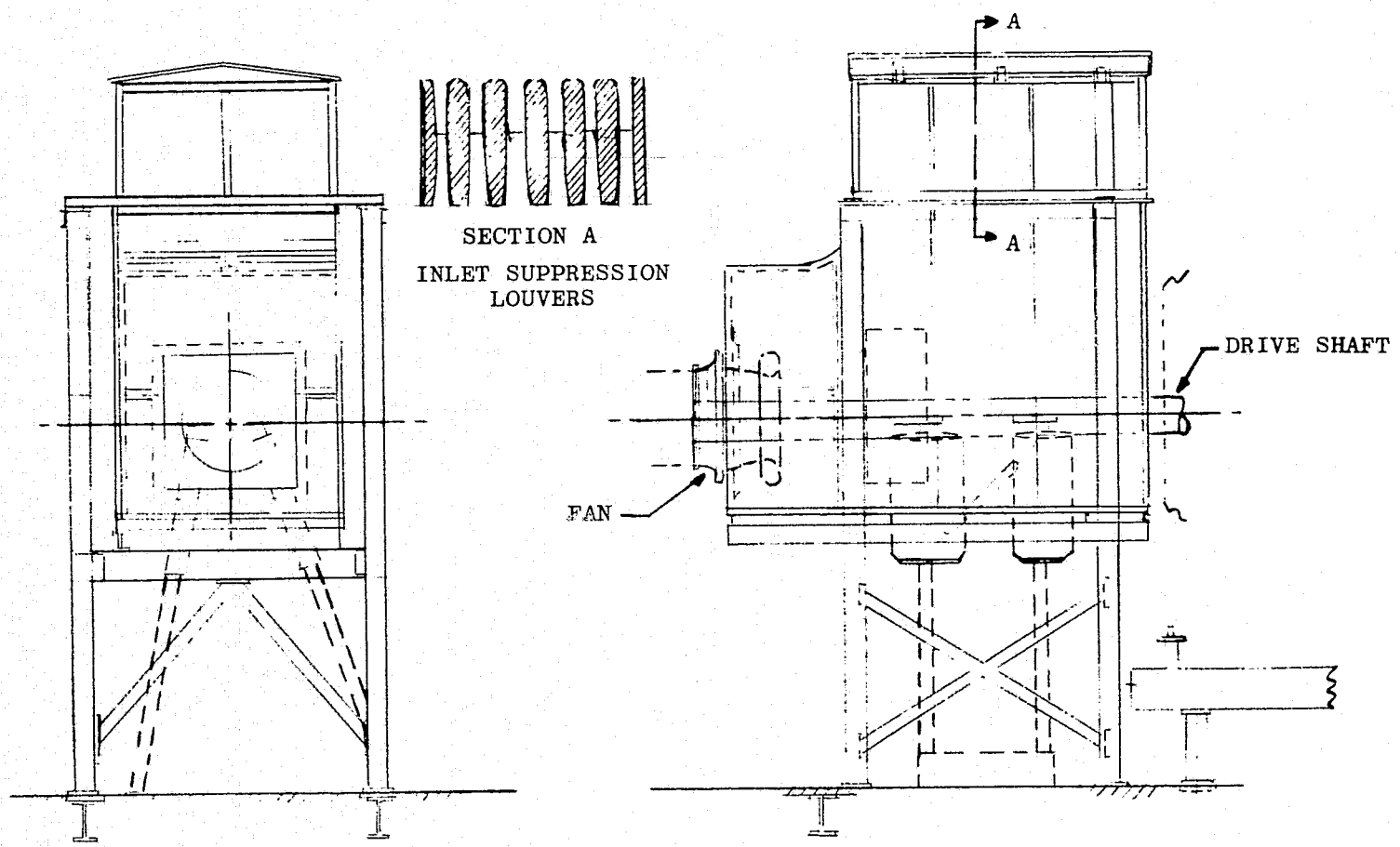

Figure 10. Inlet Suppressor, GE Peebles Site IV.

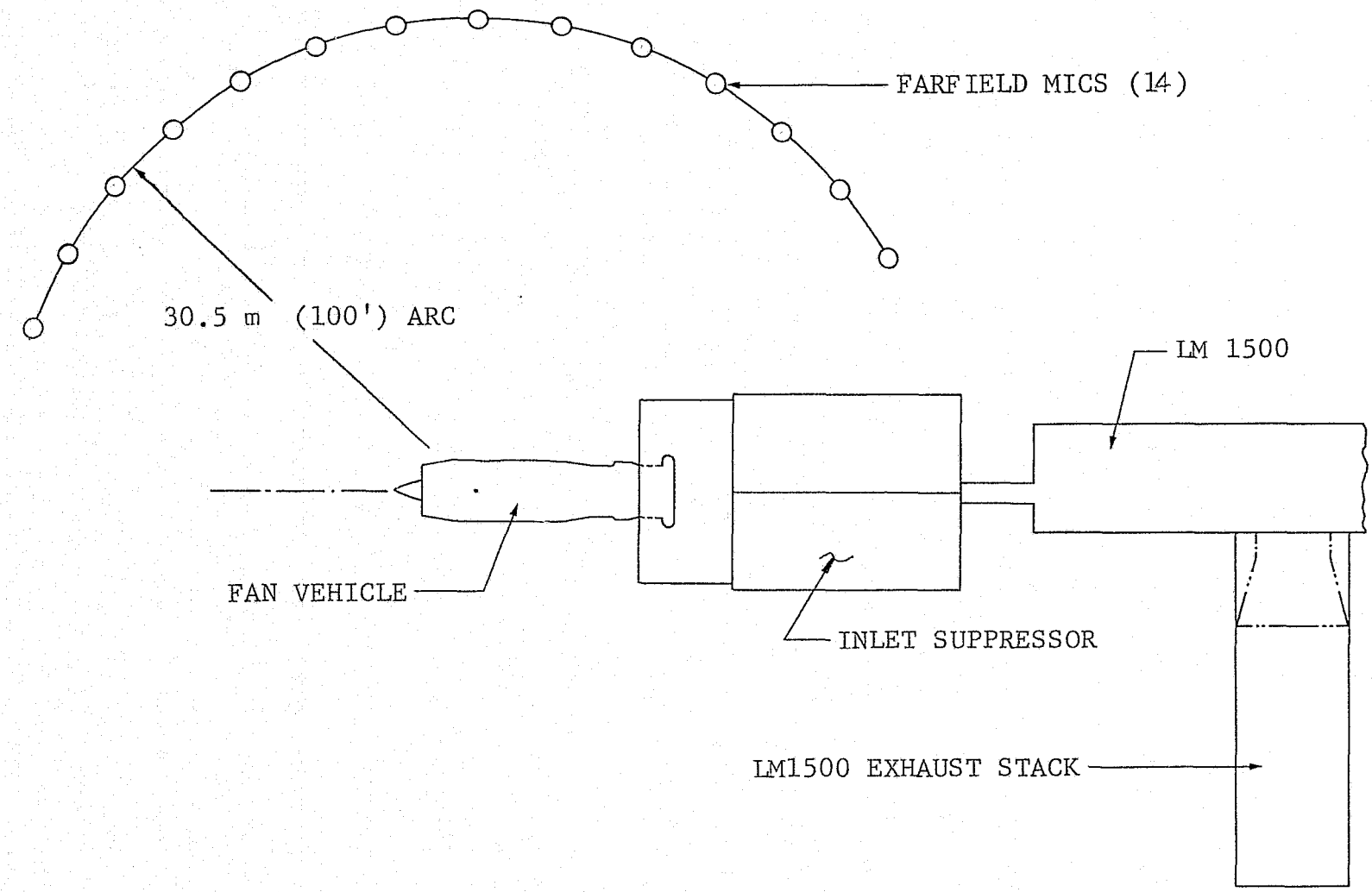

Figure 11. Front-Drive Tests Sound Field, GE Peebles Site IV.

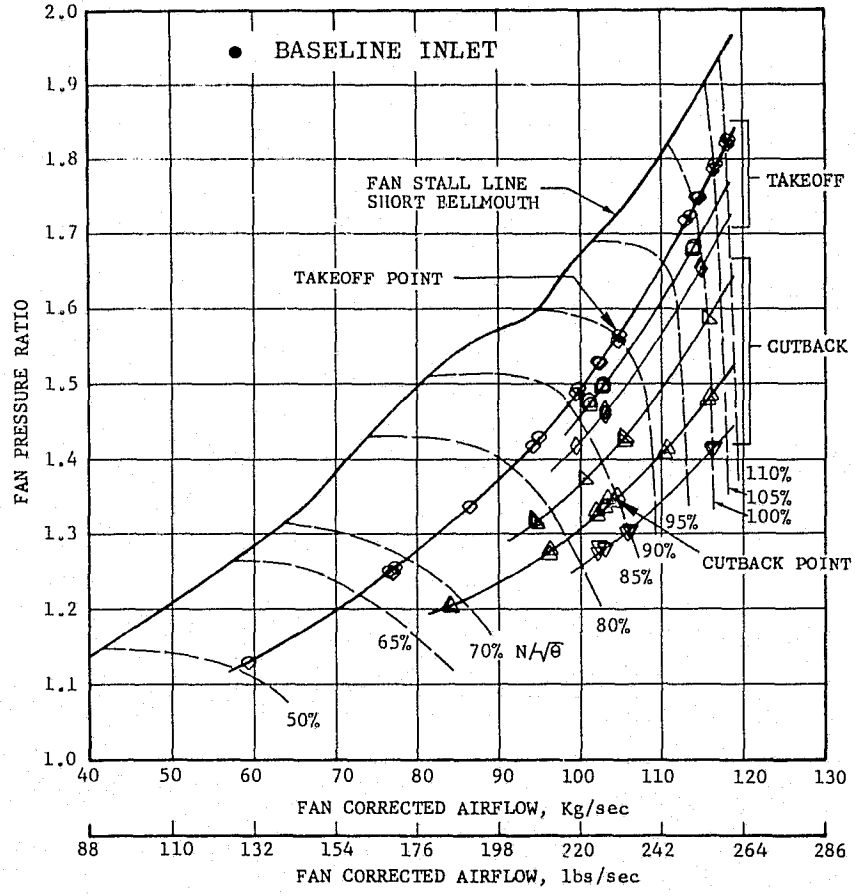

Figure 12. Acoustic Data Points for Takeoff and Cutback, Rear Drive.

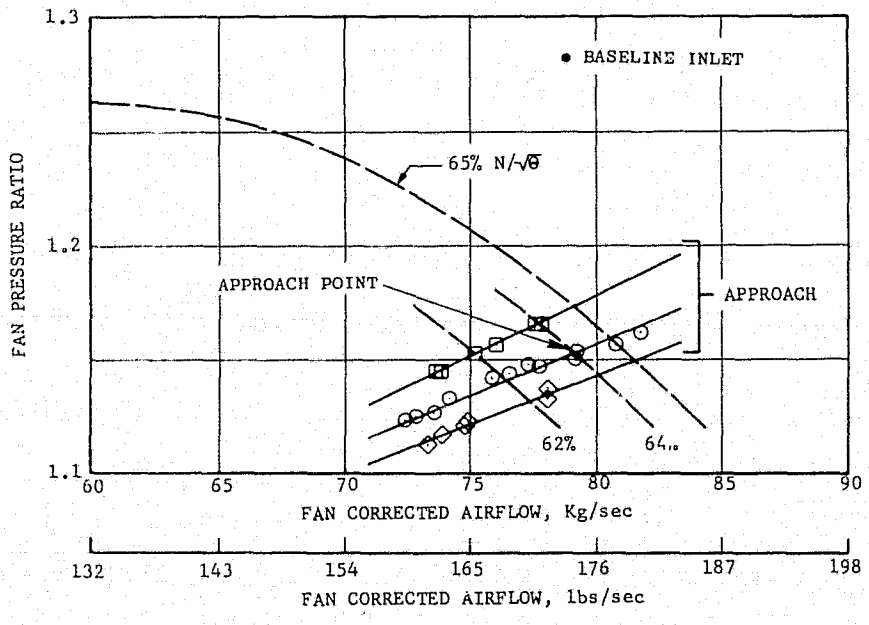

Figure 13. Acoustic Data Points for Approach, Rear Drive.

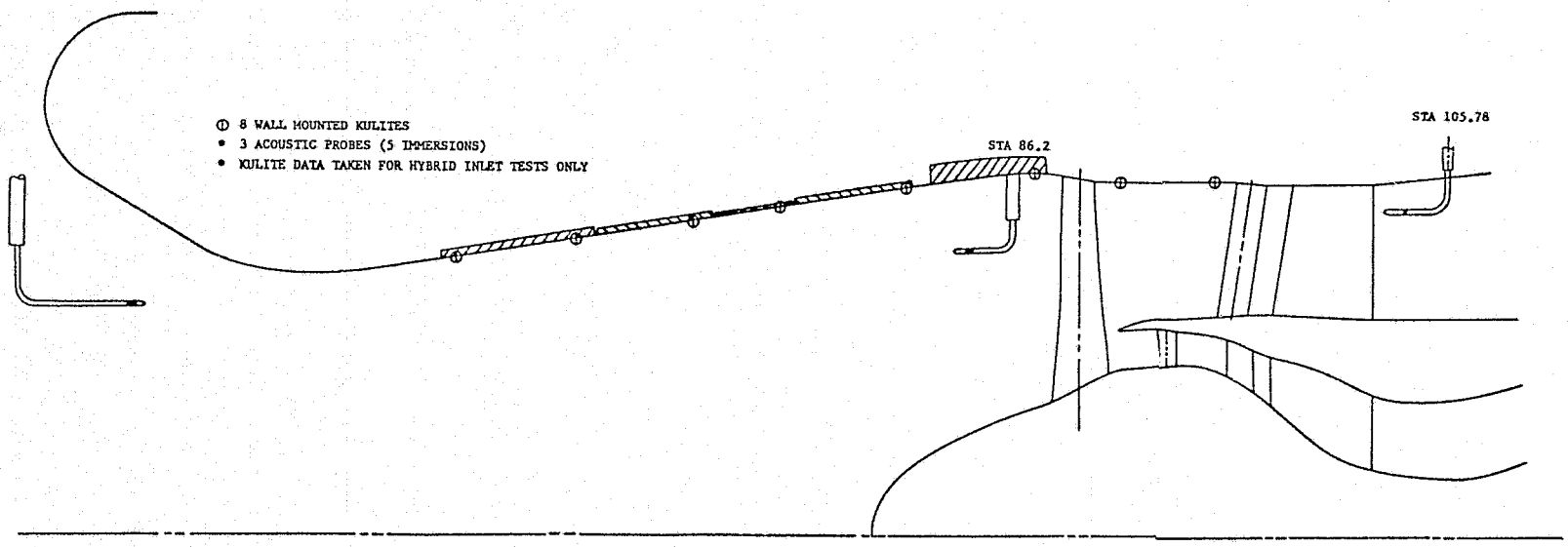

Figure 14. Internal Acoustic Instrumentation, Rear Drive.

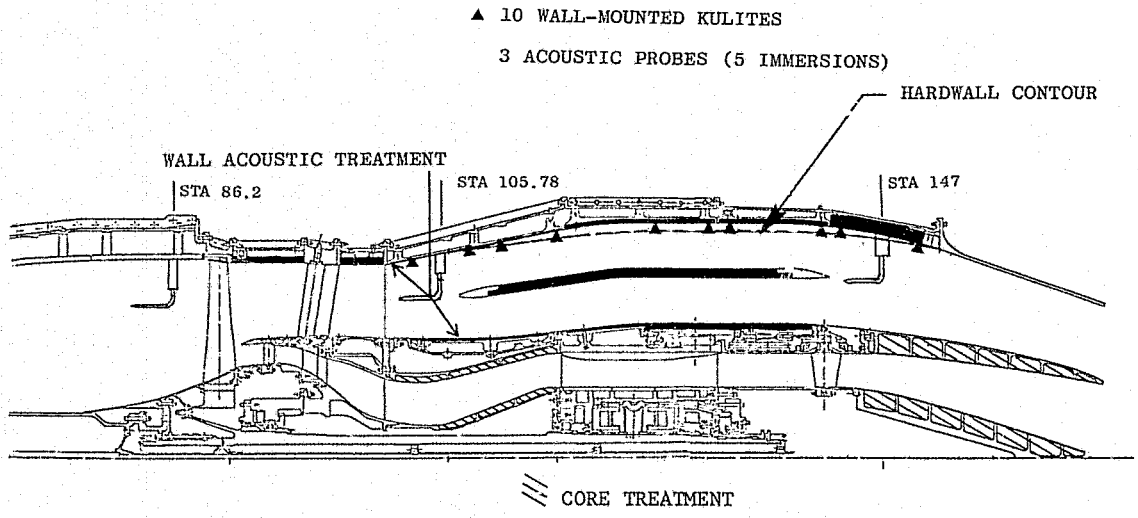

Figure 15. Exhaust Duct Instrumentation Locations, Front Drive.

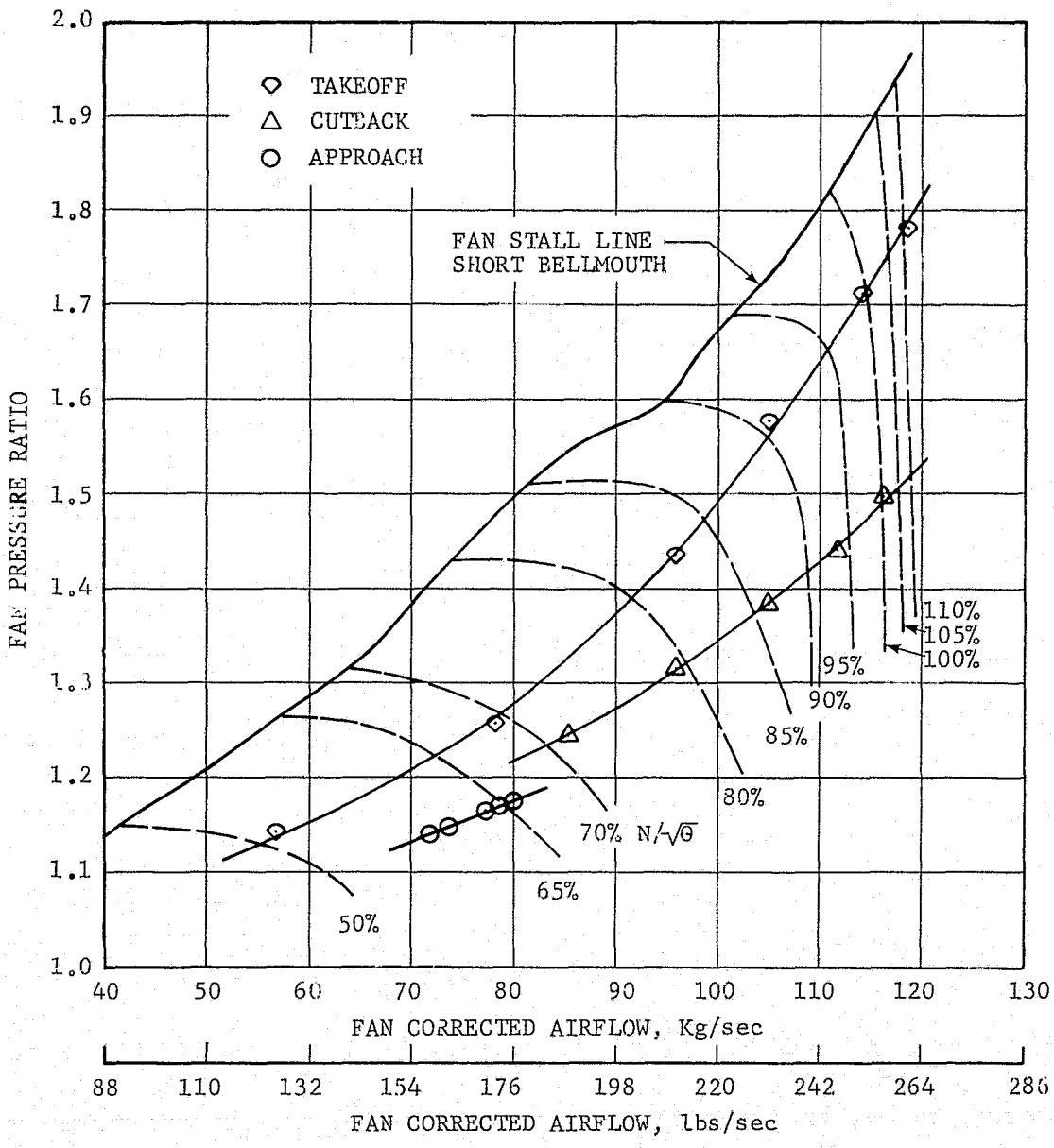

Figure 16. Acoustic Data Points for Takeoff, Cutback, and Approach, Front Drive.

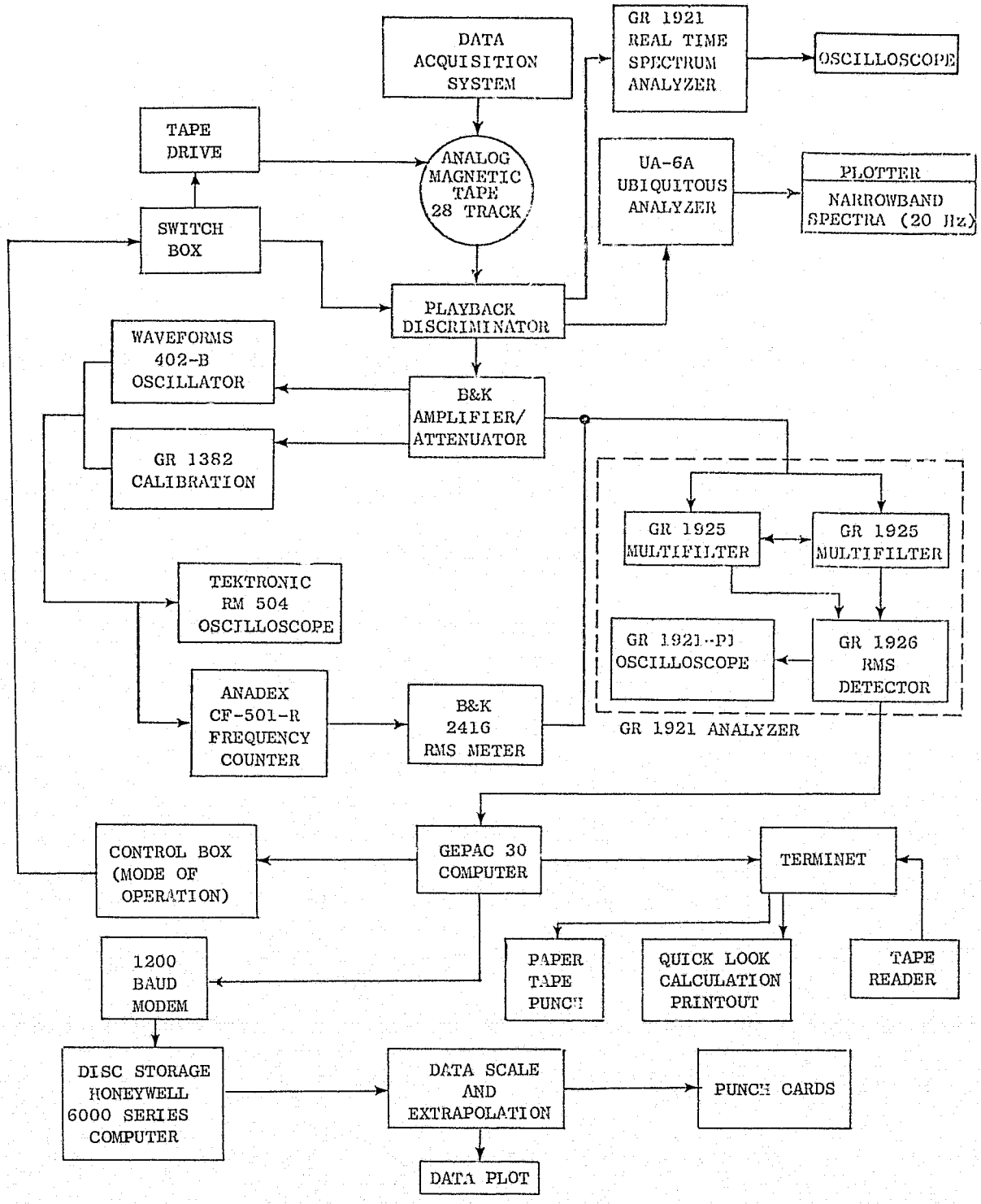

Figure 17. Acoustic Data Reduction System.

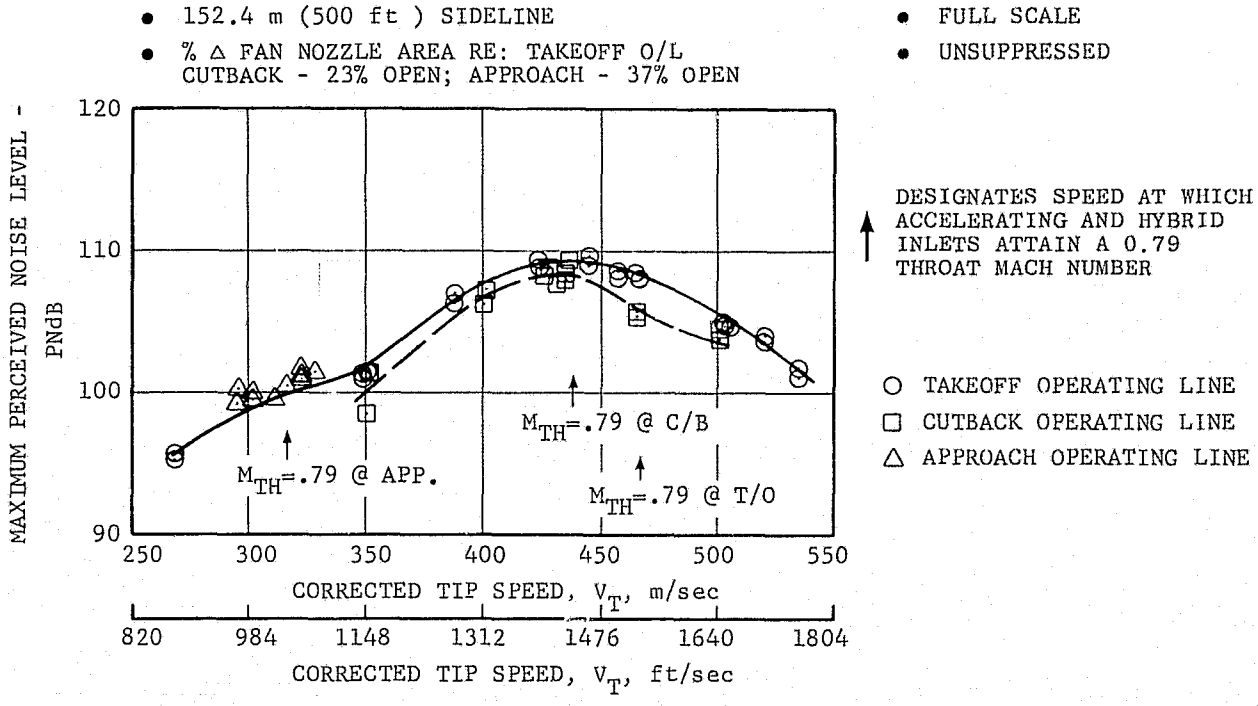

Figure 18. Effect of Speed on Maximum PNL, Baseline Bellmouth Inlet (Rear-Drive Test).

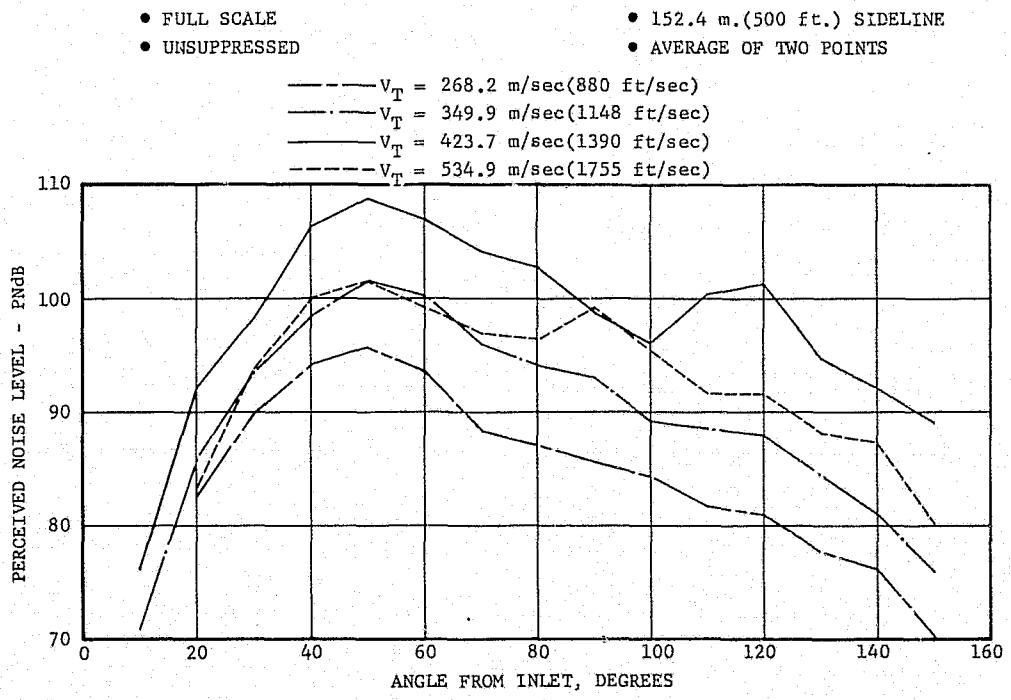

Figure 19. PNL Directivity, Baseline Bellmouth Inlet (Rear-Drive Test).

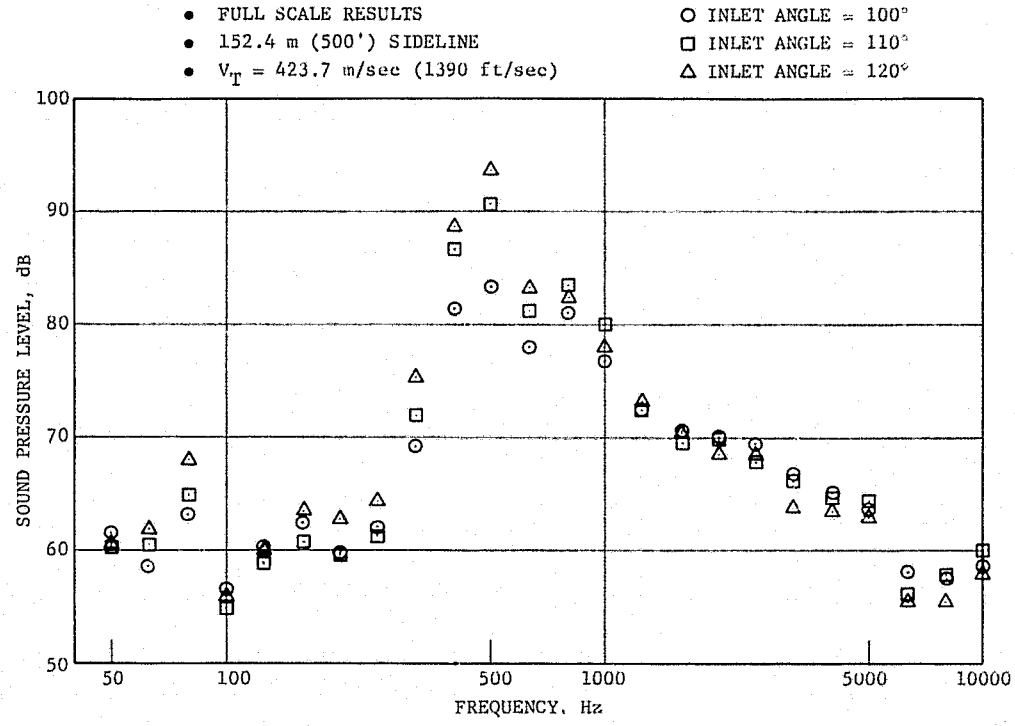

Figure 20. Comparison of SPL Spectra, Unsuppressed Baseline at Takeoff (Rear-Drive Test).

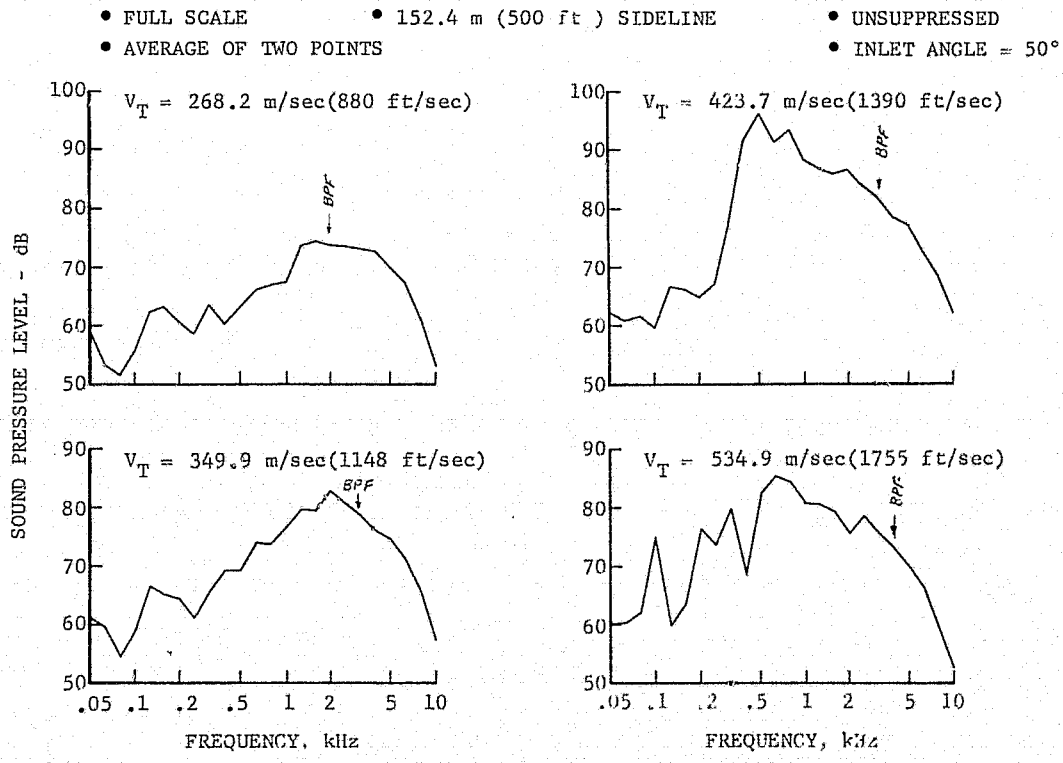

Figure 21. 1/3-Octave SPL Spectra at Various Tip Speeds, Baseline Bellmouth Inlet (Rear-Drive Test).

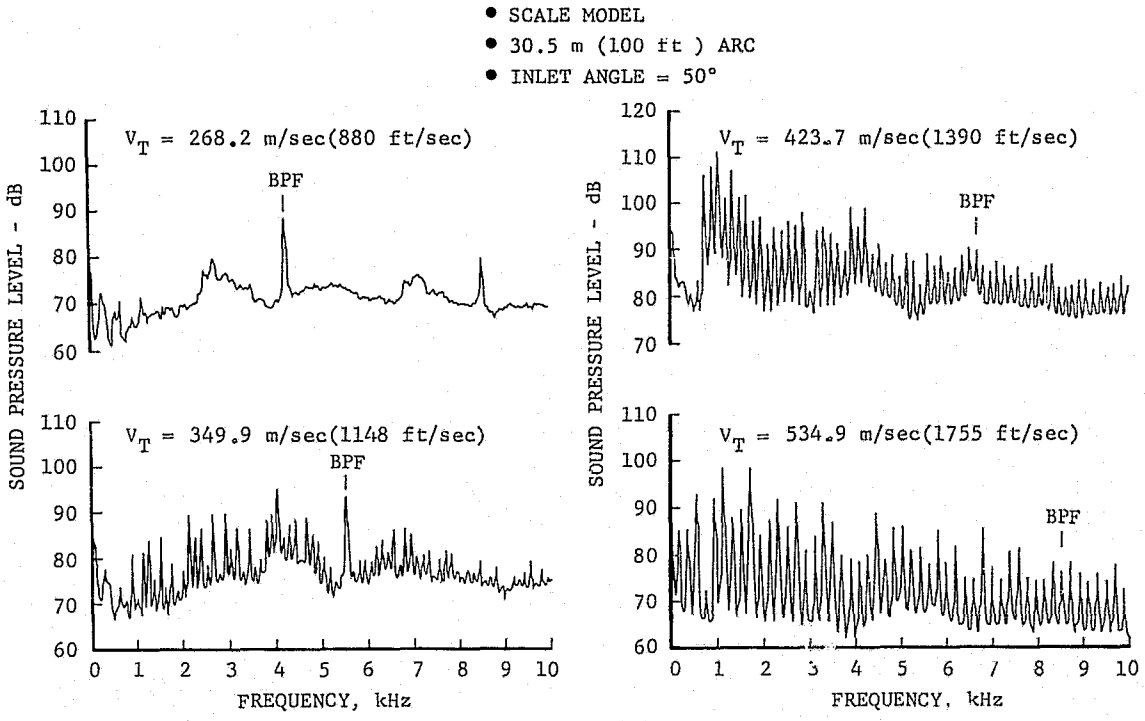

Figure 22. Farfield Narrowband Comparisons at Various Tip Speeds, Baseline Bellmouth Inlet (Rear-Drive Test).

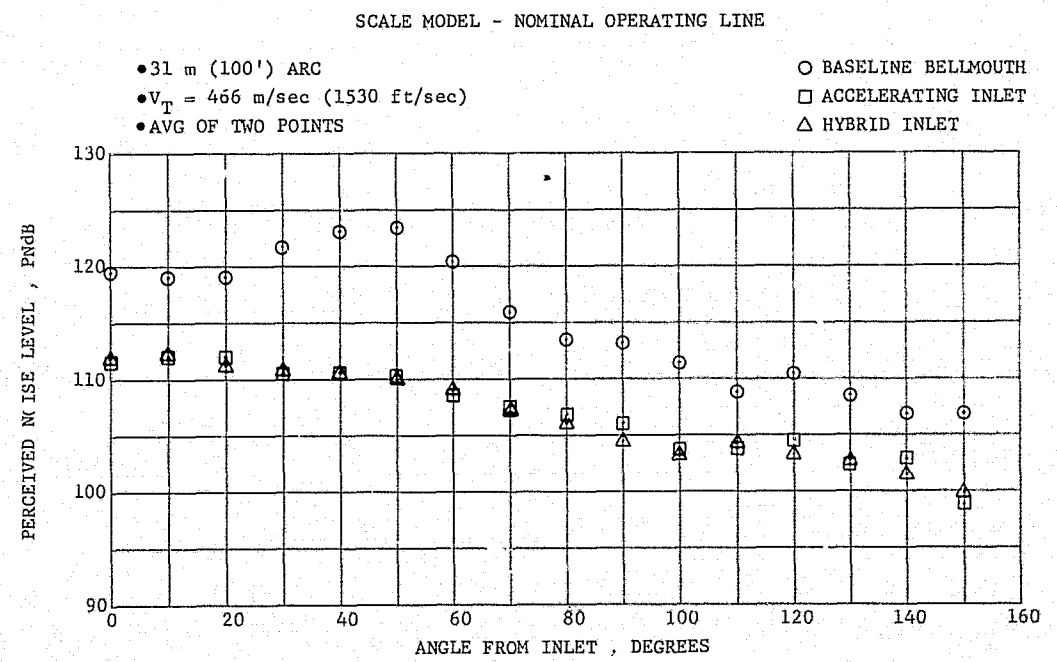

Figure 23. Scale-Model PNL Directivity at Takeoff, M_{TH} = 0.79 (Rear-Drive Test).

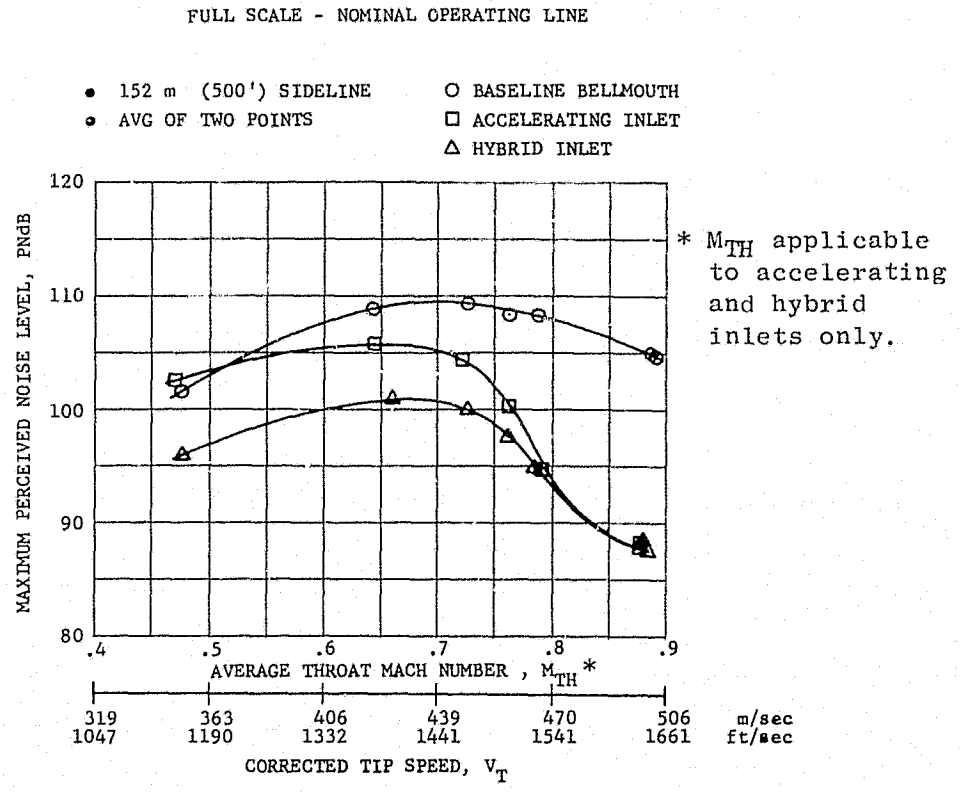

Figure 24. Maximum PNL Vs. Average Throat Mach Number, at Takeoff (Rear-Drive Test).

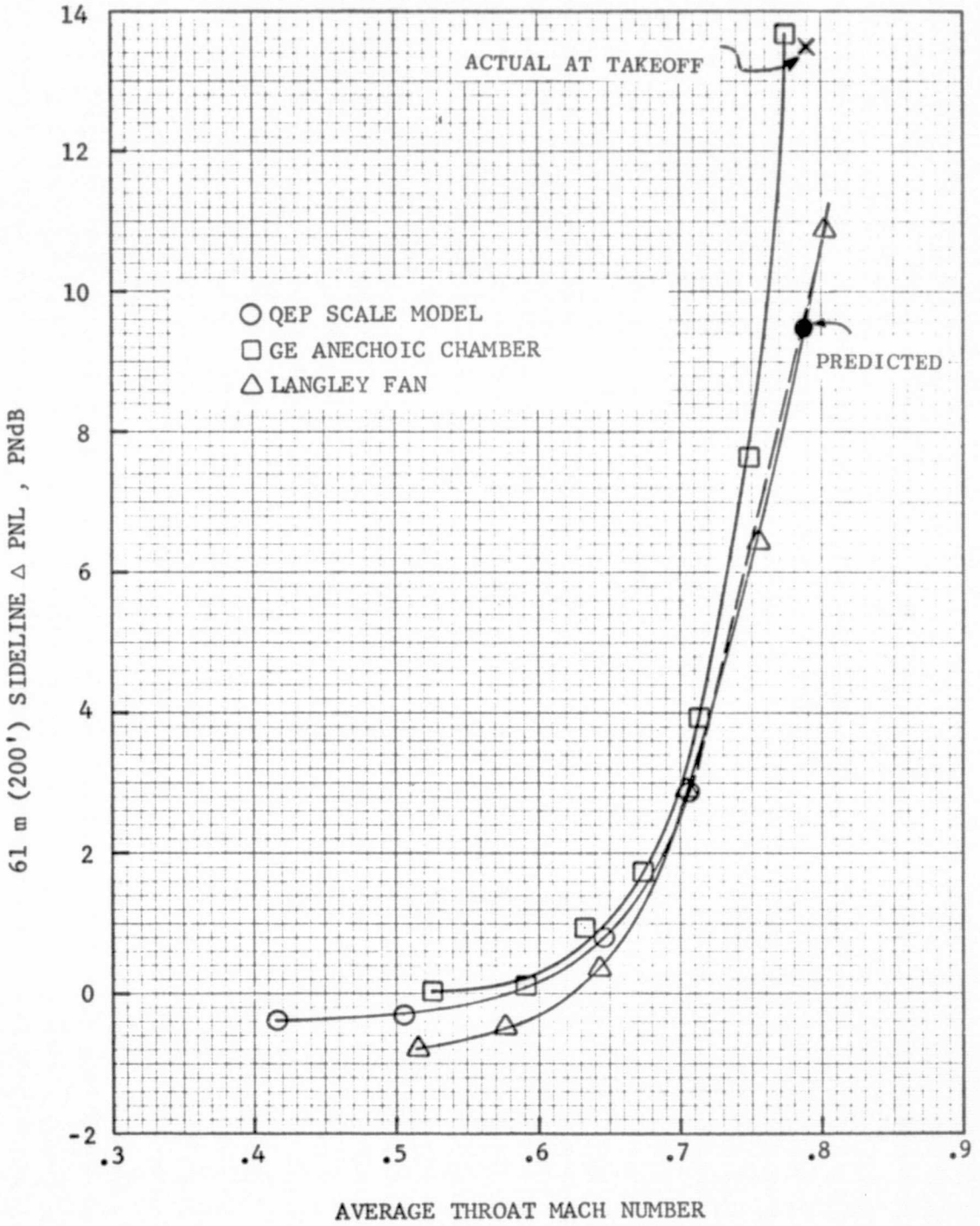

Figure 25. Inlet Acceleration Effects (Rear-Drive Test).

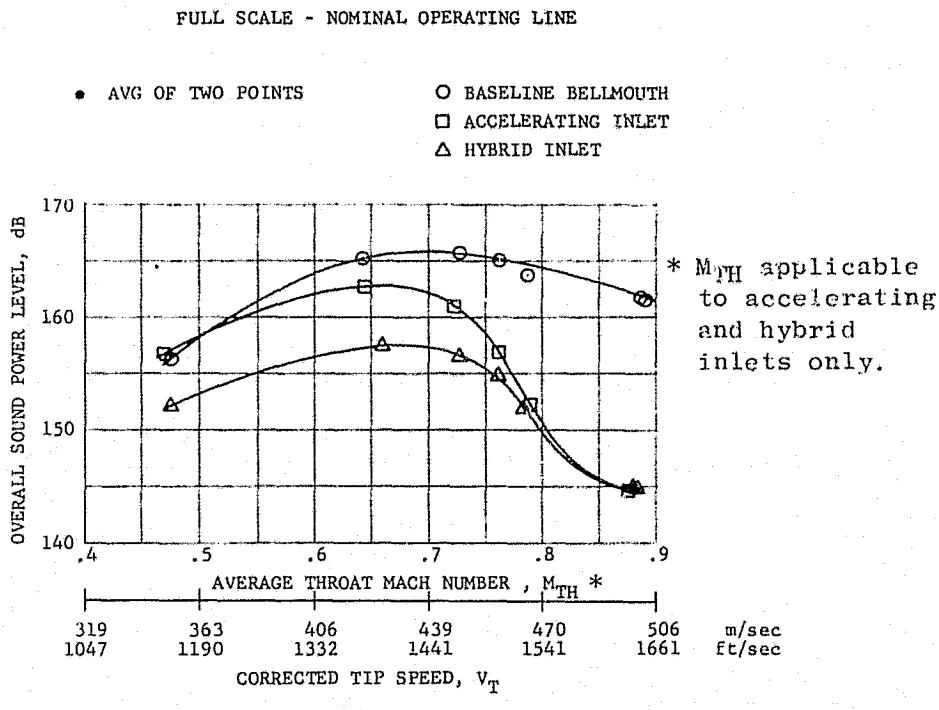

Figure 26. Overall Power Level Vs. Average Throat Mach Number, at Takeoff (Rear-Drive Test).

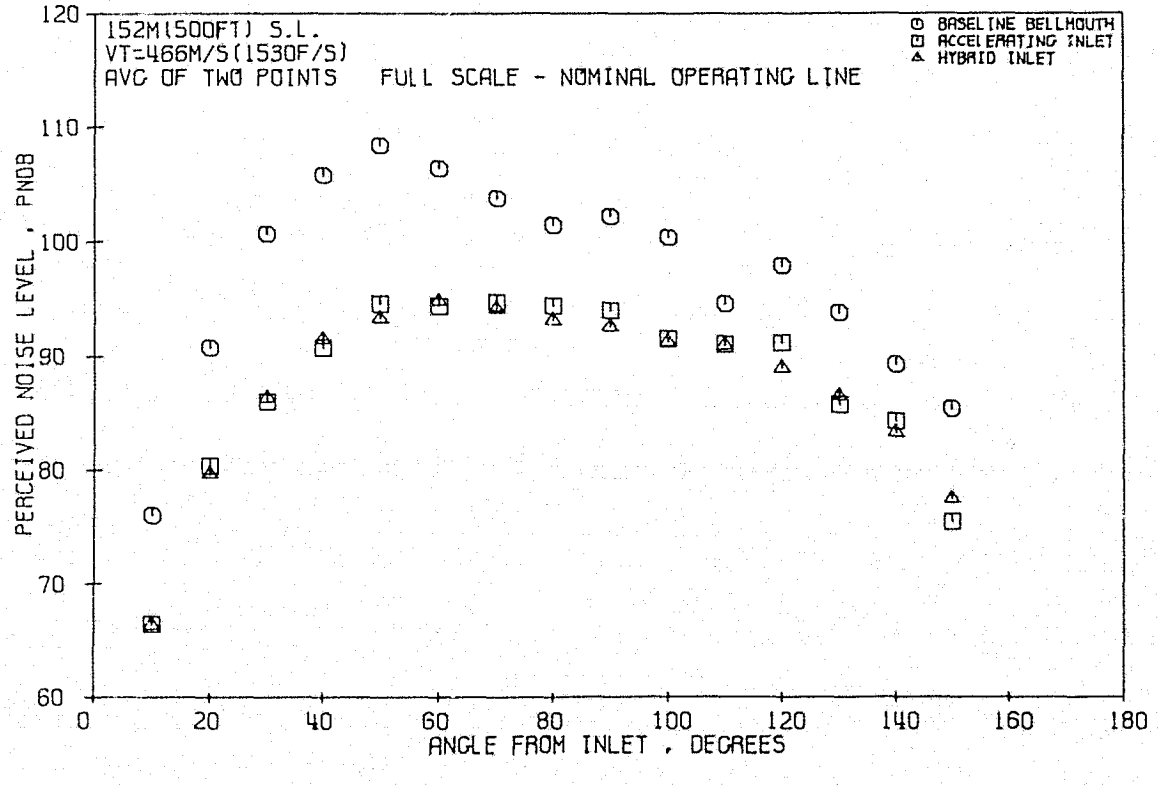

Figure 27. PNL Directivity of Takeoff, M_{TH} = 0.79 (Rear-Drive Test).

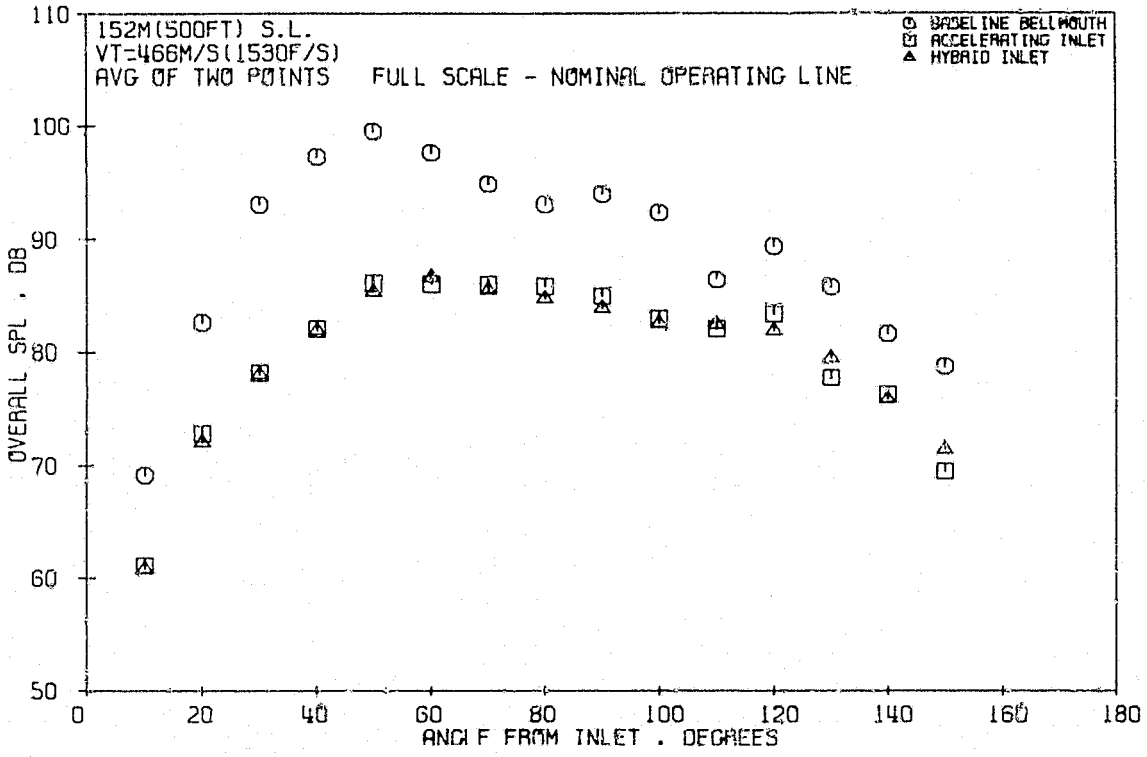

Figure 28. Variation of **OASPL with Inlet Angle at Takeoff, M_{TH} = 0.79 (Rear-Drive Test).**

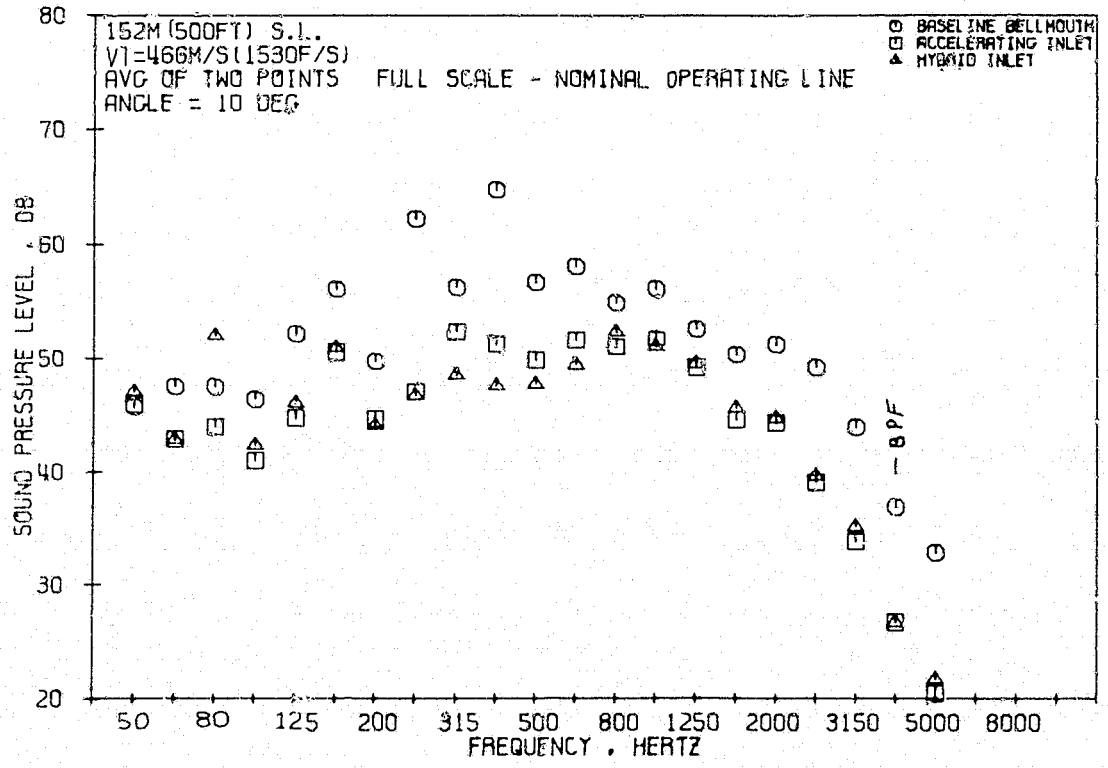

Figure 29. 1/3-Octave Spectral Comparisons at Takeoff, M_{TH} = 0.79, 10° Angle (Rear-Drive Test).

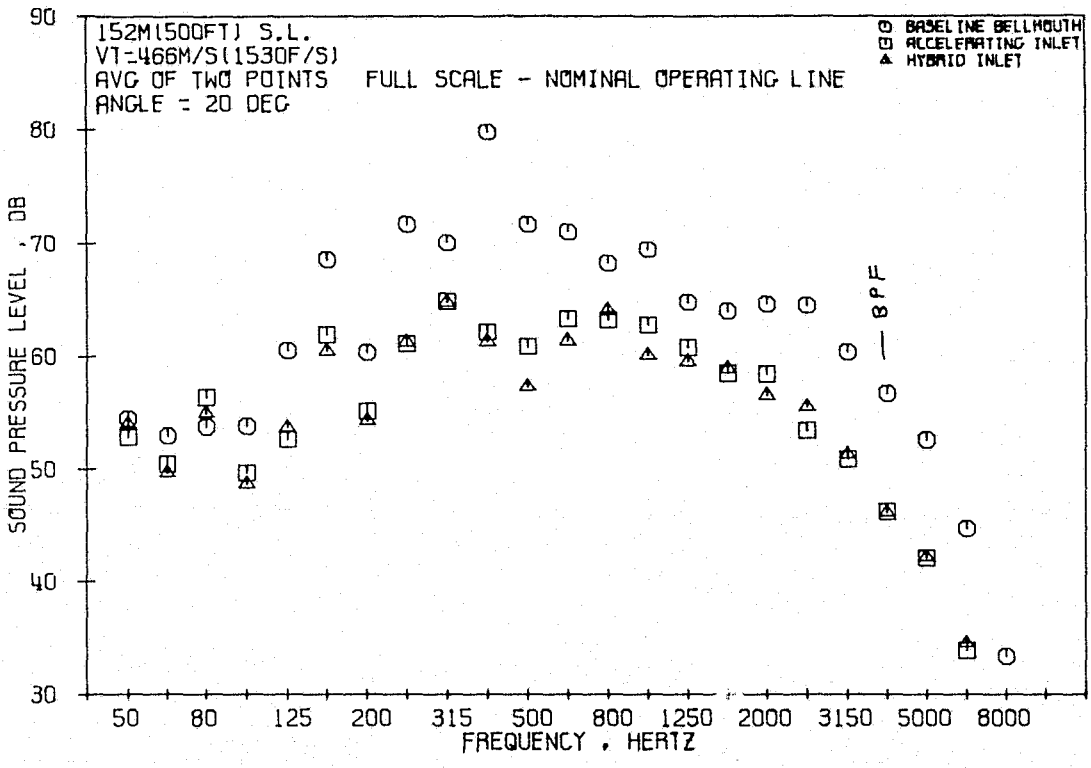

Figure 30. 1/3-Octave Spectral Comparisons at Takeoff, M_{TH} = 0.79, 20° Angle (Rear-Drive Test).

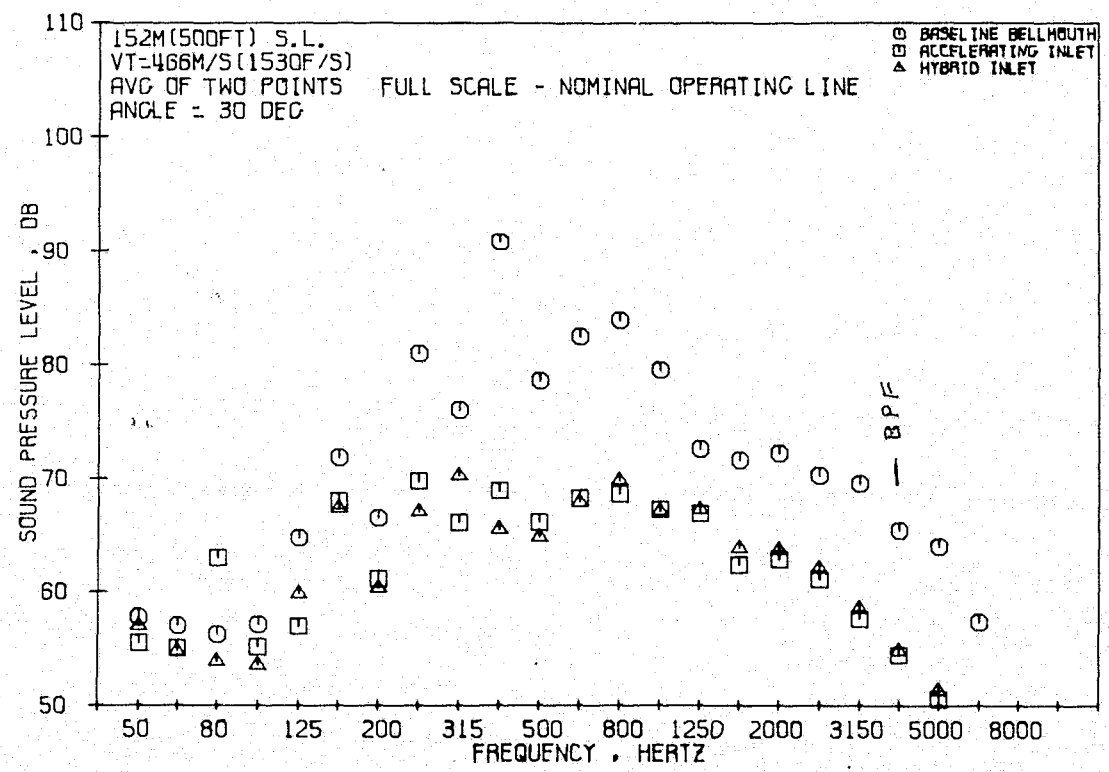

Figure 31. 1/3-Octave Spectral Comparisons at Takeoff, M_{TH} = 0.79, 30° Angle (Rear-Drive Test).

C. 2

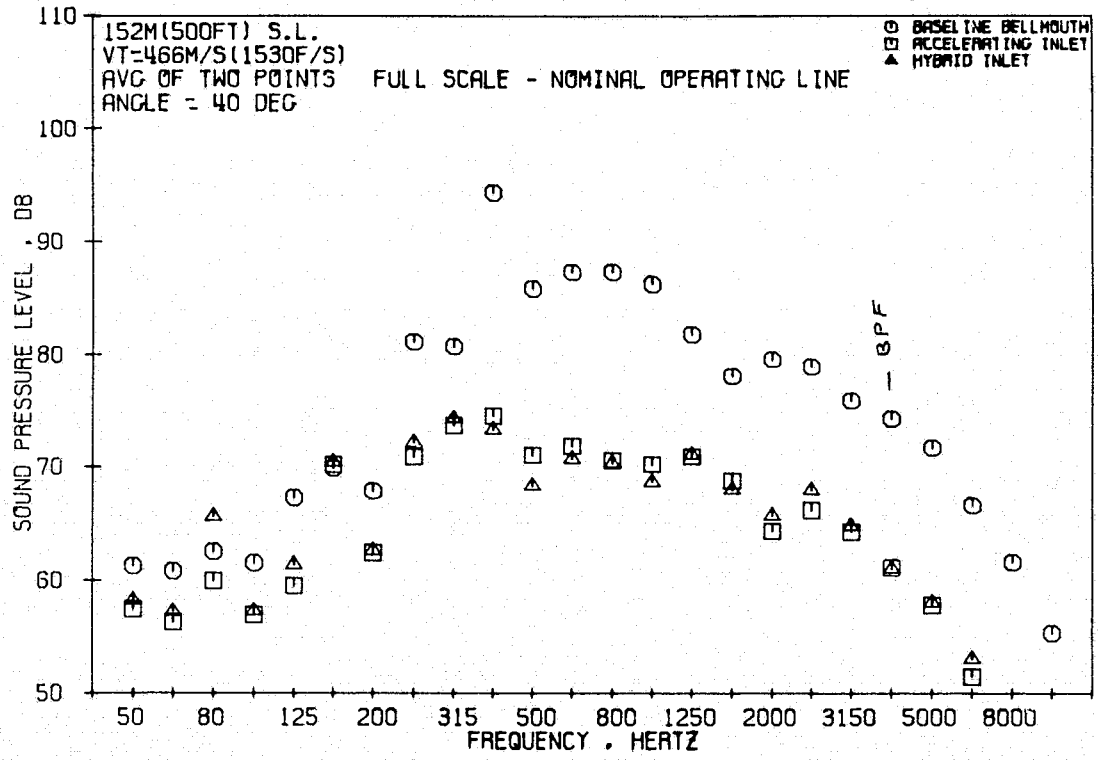

Figure 32. 1/3-Octave Spectral Comparisons at Takeoff, M_{TH} = 0.79, 40° Angle (Rear-Drive Test).

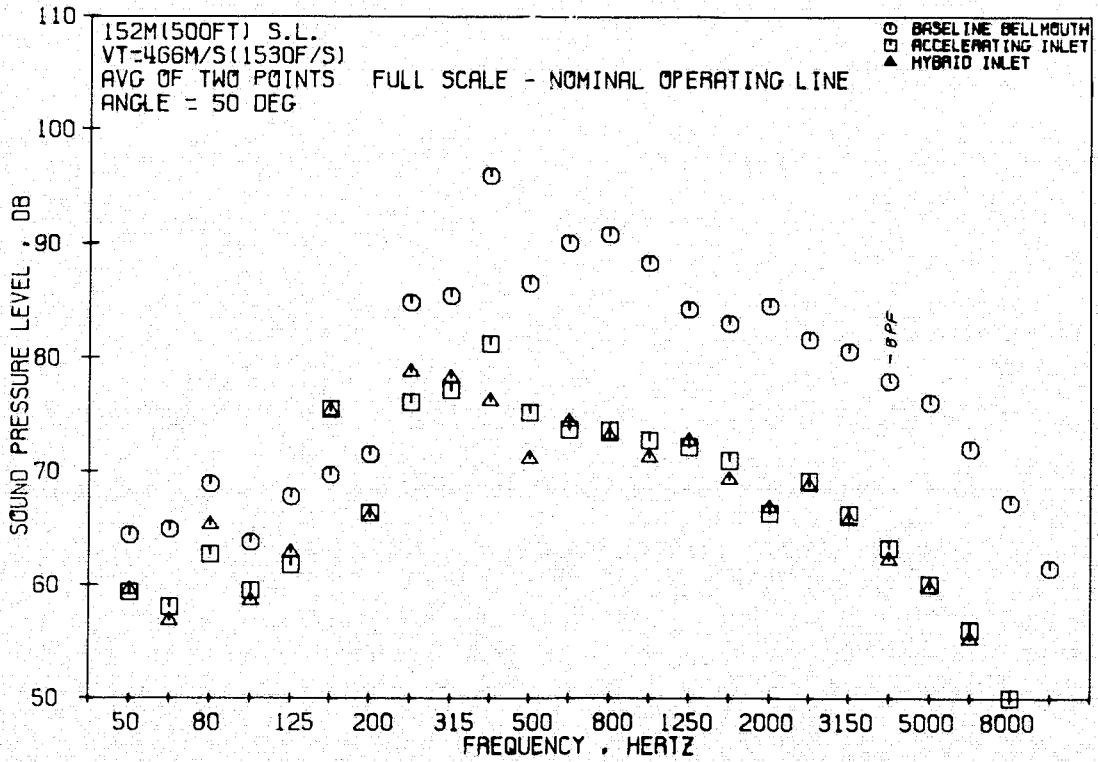

Figure 33. 1/3-Octave Spectral Comparisons at Takeoff, M_{TH} = 0.79, 50° Angle (Rear-Drive Test).

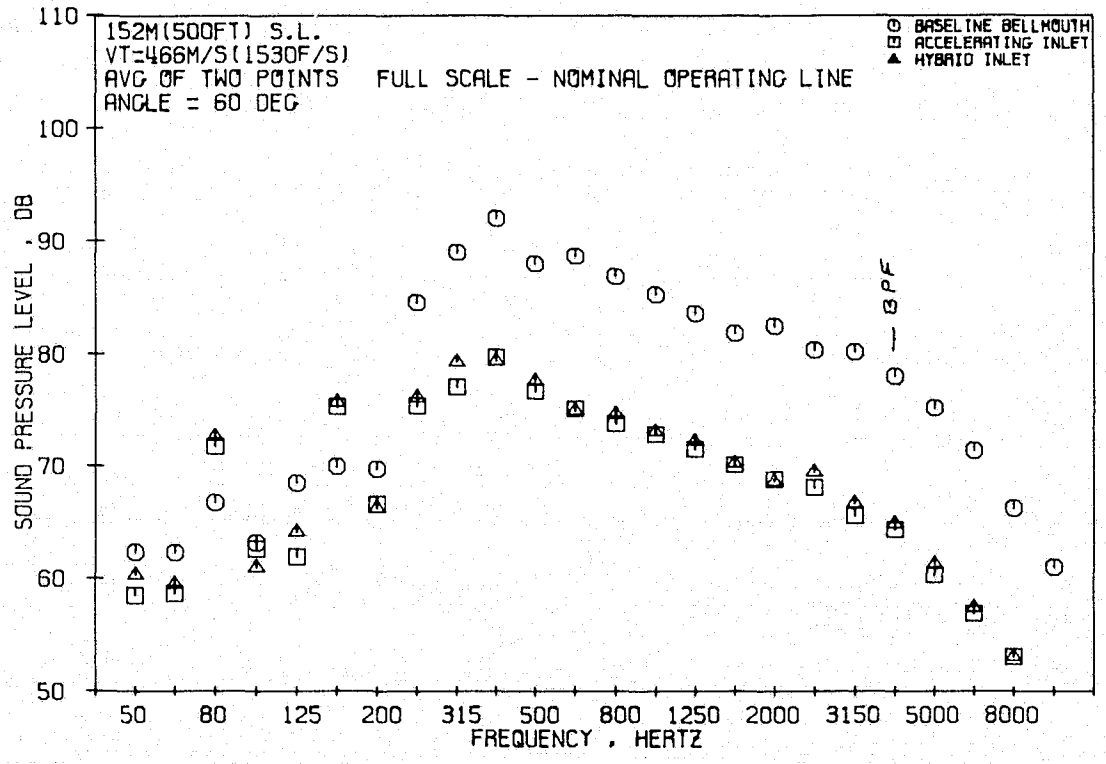

Figure 34. 1/3-Octave Spectral Comparisons at Takeoff, M_{TH} = 0.79, 60° Angle (Rear-Drive Test).

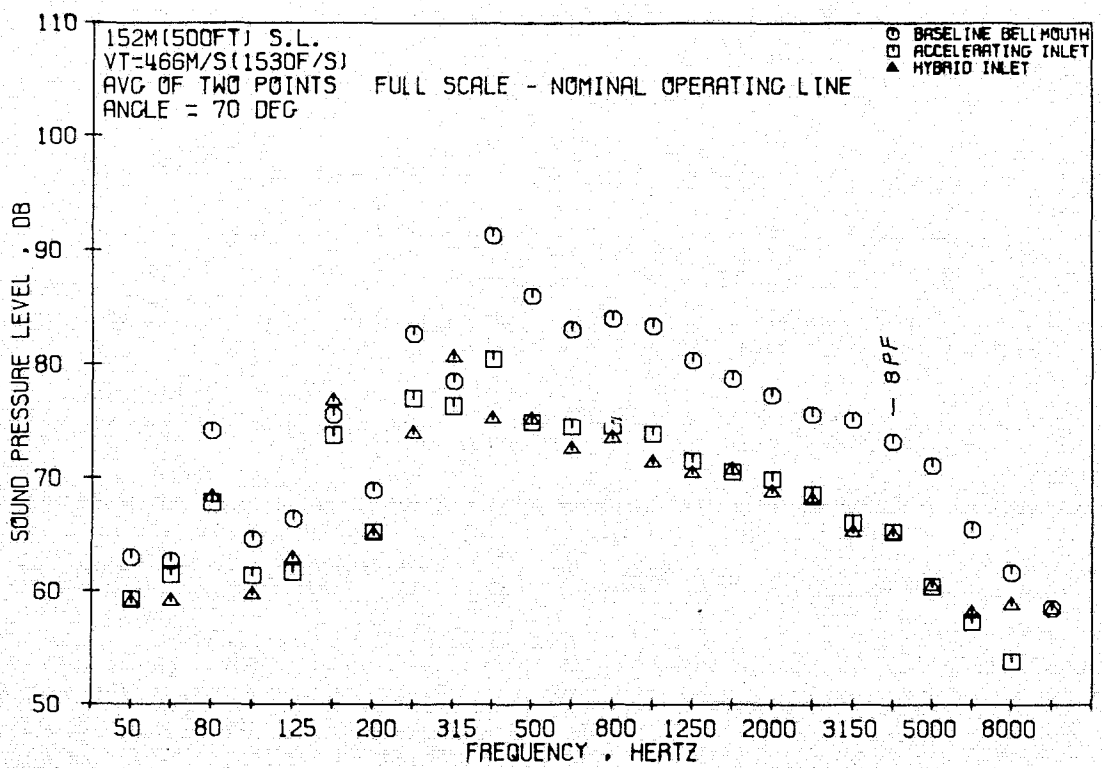

Figure 35. 1/3-Octave Spectral Comparisons at Takeoff, M_{TH} = 0.79, 70° Angle (Rear-Drive Test).

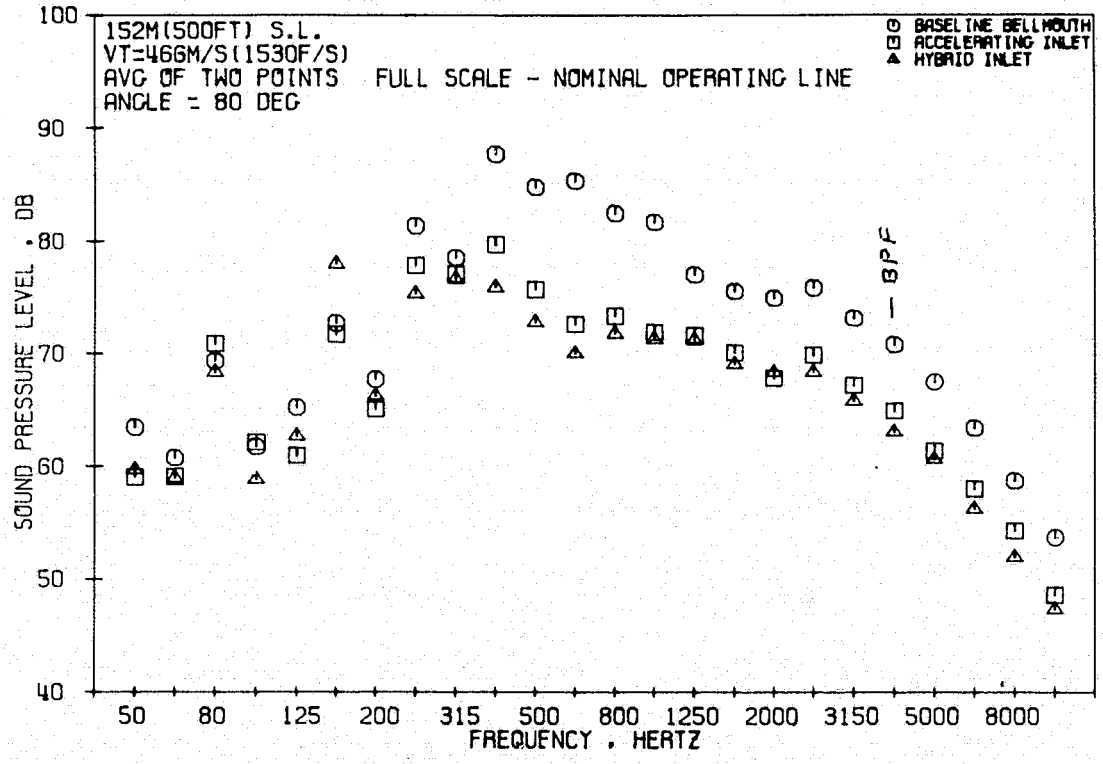

Figure 36. 1/3-Octave Spectral Comparisons at Takeoff, M_{TH} = 0.79, 80° Angle (Rear-Drive Test).

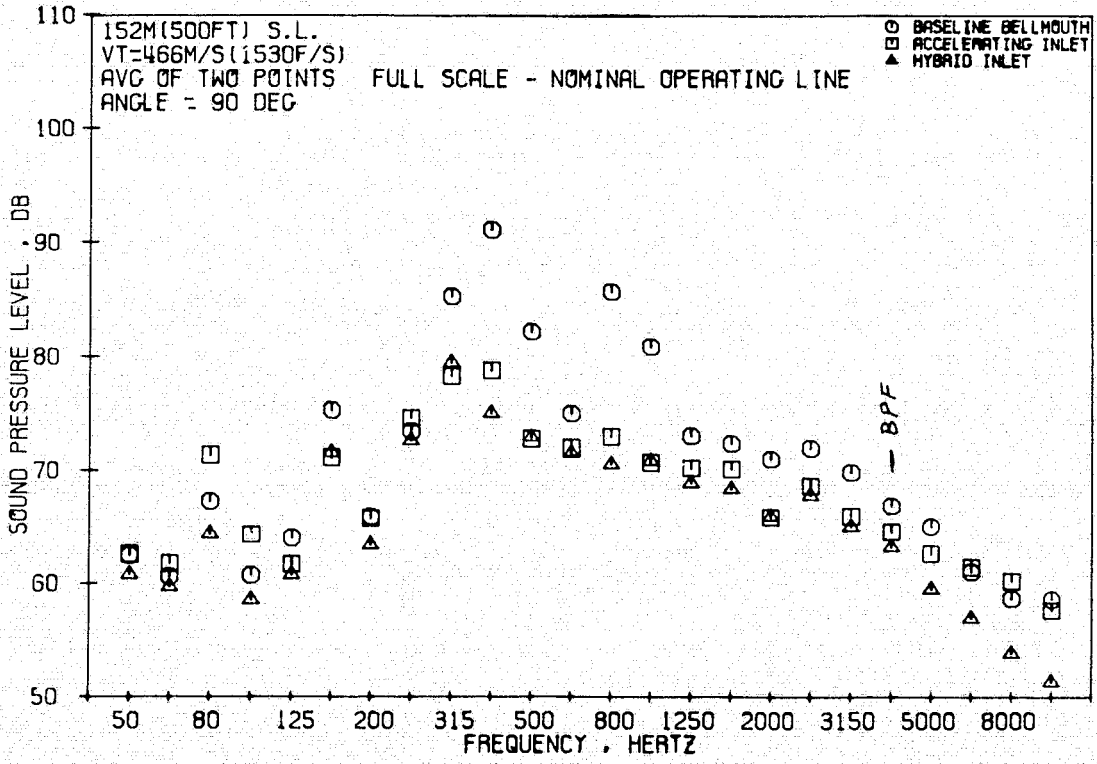

Figure 37. 1/3-Octave Spectral Comparisons at Takeoff, M_{TH} = 0.79, 90° Angle (Rear-Drive Test).

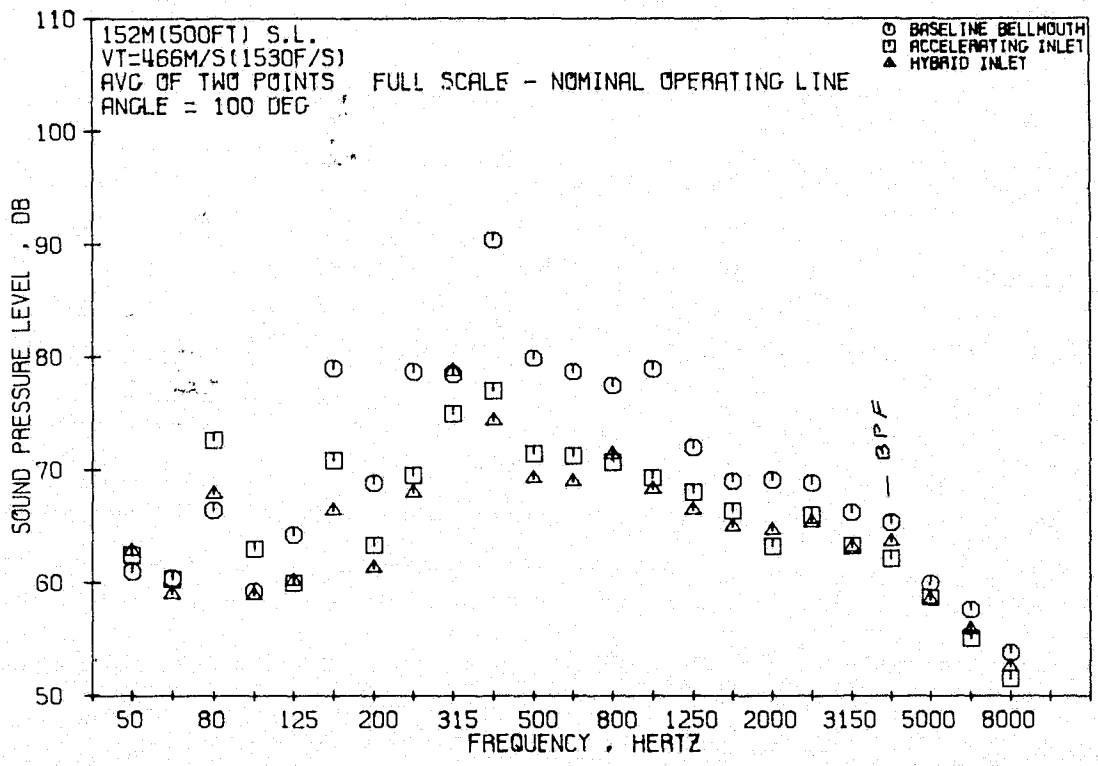

Figure 38. 1/3-Octave Spectral Comparisons at Takeoff, M_{TH} = 0.79, 100° Angle (Rear-Drive Test).

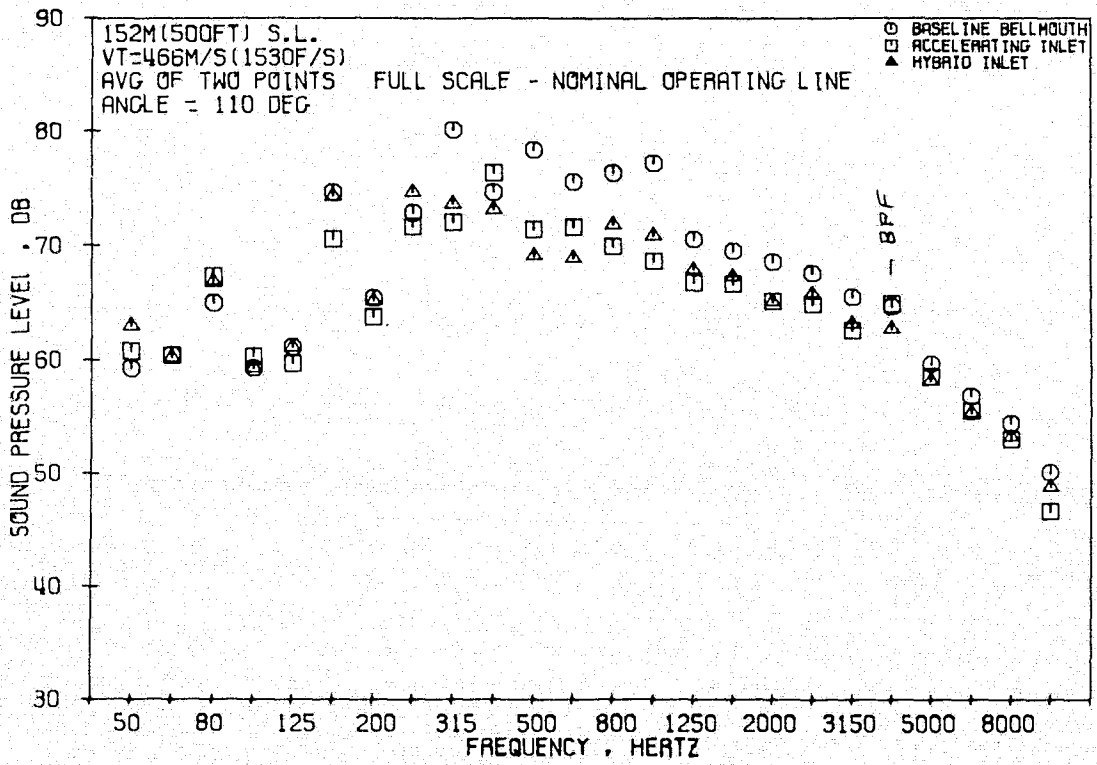

Figure 39. 1/3-Octave Spectral Comparisons at Takeoff, M_{TH} = 0.79, 110° Angle (Rear-Drive Test).

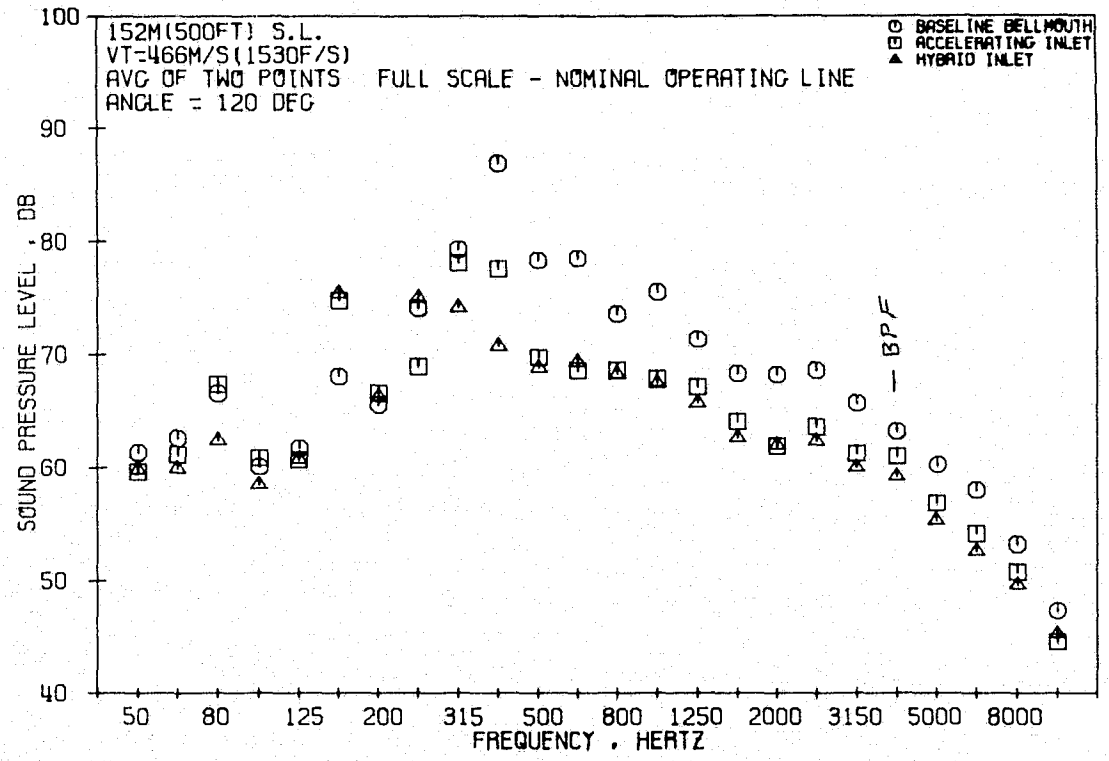

Figure 40. 1/3-Octave Spectral Comparisons at Takeoff, M_{TH} = 0.79, 120° Angle (Rear-Drive Test).

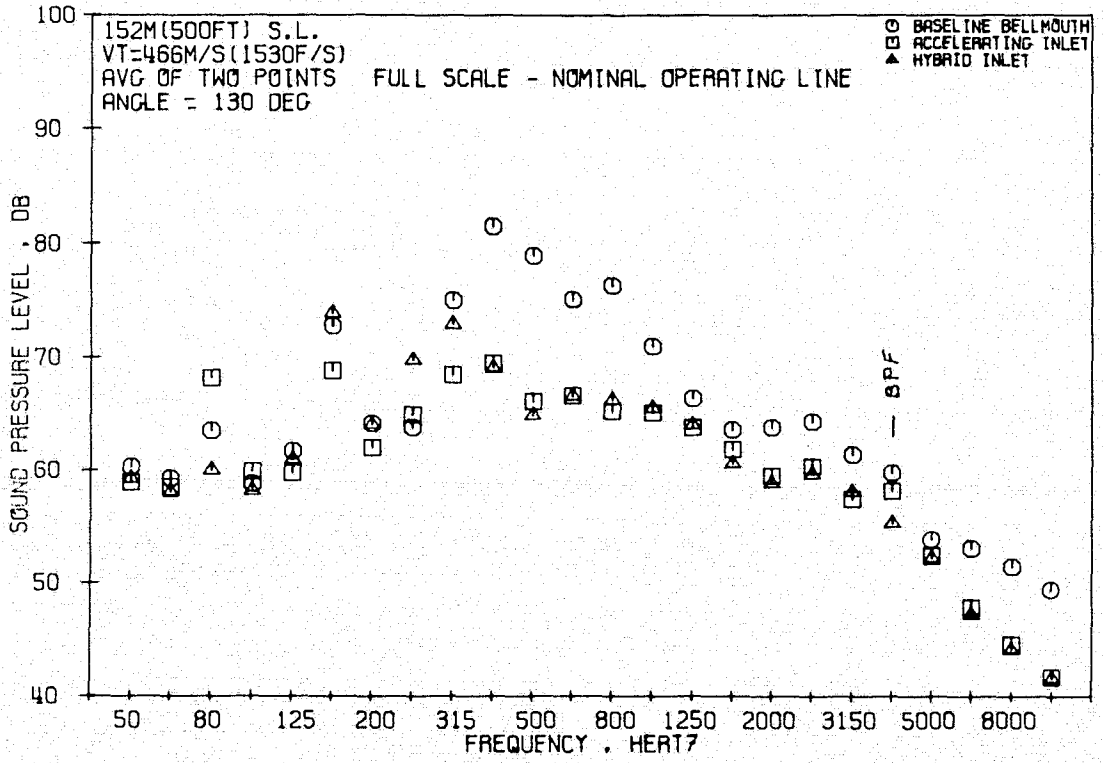

Figure 41. 1/3-Octave Spectral Comparisons at Takeoff, M_{TH} = 0.79, 130° Angle (Rear-Drive Test).

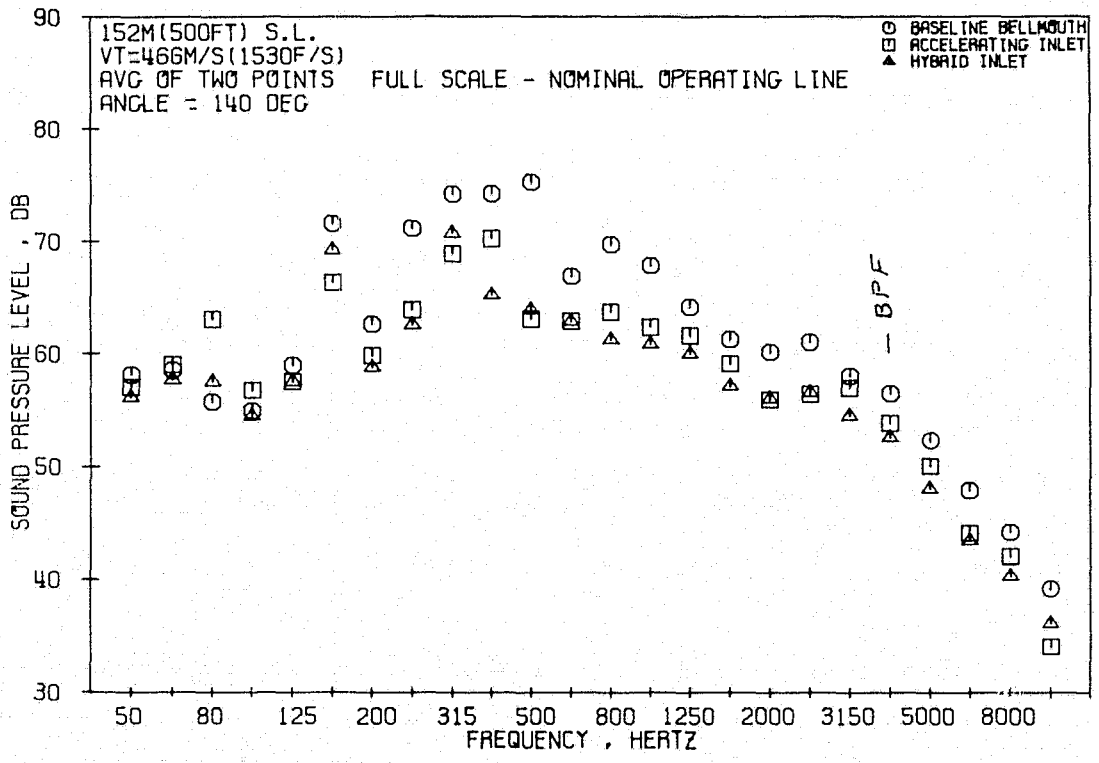

Figure 42. 1/3-Octave Spectral Comparisons at Takeoff, M_{TH} = 0.79, 140° Angle (Rear-Drive Test).

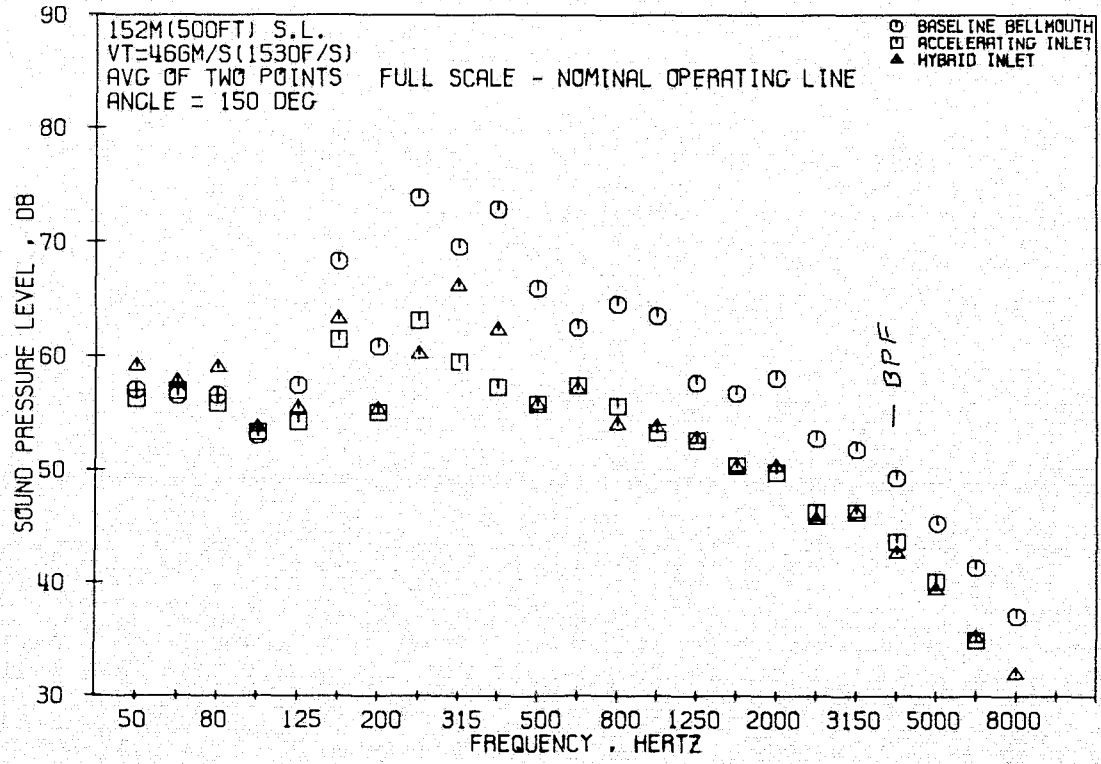

Figure 43. 1/3-Octave Spectral Comparisons at Takeoff, M_{TH} = 0.79, 150° Angle (Rear-Drive Test).

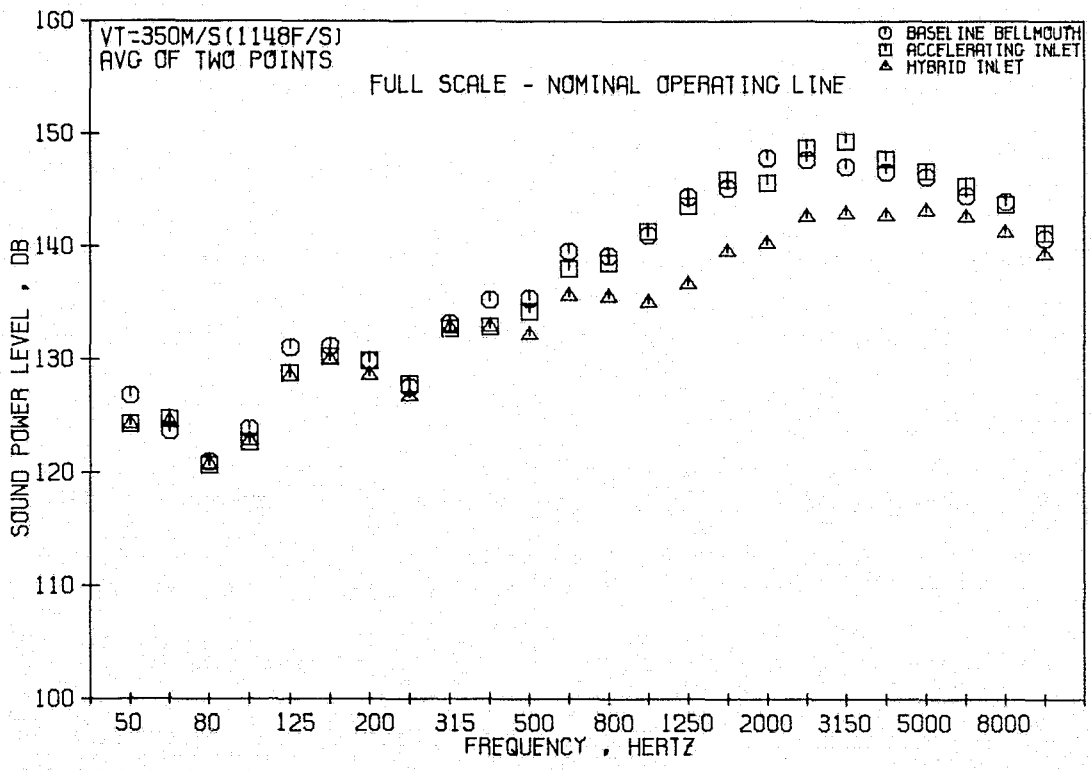

Figure 44. 1/3-Octave PWL Comparisons at Takeoff, M_{TH} = 0.47 (Rear-Drive Test).

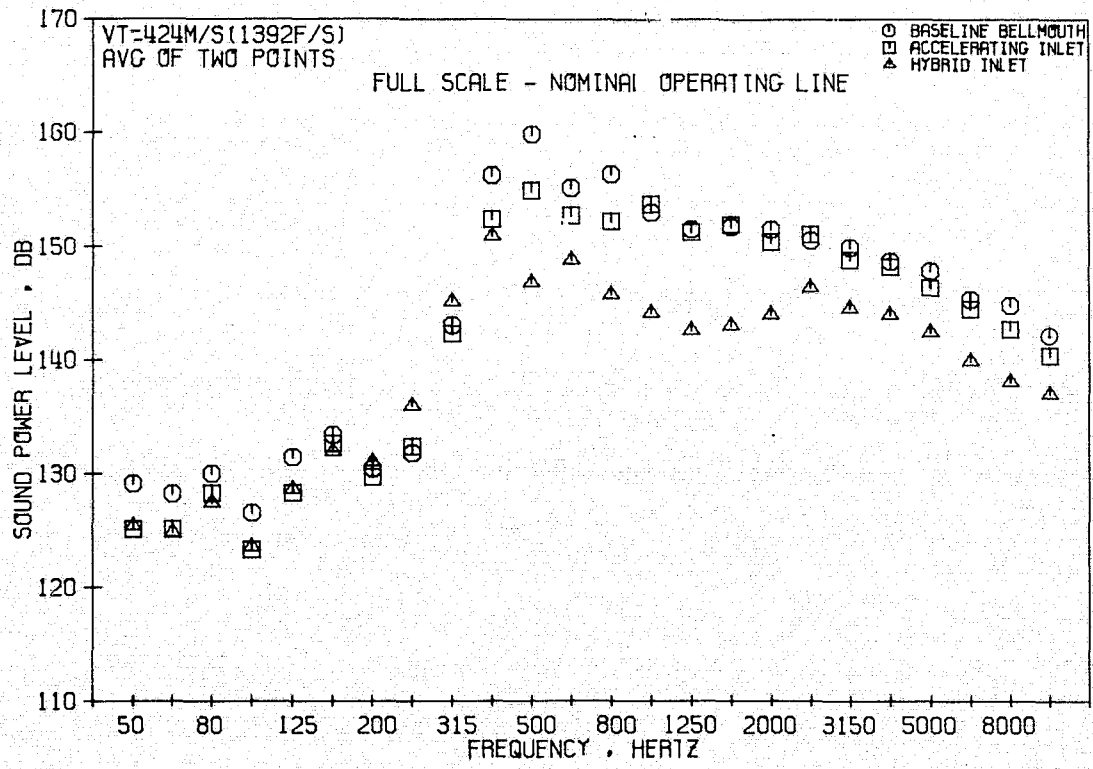

Figure 45. 1/3-Octave PWL Comparisons at Takeoff, M_{TH} = 0.65 (Rear-Drive Test).

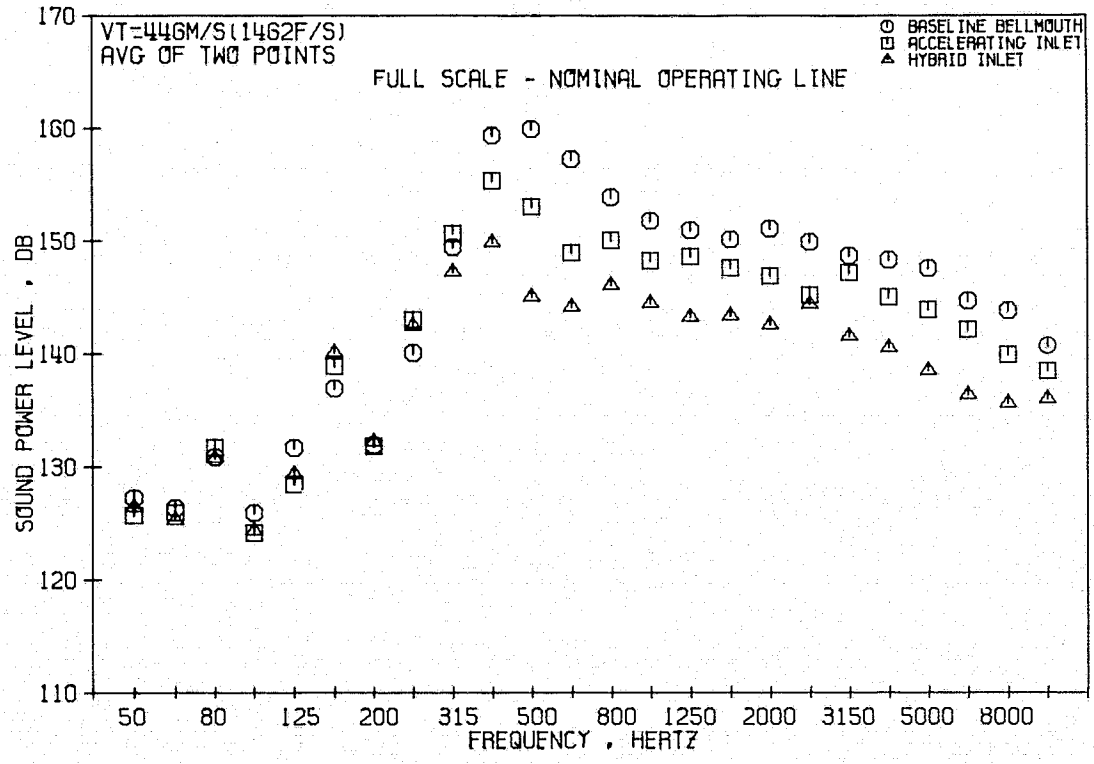

Figure 46. 1/3-Octave PWL Comparisons at Takeoff, M_{TH} = 0.72 (Rear-Drive Test).

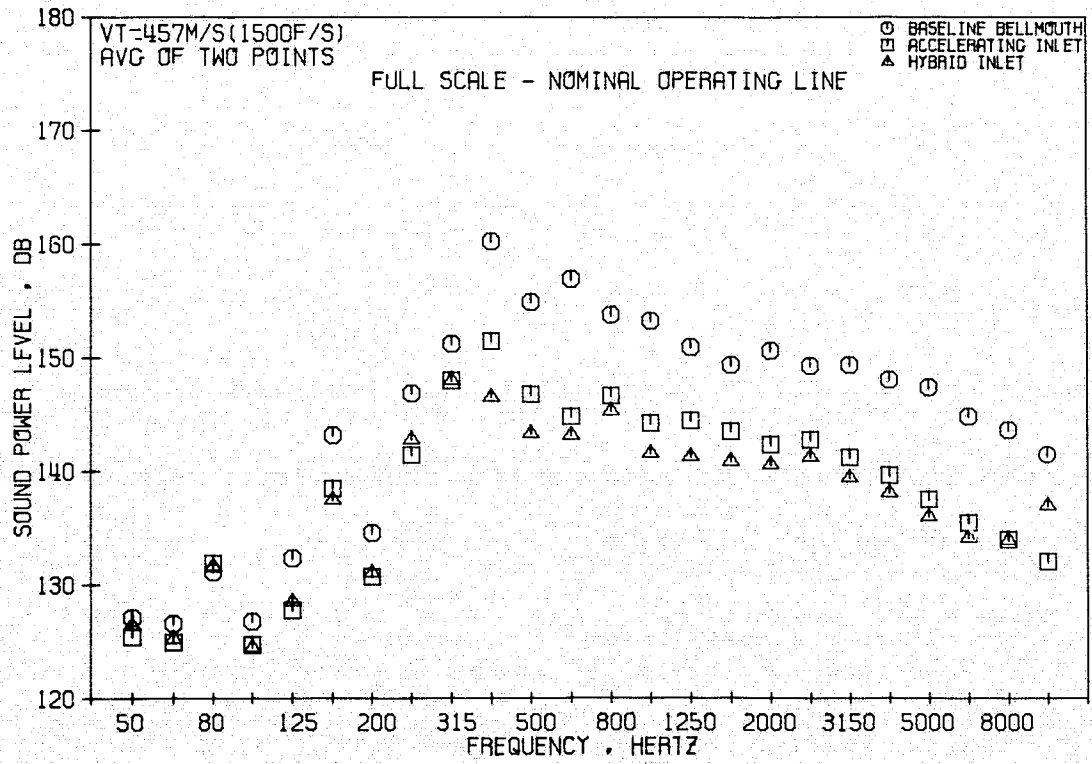

Figure 47. 1/3-Octave PWL Comparisons at Takeoff, M_{TH} = 0.76 (Rear-Drive Test).

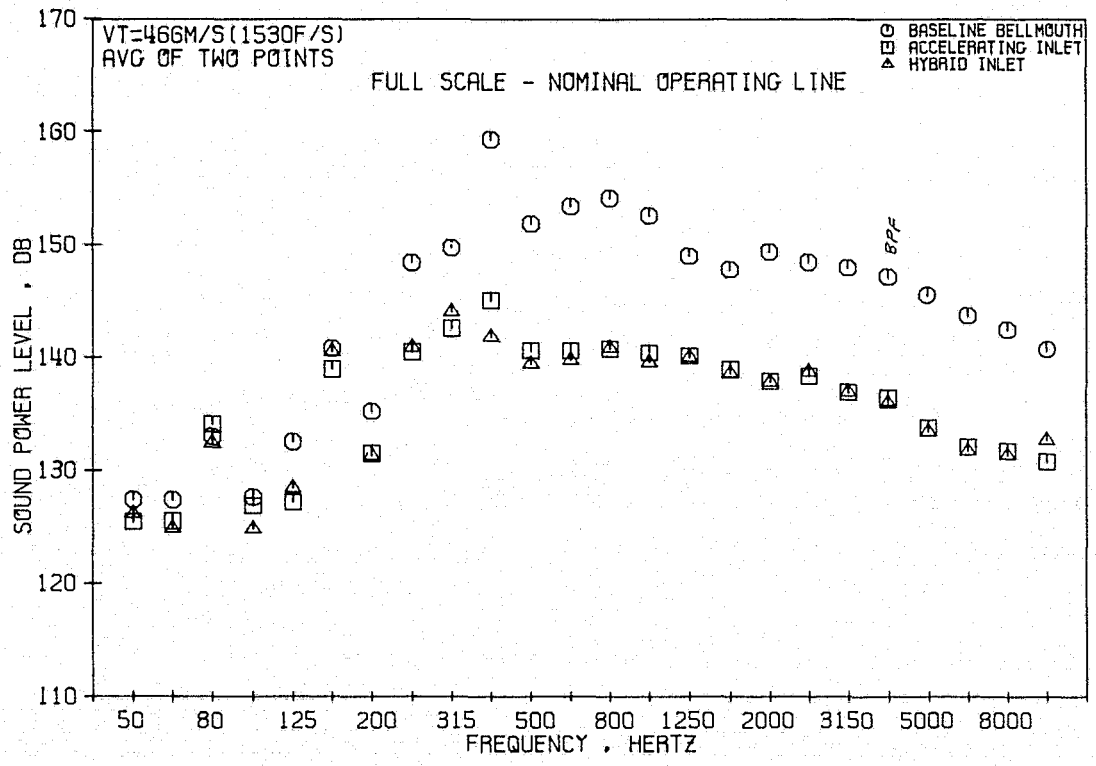

Figure 48. 1/3-Octave PWL Comparisons at Takeoff, M_{TH} = 0.79 (Rear-Drive Test).

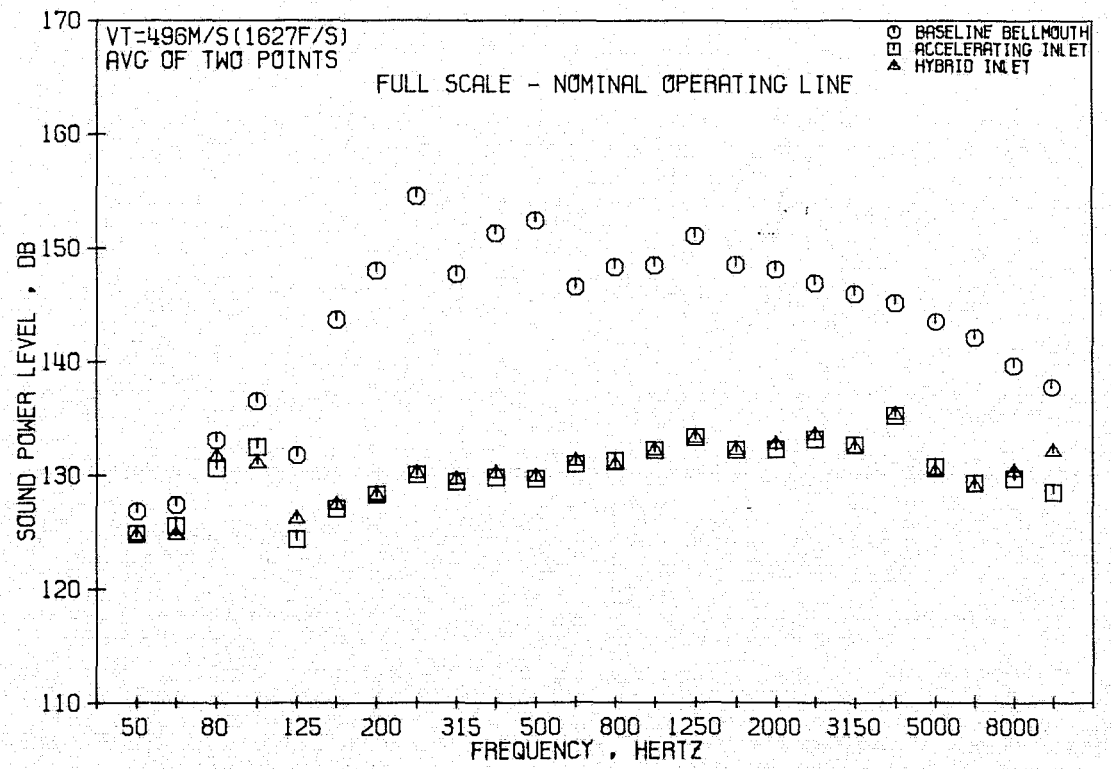

Figure 49. 1/3-Octave PWL Comparisons at Takeoff, M_{TH} = 0.87 (Rear-Drive Test).

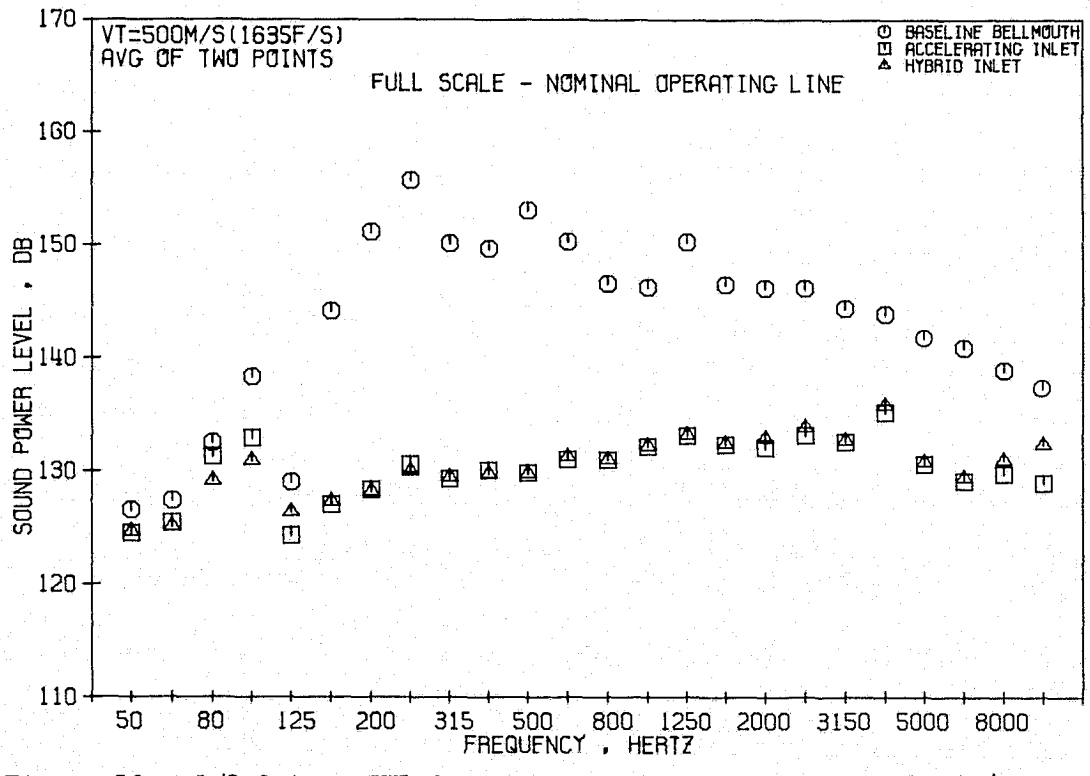

Figure 50. 1/3-Octave PWL Comparisons at Takeoff, M_{TH} = 0.88 (Rear-Drive Test).

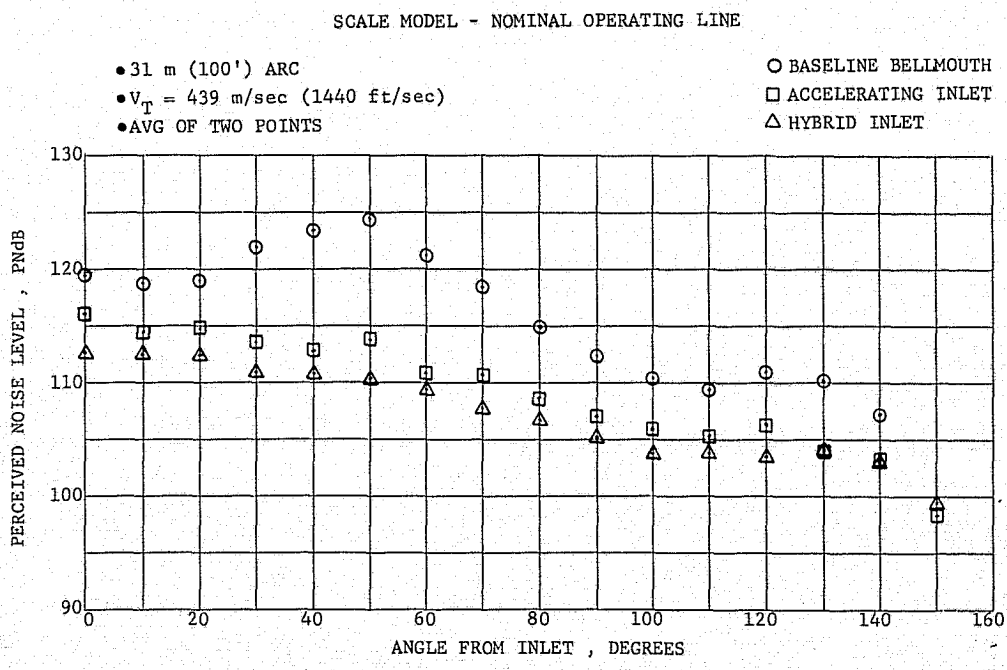

Figure 51. Scale-Model PNL Directivity at Cutback, M_{TH} = 0.79 (Rear-Drive Test).

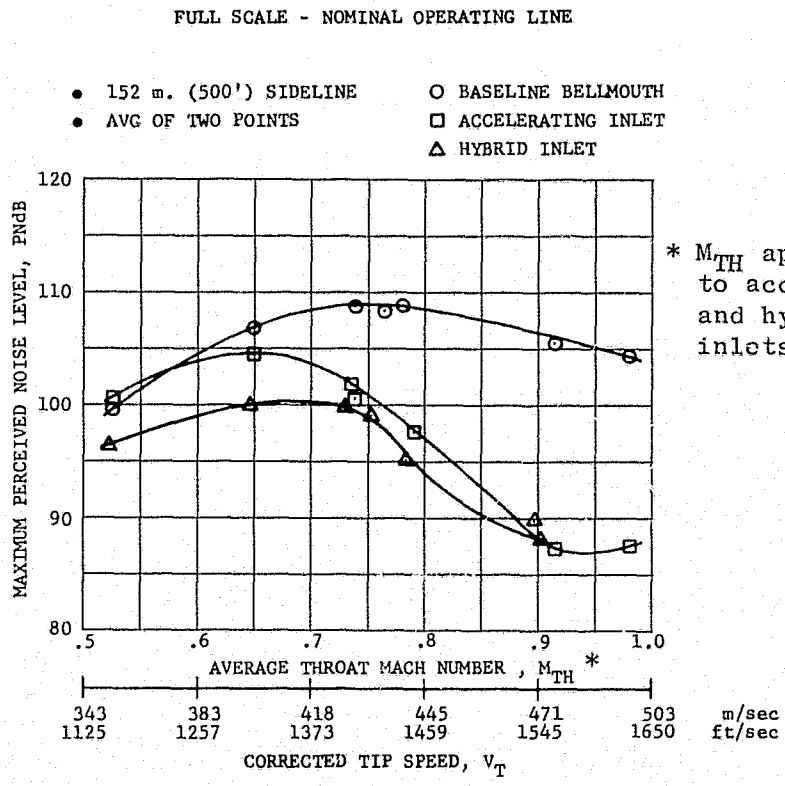

Figure 52. Maximum PNL Vs. Average Throat Mach Number, at Cutback (Rear-Drive Test).

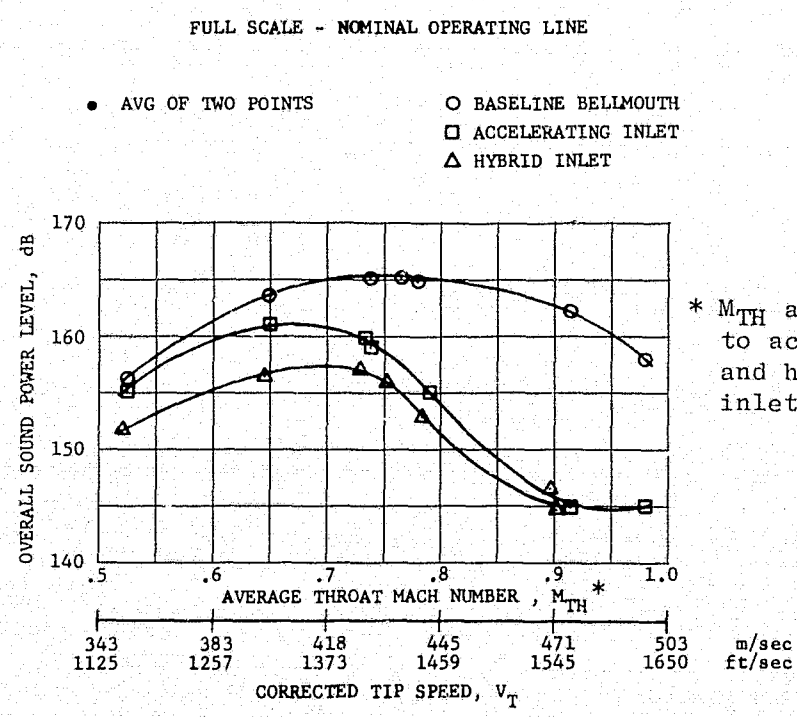

Figure 53. Overall Power Level Vs. Average Throat Mach Number, at Cutback (Rear-Drive Test).

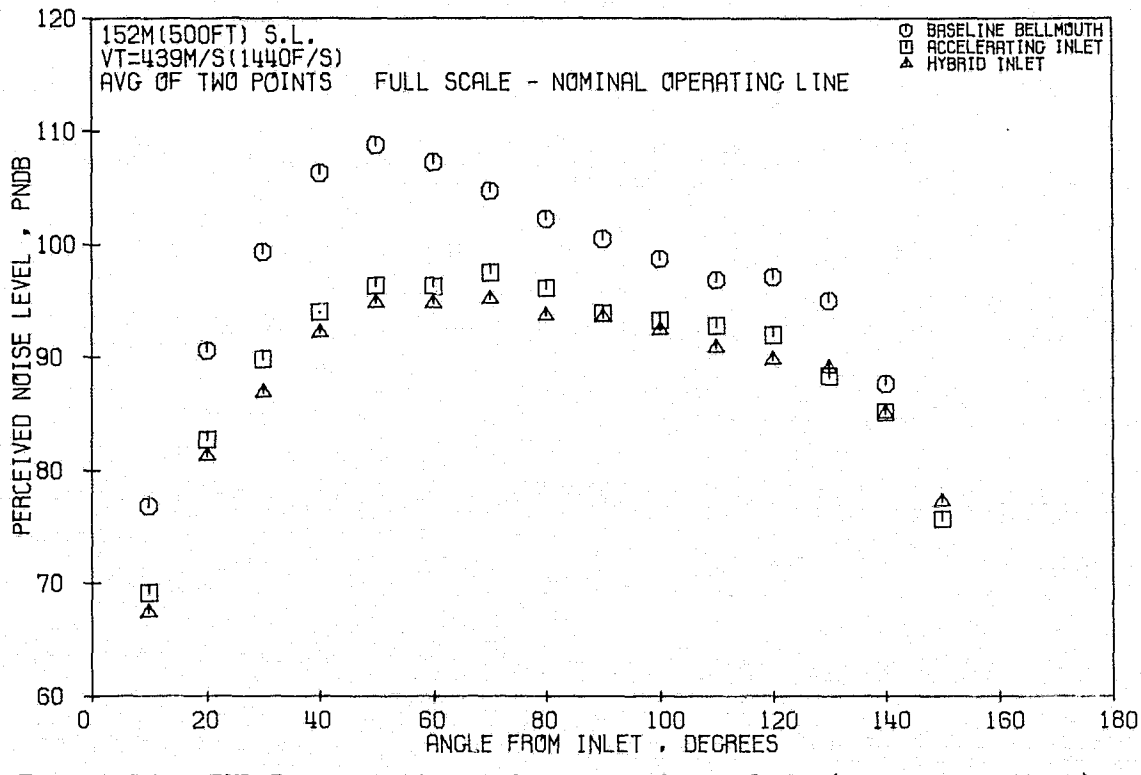

Figure 54. PNL Directivity at Cutback, M_{TH} = 0.79 (Rear-Drive Test).

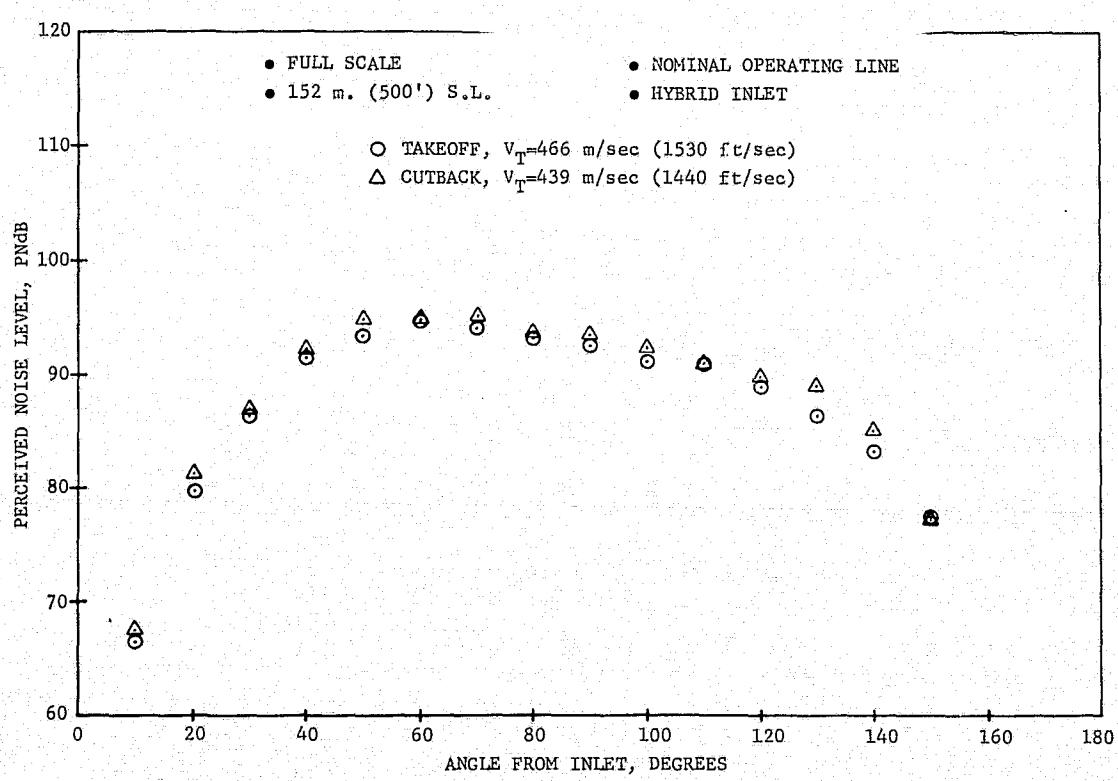

Figure 55. Comparison of PNL Directivity, Takeoff Vs. Cutback, M_{TH} = 0.79 (Rear-Drive Test).

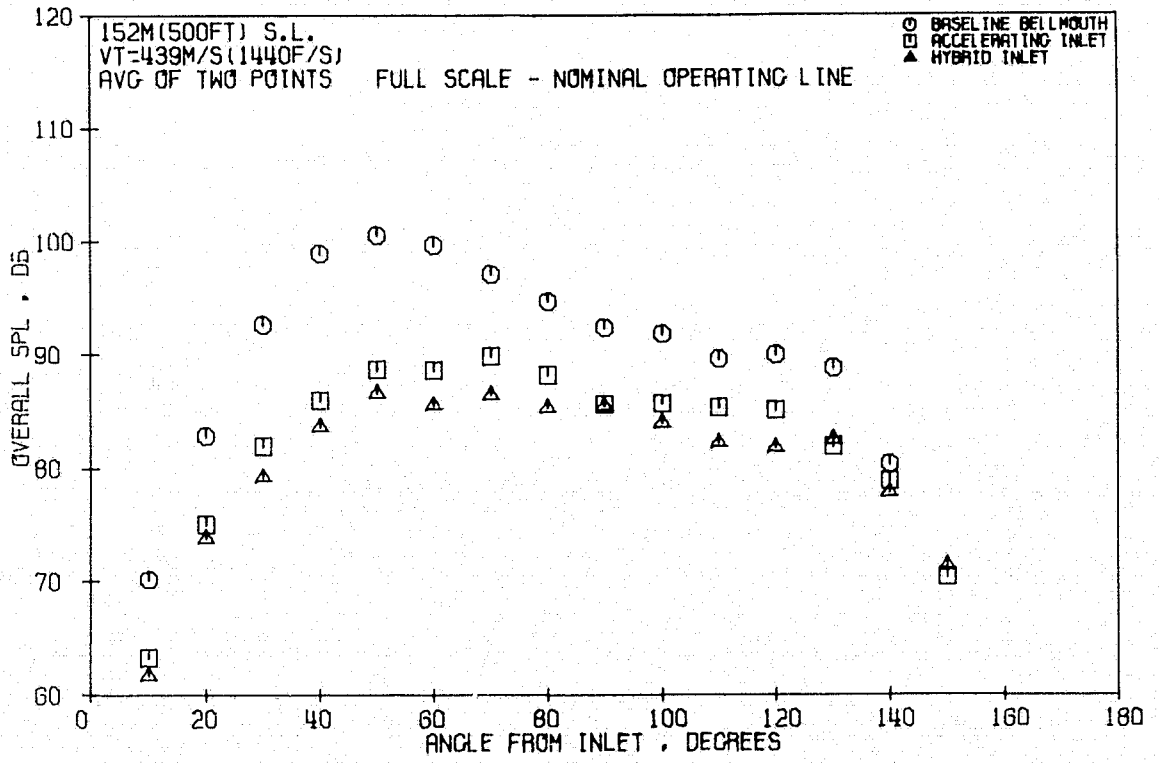

Figure 56. Variation of OASPL with Inlet Angle at Cutback, M_{TH} = 0.79 (Rear-Drive Test).

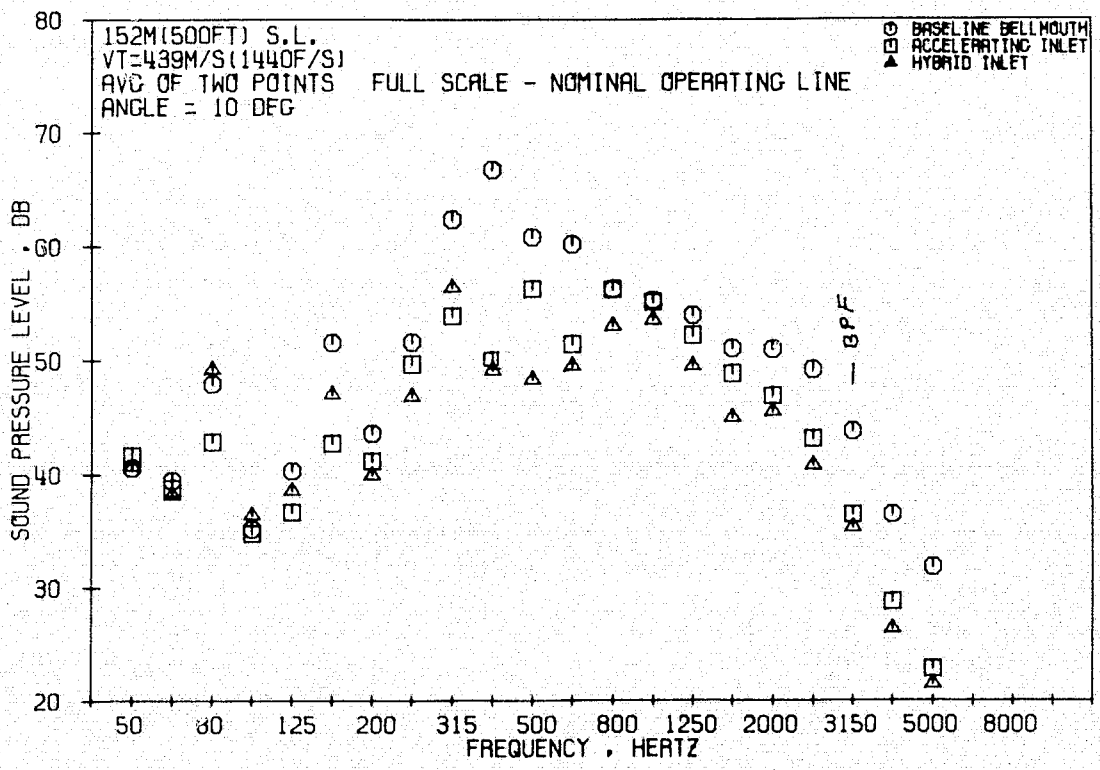

Figure 57. 1/3-Octave Spectral Comparisons at Cutback, M_{TH} = 0.79, 10° Angle (Rear-Drive Test).

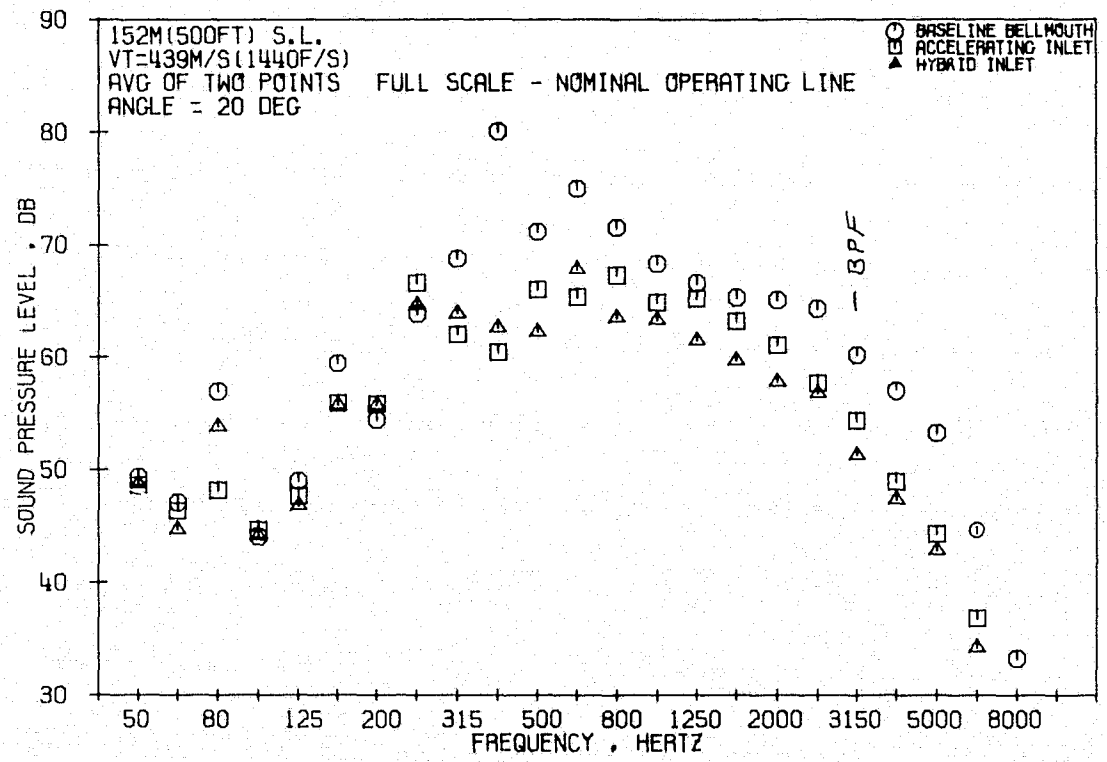

Figure 58. 1/3-Octave Spectral Comparisons at Cutback, M_{TH} = 0.79, 20° Angle (Rear-Drive Test).

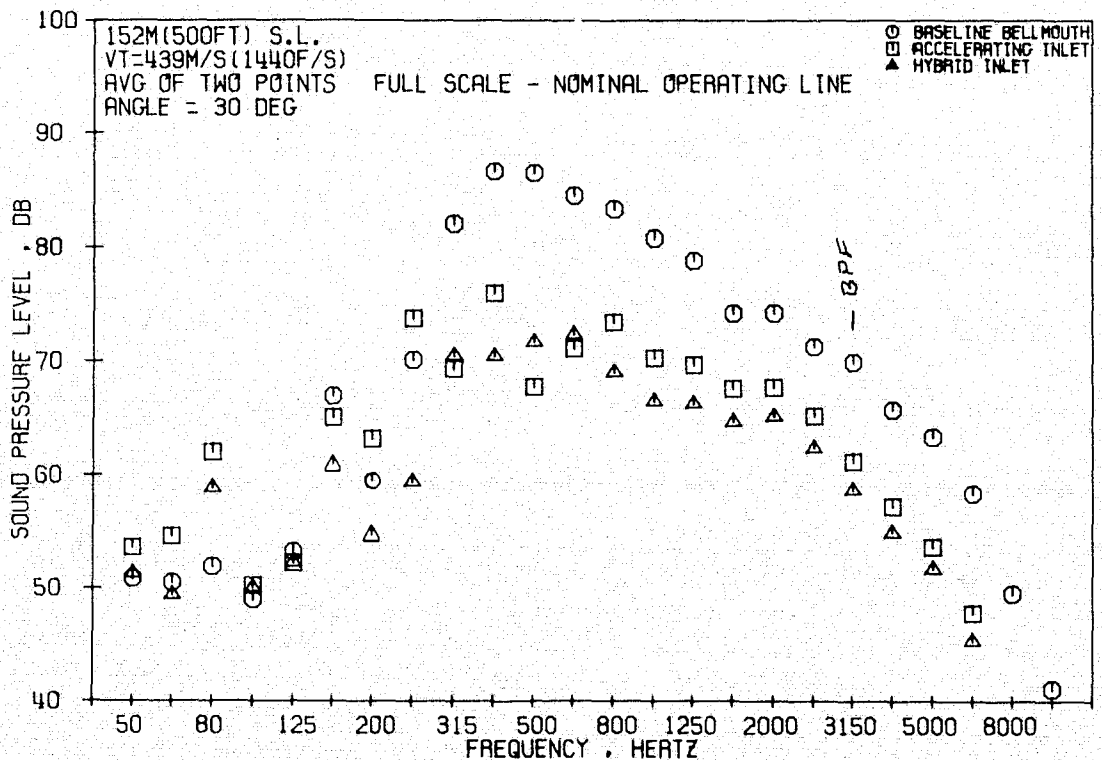

Figure 59. 1/3-Octave Spectral Comparisons at Cutback, M_{TH} = 0.79, 30° Angle (Rear-Drive Test).

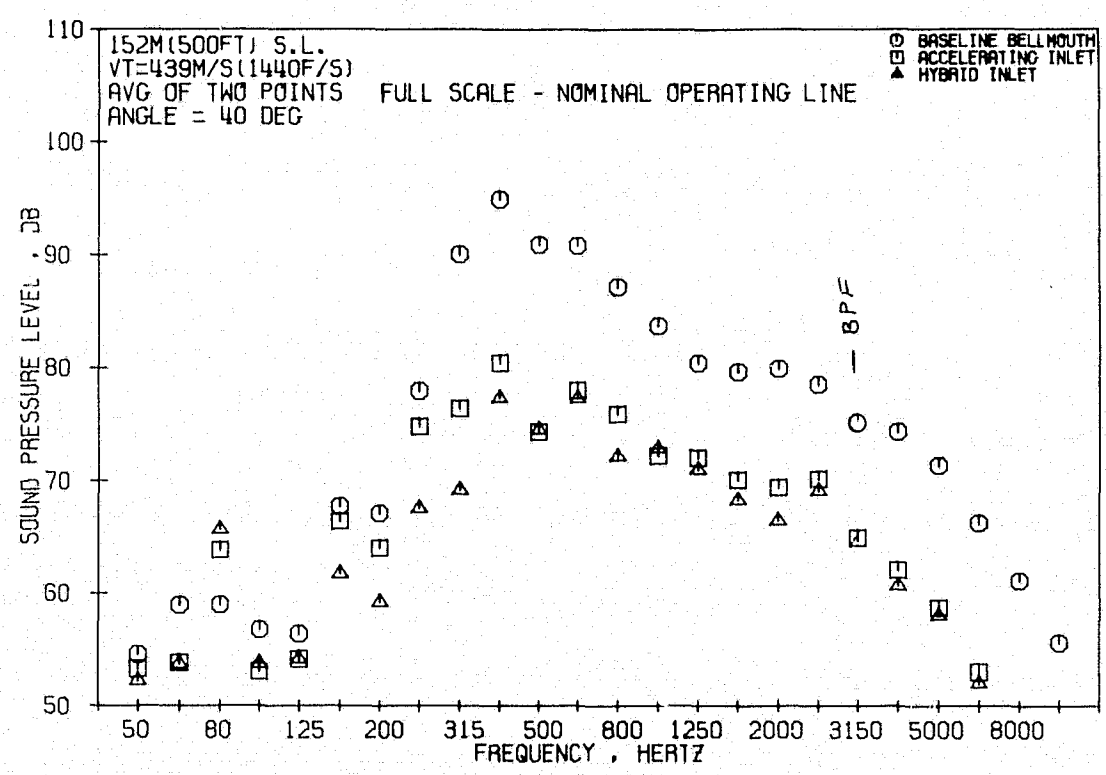

Figure 60. 1/3-Octave Spectral Comparisons at Cutback, M_{TH} = 0.79, 40° Angle (Rear-Drive Test).

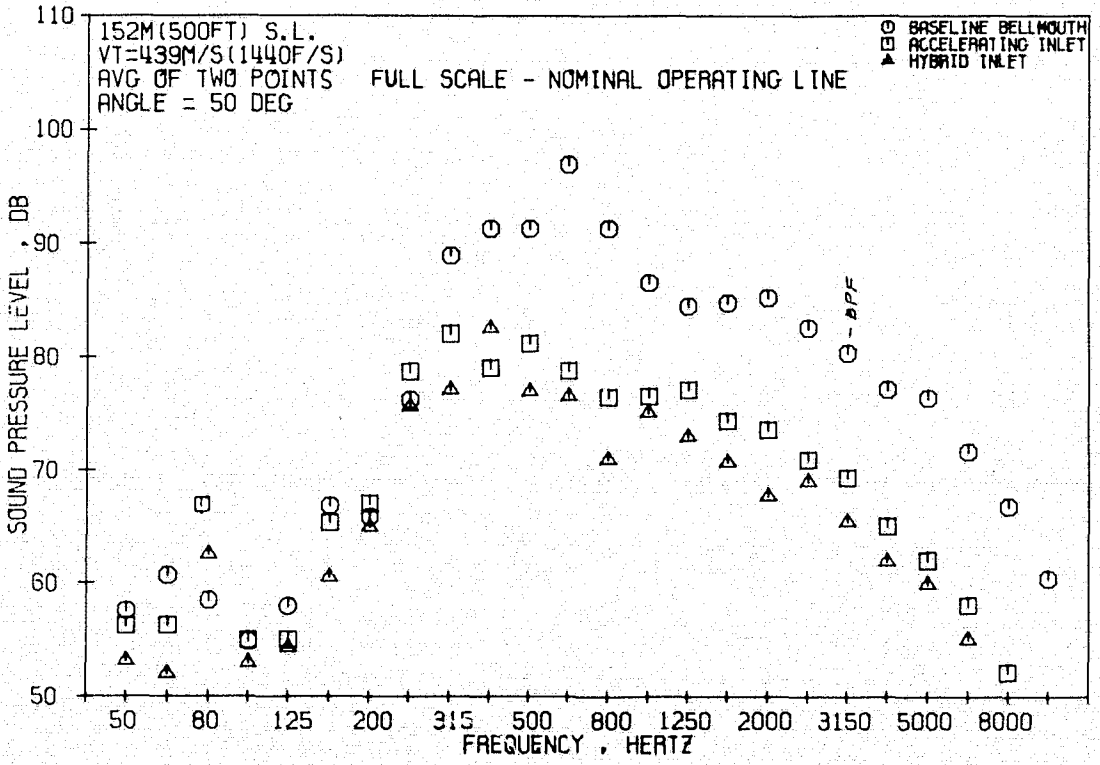

Figure 61. 1/3-Octave Spectral Comparisons at Cutback, M_{TH} = 0.79, 50° Angle (Rear-Drive Test).

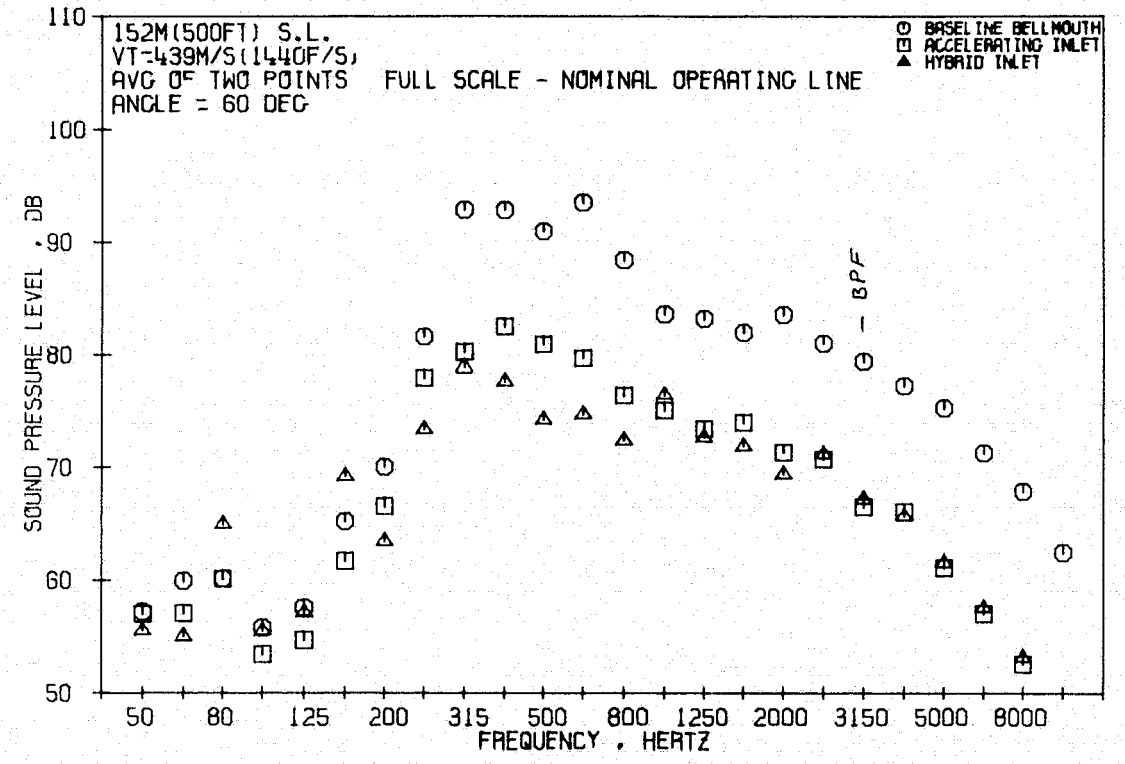

Figure 62. 1/3-Octave Spectral Comparisons at Cutback, M_{TH} = 0.79, 60° Angle (Rear-Drive Test).

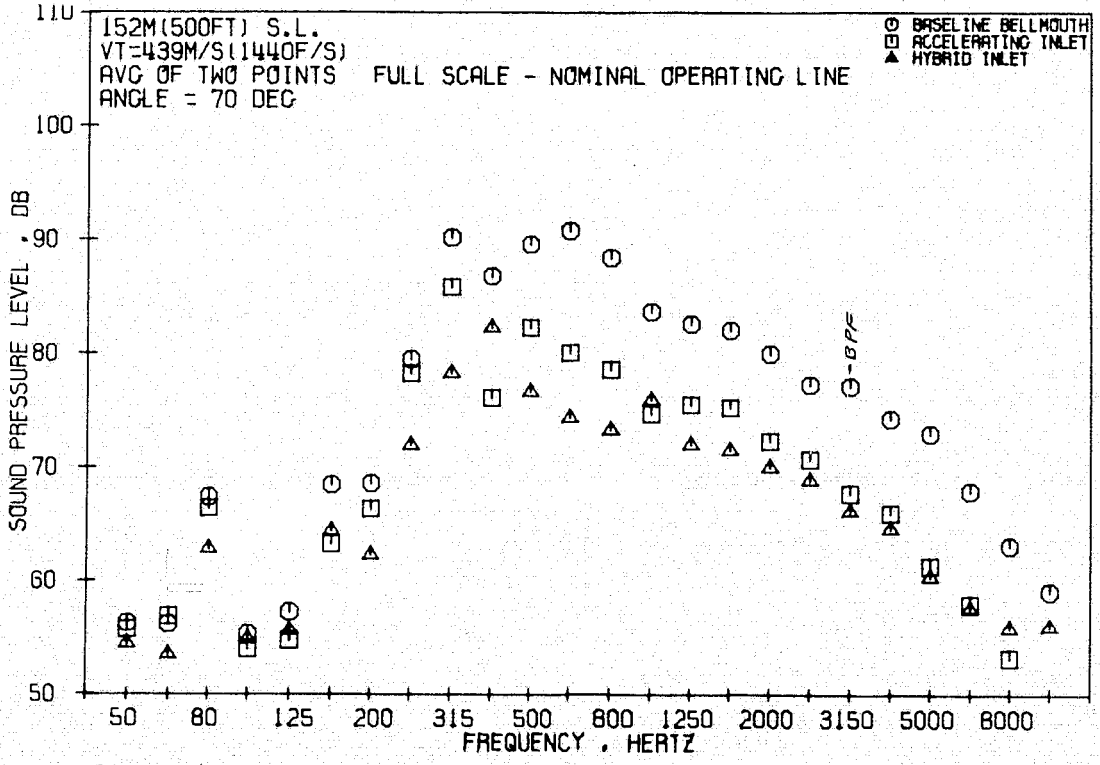

Figure 63. 1/3-Octave Spectral Comparisons at Cutback, M_{TH} = 0.79, 70° Angle (Rear-Drive Test).

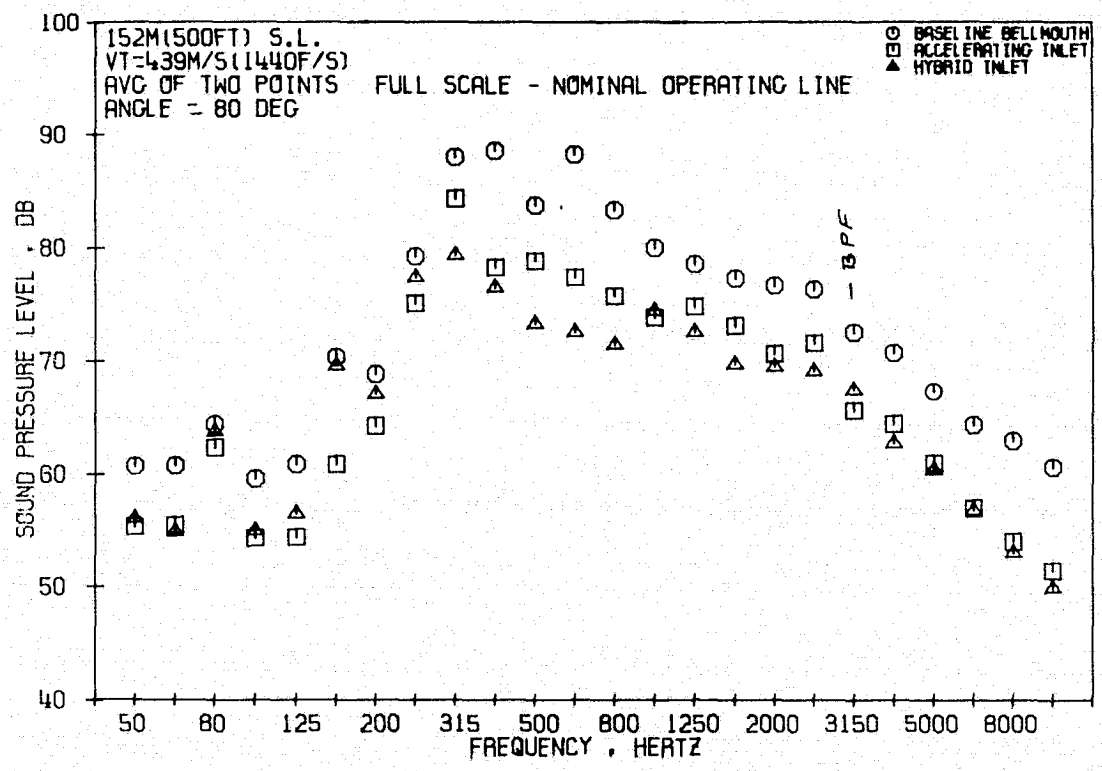

Figure 64. 1/3-Octave Spectral Comparisons at Cutback, M_{TH} = 0.79, 80° Angle (Rear-Drive Test).

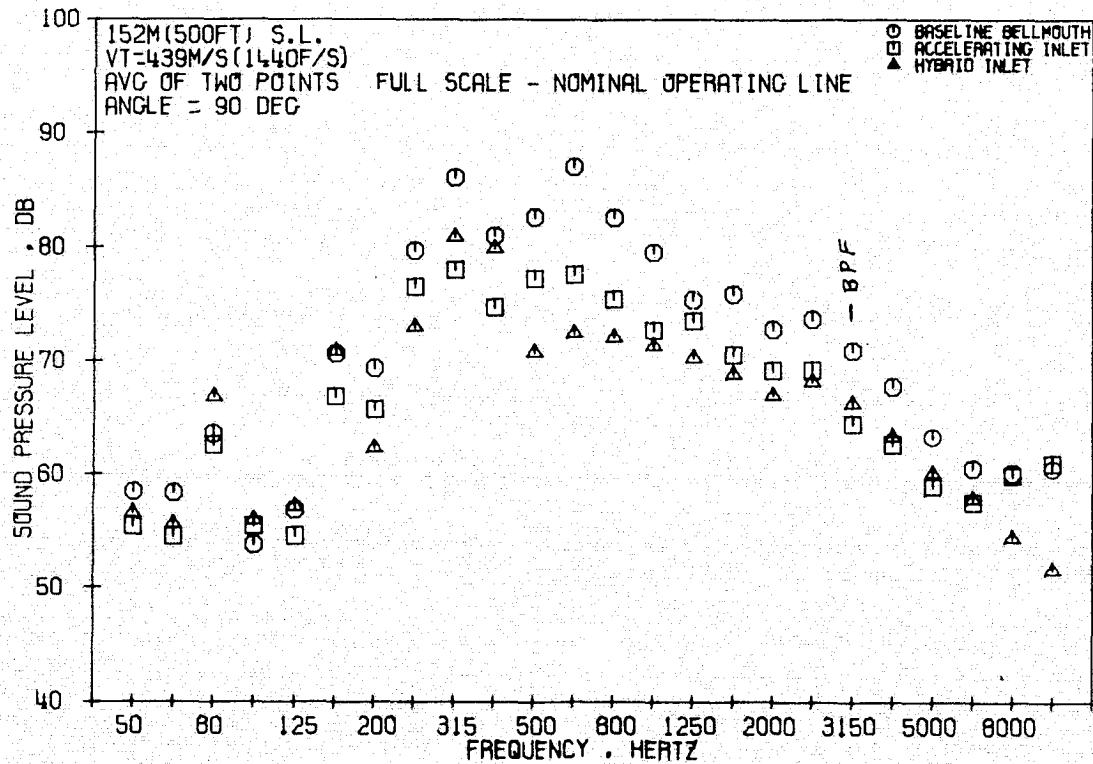

Figure 65. 1/3-Octave Spectral Comparisons at Cutback, M_{TH} = 0.79, 90° Angle (Rear-Drive Test).

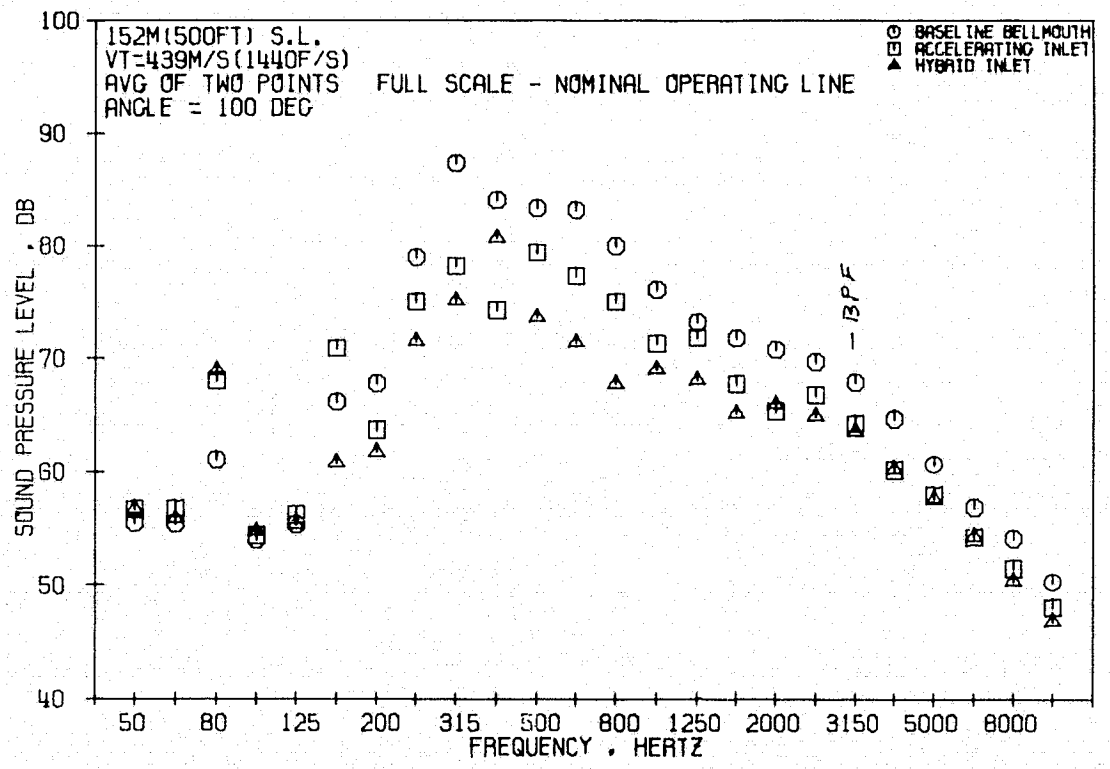

Figure 66. 1/3-Octave Spectral Comparisons at Cutback, M_{TH} = 0.79, 100° Angle (Rear-Drive Test).

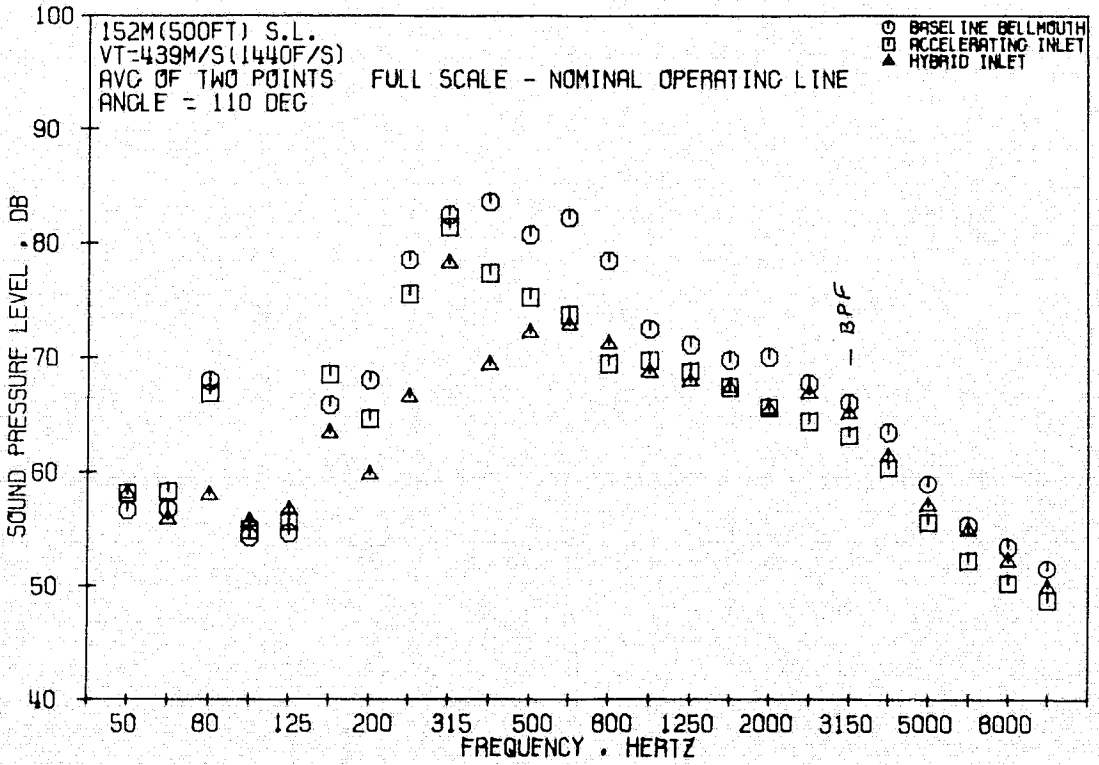

Figure 67. 1/3-Octave Spectral Comparisons at Cutback, M_{TH} = 0.79, 110° Angle (Rear-Drive Test).

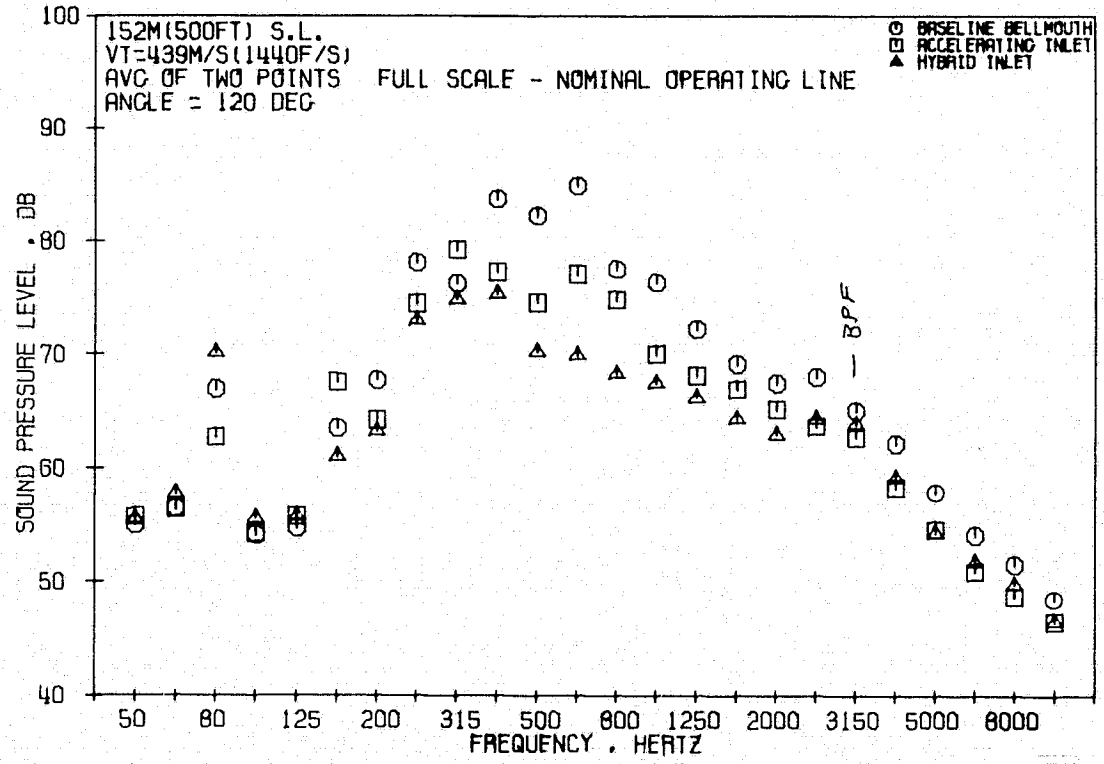

Figure 68. 1/3-Octave Spectral Comparisons at Cutback, M_{TH} = 0.79, 120° Angle (Rear-Drive Test).

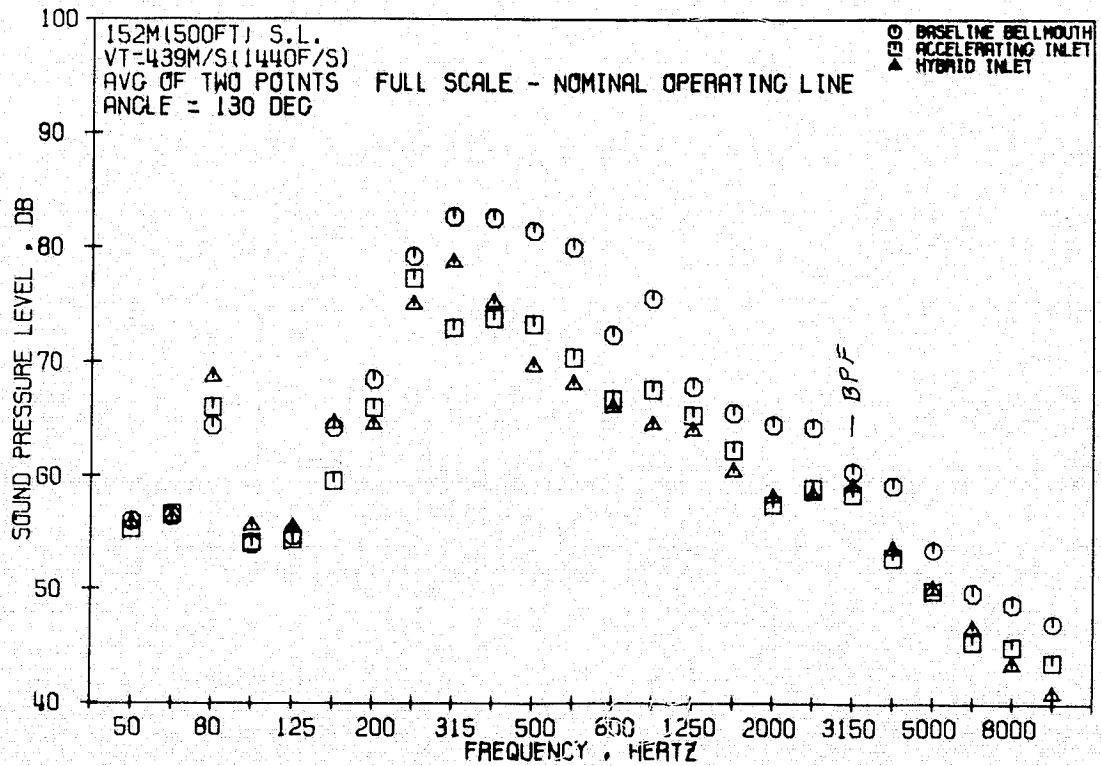

Figure 69. 1/3-Octave Spectral Comparisons at Cutback, M_{TH} = 0.79, 130° Angle (Rear-Drive Test).

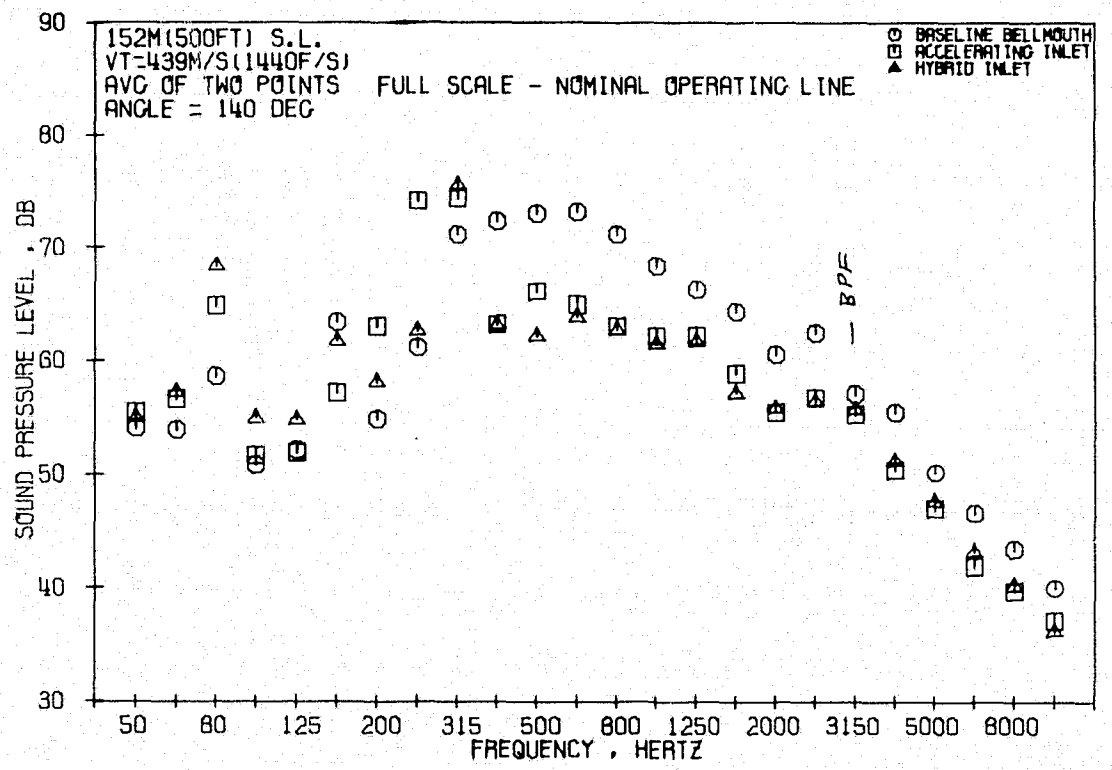

Figure 70. 1/3-Octave Spectral Comparisons at Cutback, M_{TH} = 0.79, 140° Angle (Rear-Drive Test).

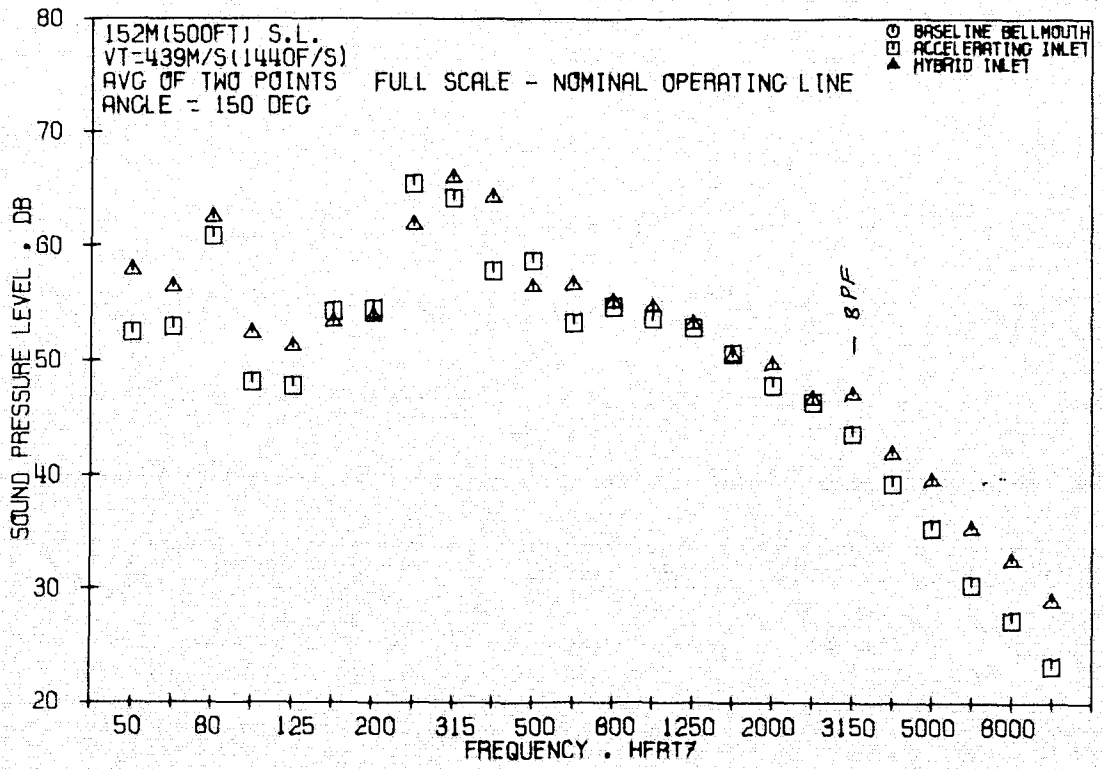

Figure 71. 1/3-Octave Spectral Comparisons at Cutback, M_{TH} = 0.79, 150° Angle (Rear-Drive Test).

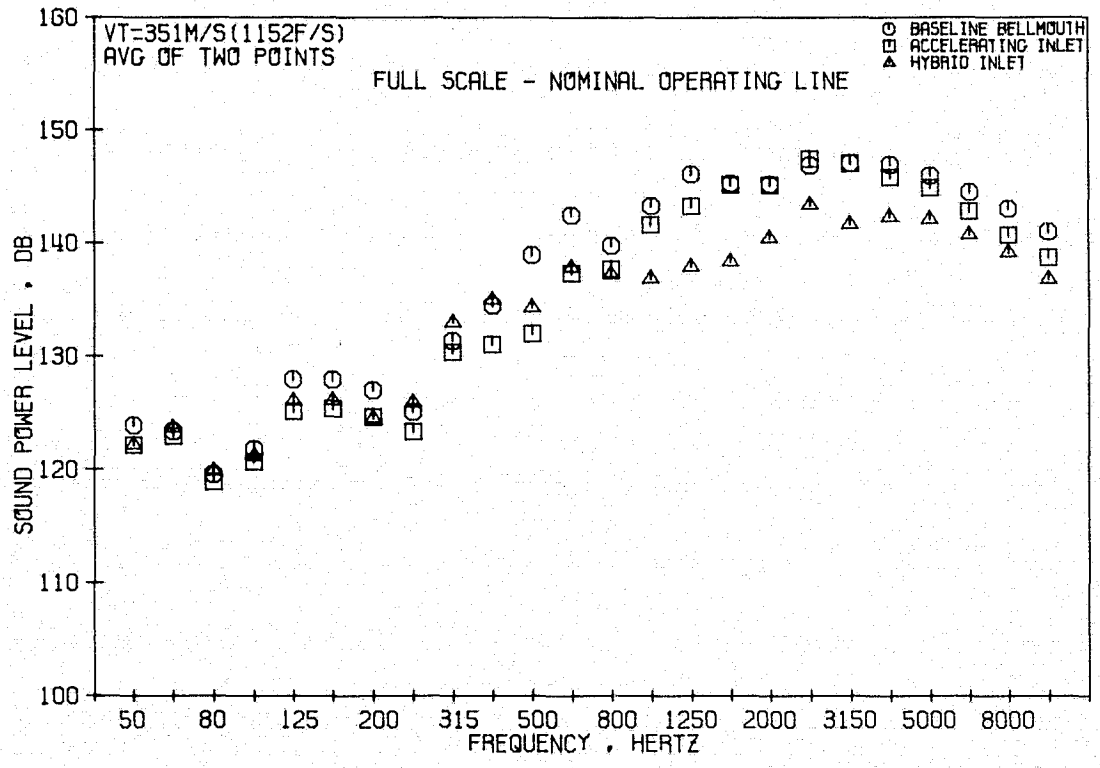

Figure 72. 1/3-Octave PWL Comparisons at Cutback, M_{TH} = 0.52 (Rear-Drive Test).

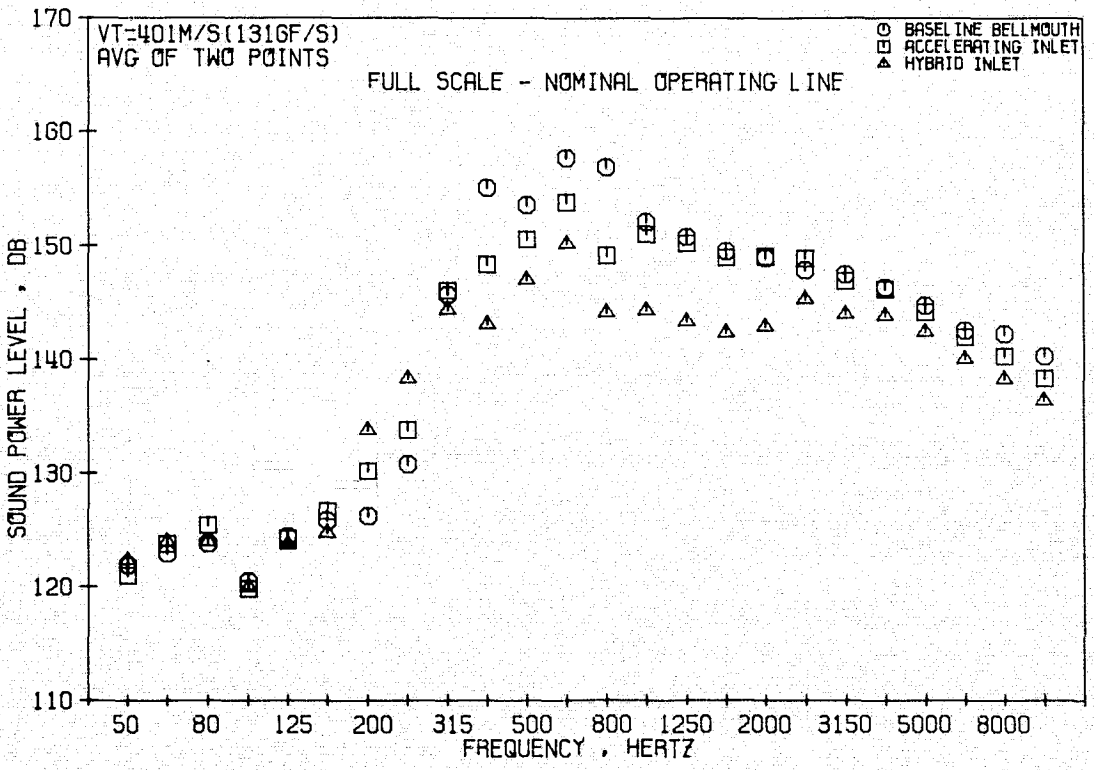

Figure 73. 1/3-Octave PWL Comparisons at Cutback, M_{TH} = 0.65 (Rear-Drive Test).

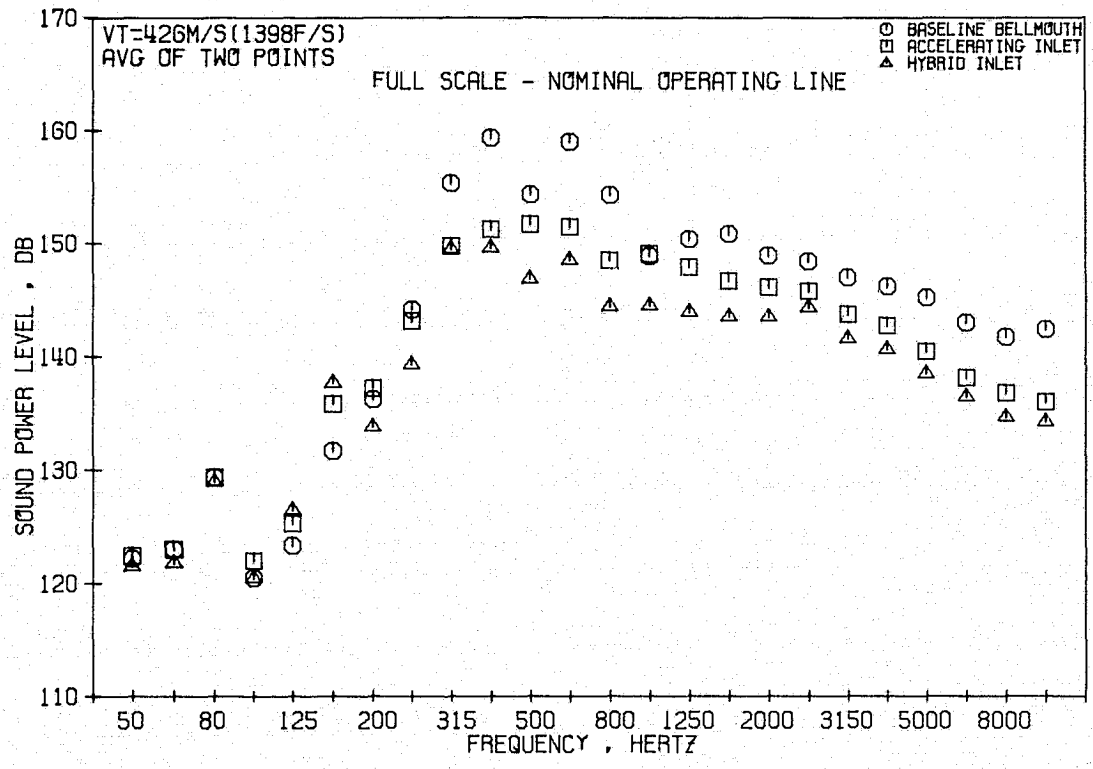

Figure 74. 1/3-Octave PWL Comparisons at Cutback, M_{TH} = 0.73 (Rear-Drive Test).

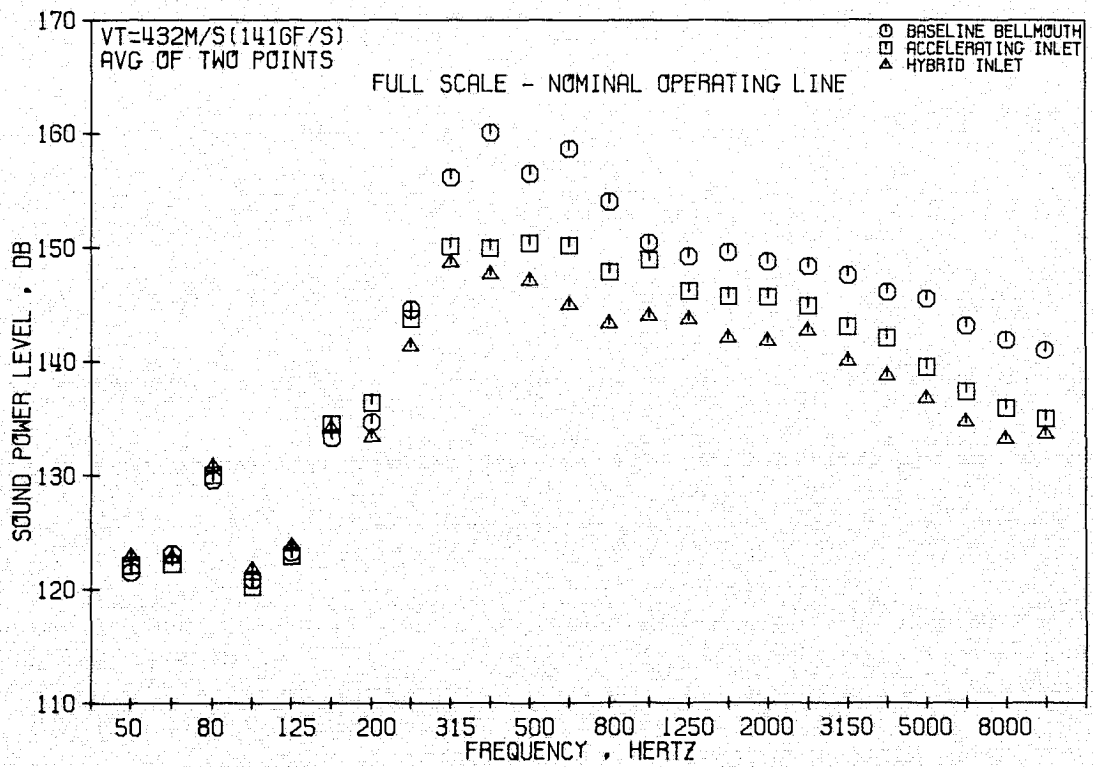

Figure 75. 1/3-Octave PWL Comparisons at Cutback, M_{TH} = 0.75 (Rear-Drive Test).

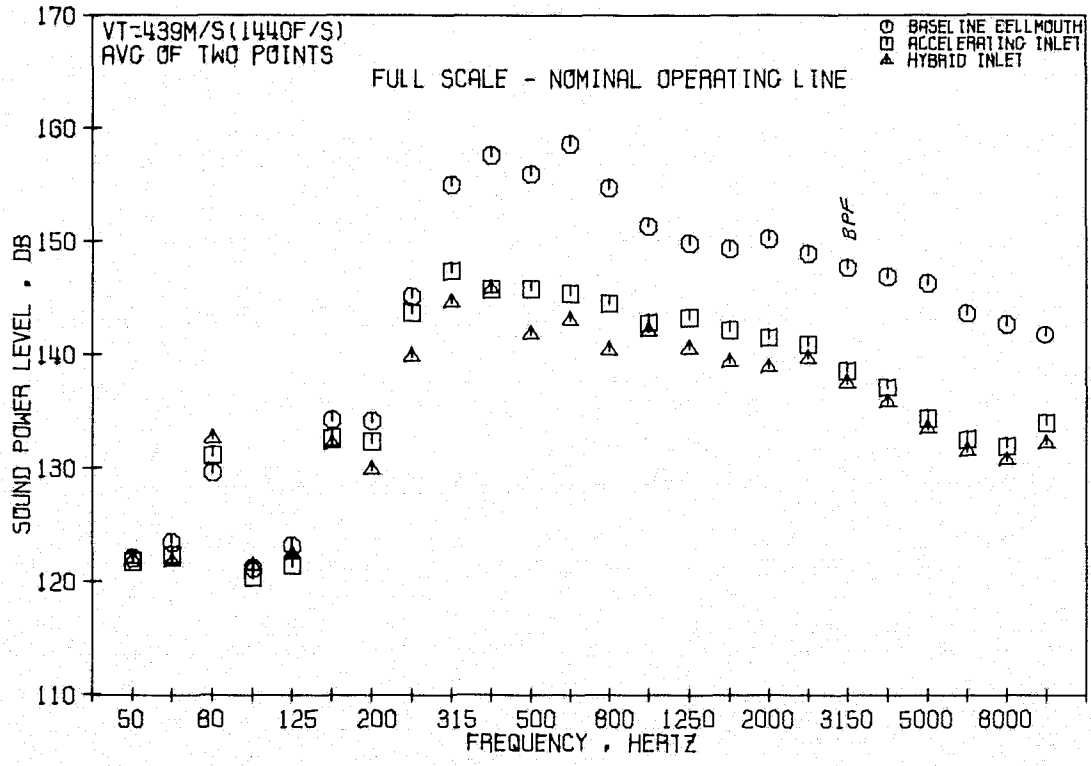

Figure 76. 1/3-Octave PWL Comparisons at Cutback, M_{TH} = 0.79 (Rear-Drive Test).

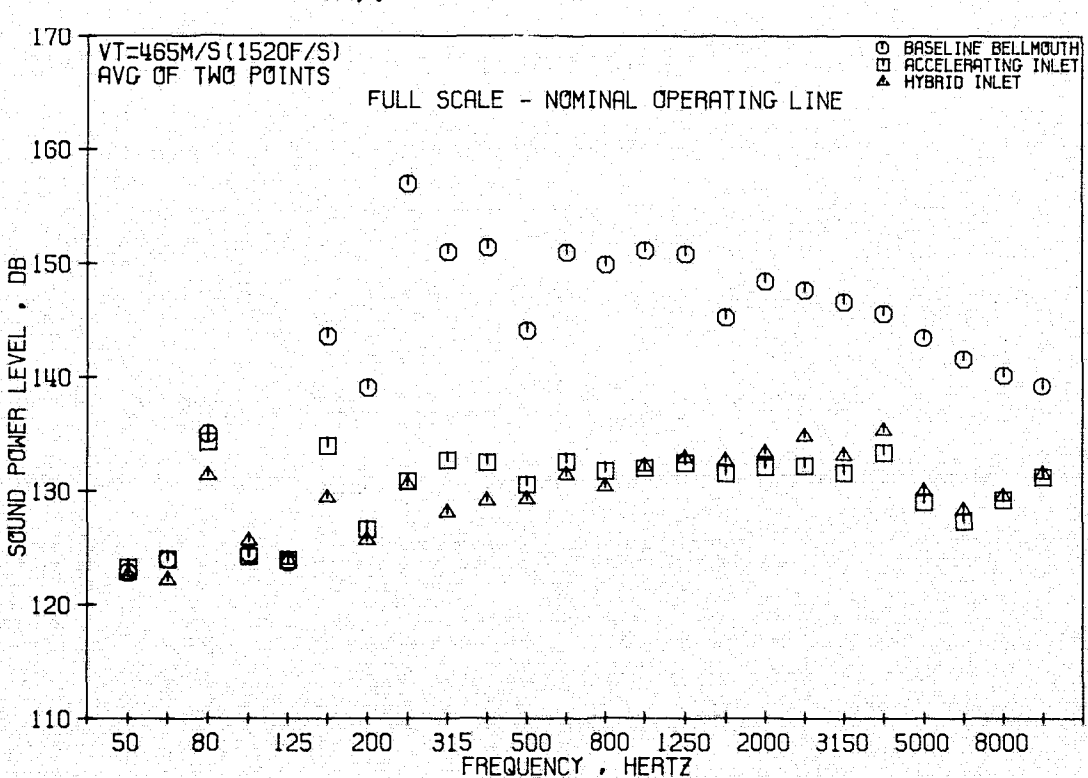

Figure 77. 1/3-Octave PWL Comparisons at Cutback, M_{TH} = 0.90 (Rear-Drive Test).

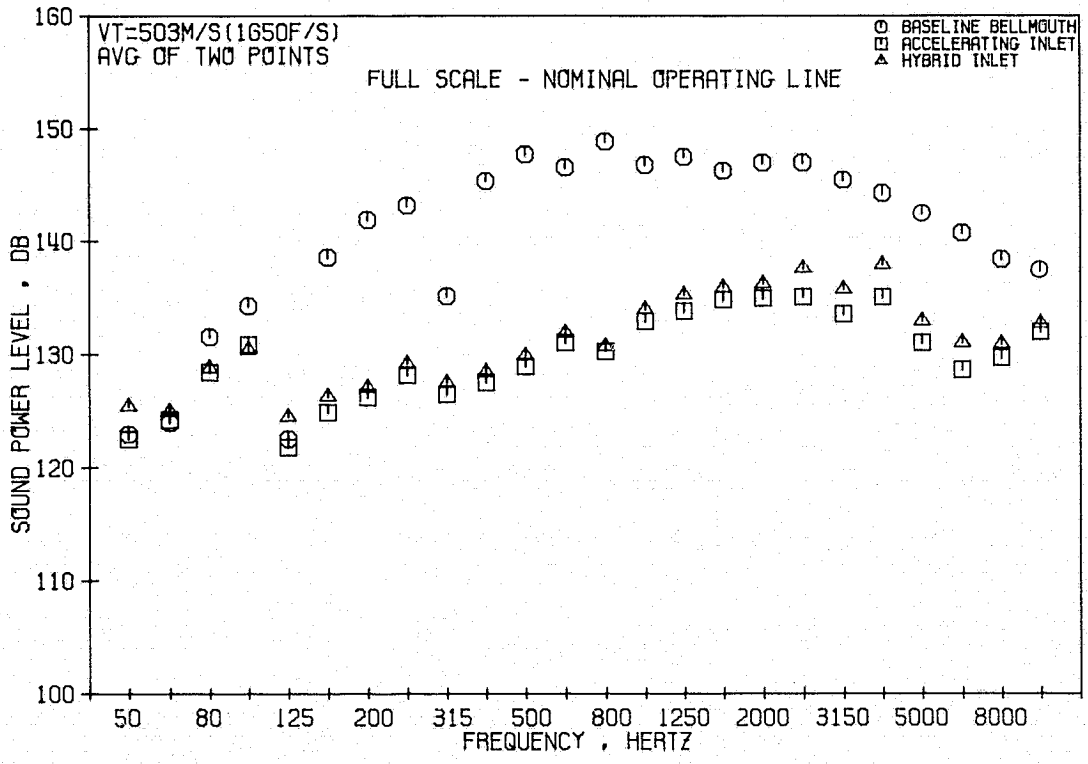

Figure 78. 1/3-Octave PWL Comparisons at Cutback, M_{TH} = 0.94 (Rear-Drive Test).

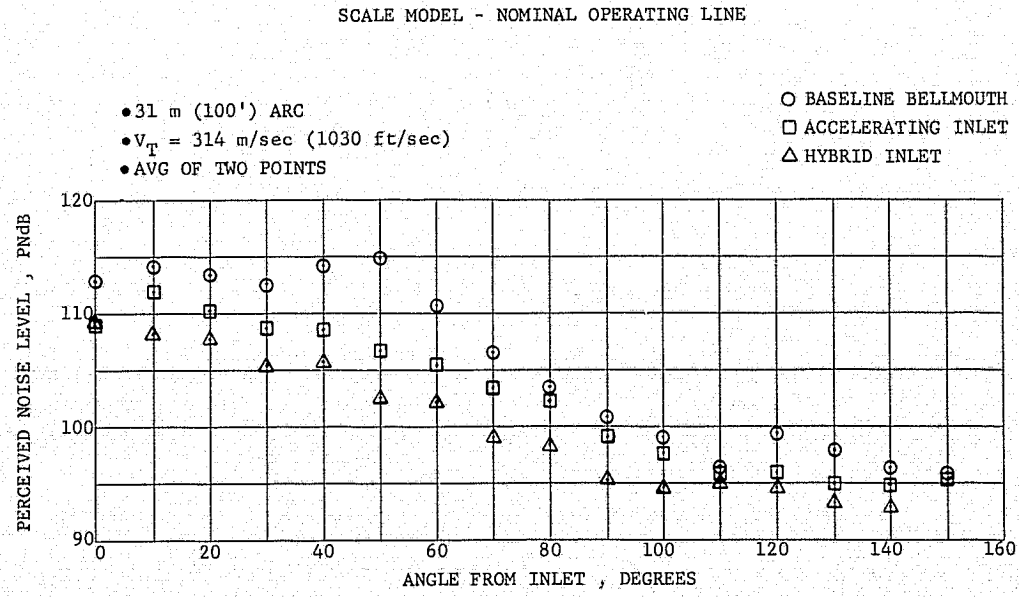

Figure 79. Scale-Model PNL Directivity at Approach, M_{TH} = 0.79 (Rear-Drive Test).

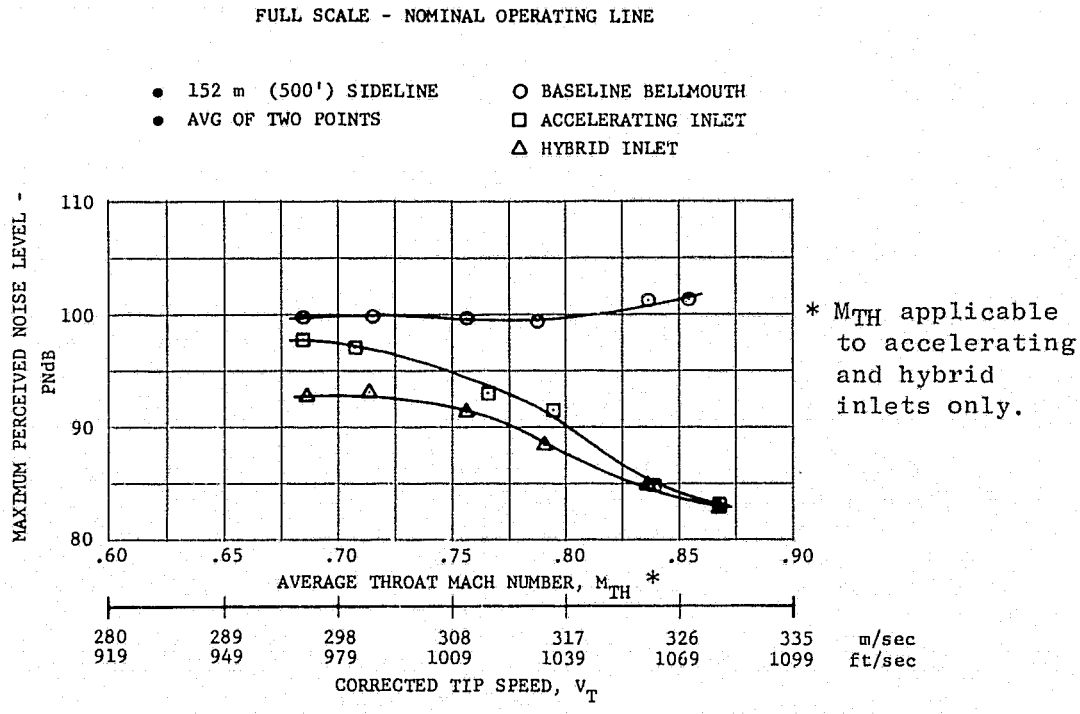

Figure 80. Maximum PNL Vs. Average Throat Mach Number, at Approach (Rear-Drive Test).

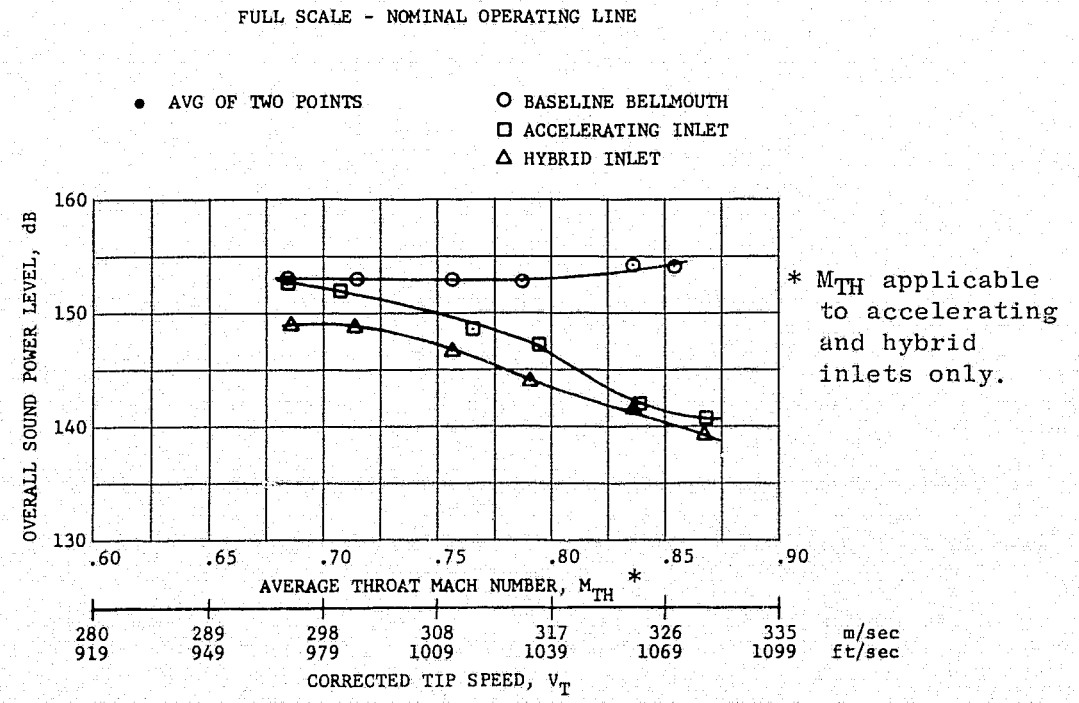

Figure 81. Overall Power Level Vs. Average Throat Mach Number, at Approach (Rear-Drive Test).

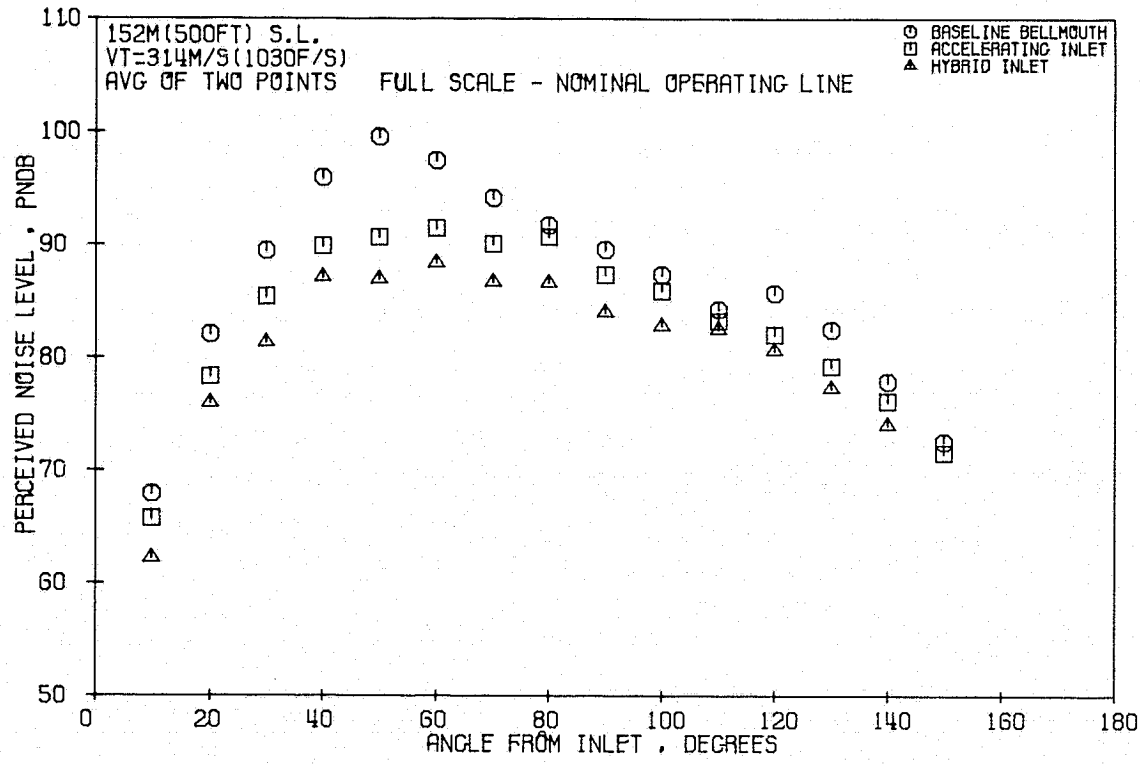

Figure 82. PNL Directivity at Approach, M_{TH} = 0.79 (Rear-Drive Test).

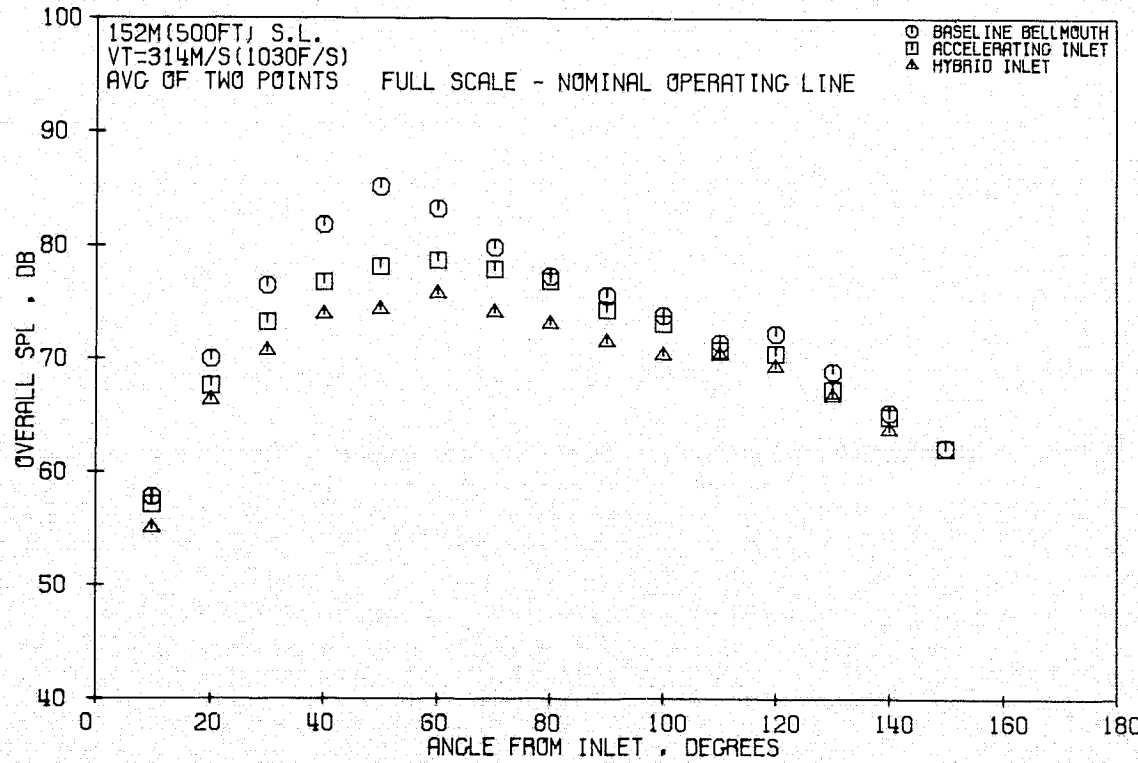

Figure 83. Variation of OASPL with Inlet Angle at Approach, M_{TH} = 0.79 (Rear-Drive Test).

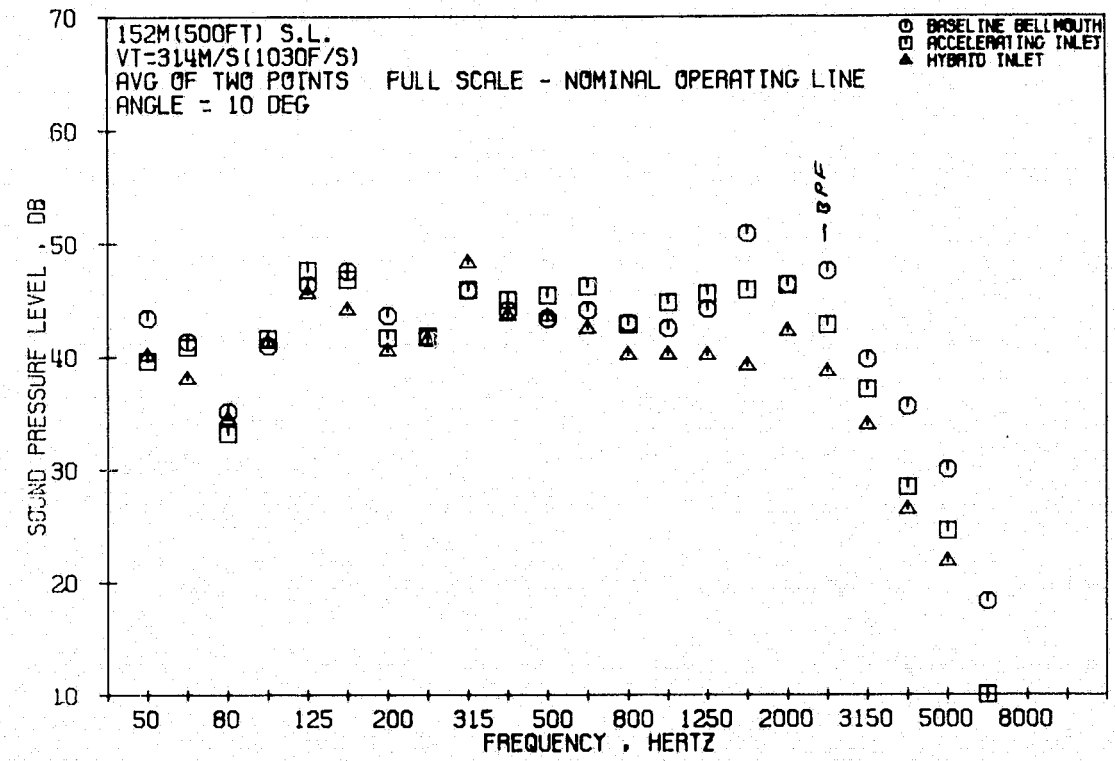

Figure 84. 1/3-Octave Spectral Comparisons at Approach, M_{TH} = 0.79, 10° Angle (Rear-Drive Test).

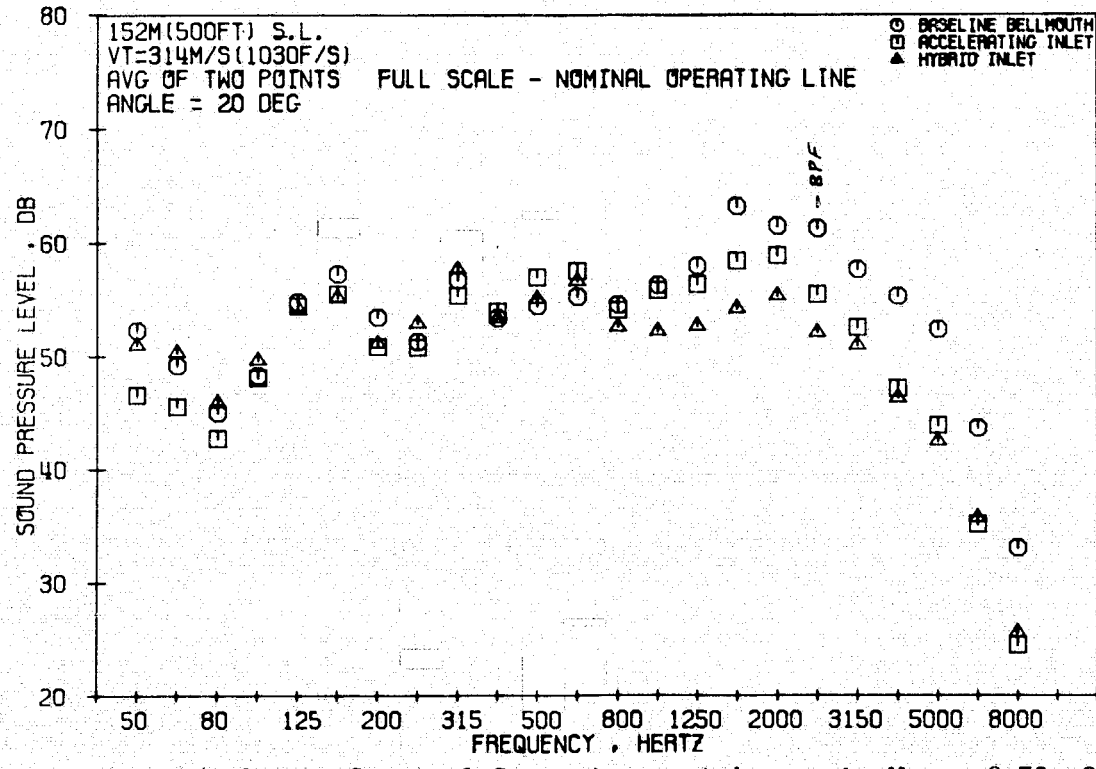

Figure 85. 1/3-Octave Spectral Comparisons at Approach, M_{TH} = 0.79, 20° Angle (Rear-Drive Test).

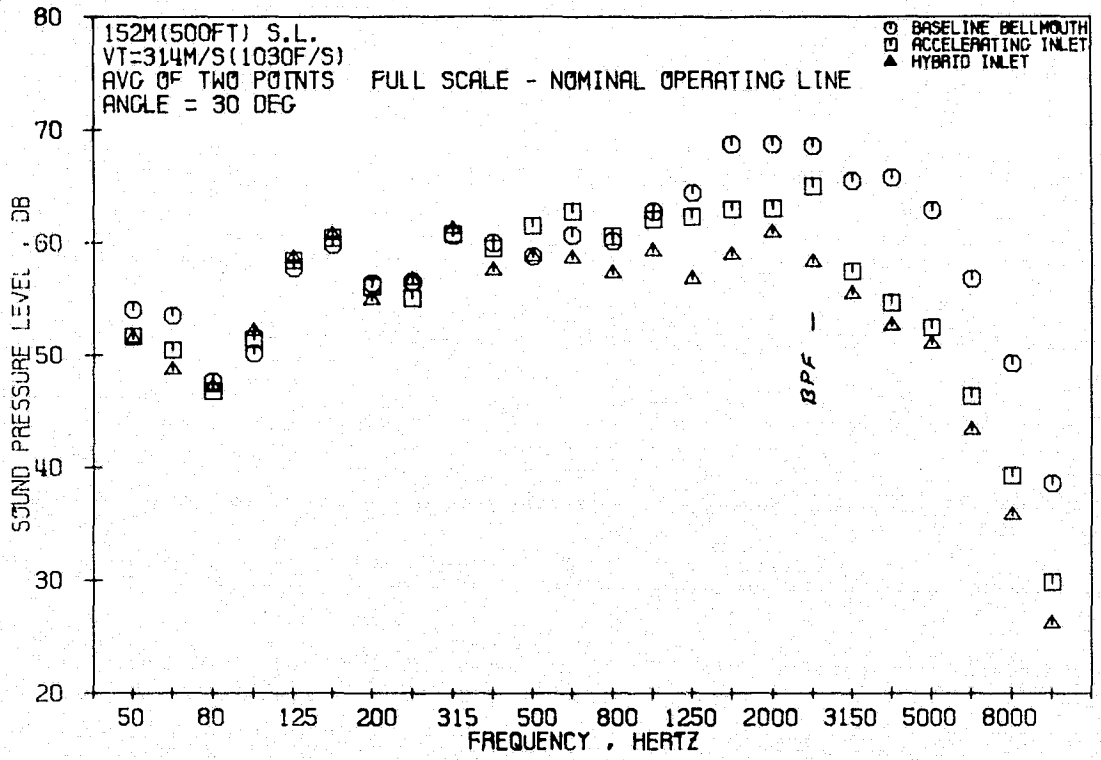

Figure 86. 1/3-Octave Spectral Comparisons at Approach, M_{TH} = 0.79, 30° Angle (Rear-Drive Test).

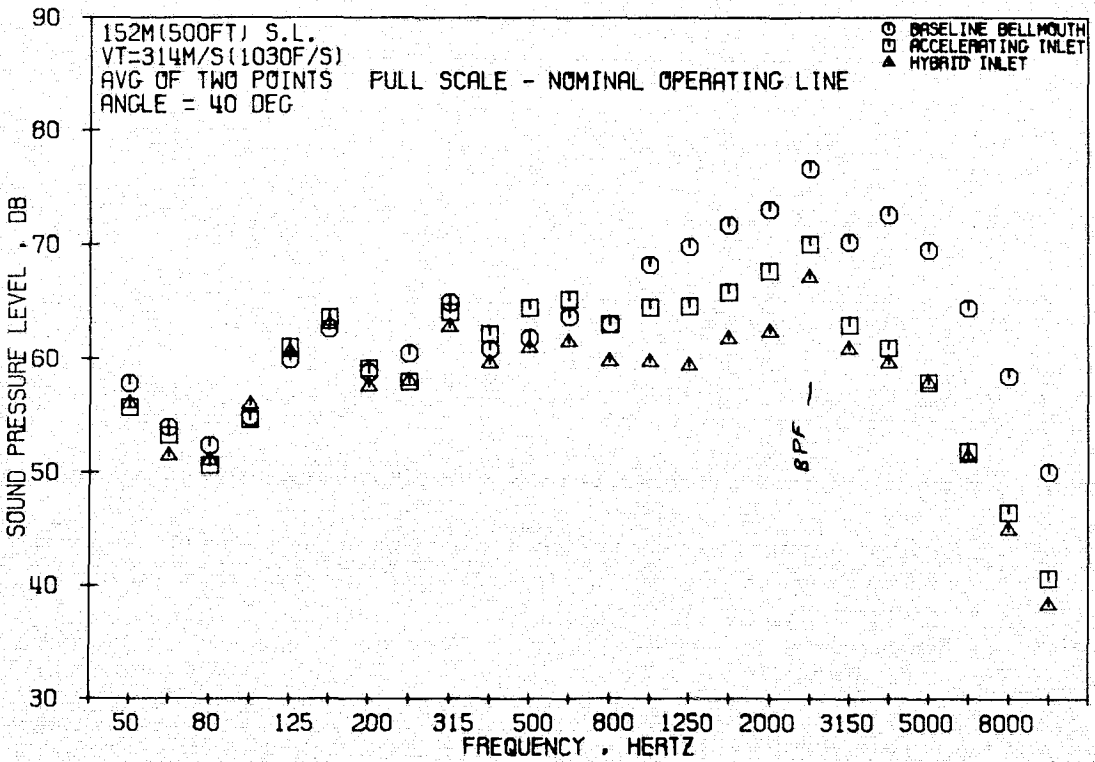

Figure 87. 1/3-Octave Spectral Comparisons at Approach, M_{TH} = 0.79, 40° Angle (Rear-Drive Test).

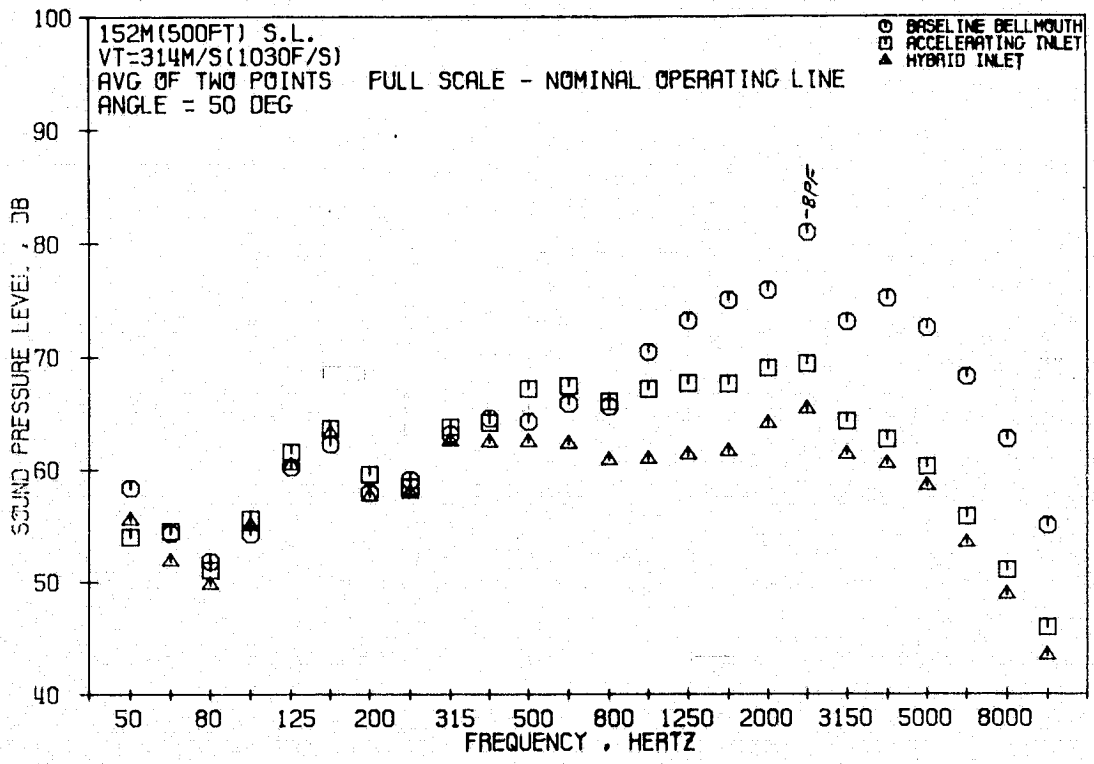

Figure 88. 1/3-Octave Spectral Comparisons at Approach, M_{TH} = 0.79, 50° Angle (Rear-Drive Test).

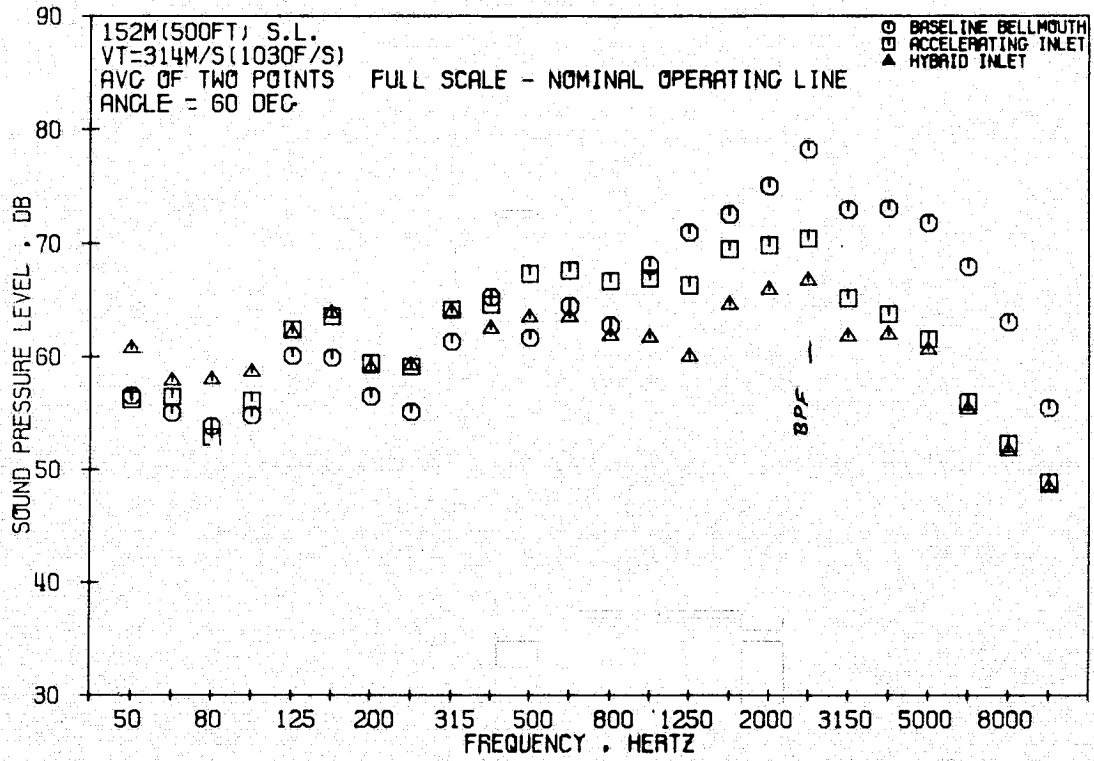

Figure 89. 1/3-Octave Spectral Comparisons at Approach, M_{TH} = 0.79, 60° Angle (Rear-Drive Test).

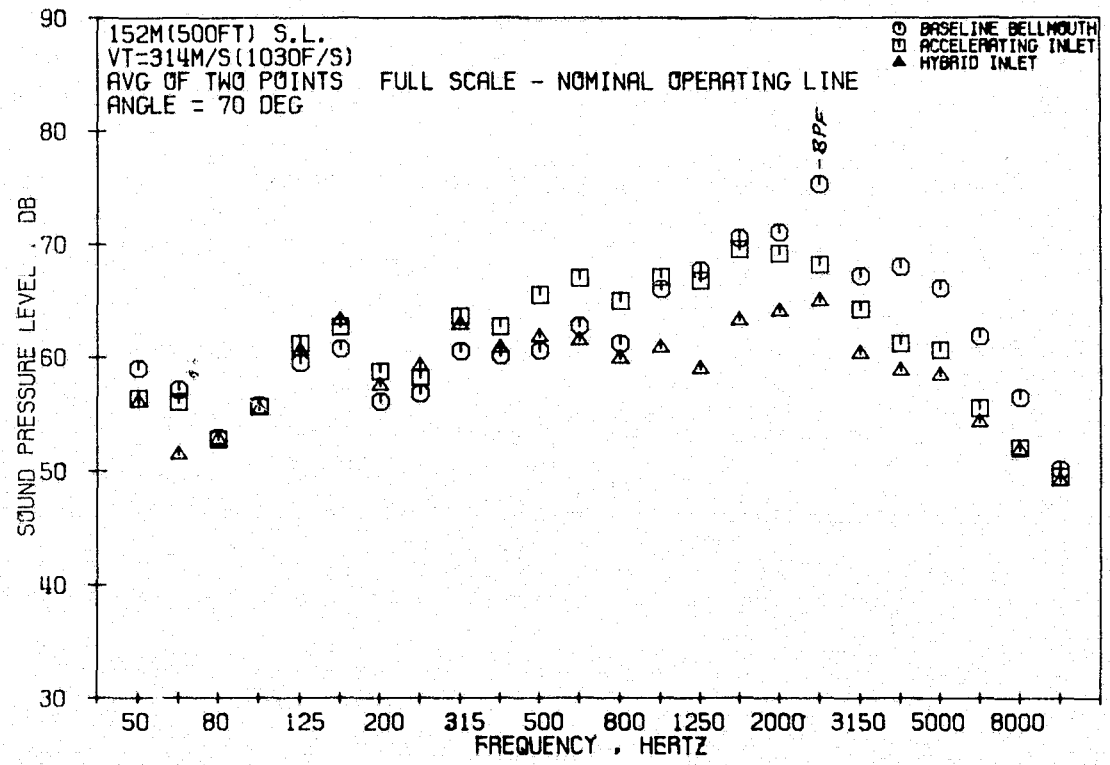

Figure 90. 1/3-Octave Spectral Comparisons at Approach, M_{TH} = 0.79, 70° Angle (Rear-Drive Test).

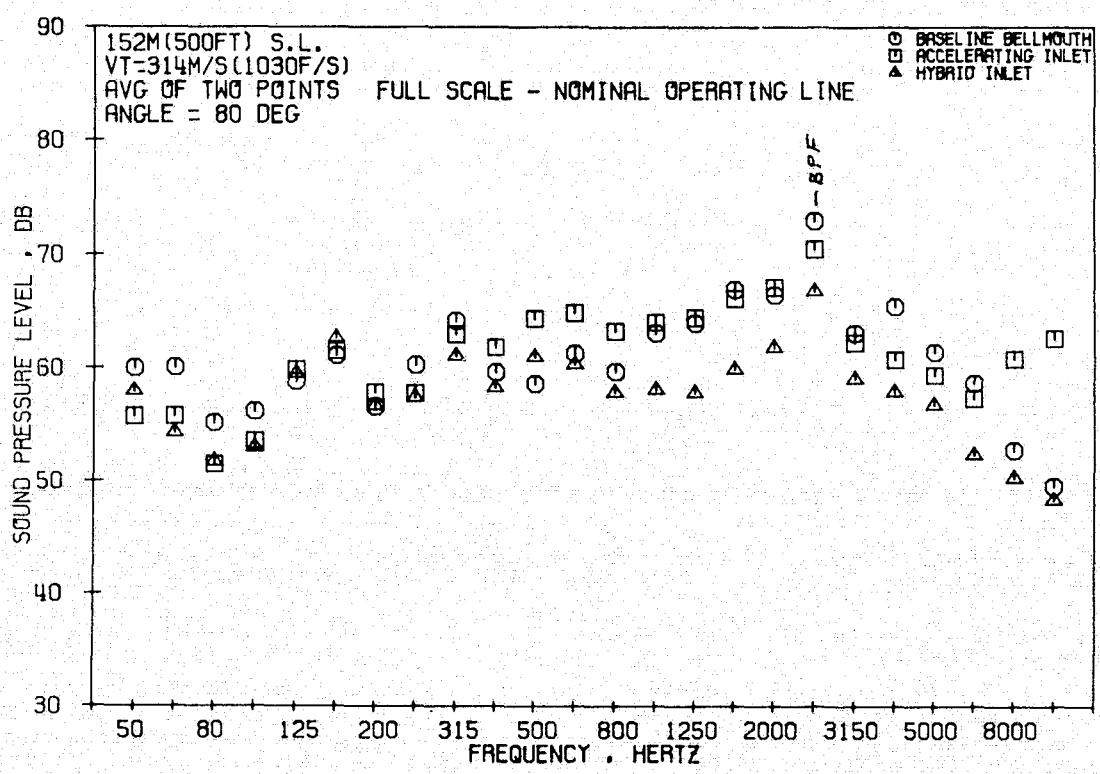

Figure 91. 1/3-Octave Spectral Comparisons at Approach, M_{TH} = 0.79, 80° Angle (Rear-Drive Test).

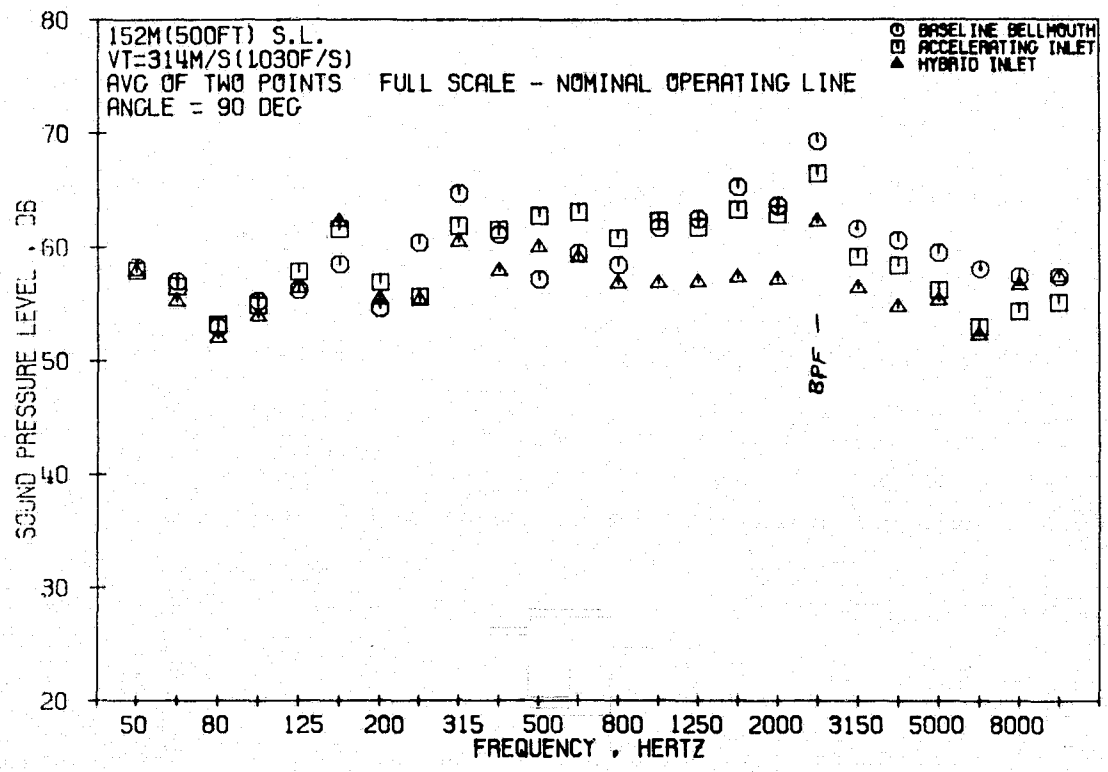

Figure 92. 1/3-Octave Spectral Comparisons at Approach, M_{TH} = 0.79, 90° Angle (Rear-Drive Test).

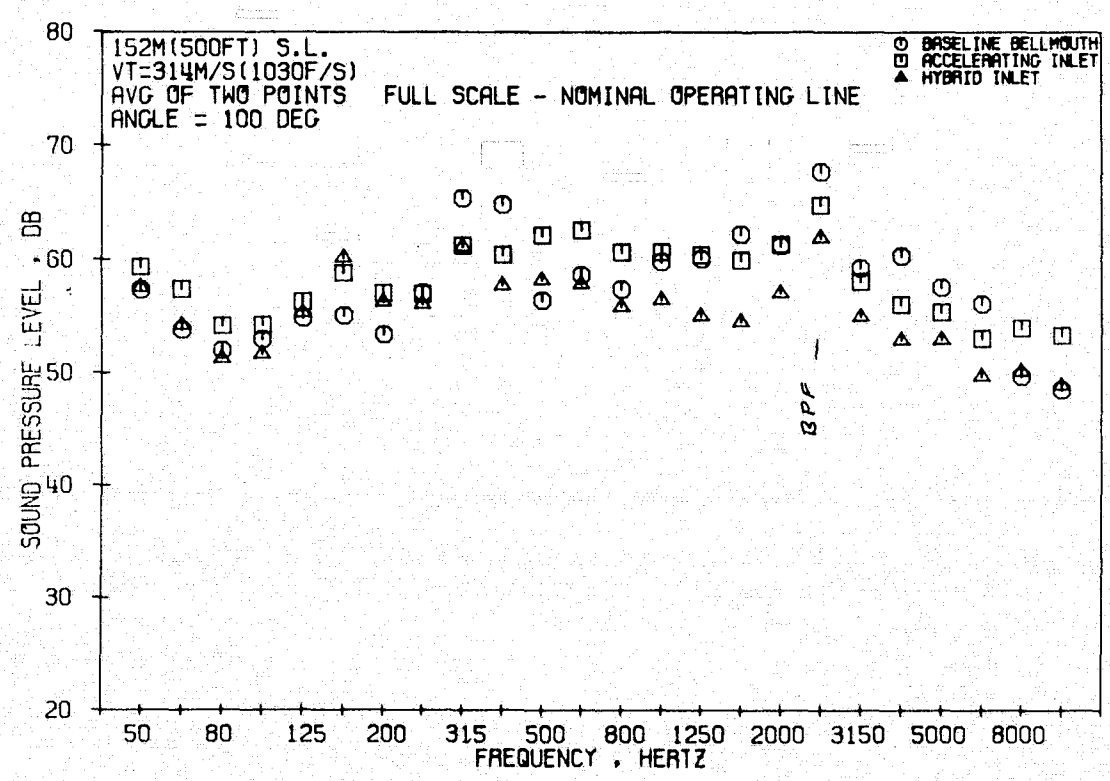

Figure 93. 1/3-Octave Spectral Comparisons at Approach, M_{TH} = 0.79, 100° Angle (Rear-Drive Test).

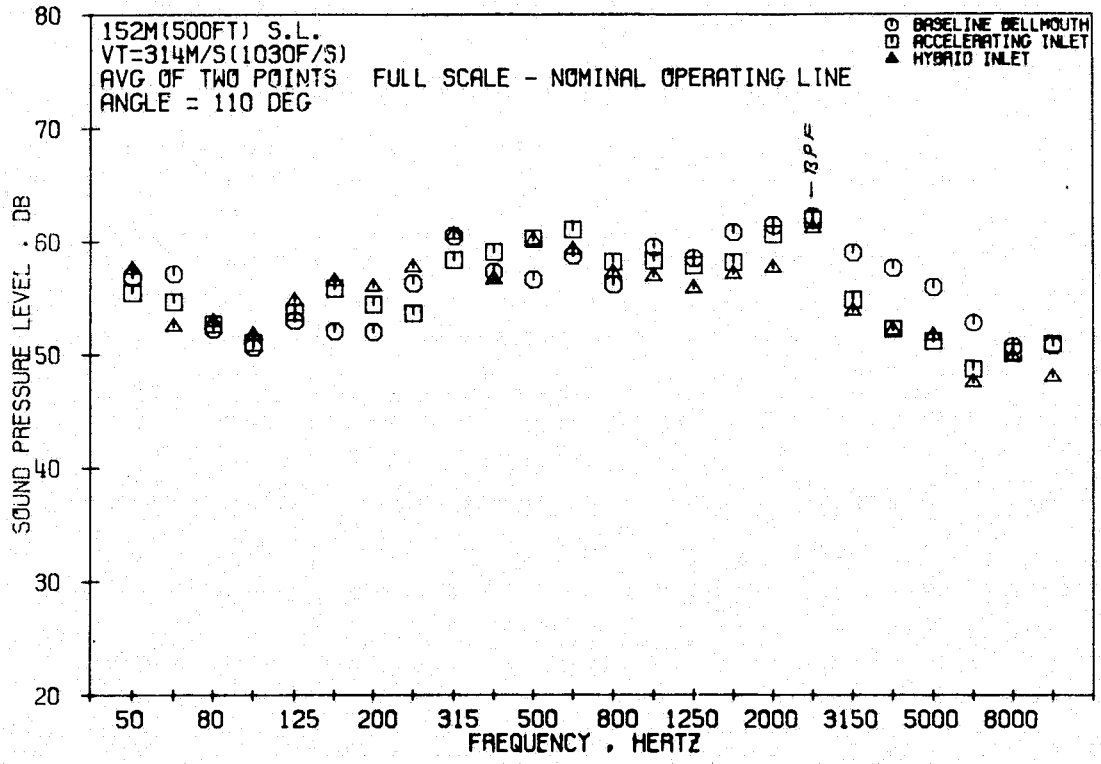

Figure 94. 1/3-Octave Spectral Comparisons at Approach, M_{TH} = 0.79, 110° Angle (Rear-Drive Test).

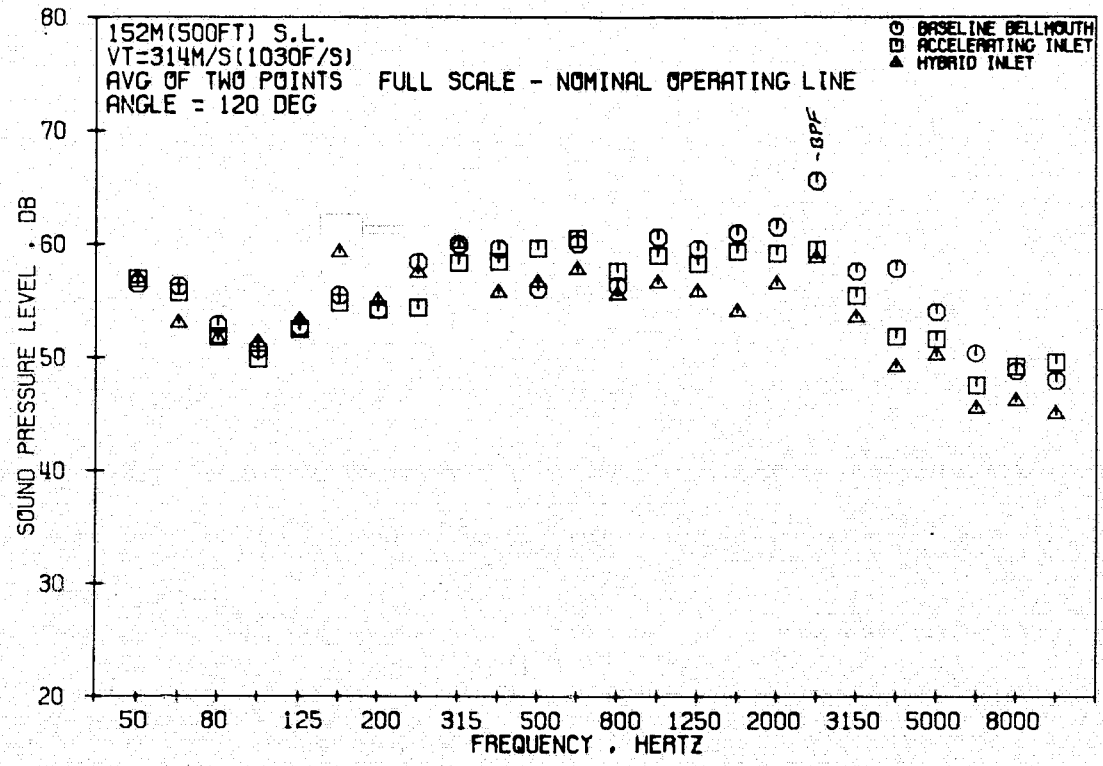

Figure 95. 1/3-Octave Spectral Comparisons at Approach, M_{TH} = 0.79, 120° Angle (Rear-Drive Test).

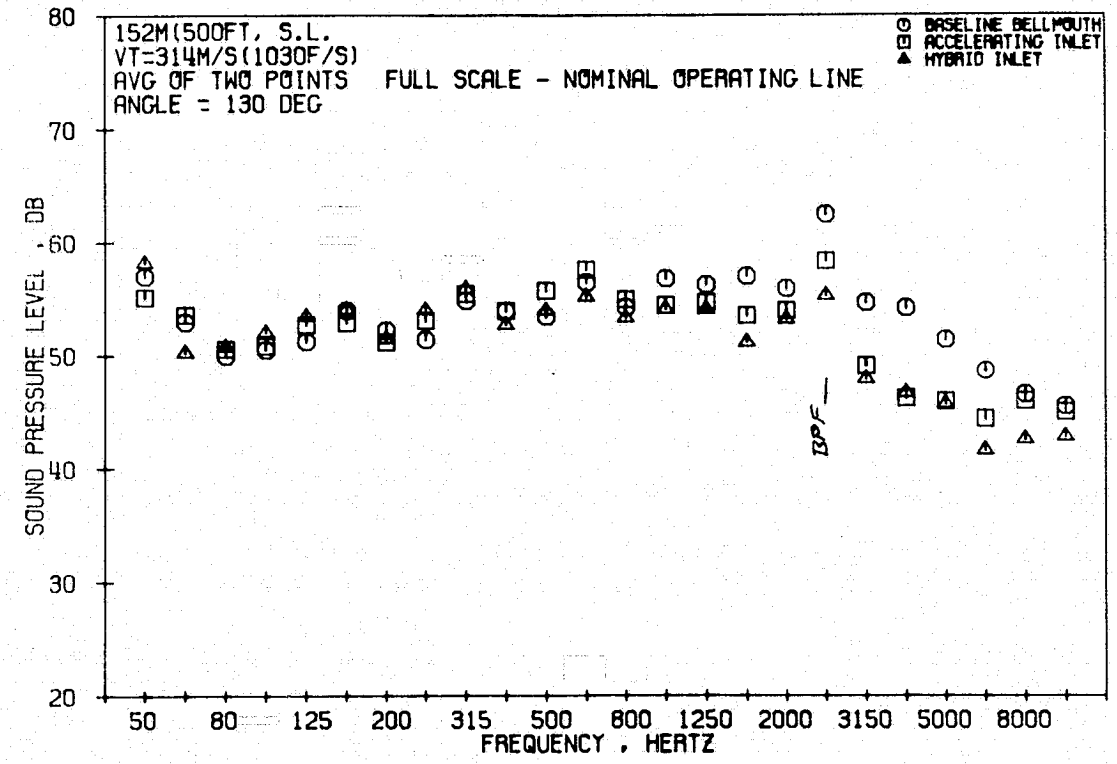

Figure 96. 1/3-Octave Spectral Comparisons at Approach, M_{TH} = 0.79, 130° Angle (Rear-Drive Test).

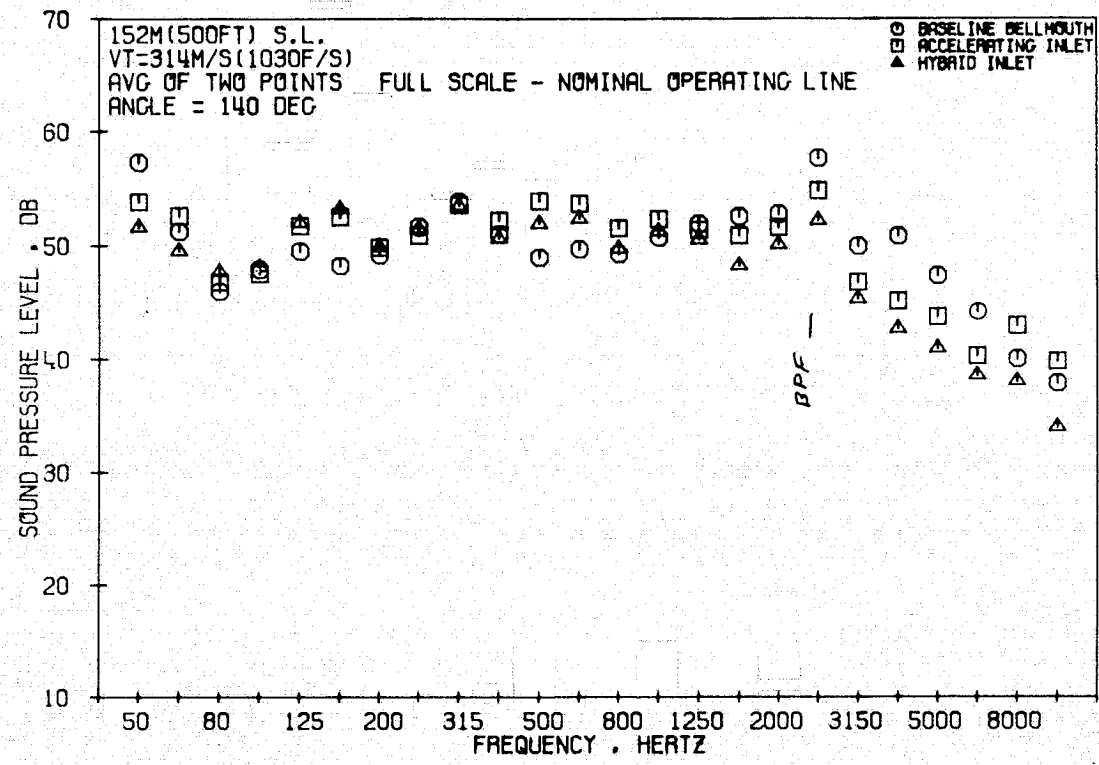

Figure 97. 1/3-Octave Spectral Comparisons at Approach, M_{TH} = 0.79, 140° Angle (Rear-Drive Test).

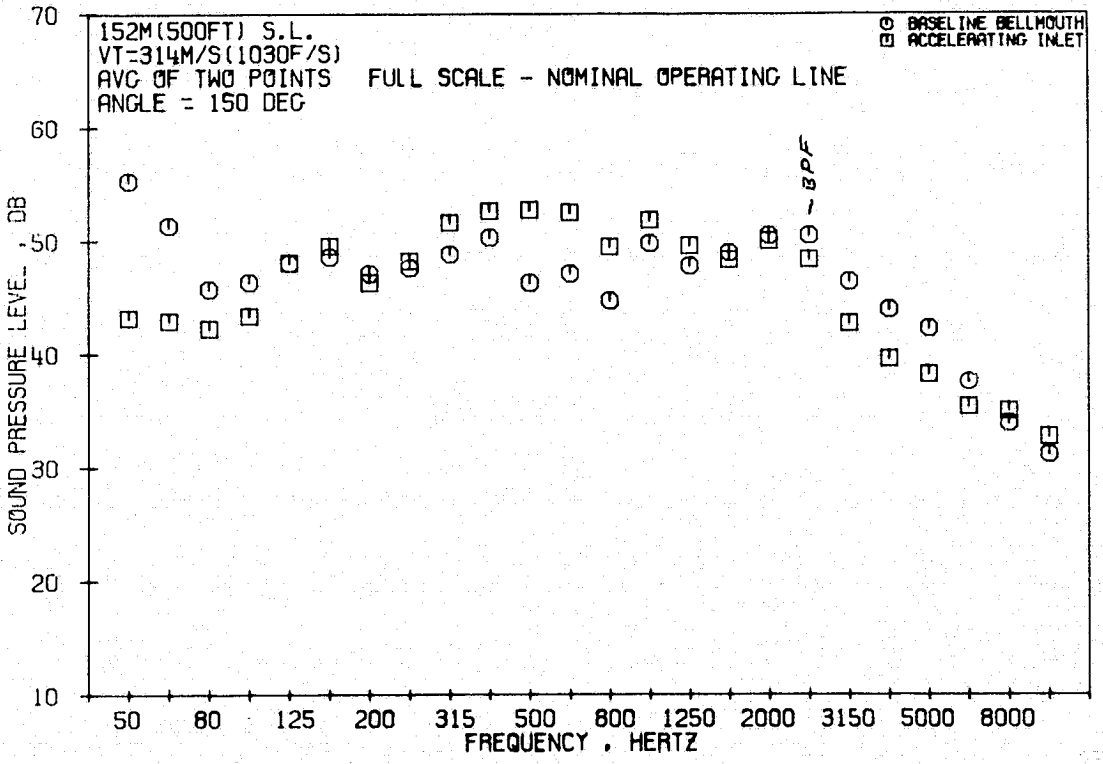

Figure 98. 1/3-Octave Spectral Comparisons at Approach, M_{TH} = 0.79, 150° Angle (Rear-Drive Test).

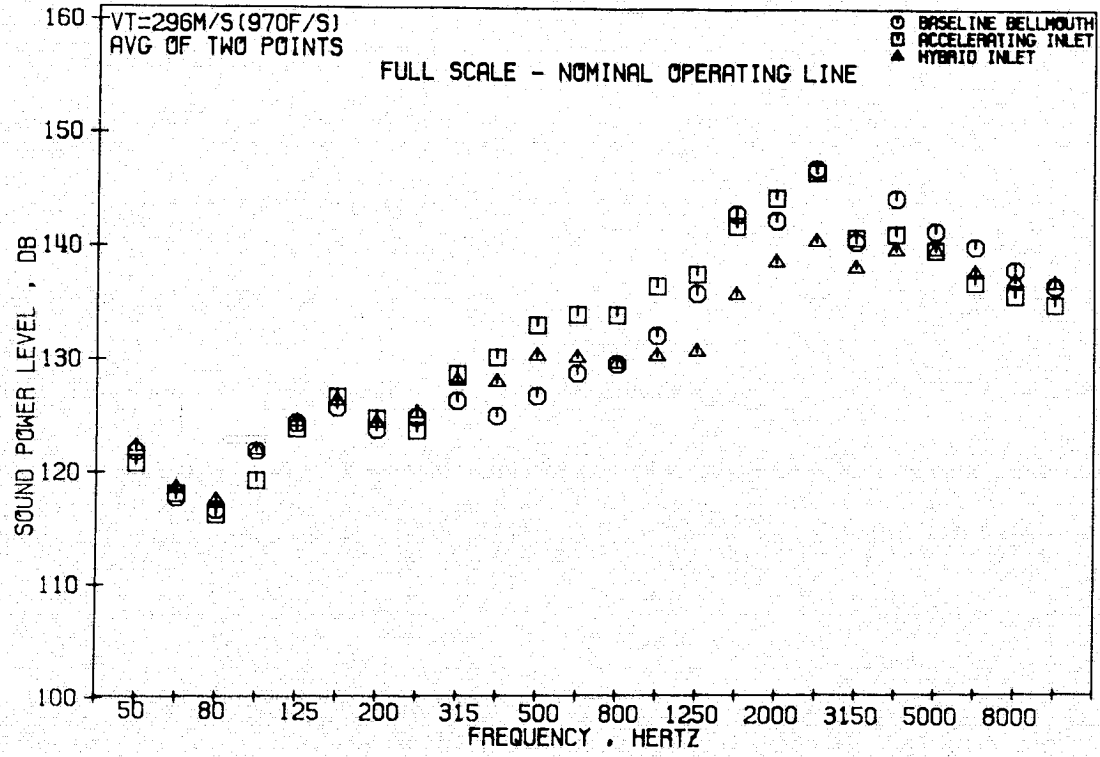

Figure 99. 1/3-Octave PWL Comparisons at Approach, M_{TH} = 0.68 (Rear-Drive Test).

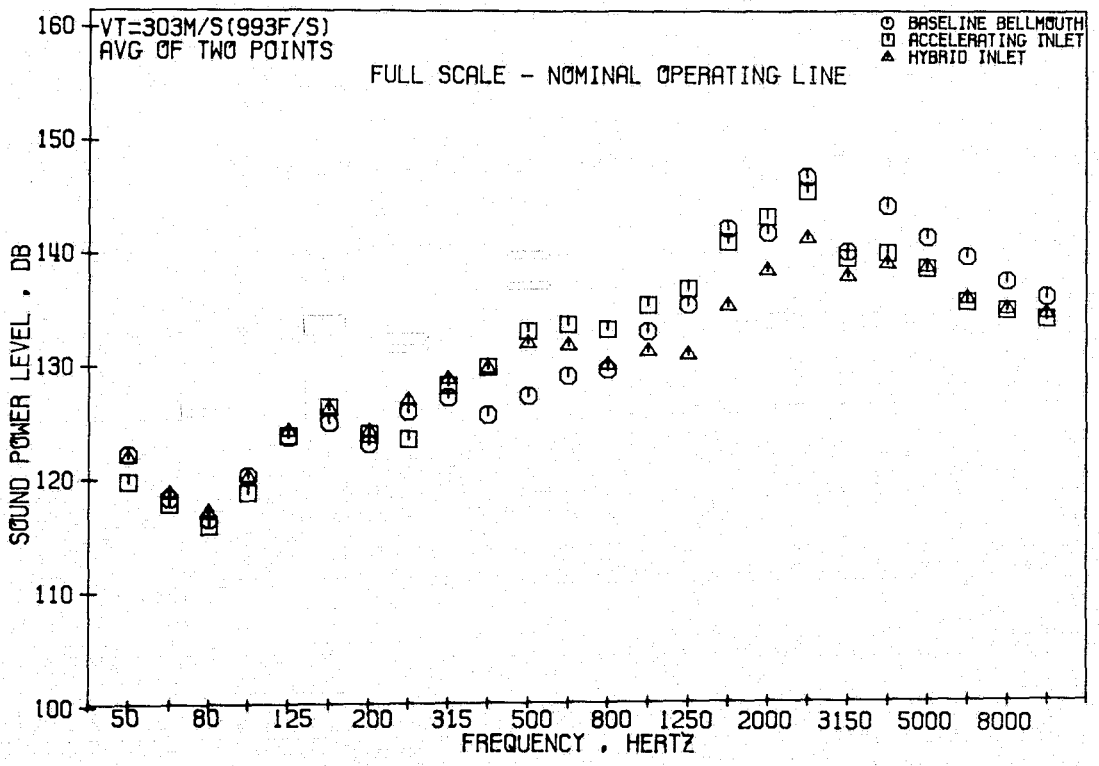

Figure 100. 1/3-Octave PWL Comparisons at Approach, M_{TH} = 0.71 (Rear-Drive Test).

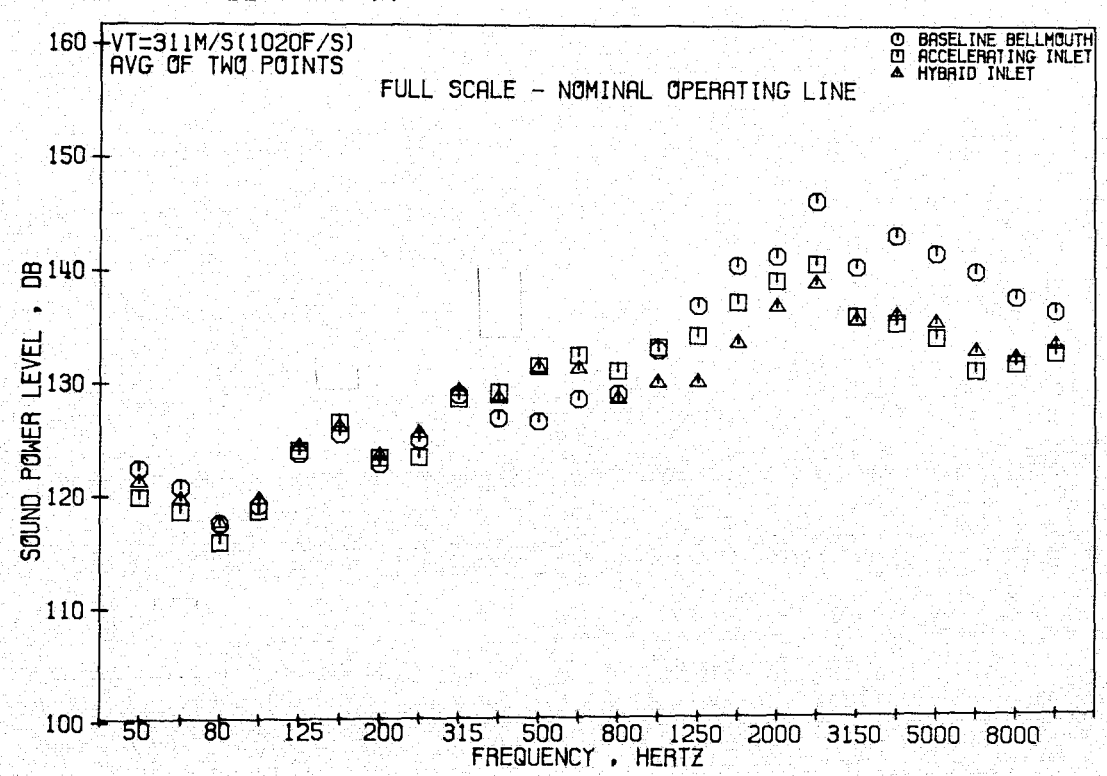

Figure 101. 1/3-Octave PWL Comparisons at Approach, M_{TH} = 0.76 (Rear-Drive Test).

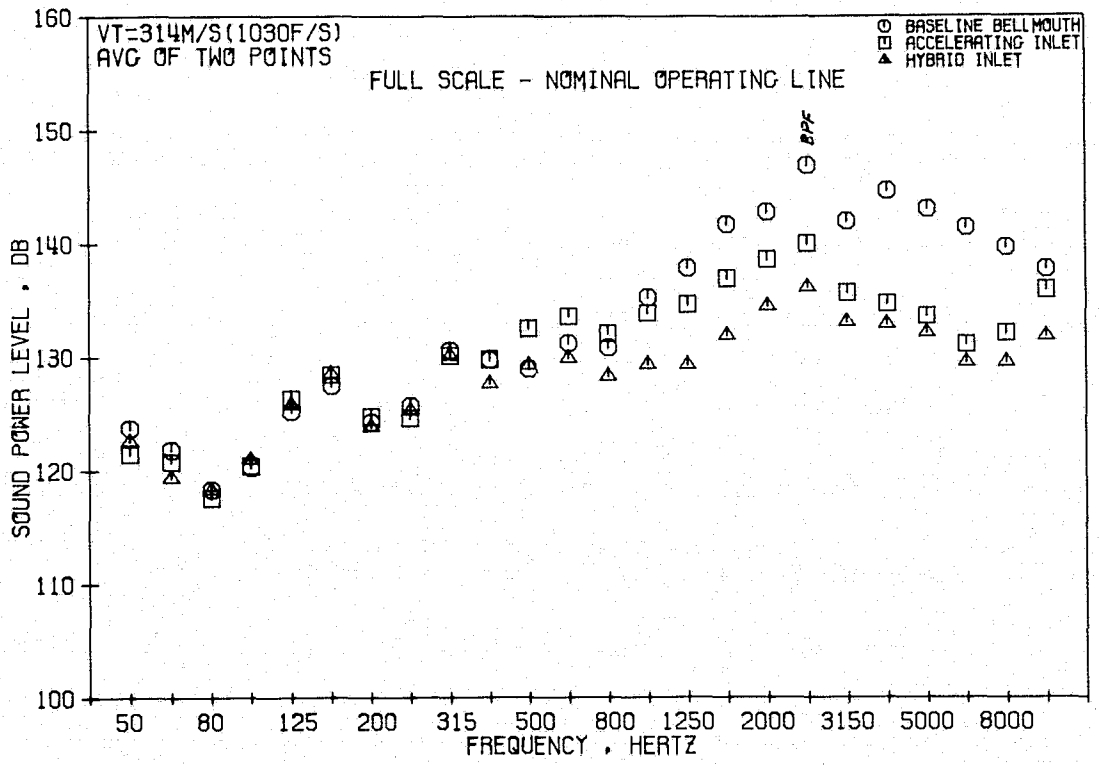

Figure 102. 1/3-Octave PWL Comparisons at Approach, M_{TH} = 0.79 (Rear-Drive Test).

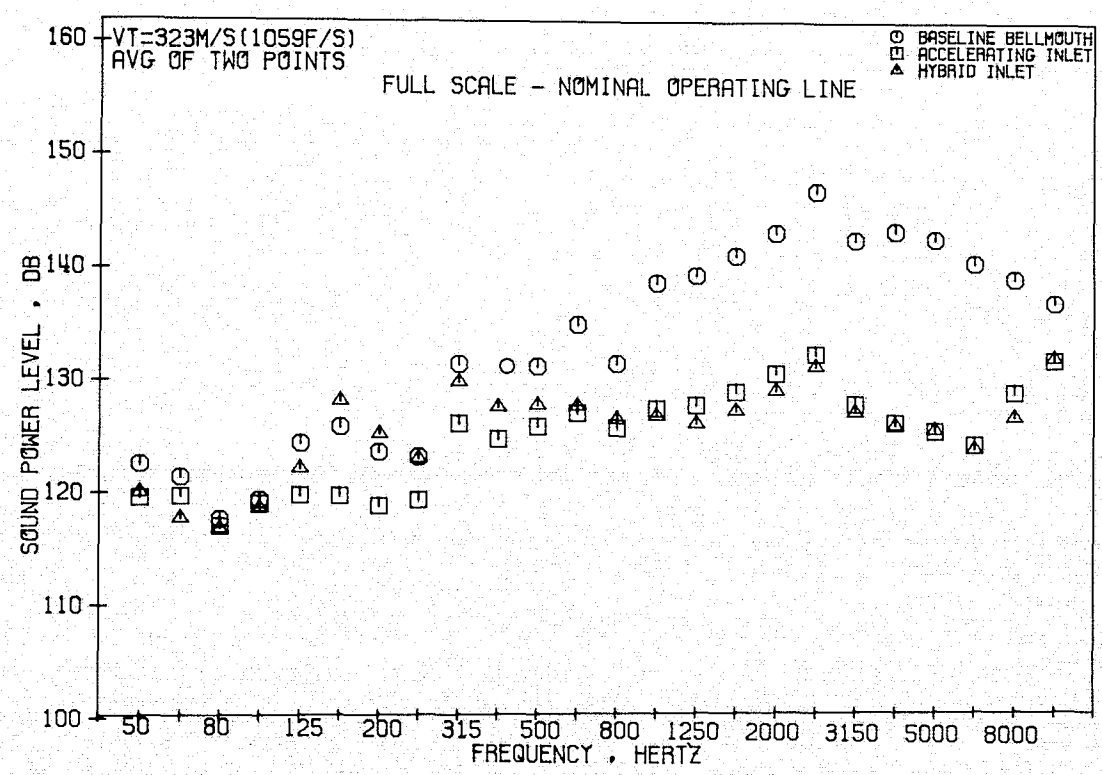

Figure 103. 1/3-Octave PWL Comparisons at Approach, M_{TH} = 0.84 (Rear-Drive Test).

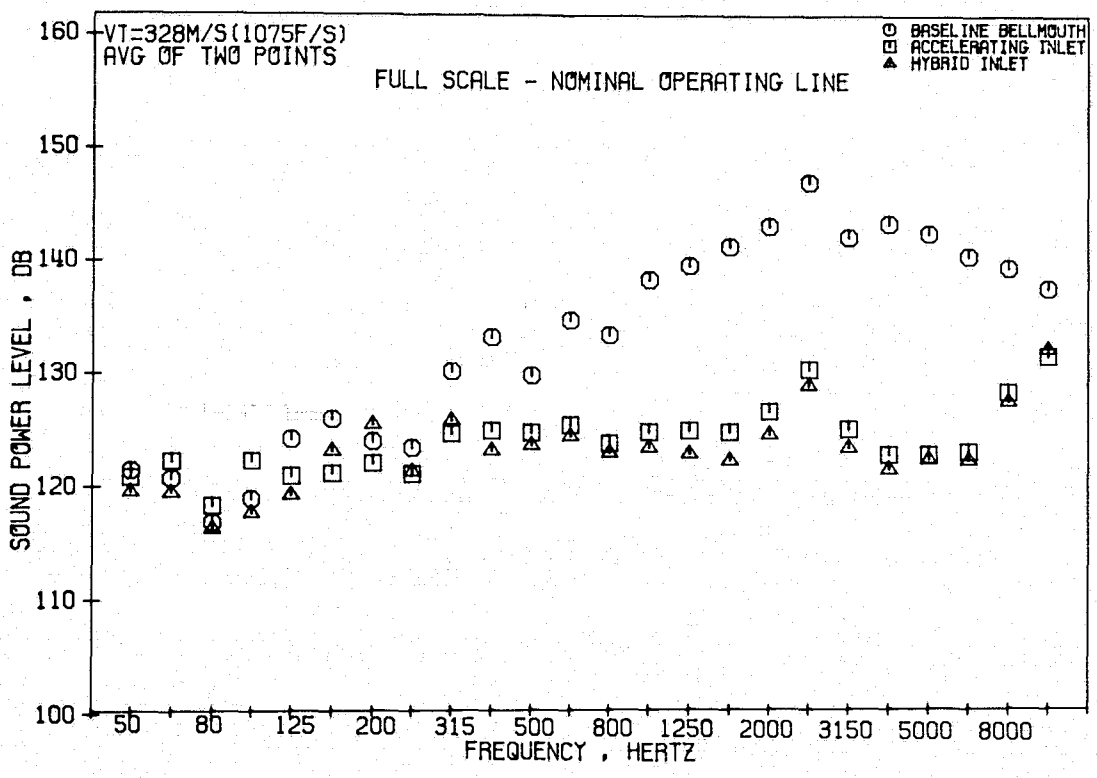

Figure 104. 1/3-Octave PWL Comparisons at Approach, M_{TH} = 0.90 (Rear-Drive Test).

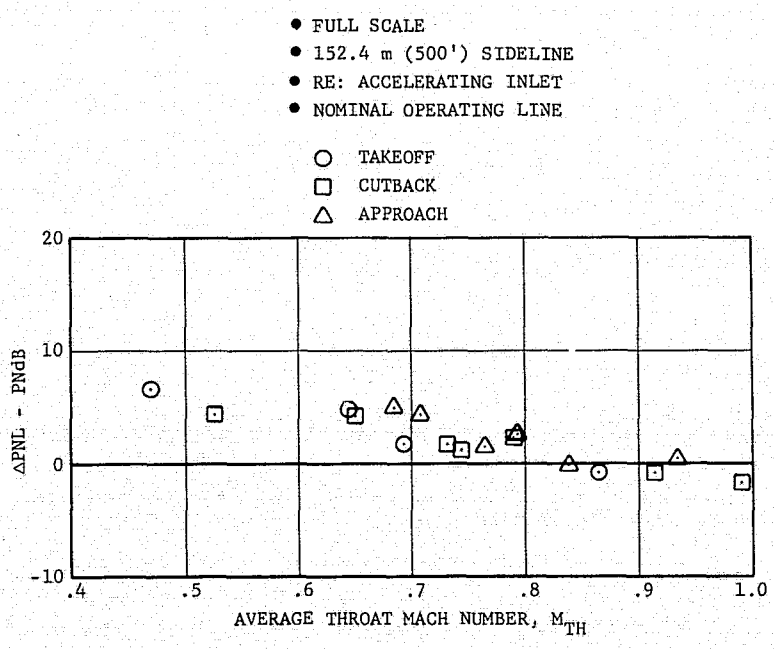

Figure 105. Inlet Suppression Due to Treatment Effectiveness Vs. Average Throat Mach Number (Rear-Drive Test).

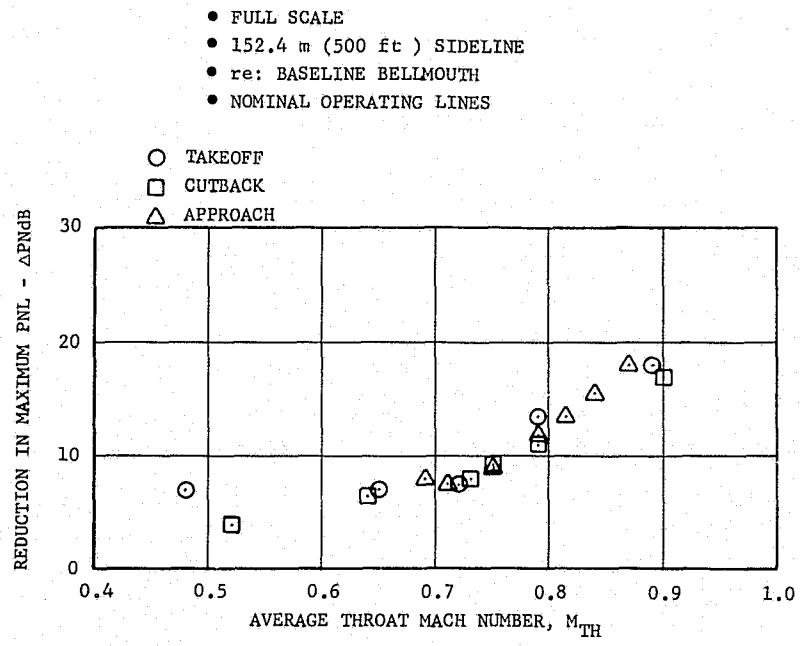

Figure 106. Total Hybrid-Inlet Suppression Vs. Average Throat Mach Number (Rear-Drive Test).

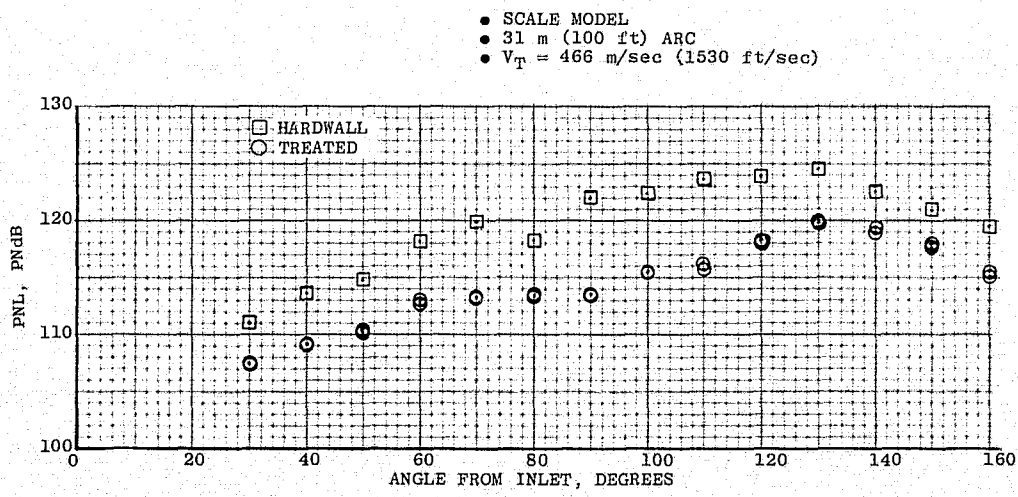

Figure 107. Scale-Model PNL Directivity at Takeoff (Front-Drive Test).

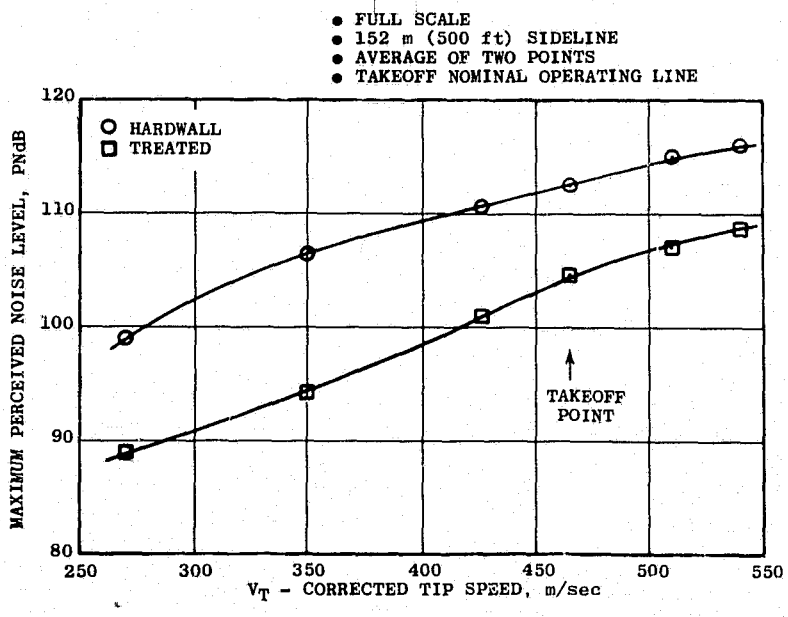

Figure 108. Maximum PNL Vs. Corrected Tip Speed at Takeoff (Front-Drive Test).

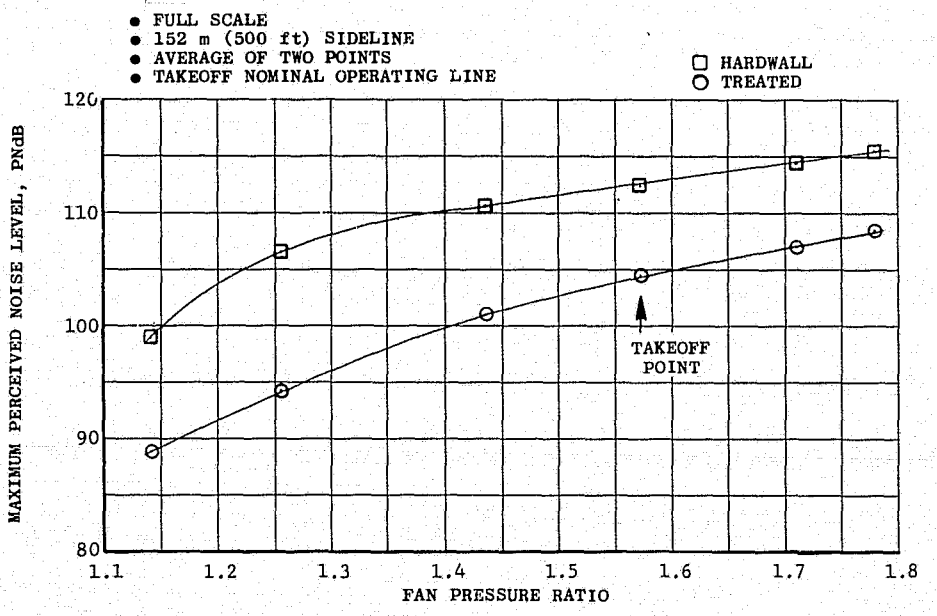

Figure 109. Maximum PNL Vs. Fan Pressure Ratio at Takeoff (Front-Drive Test).

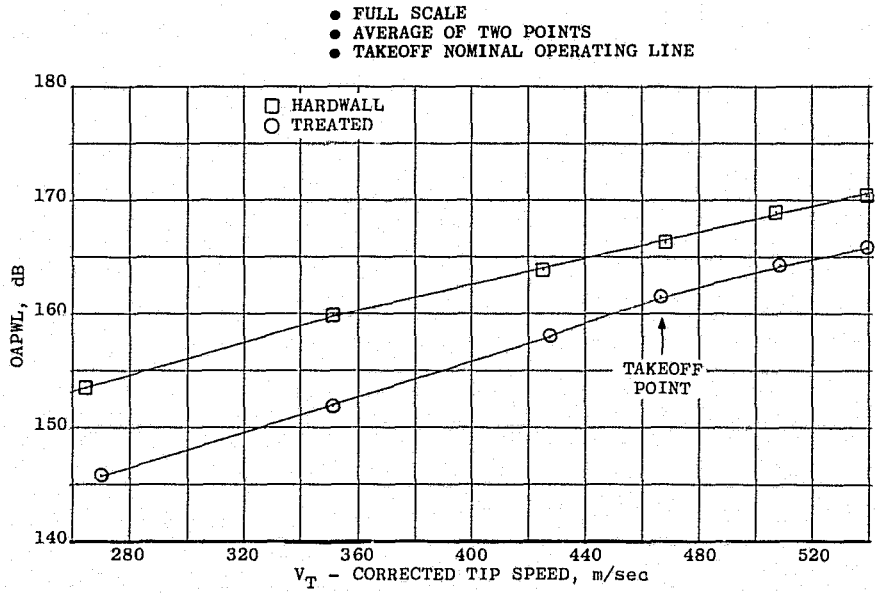

Figure 110. Overall Sound Power Level Vs. Corrected Tip Speed at Takeoff (Front-Drive Test).

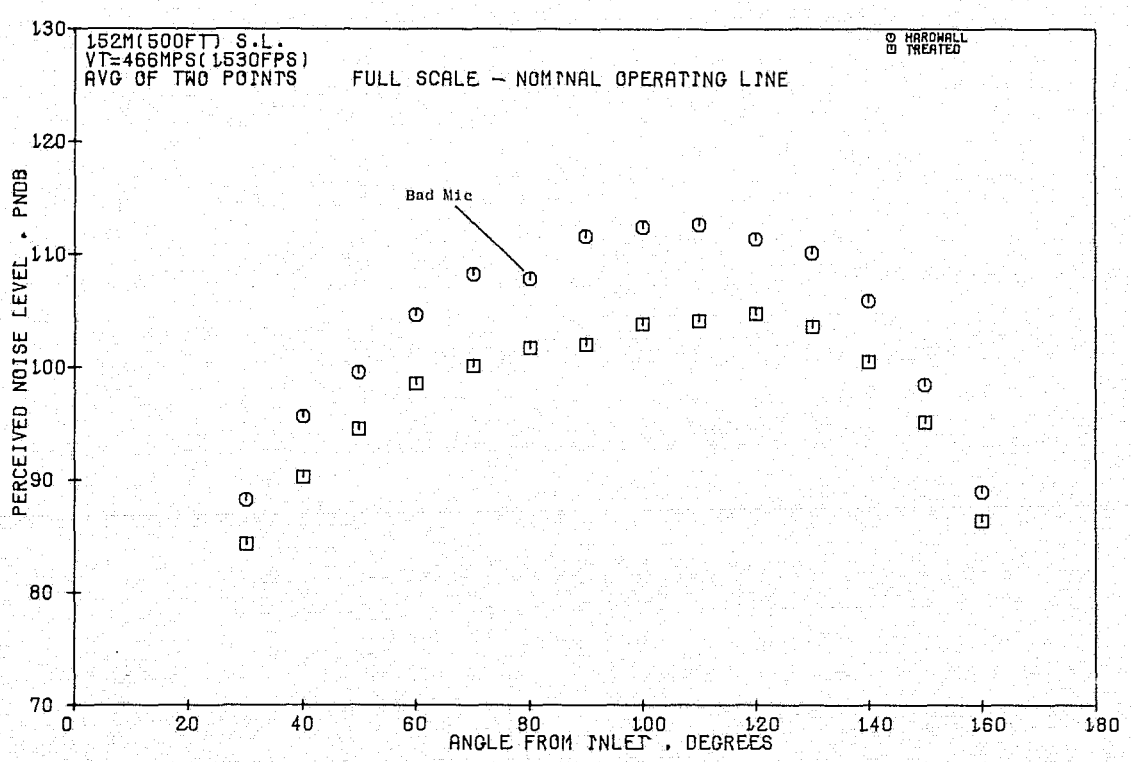

Figure 111. PNL Directivity at Takeoff (Front-Drive Test).

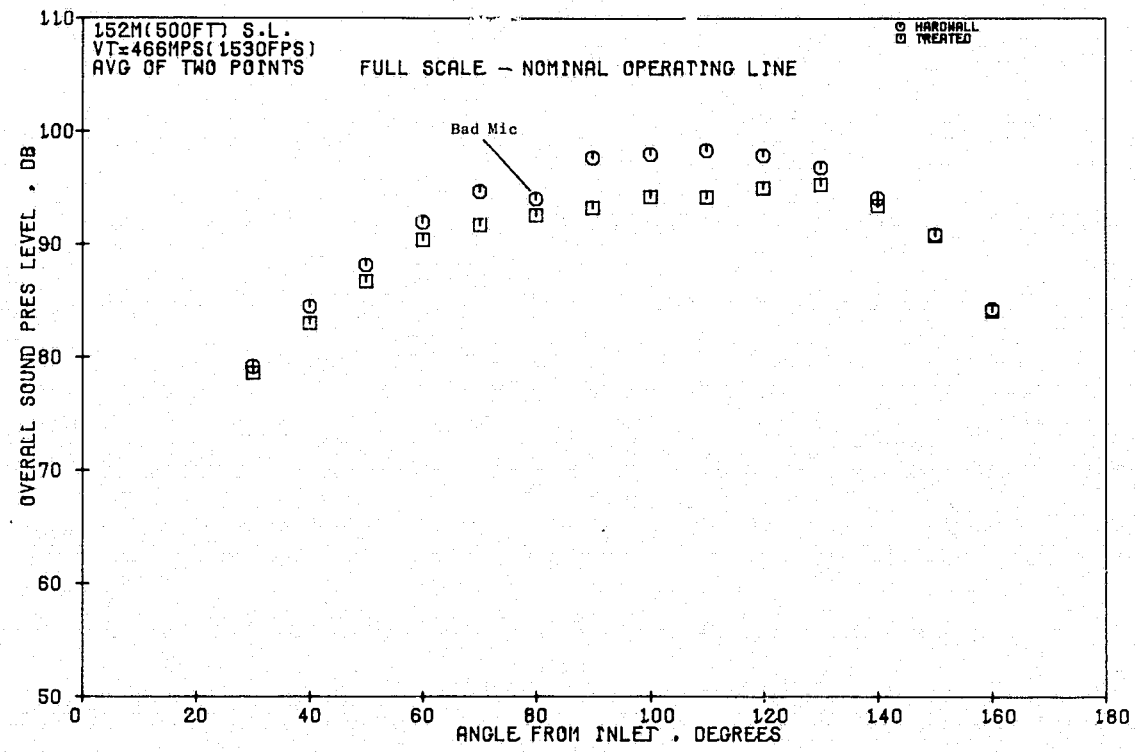

Figure 112. Variation of OASPL with Inlet Angle at Takeoff (Front-Drive Test).

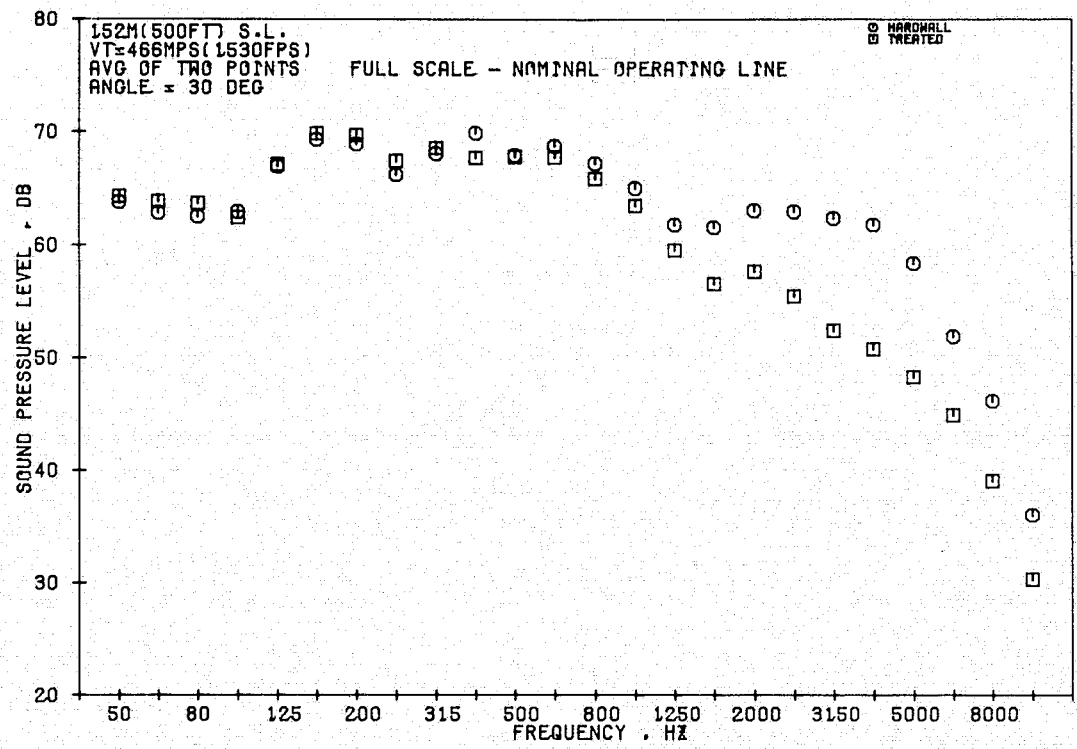

Figure 113. 1/3-Octave Spectra Comparisons at Takeoff, 30° Angle (Front-Drive Test).

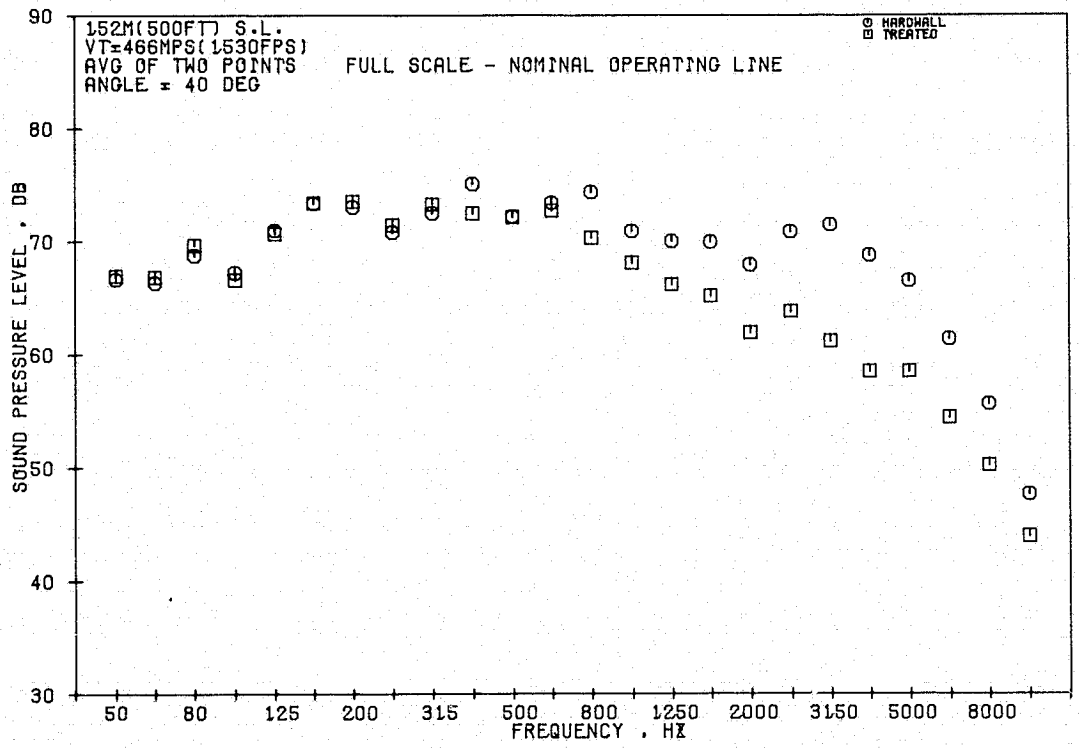

Figure 114. 1/3-Octave Spectra Comparisons at Takeoff, 40° Angle (Front-Drive Test).

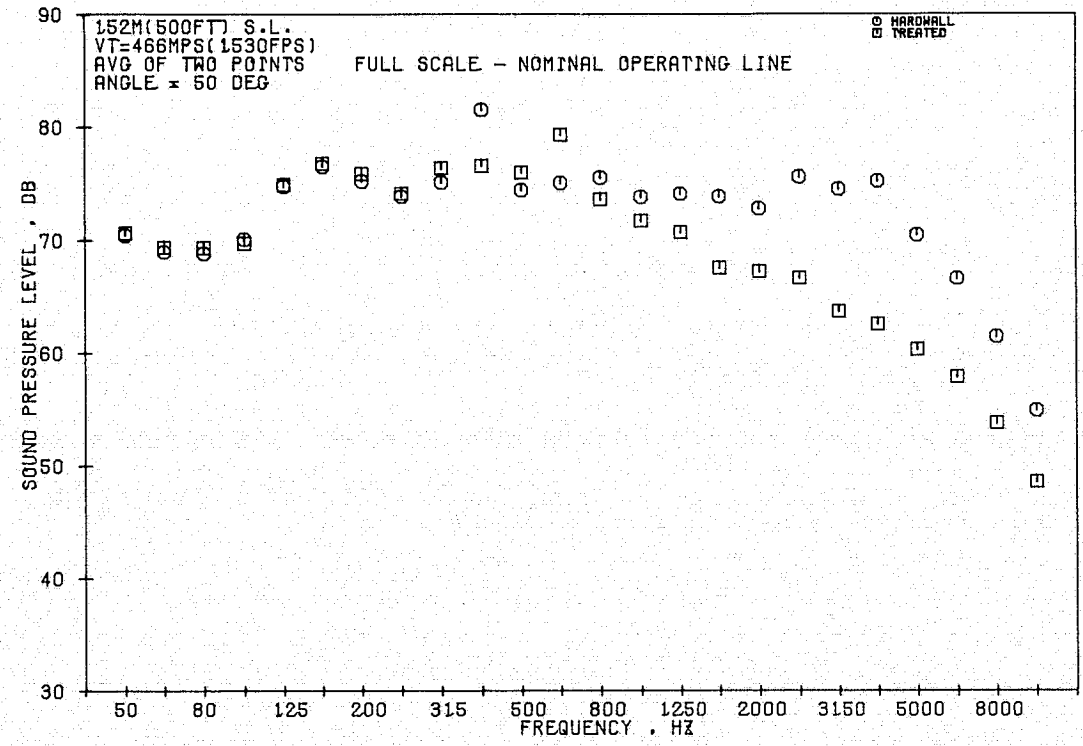

Figure 115. 1/3-Octave Spectra Comparisons at Takeoff, 50° Angle (Front-Drive Test).

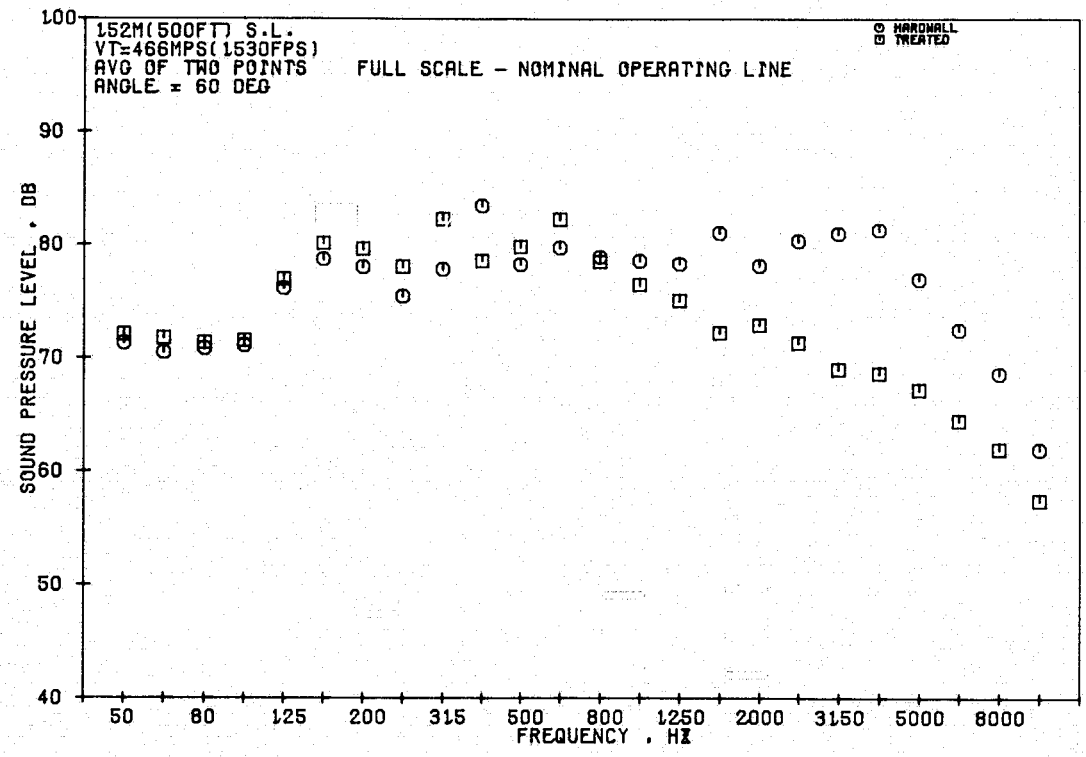

Figure 116. 1/3-Octave Spectra Comparisons at Takeoff, 60° Angle (Front-Drive Test).

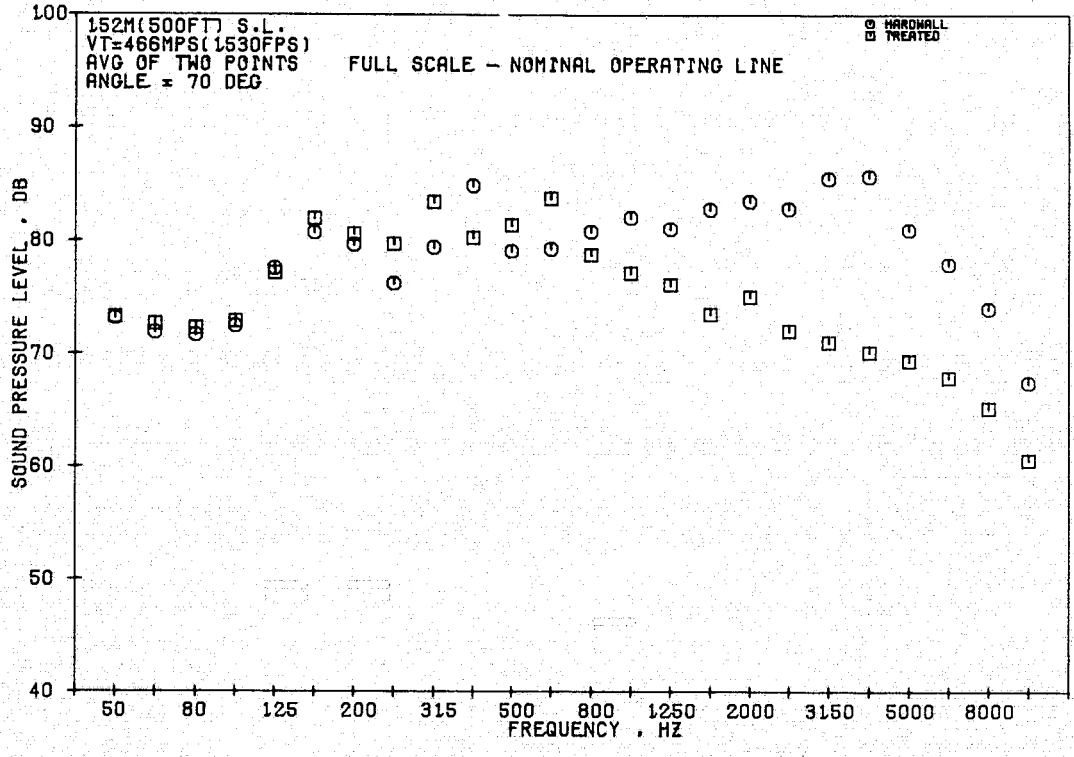

Figure 117. 1/3-Octave Spectra Comparisons at Takeoff, 70° Angle (Front-Drive Test).

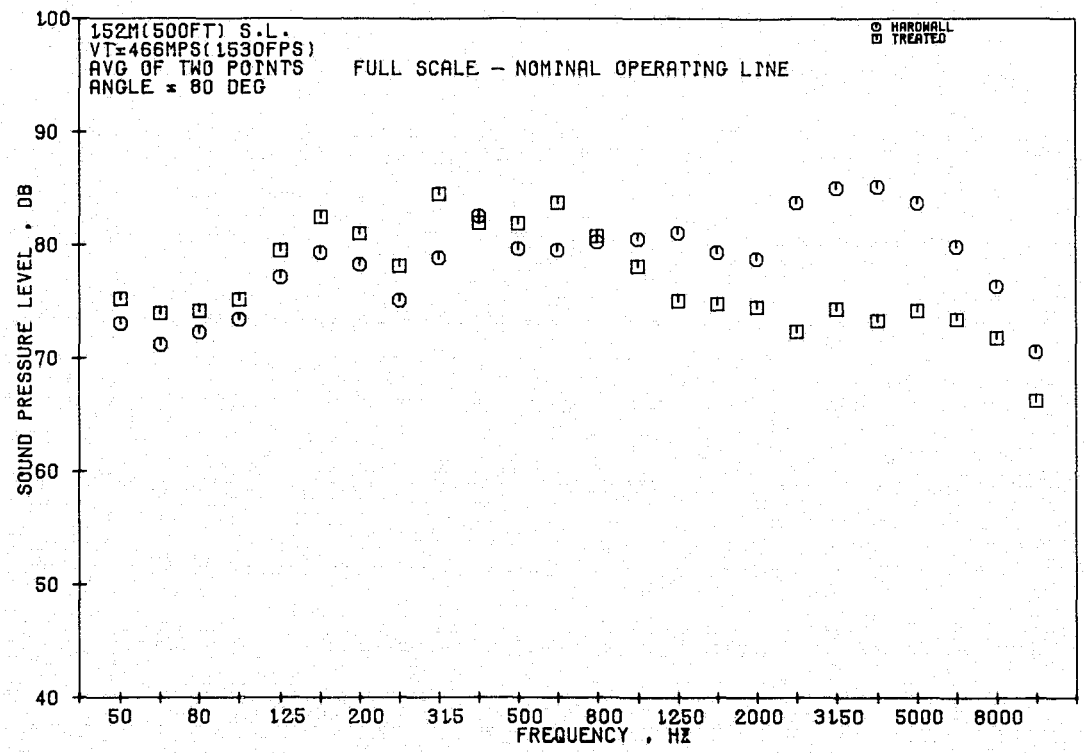

Figure 118. 1/3-Octave Spectra Comparisons at Takeoff, 80° Angle (Front-Drive Test).

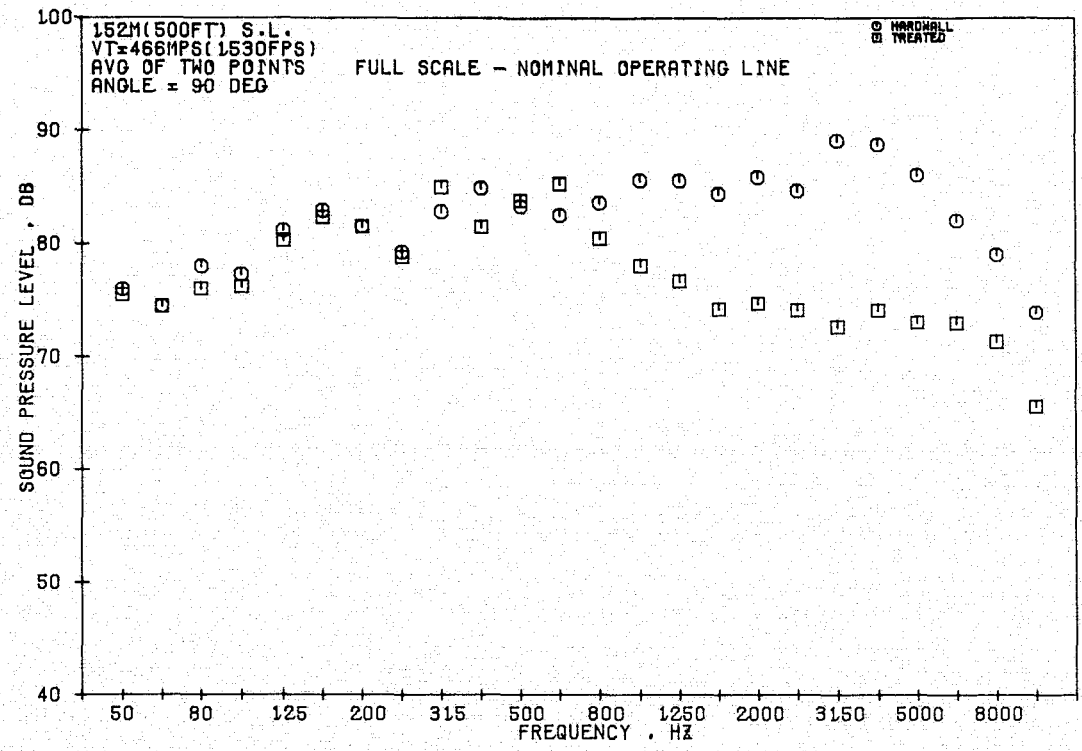

Figure 119. 1/3-Octave Spectra Comparisons at Takeoff, 90° Angle (Front-Drive Test).

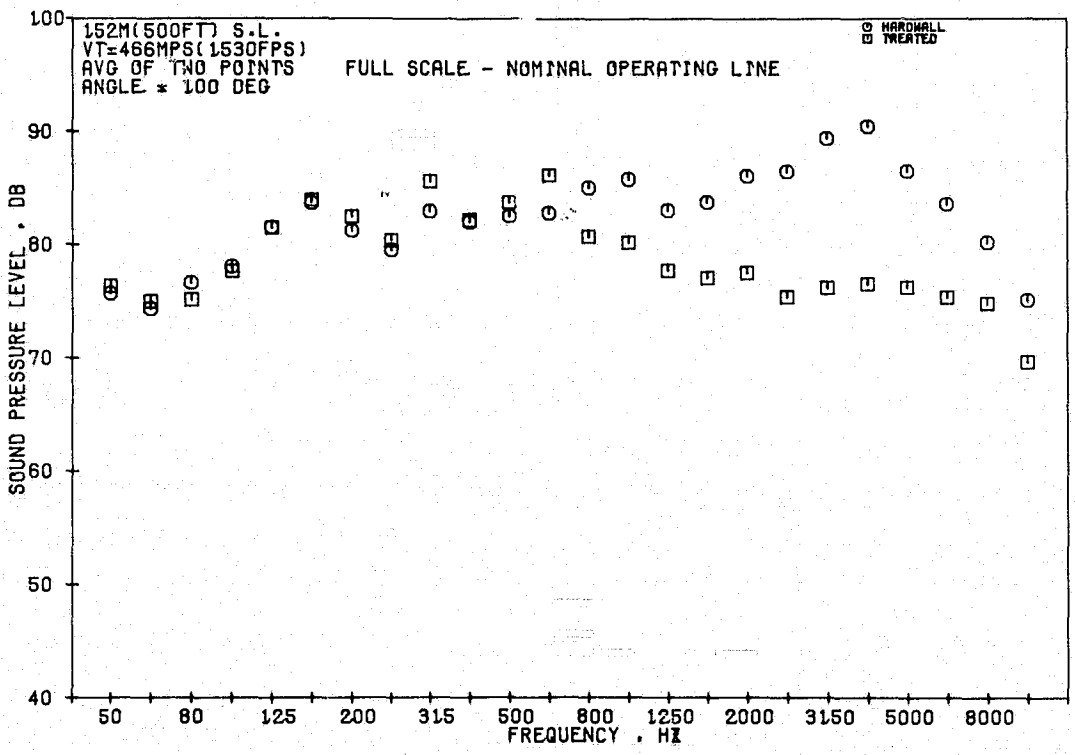

Figure 120. 1/3-Octave Spectra Comparisons at Takeoff, 100° Angle (Front-Drive Test).

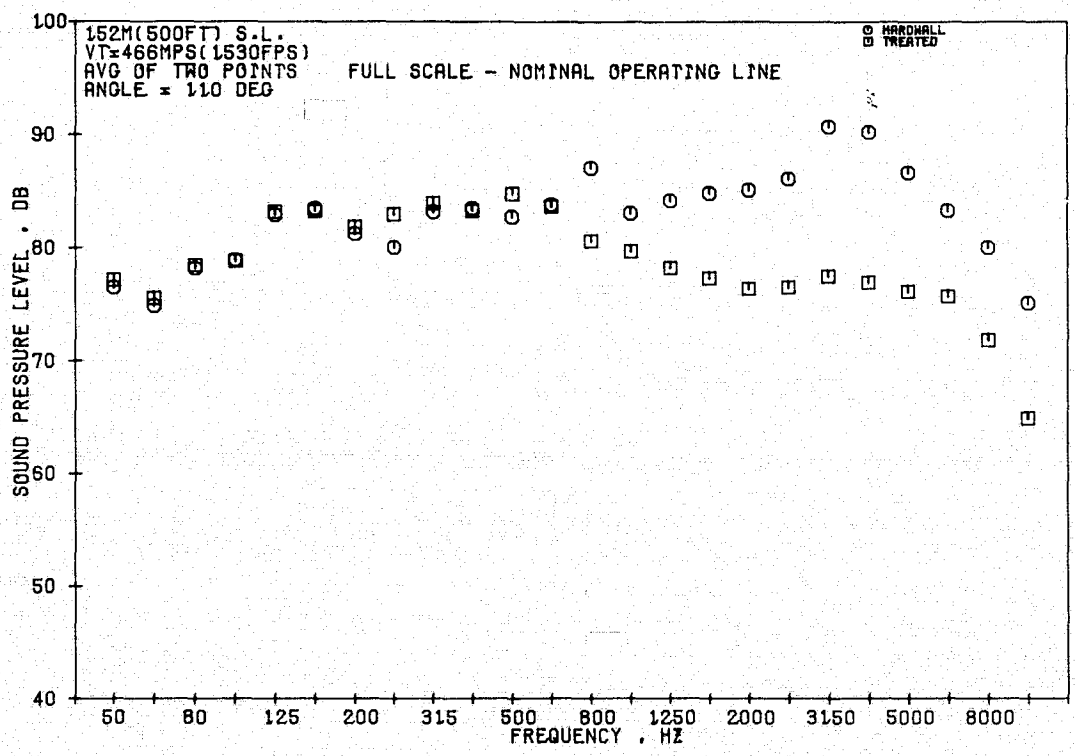

Figure 121. 1/3-Octave Spectra Comparisons at Takeoff, 110° Angle (Front-Drive Test).

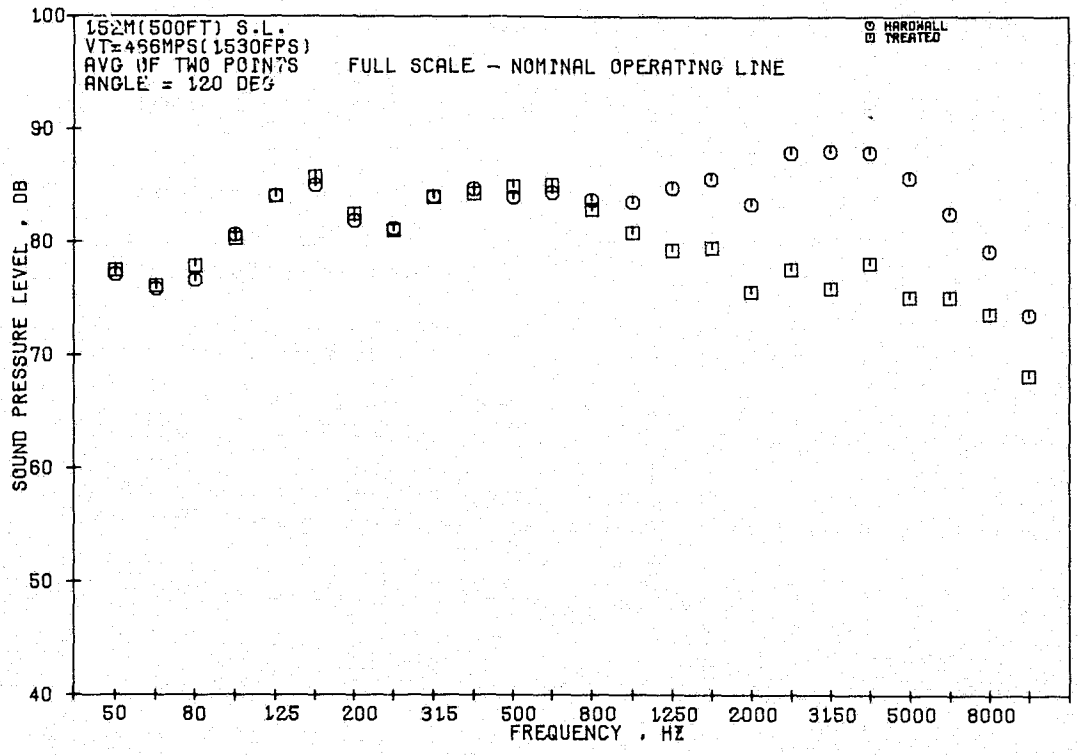

Figure 122. 1/3-Octave Spectra Comparisons at Takeoff, 120° Angle (Front-Drive Test).

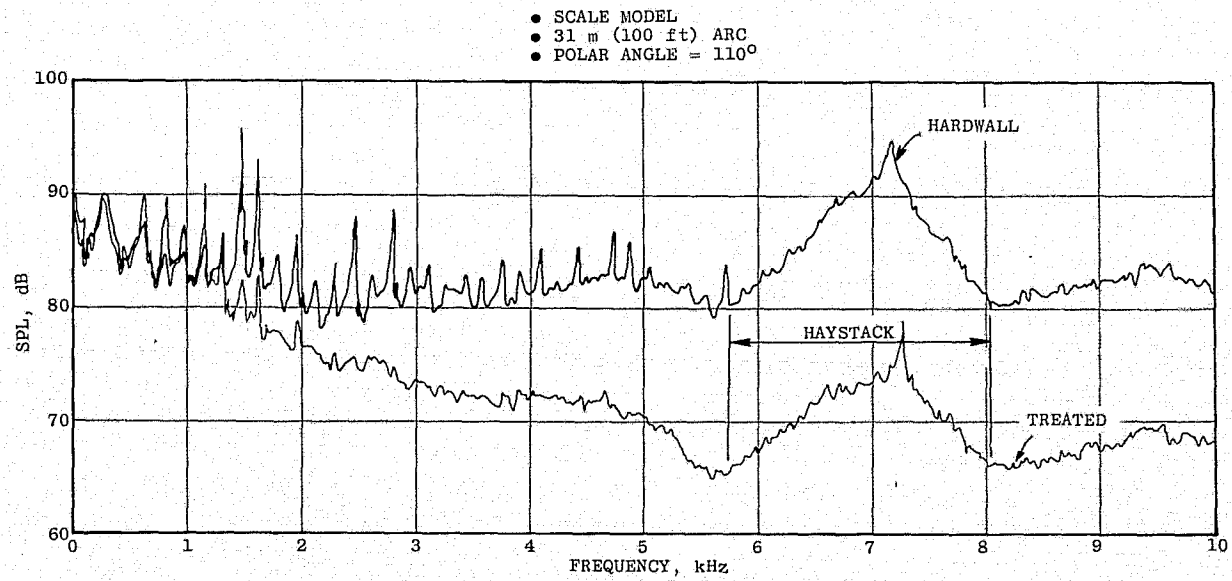

Figure 123. Farfield Narrowband Comparison for the Treated and the Hardwall Configurations at Takeoff, 110° Angle (Front-Drive Test).

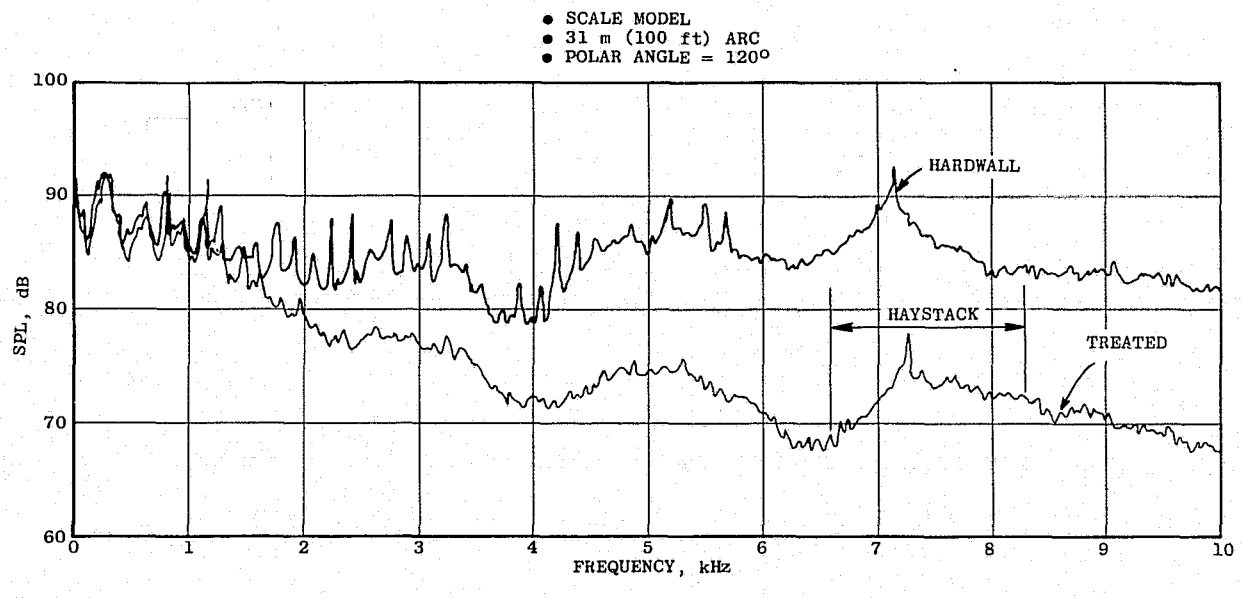

Figure 124. Farfield Narrowband Comparison for the Treated and the Hardwall Configurations at Takeoff, 120° Angle (Front-Drive Test).

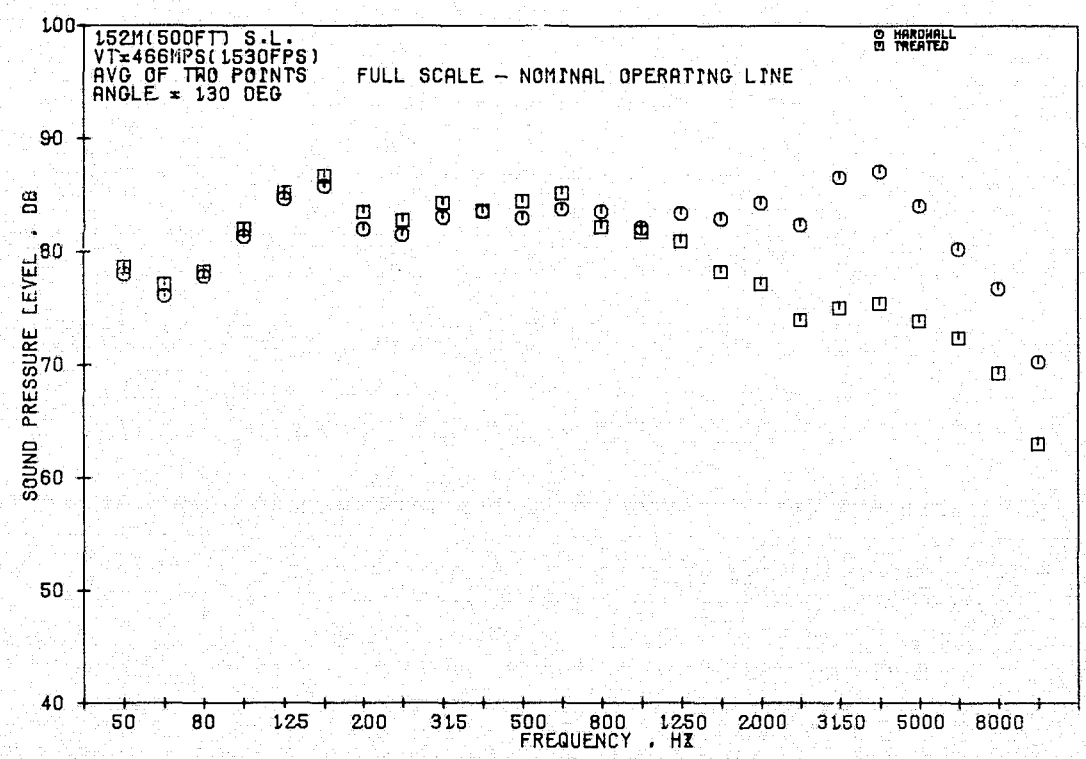

Figure 125. 1/3-Octave Spectra Comparisons at Takeoff, 130° Angle (Front-Drive Test).

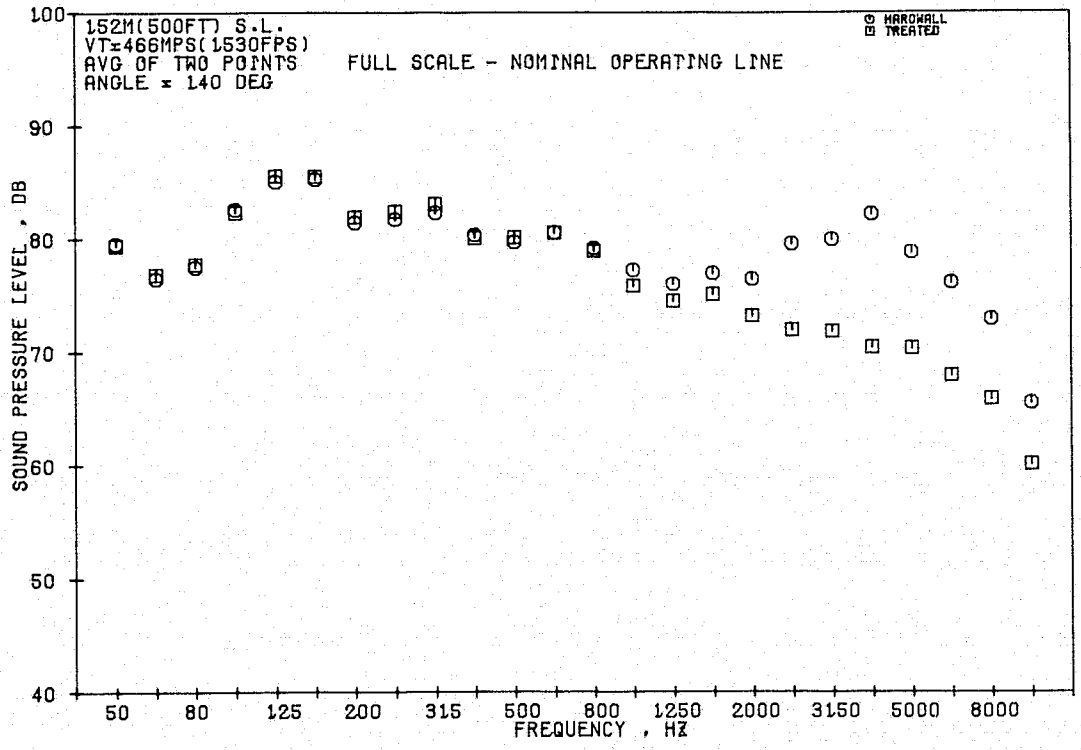

Figure 126. 1/3-Octave Spectra Comparisons at Takeoff, 140° Angle (Front-Drive Test).

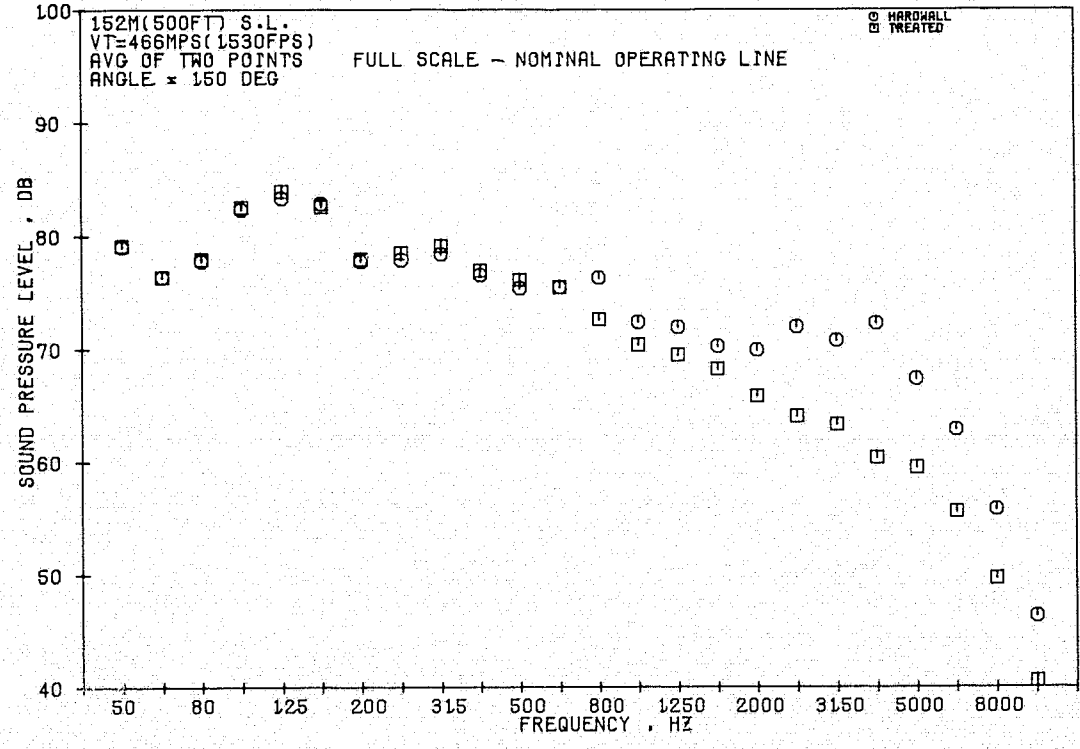

Figure 127. 1/3-Octave Spectra Comparisons at Takeoff, 150° Angle (Front-Drive Test).

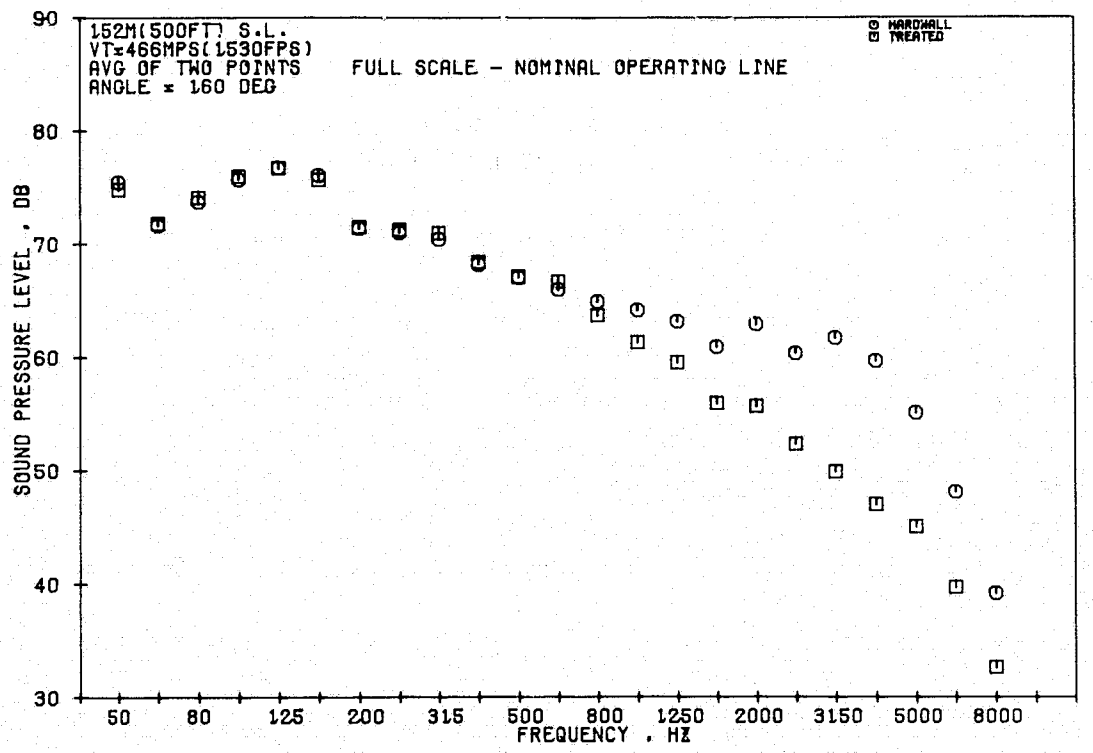

Figure 128. 1/3-Octave Spectra Comparisons at Takeoff, 160° Angle (Front-Drive Test).

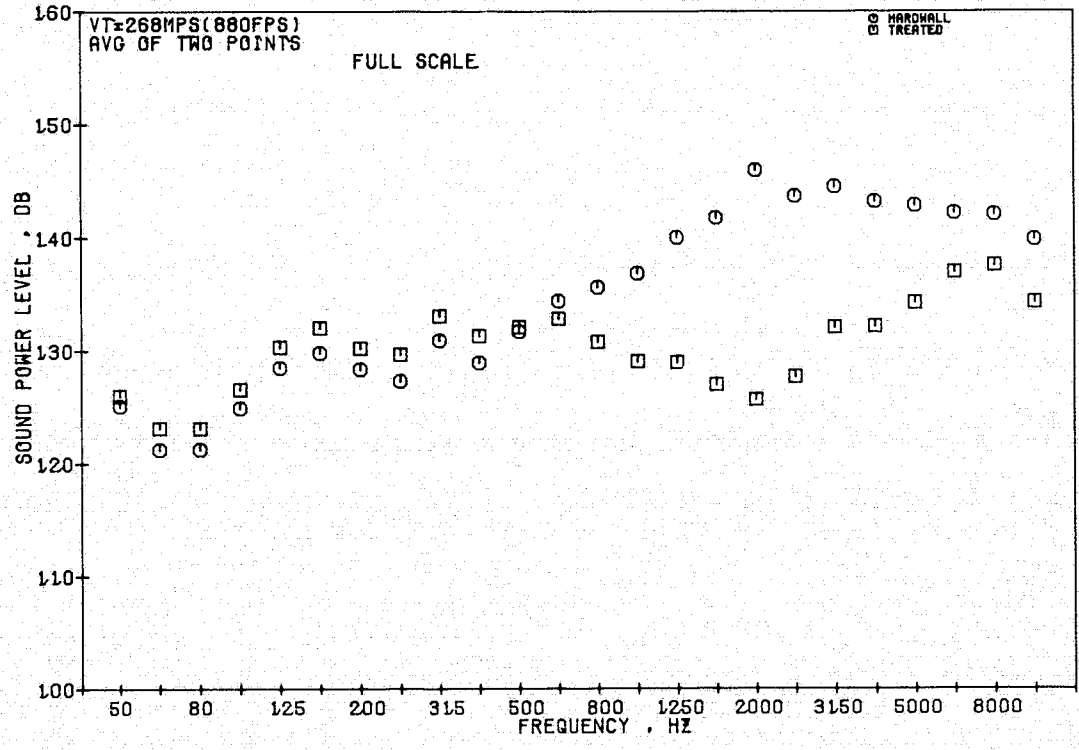

Figure 129. 1/3-Octave PWL Comparisons at Takeoff, V_T = 268 m/sec (Front-Drive Test).

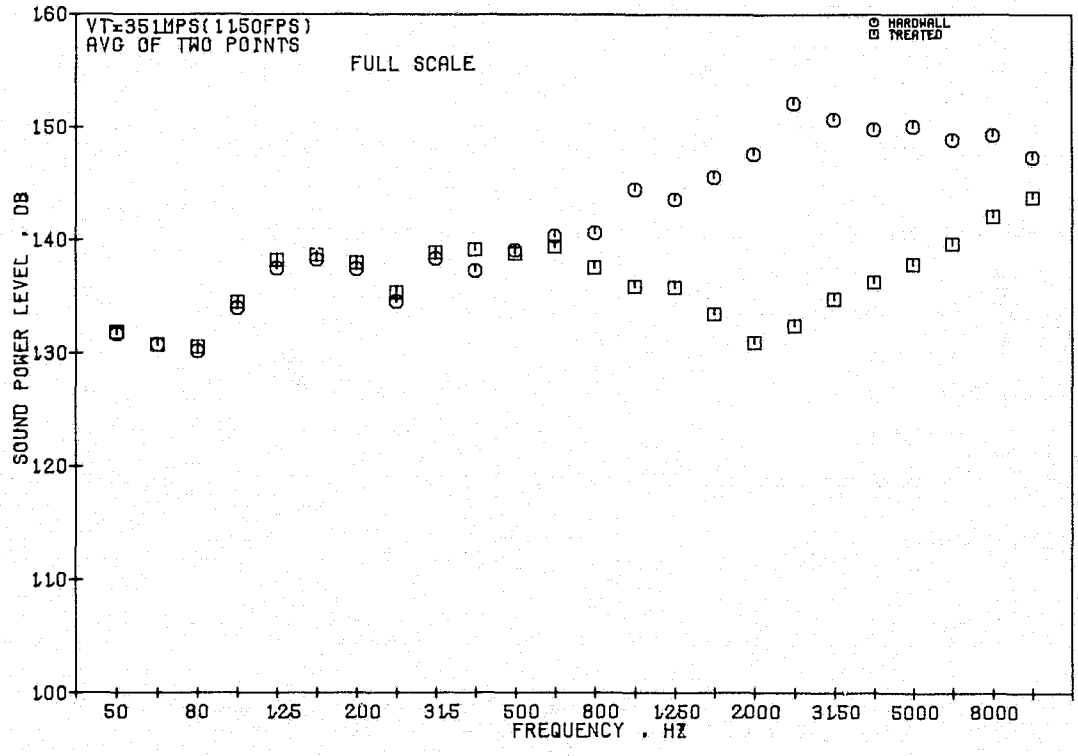

Figure 130. 1/3-Octave PWL Comparisons at Takeoff, V_T = 351 m/sec (Front-Drive Test).

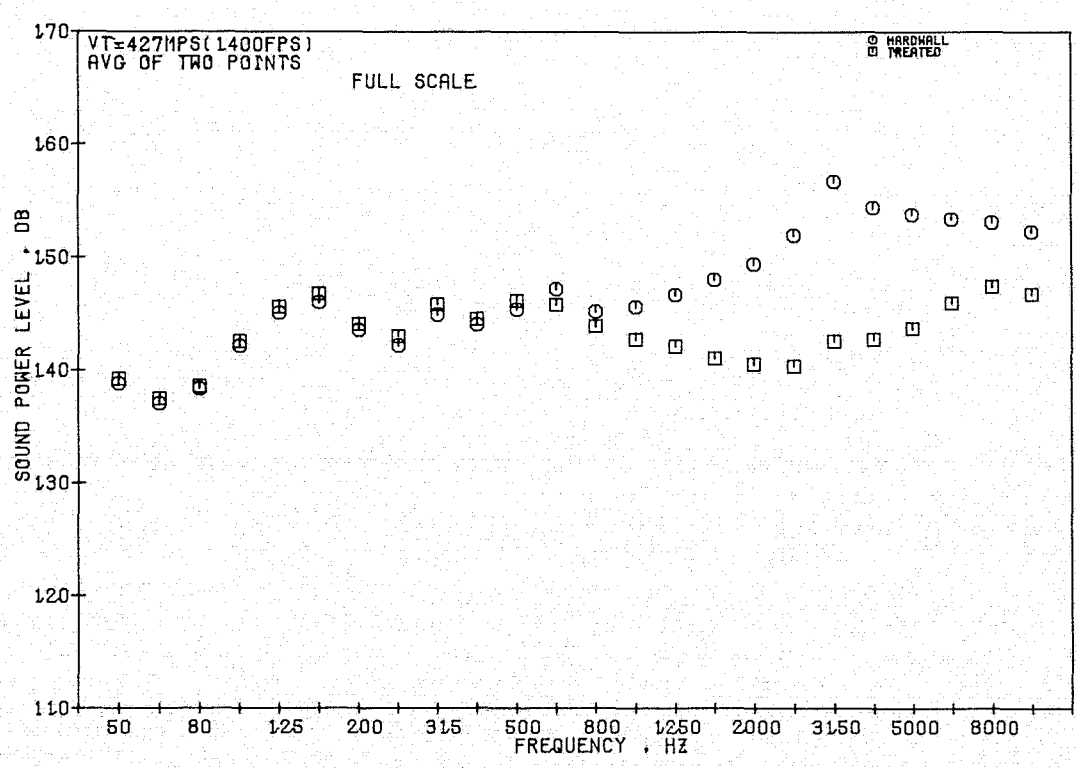

Figure 131. 1/3-Octave PWL Comparisons at Takeoff, V_T = 427 m/sec (Front-Drive Test).

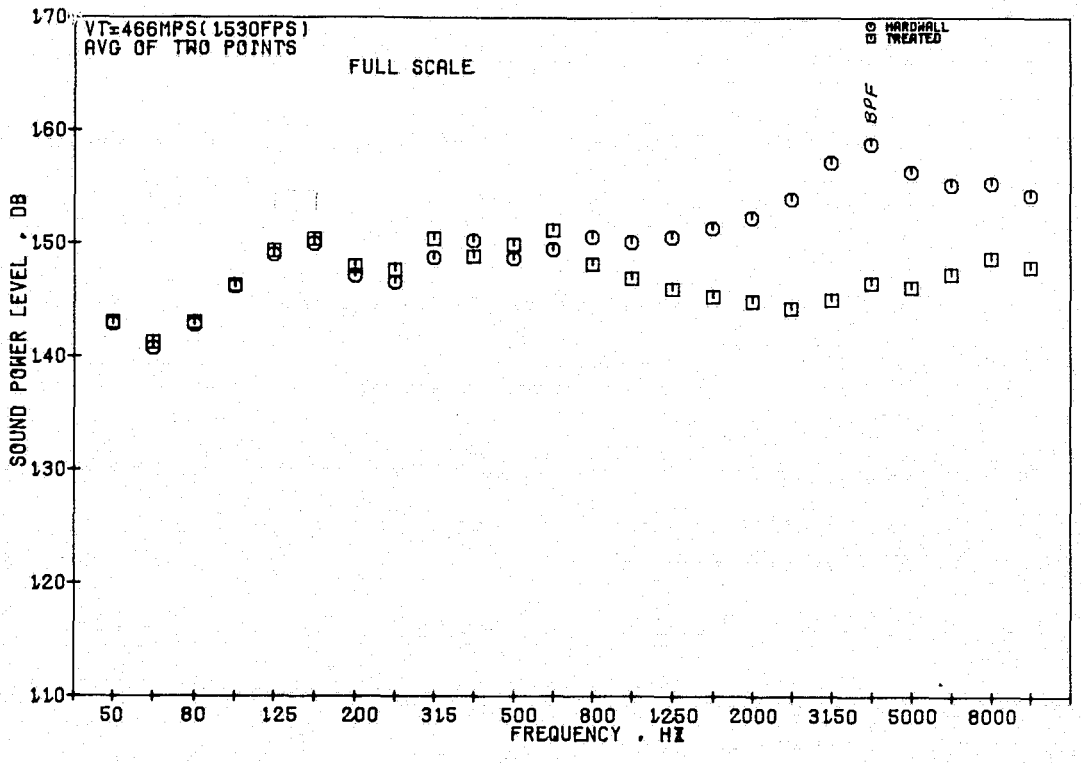

Figure 132. 1/3-Octave PWL Comparisons at Takeoff, V_T = 466 m/sec (Front-Drive Test).

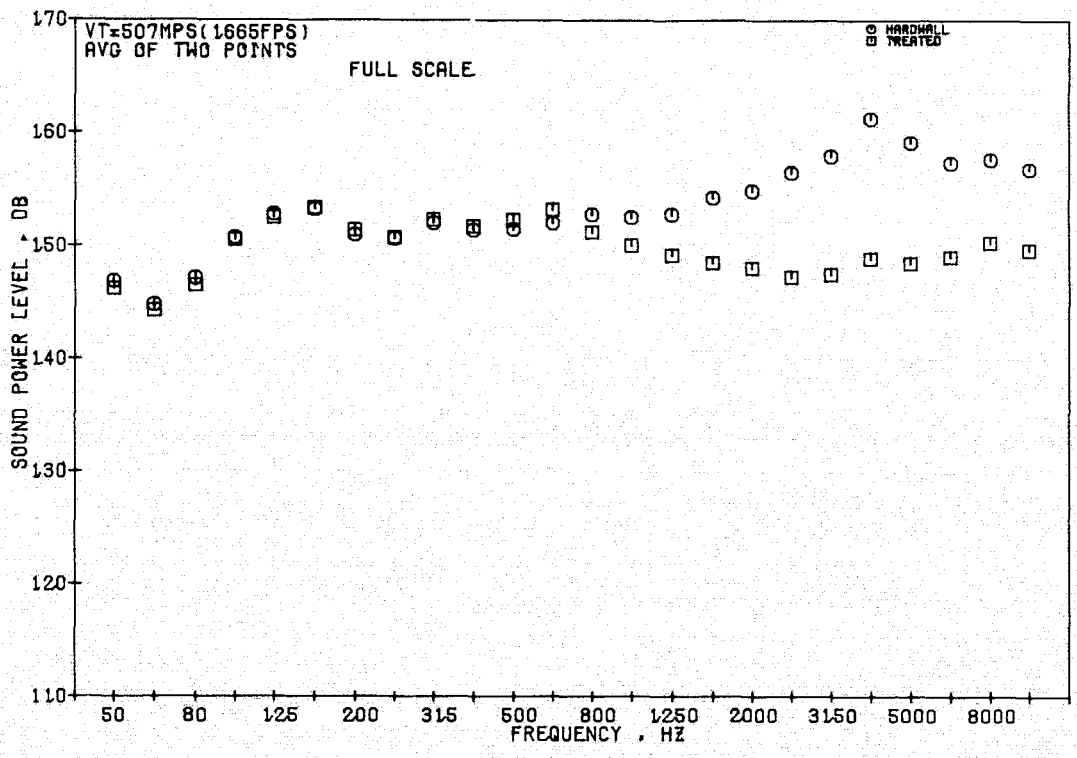

Figure 133. 1/3-Octave PWL Comparisons at Takeoff, V_T = 507 m/sec (Front-Drive Test).

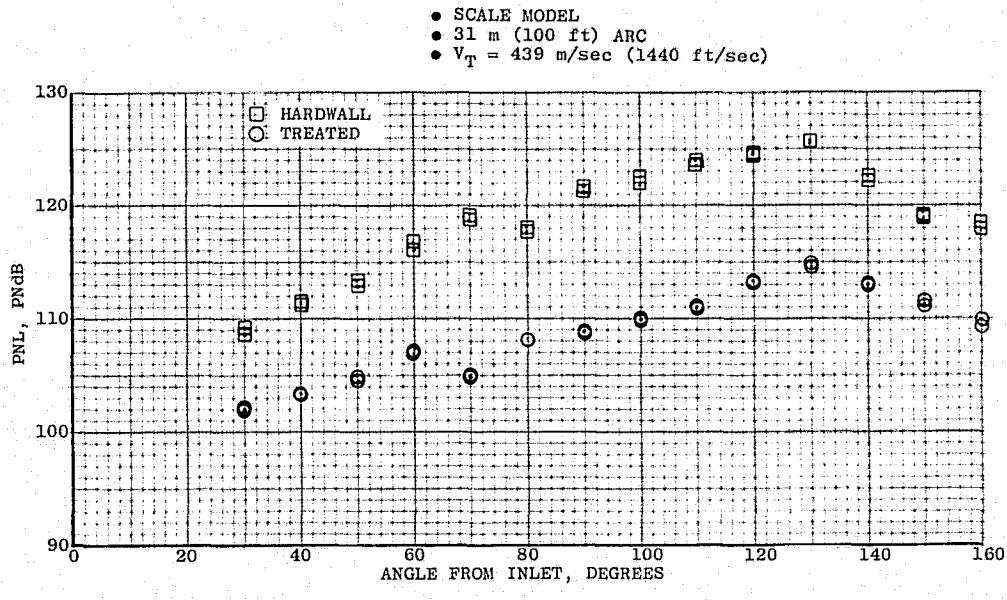

Figure 134. Scale-Model PNL Directivity at Cutback (Front-Drive Test).

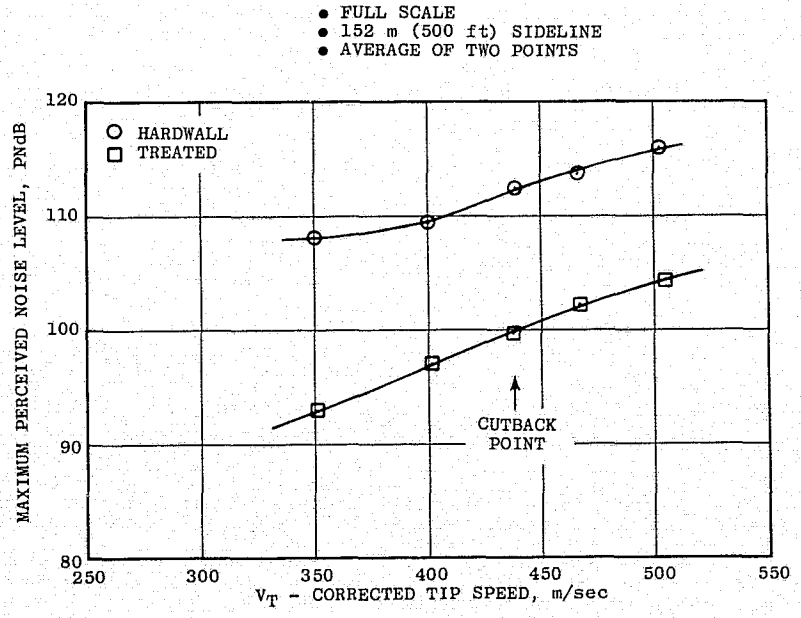

Figure 135. Maximum PNL Vs. Corrected Tip Speed at Cutback (Front-Drive Test).

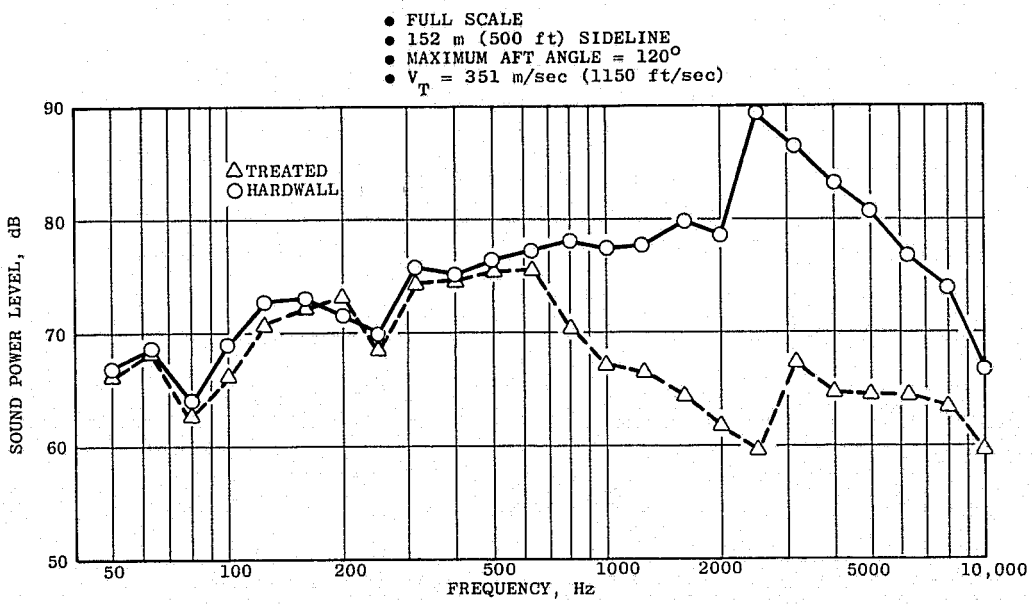

Figure 136. Maximum Aft Spectra at Cutback, V_T = 351 m/sec (Front-Drive Test).

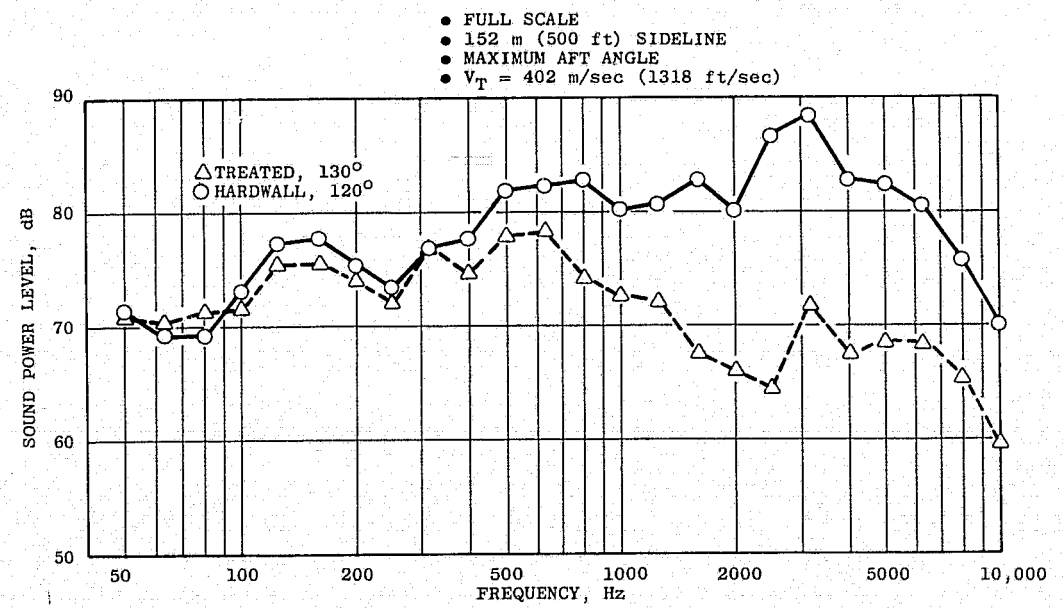

Figure 137. Maximum Aft Spectra at Cutback, V_T = 402 m/sec (Front-Drive Test).

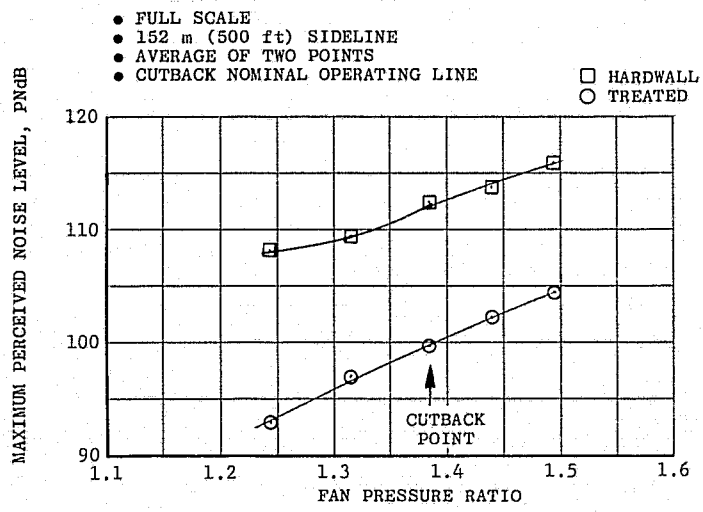

Figure 138. Maximum PNL Vs. Fan Pressure Ratio at Cutback (Front-Drive Test).

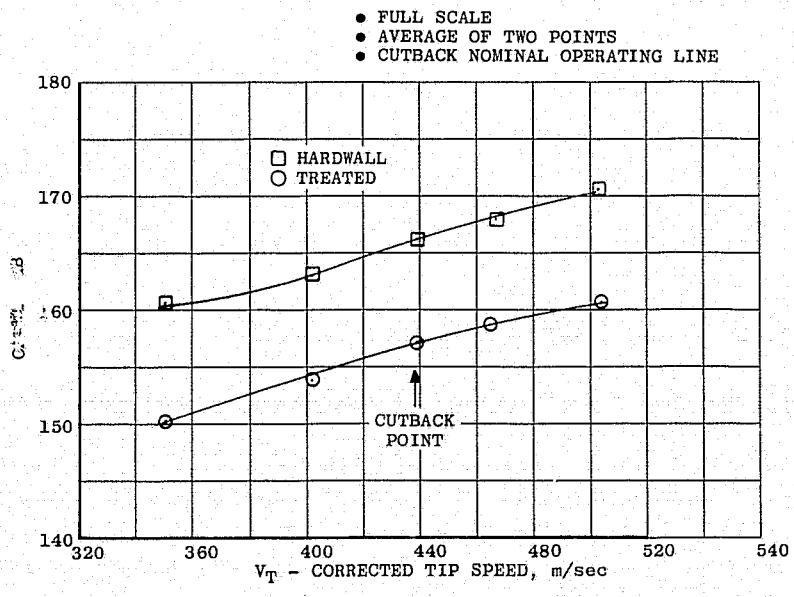

Figure 139. Overall Sound Power Level Vs. Corrected Tip Speed at Cutback (Front-Drive Test).

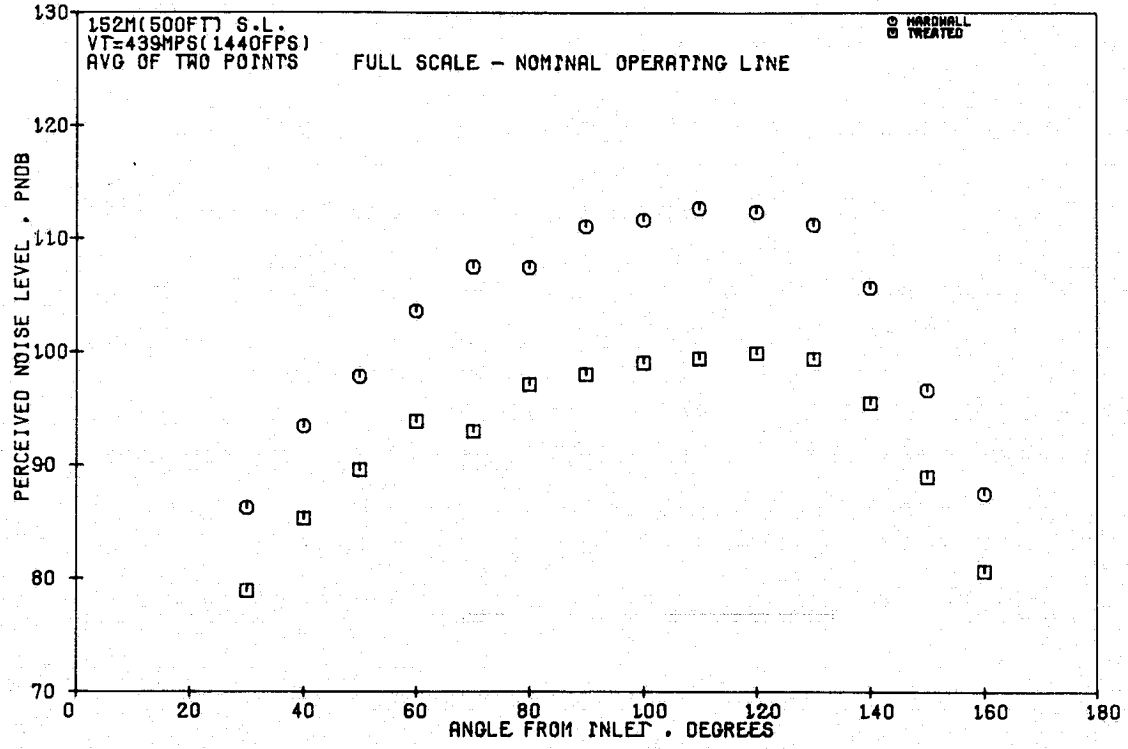

Figure 140. PNL Directivity at Cutback (Front-Drive Test).

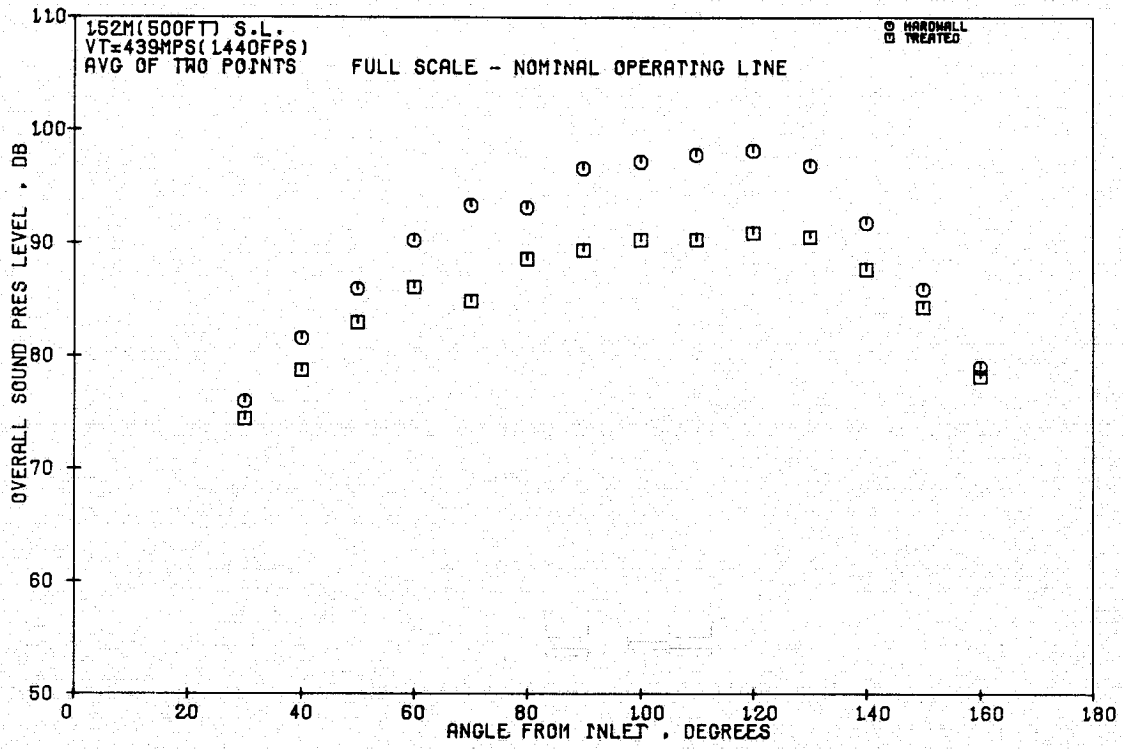

Figure 141. Variation of OASPL with Inlet Angle at Cutback (Front-Drive Test.

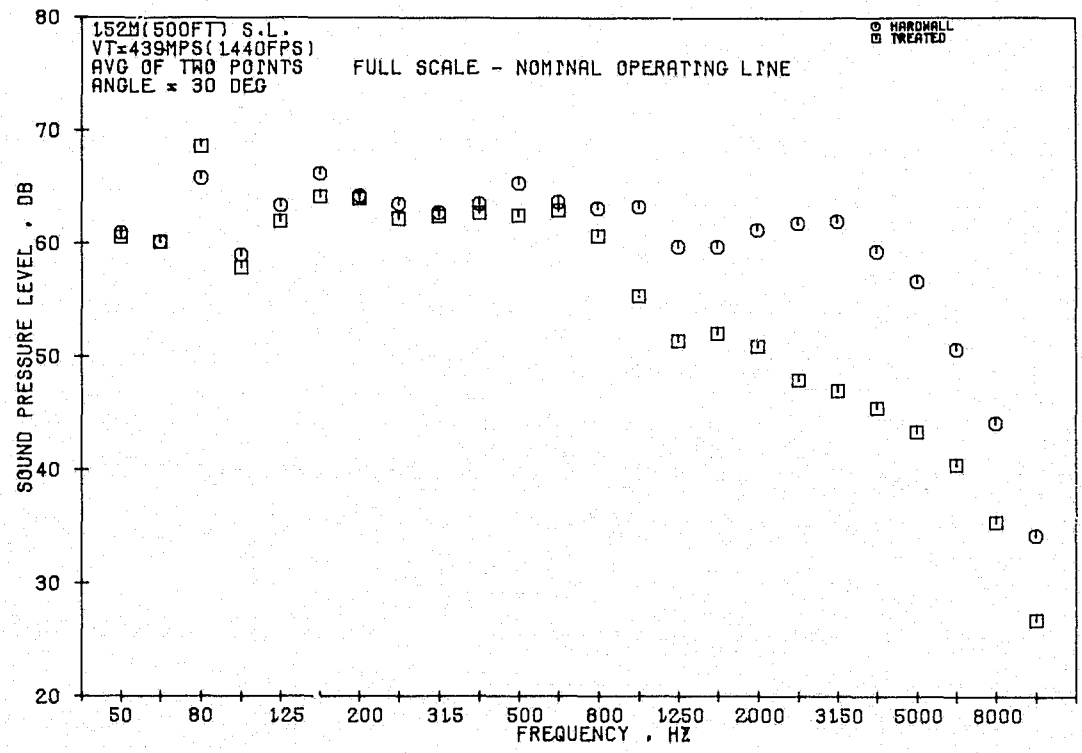

Figure 142. 1/3-Octave Spectra Comparisons at Cutback, 30° Angle (Front-Drive Test).

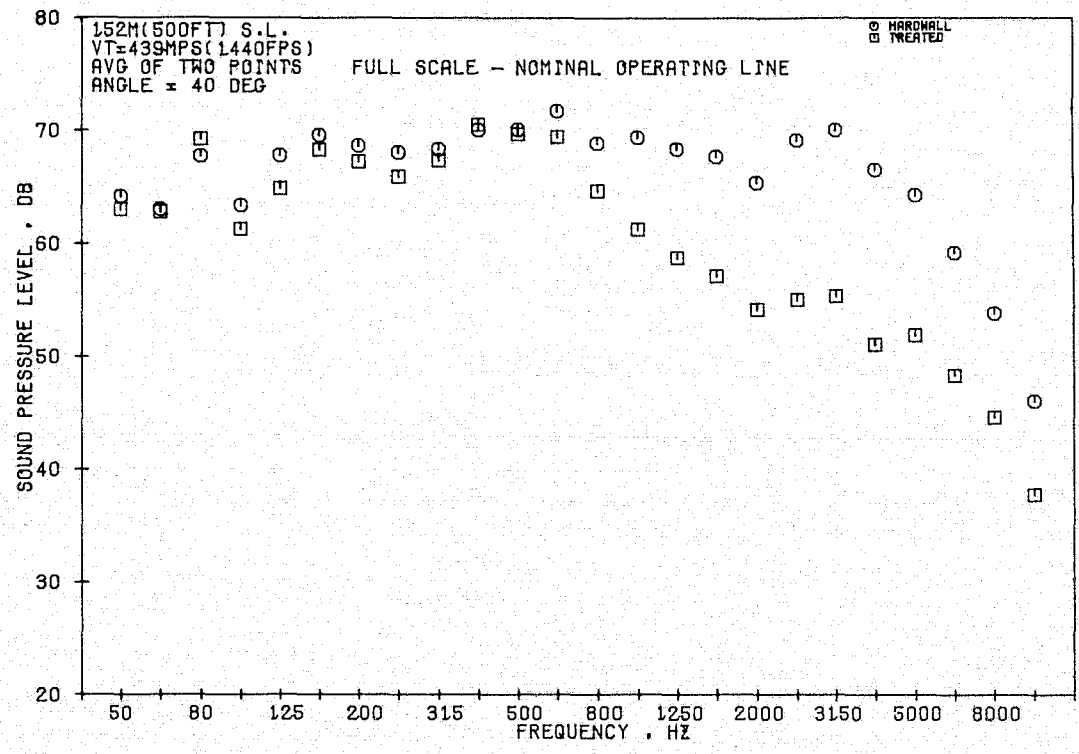

Figure 143. 1/3-Octave Spectra Comparisons at Cutback, 40° Angle (Front-Drive Test).

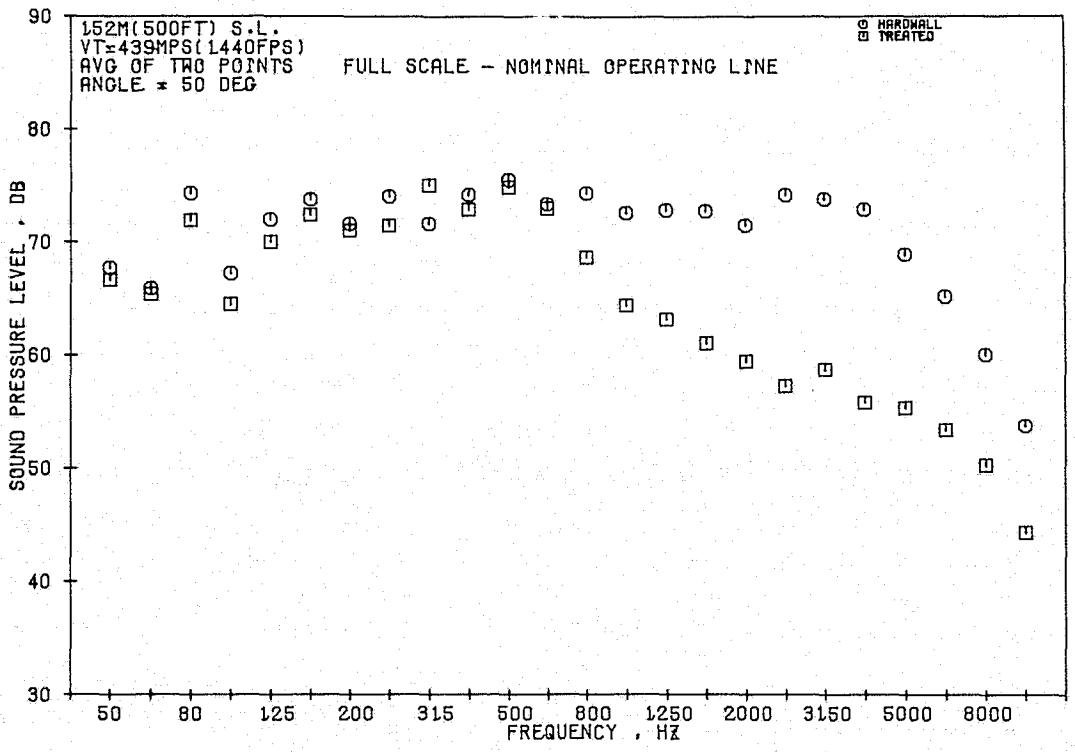

Figure 144. 1/3-Octave Spectra Comparisons at Cutback, 50° Angle (Front-Drive Test).

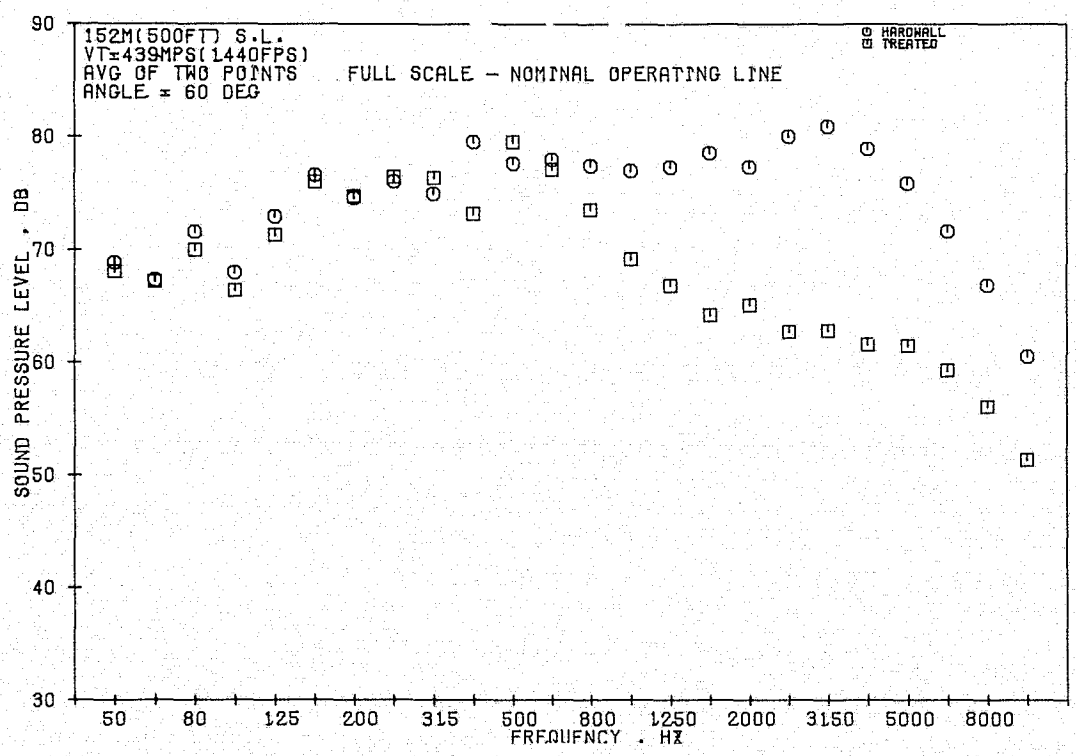

Figure 145. 1/3-Octave Spectra Comparisons at Cutback, 60° Angle (Front-Drive Test).

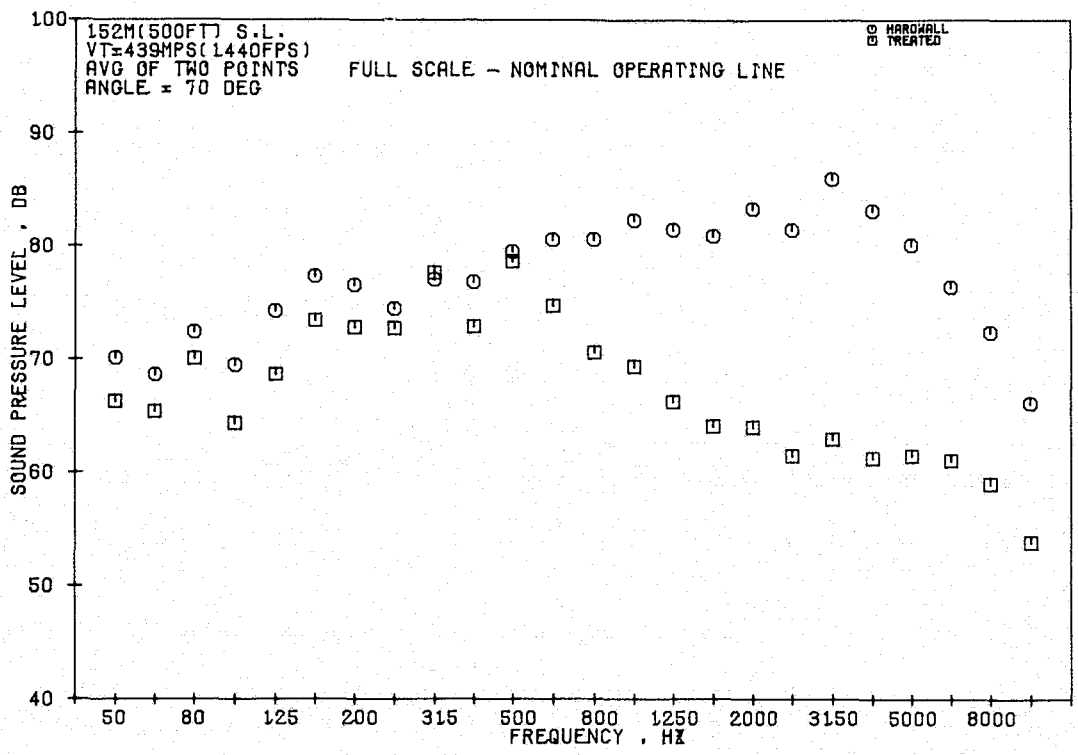

Figure 146. 1/3-Octave Spectra Comparisons at Cutback, 70° Angle (Front-Drive Test).

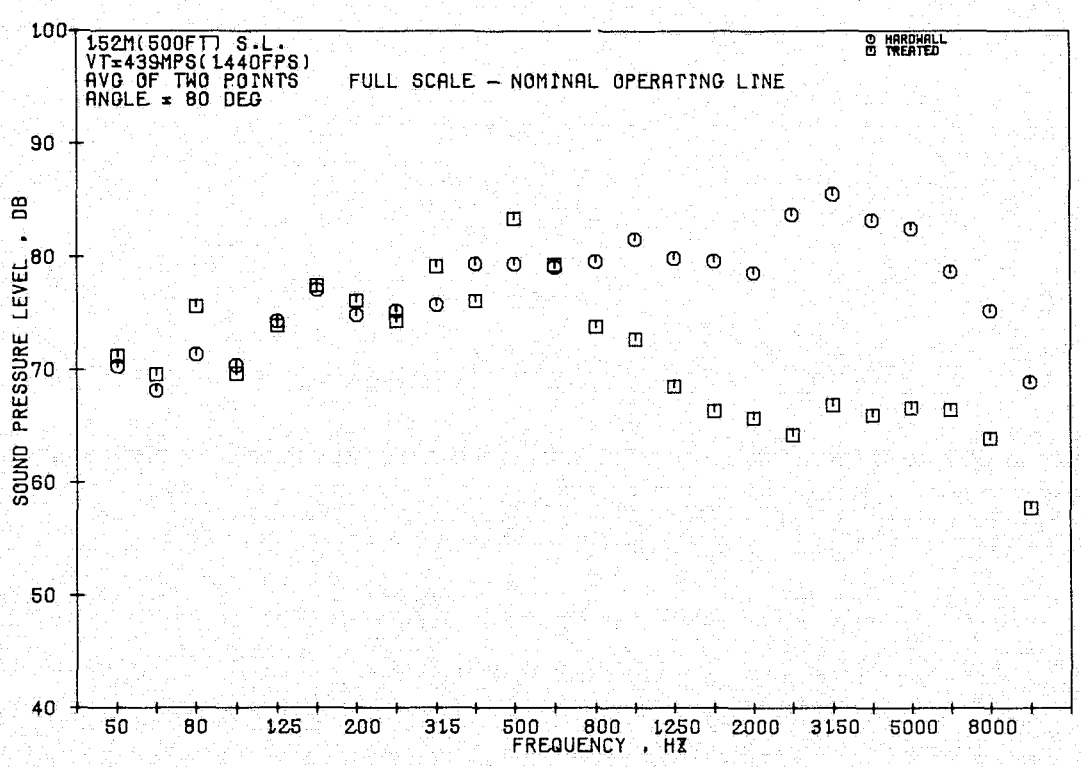

Figure 147. 1/3-Octave Spectra Comparisons at Cutback, 80° Angle (Front-Drive Test).

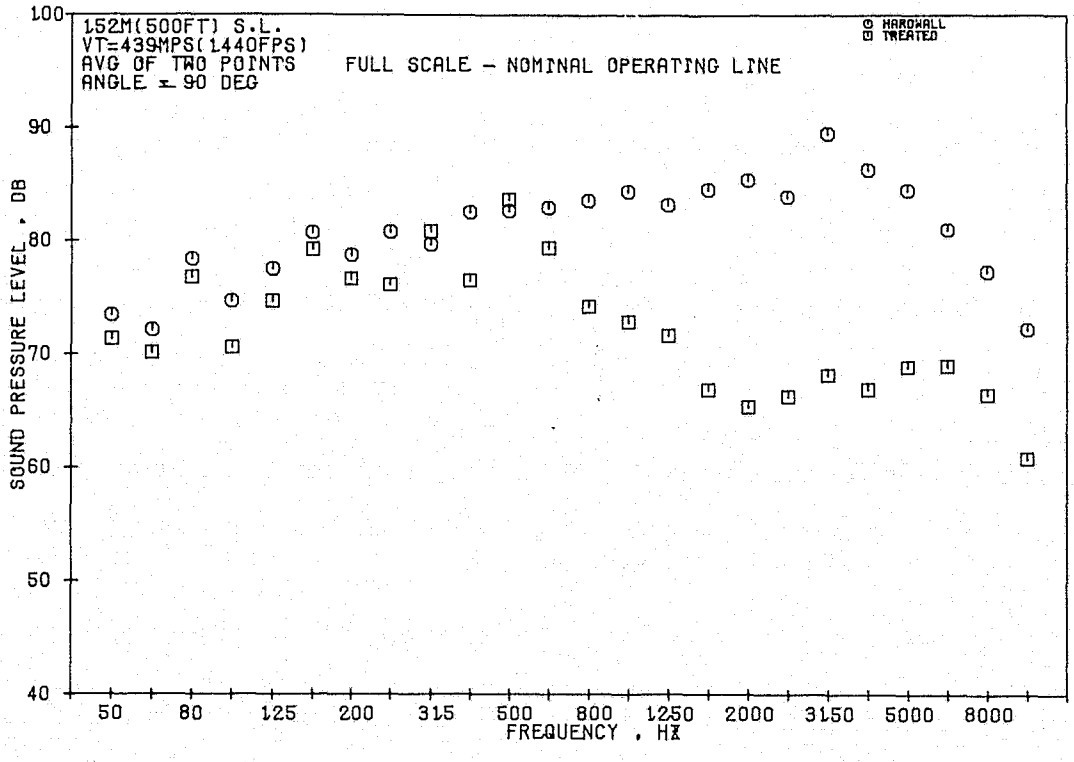

Figure 148. 1/3-Octave Spectra Comparisons at Cutback, 90° Angle (Front-Drive Test).

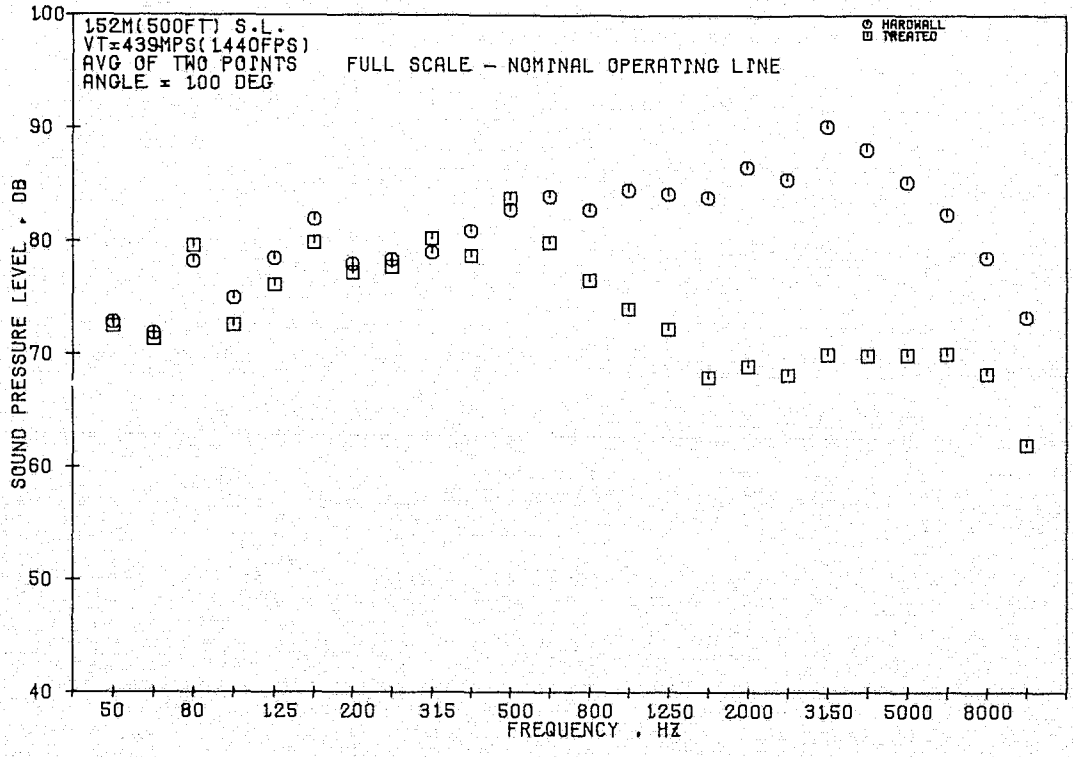

Figure 149. 1/3-Octave Spectra Comparisons at Cutback, 100° Angle (Front-Drive Test).

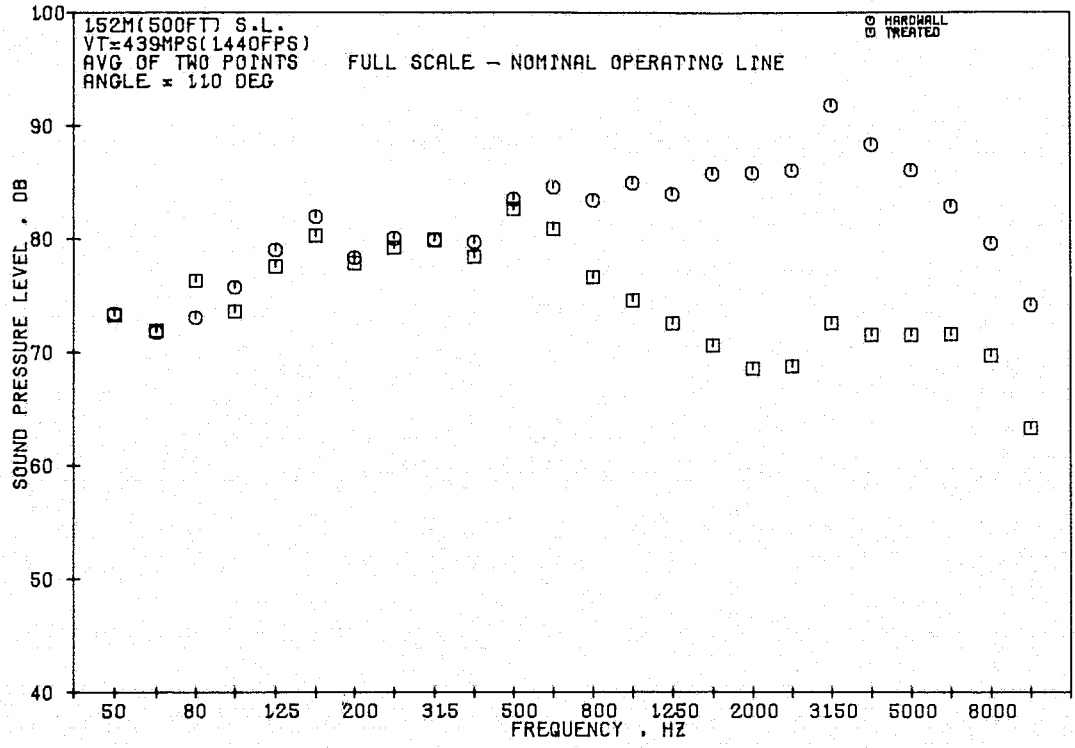

Figure 150. 1/3-Octave Spectra Comparisons at Cutback, 110° Angle (Front-Drive Test).

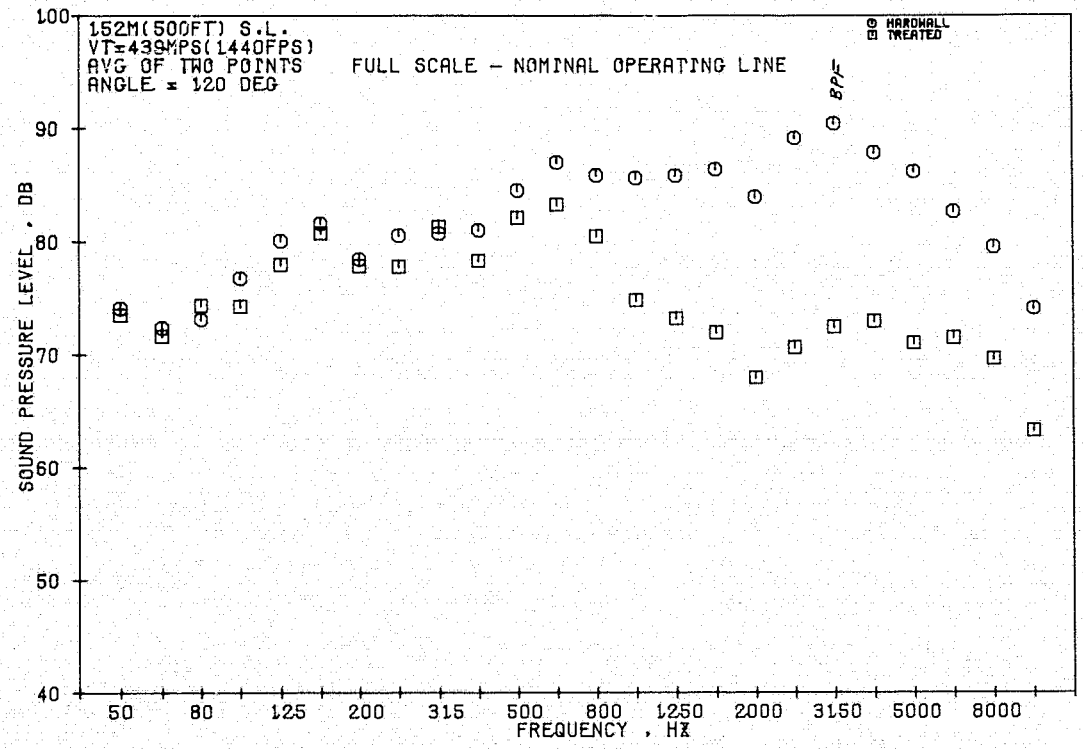

Figure 151. 1/3-Octave Spectra Comparisons at Cutback, 120° Angle (Front-Drive Test).

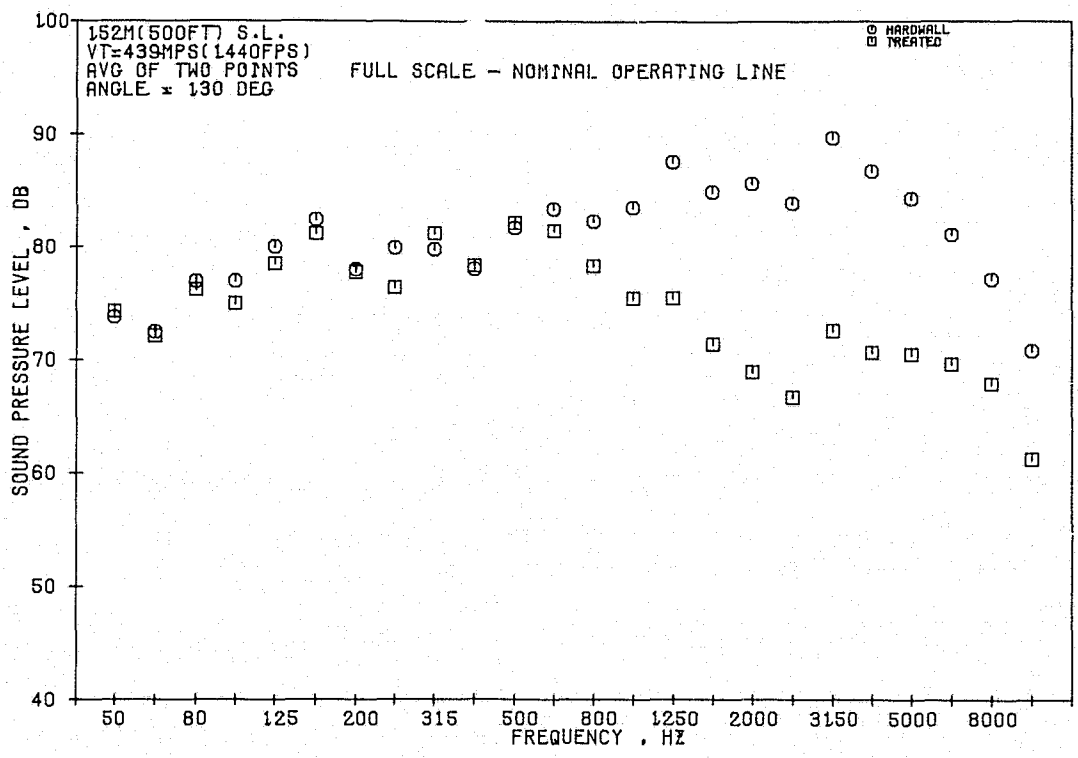

Figure 152. 1/3-Octave Spectra Comparisons at Cutback, 130° Angle (Front-Drive Test).

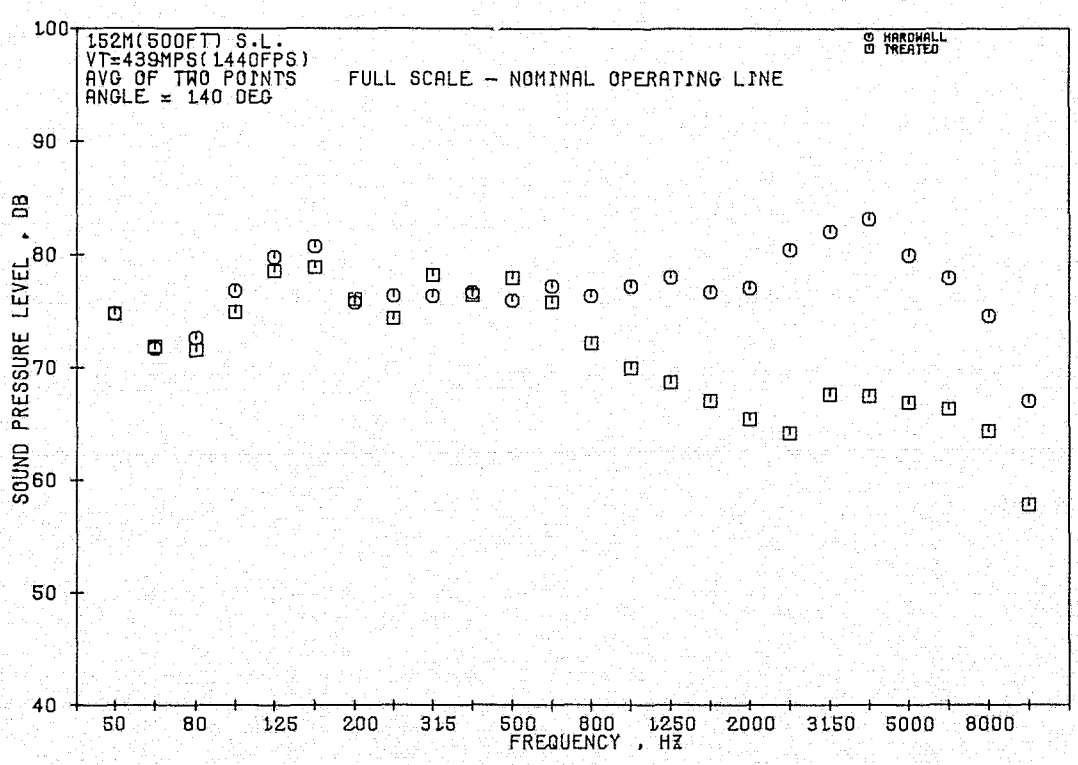

Figure 153. 1/3-Octave Spectra Comparisons at Cutback, 140° Angle (Front-Drive Test).

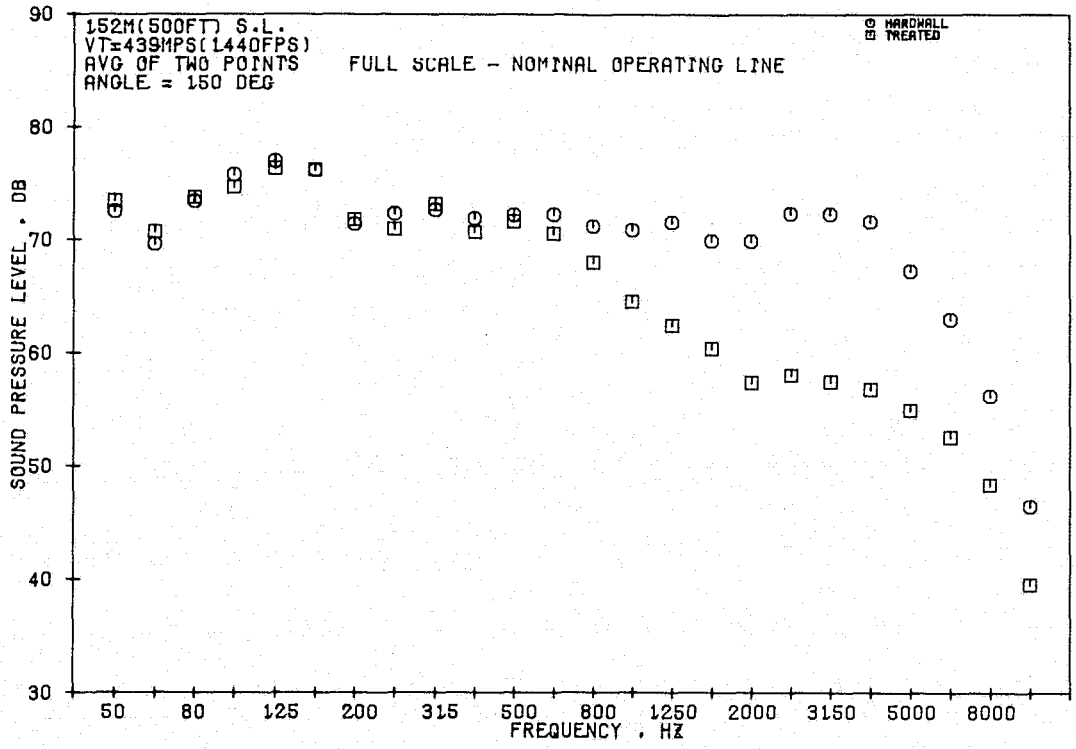

Figure 154. 1/3-Octave Spectra Comparisons at Cutback, 150° Angle (Front-Drive Test).

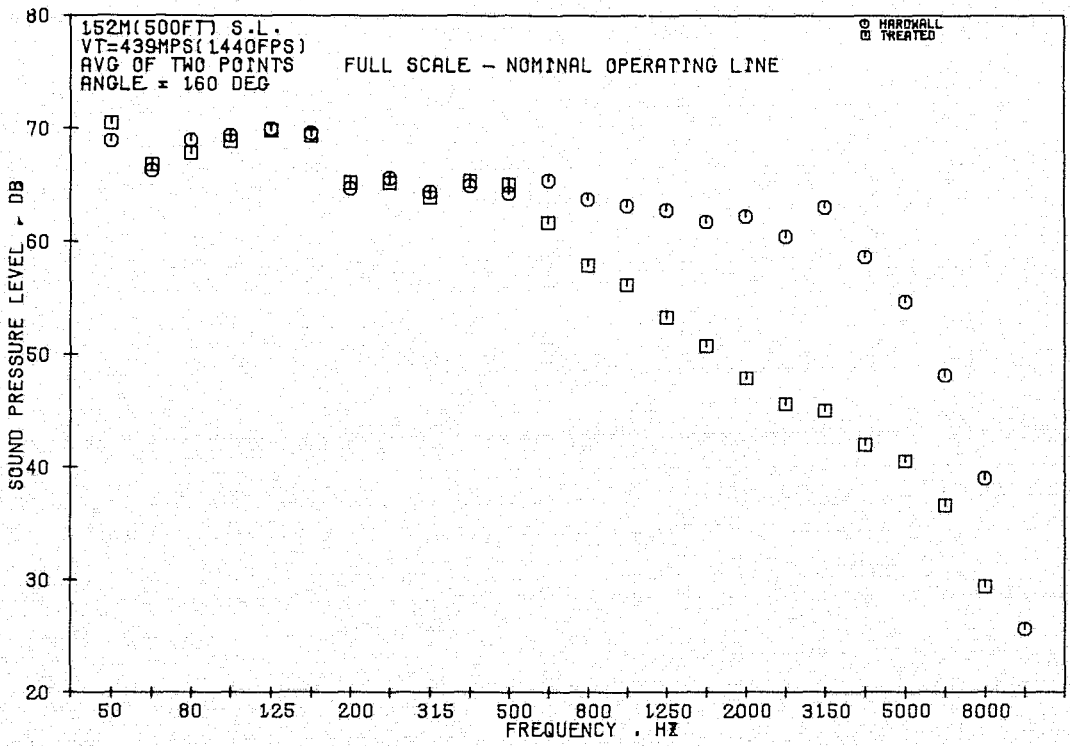

Figure 155. 1/3-Octave Spectra Comparisons at Cutback, 160° Angle (Front-Drive Test).

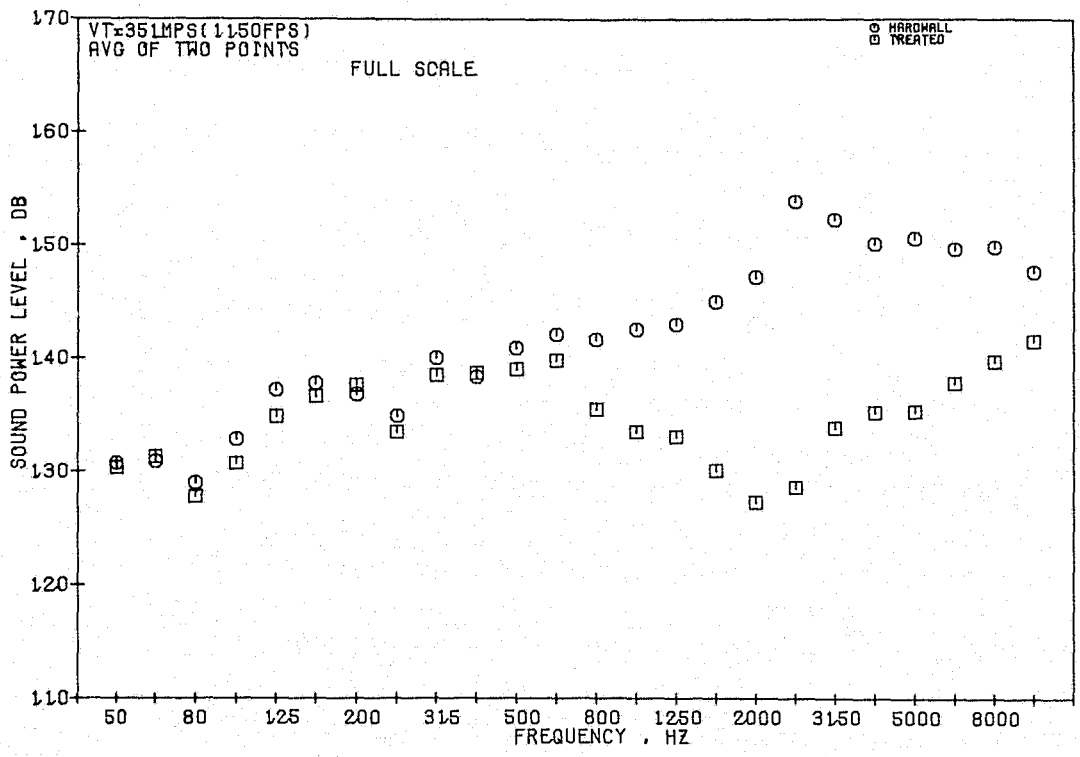

Figure 156. 1/3-Octave PWL Comparisons at Cutback, V_T = 351 m/sec (Front-Drive Test).

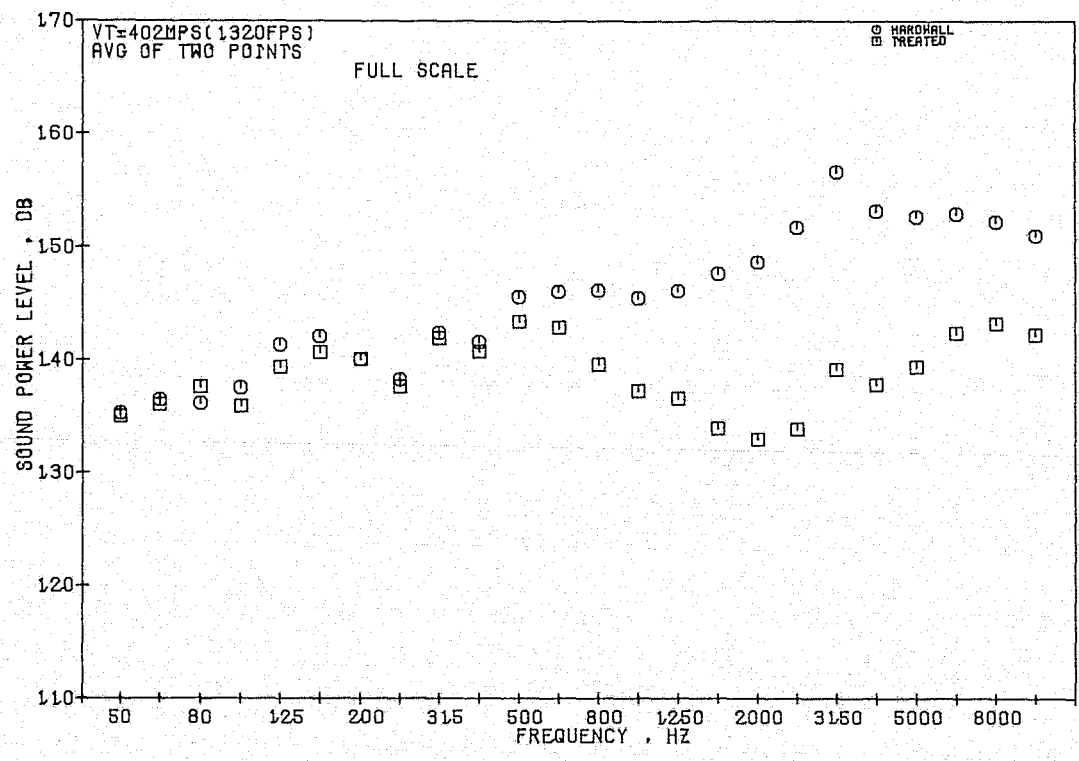

Figure 157. 1/3-Octave PWL Comparisons at Cutback, V_T = 402 m/sec (Front-Drive Test).

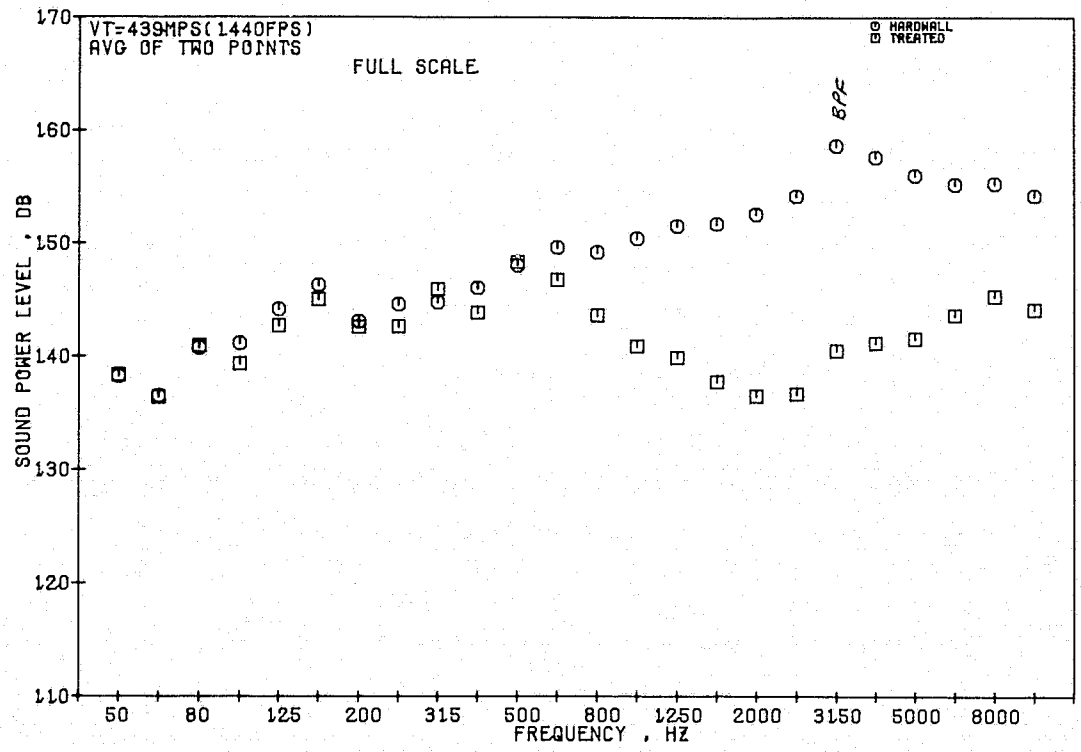

Figure 158. 1/3-Octave PWL Comparisons at Cutback, V_T = 439 m/sec (Front-Drive Test).

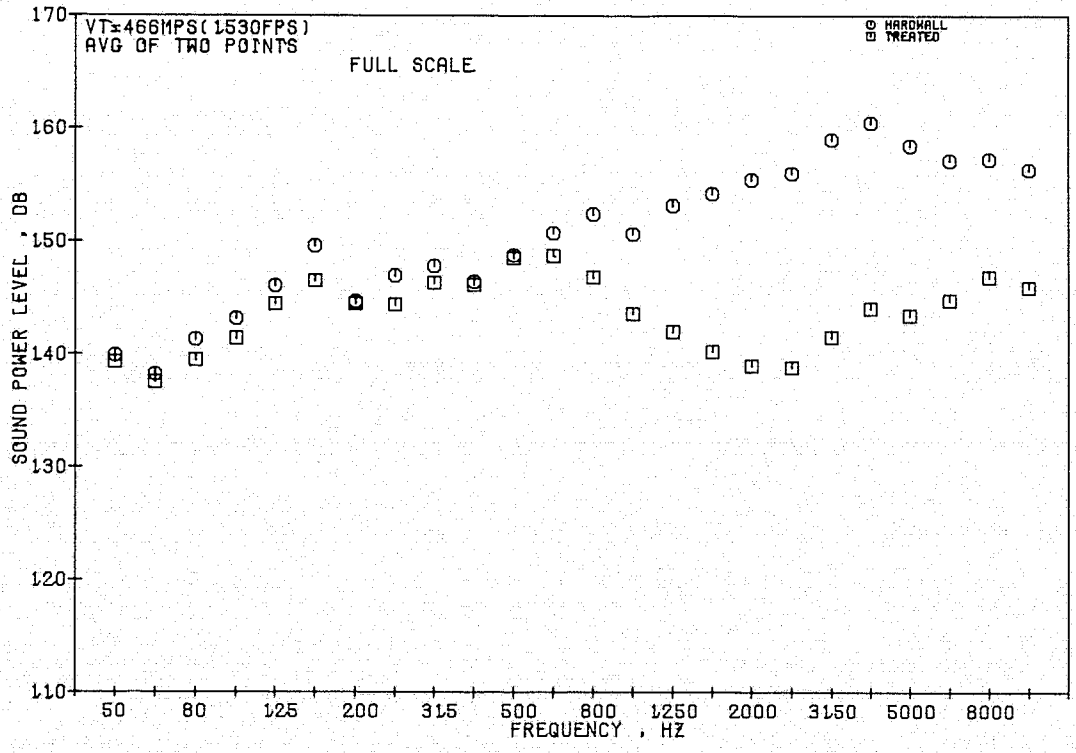

Figure 159. 1/3-Octave PWL Comparisons at Cutback, V_T = 466 m/sec (Front-Drive Test).

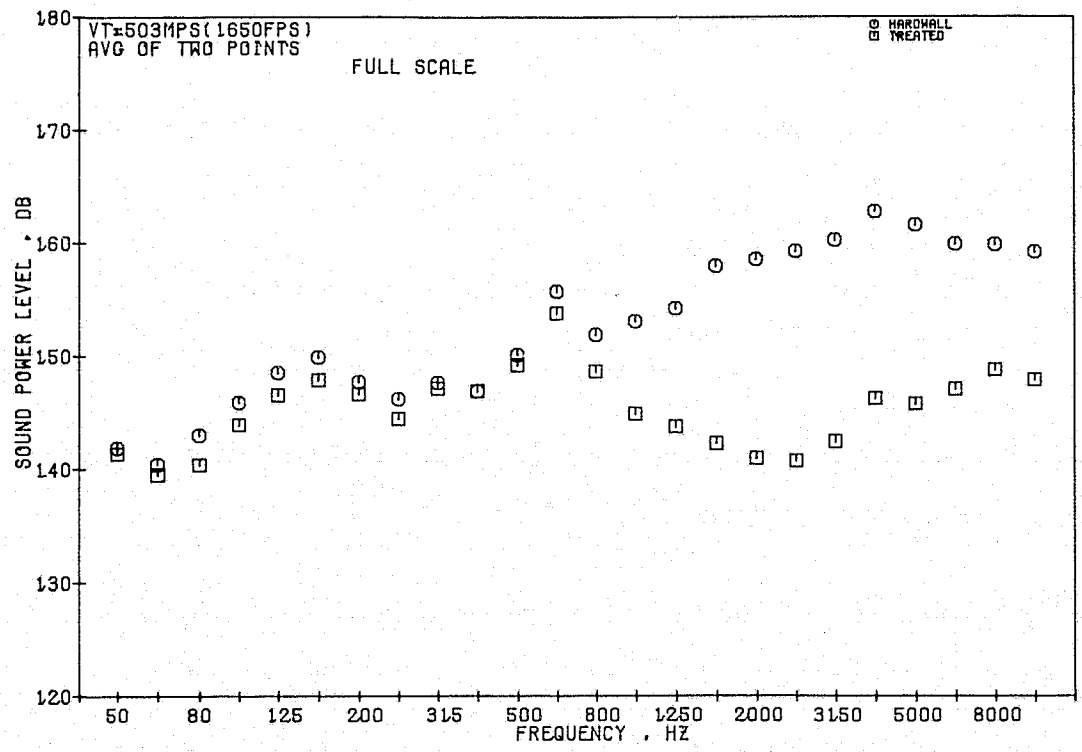

Figure 160. 1/3-Octave PWL Comparisons at Cutback, V_T = 503 m/sec (Front-Drive Test).

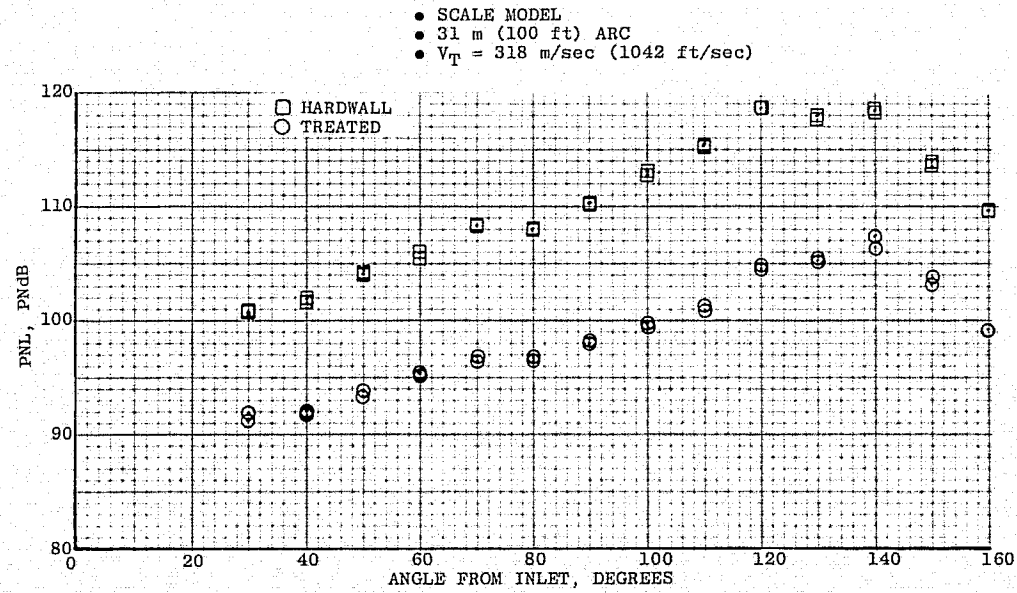

Figure 161. Scale-Model FNL Directivity at Approach (Front-Drive Test).

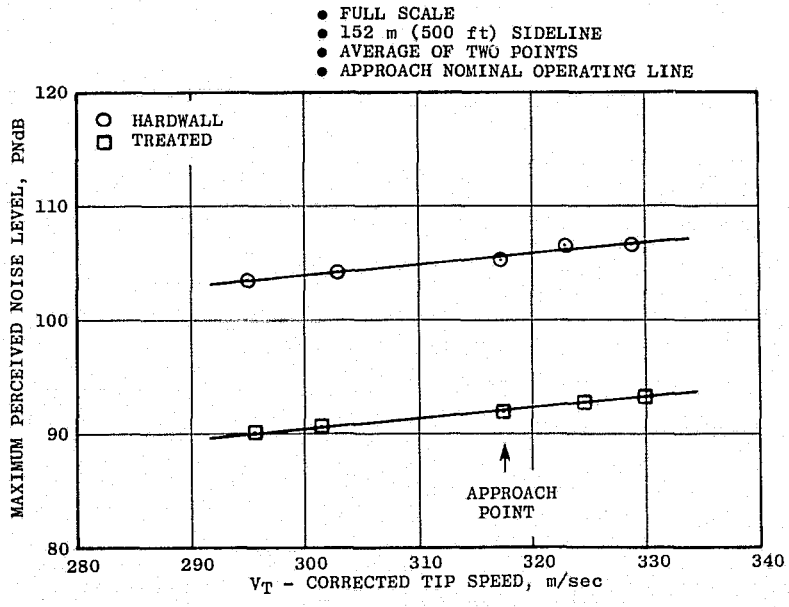

Figure 162. Maximum PNL Vs. Corrected Tip Speed at Approach (Front-Drive Test).

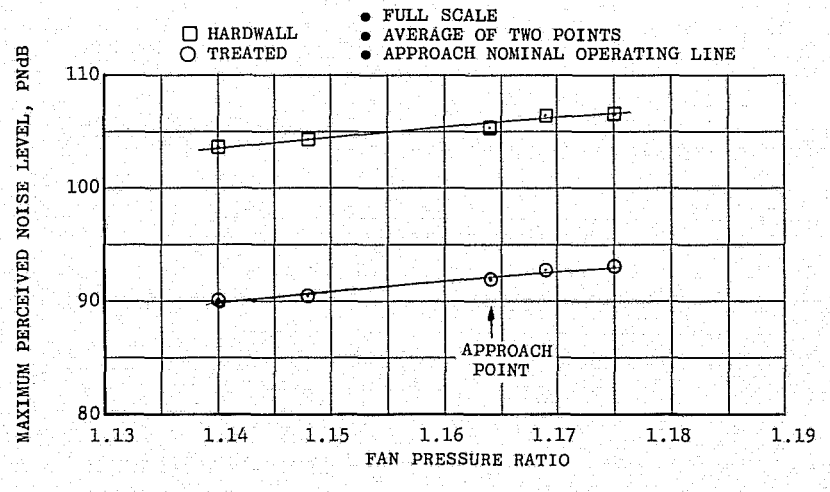

Figure 163. Maximum PNL Vs. Fan Pressure Ratio at Approach (Front-Drive Test).

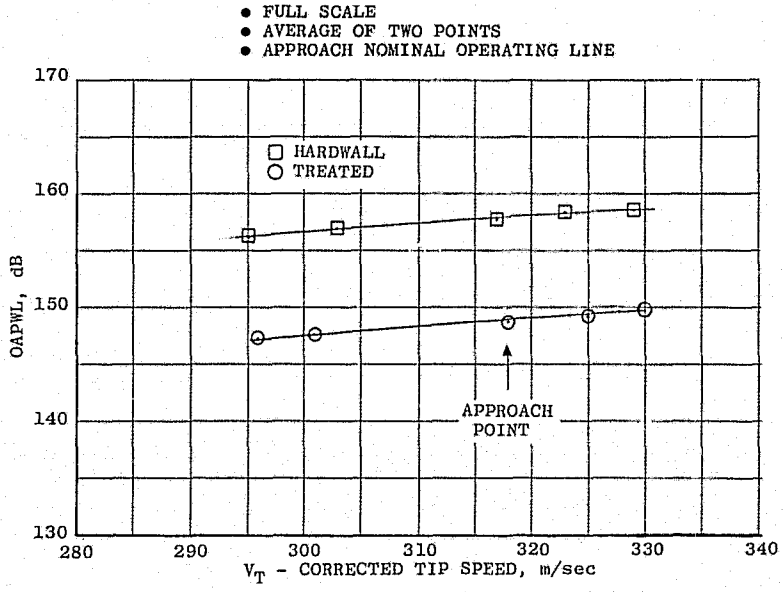

Figure 164. Overall Sound Power Level Vs. Corrected Tip Speed at Approach (Front-Drive Test).

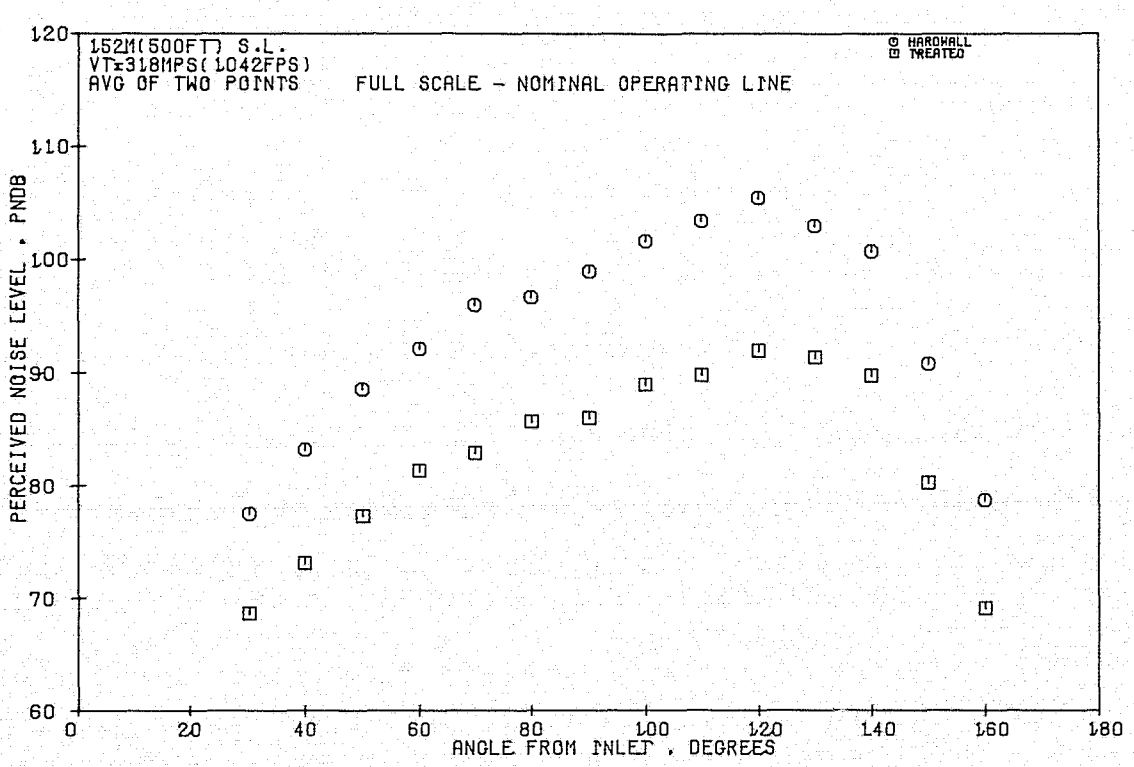

Figure 165. PNL Directivity at Approach (Front-Drive Test).

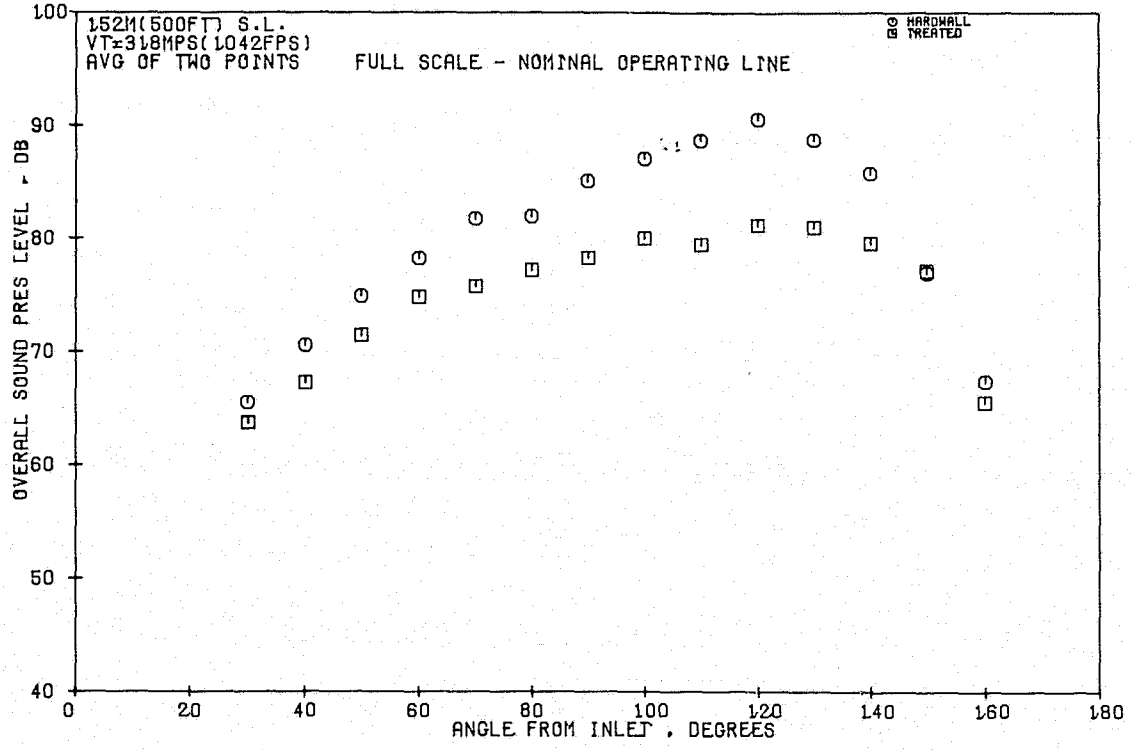

Figure 166. Variation of OASPL with Inlet Angle at Approach (Front-Drive Test).

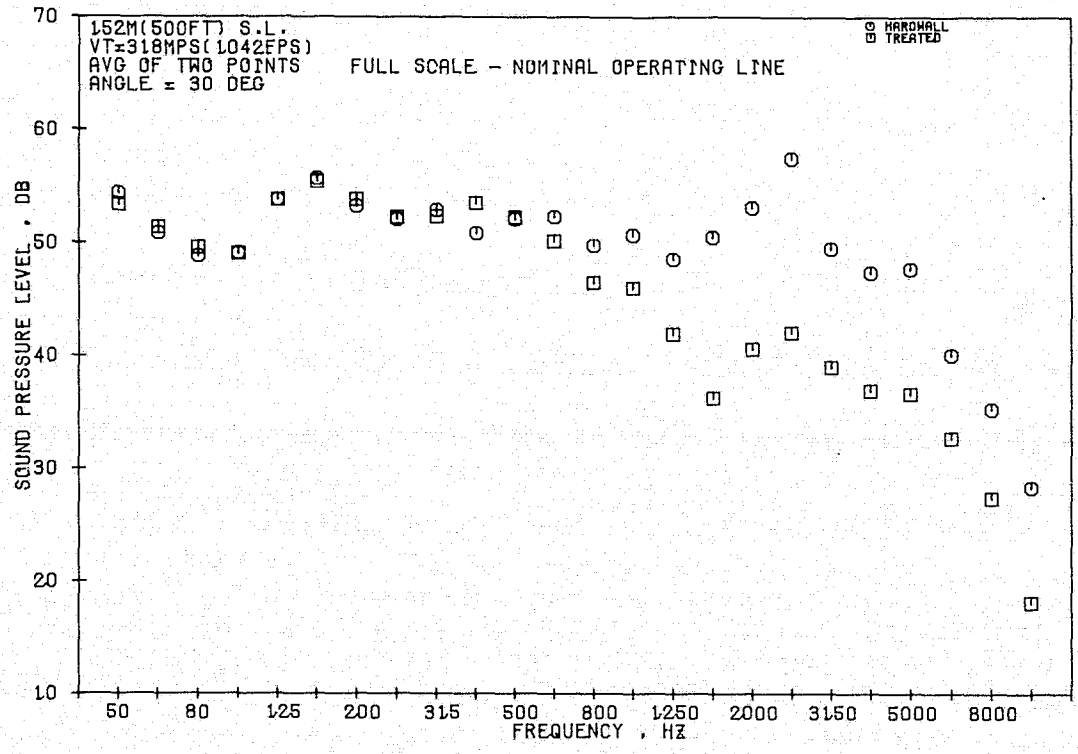

Figure 167. 1/3-Octave Spectra Comparisons at Approach, 30° Angle (Front-Drive Test).

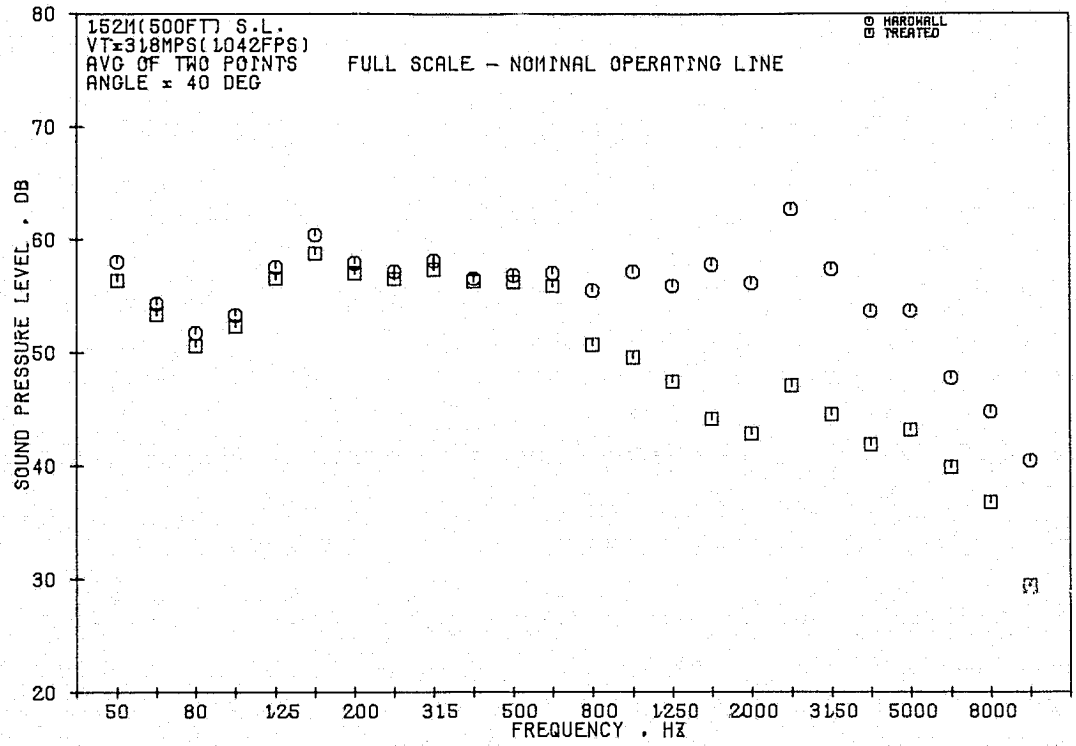

Figure 168. 1/3-Octave Spectra Comparisons at Approach, 40° Angle (Front-Drive Test).

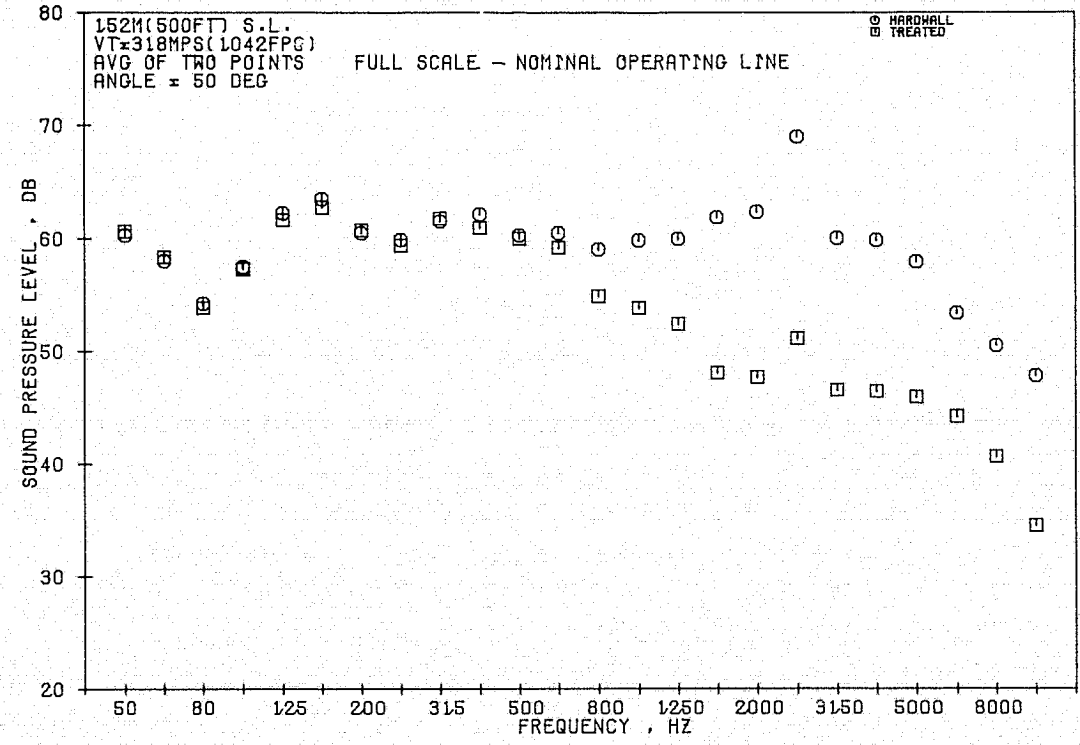

Figure 169. 1/3-Octave Spectra Comparisons at Approach, 50° Angle (Front-Drive Test).

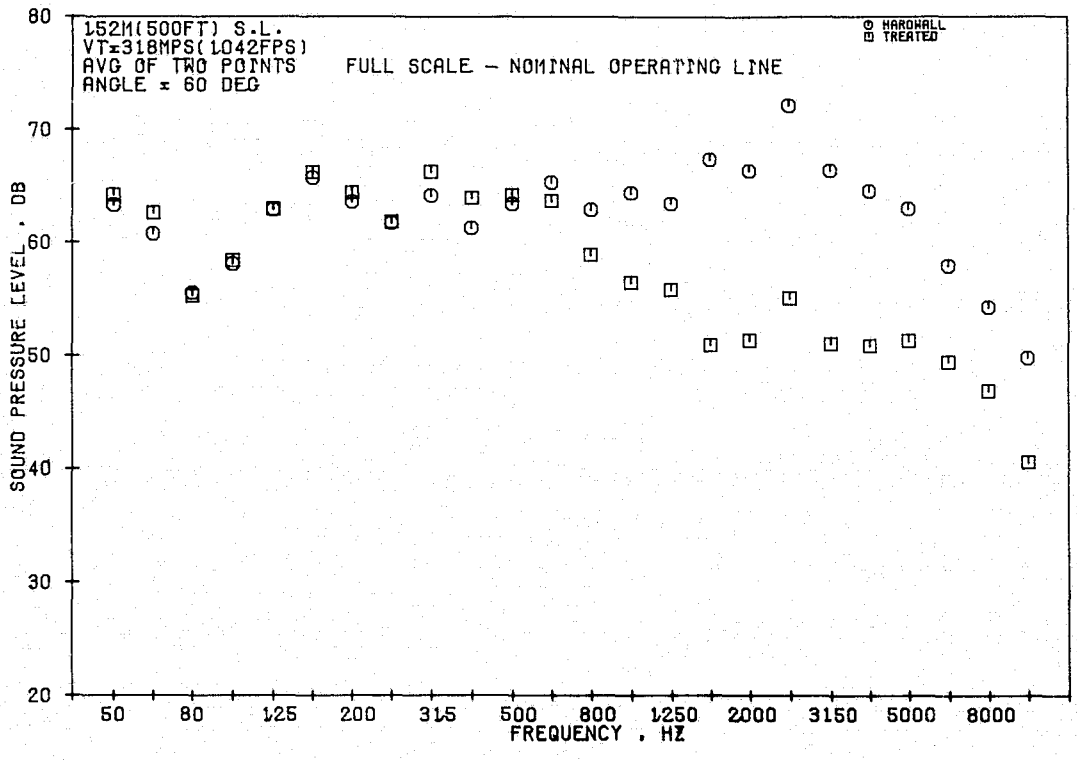

Figure 170. 1/3-Octave Spectra Comparisons at Approach, 60° Angle (Front-Drive Test).

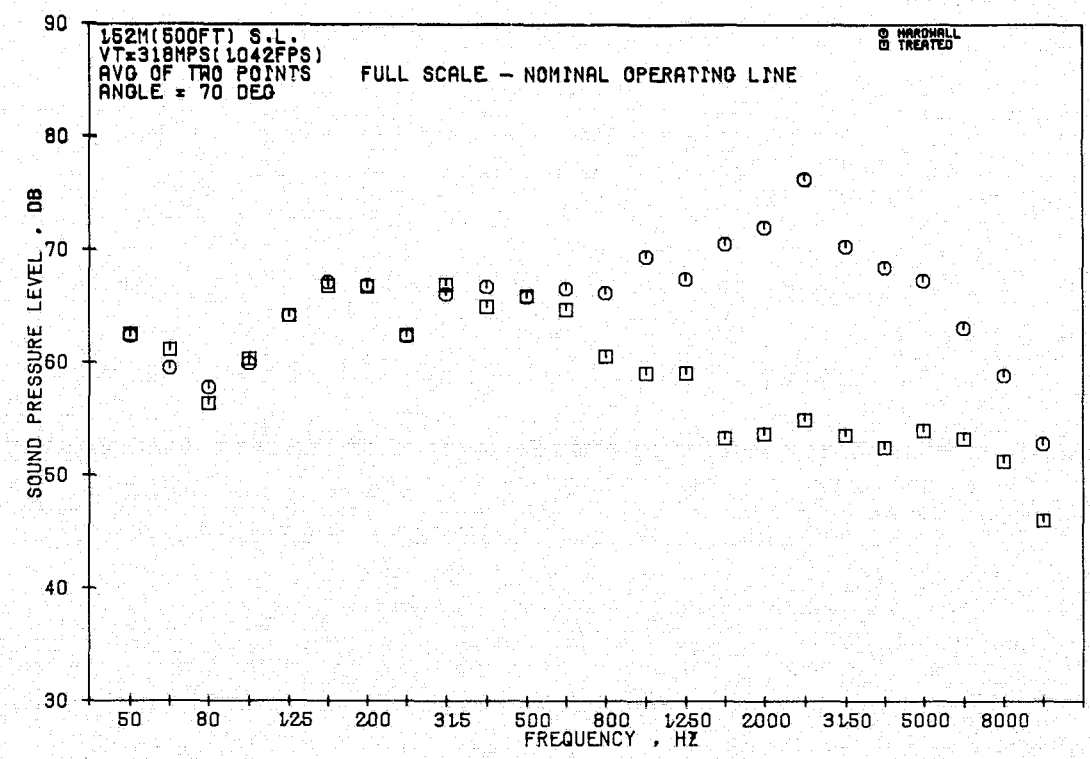

Figure 171. 1/3-Octave Spectra Comparisons at Approach, 70° Angle (Front-Drive Test).

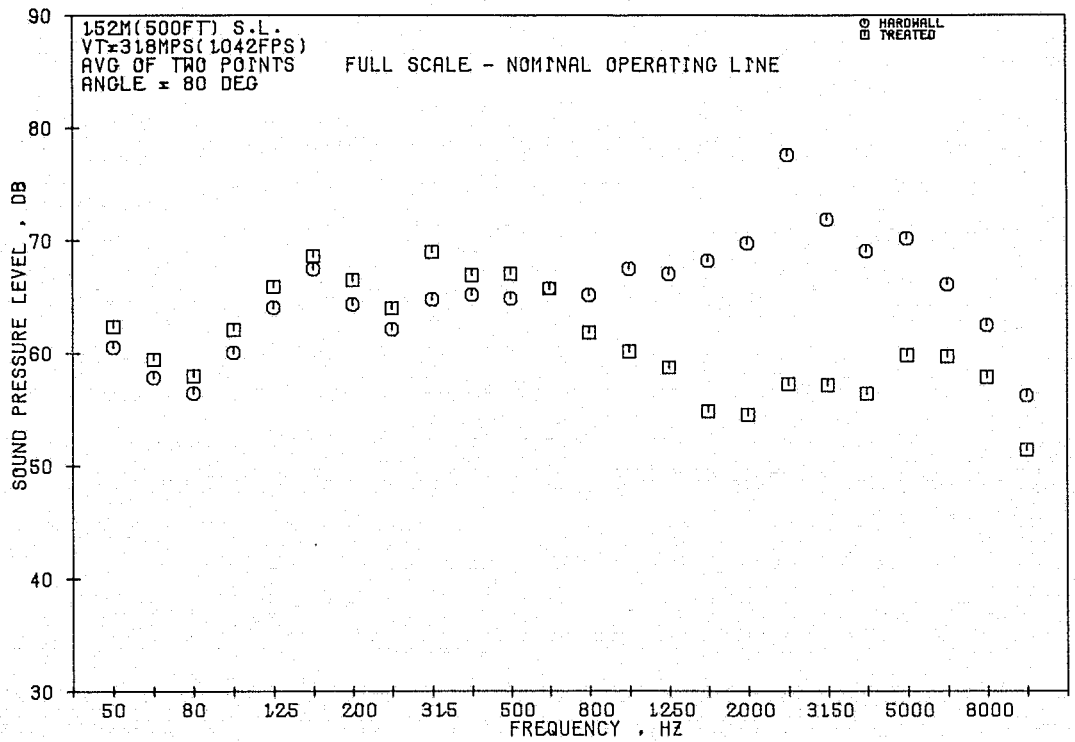

Figure 172. 1/3-Octave Spectra Comparisons at Approach, 80° Angle (Front-Drive Test).

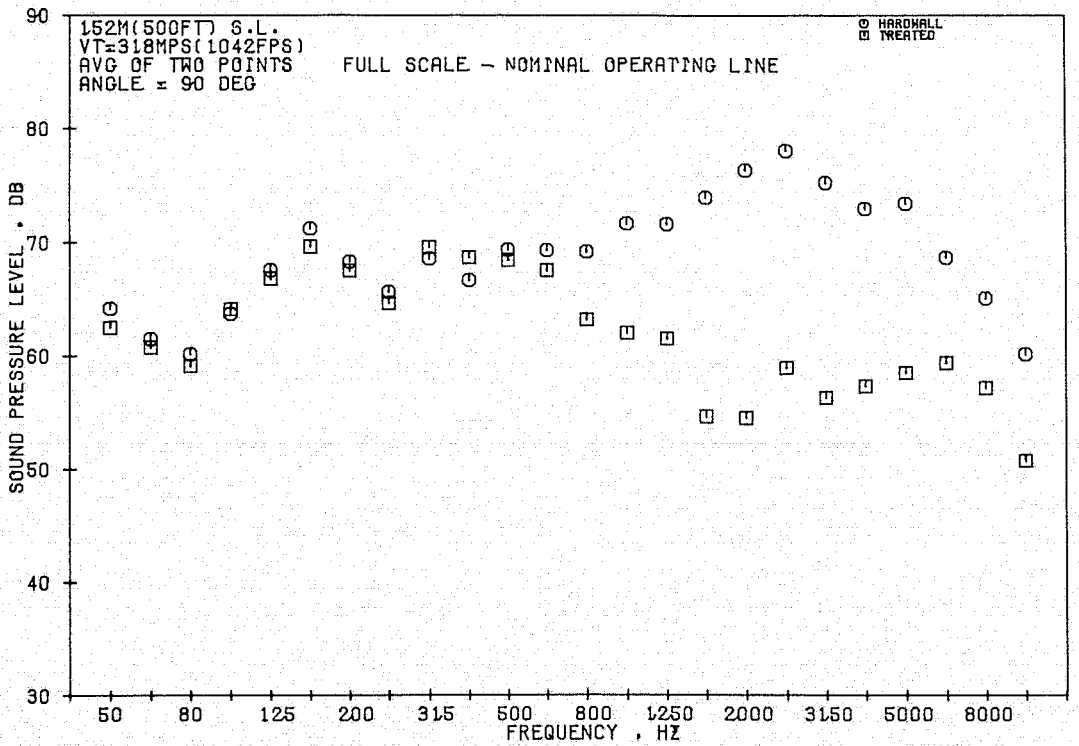

Figure 173. 1/3-Octave Spectra Comparisons at Approach, 90° Angle (Front-Drive Test).

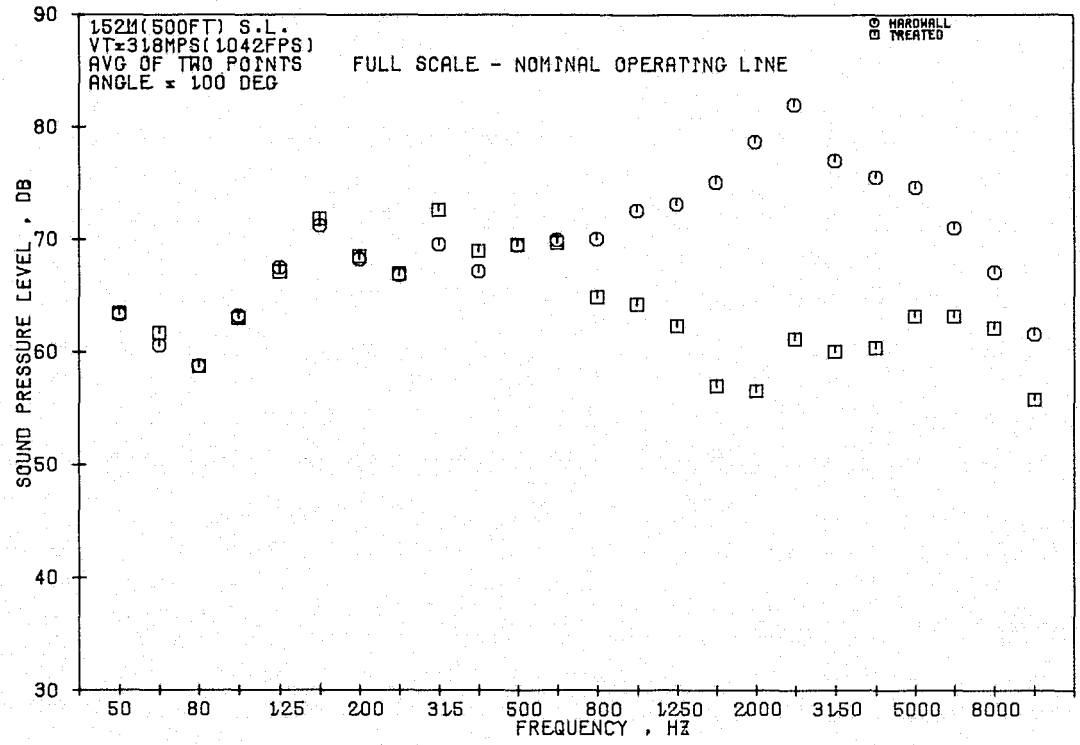

Figure 174. 1/3-Octave Spectra Comparisons at Approach, 100° Angle (Front-Drive Test).

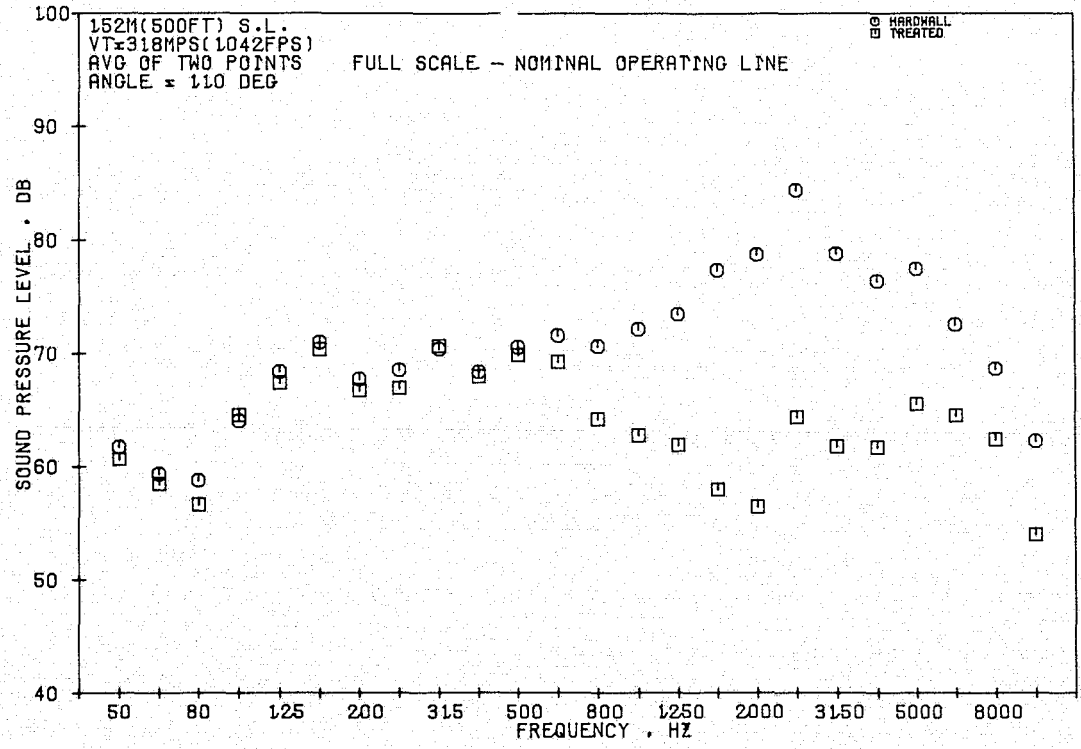

Figure 175. 1/3-Octave Spectra Comparisons at Approach, 110° Angle (Front-Drive Test).

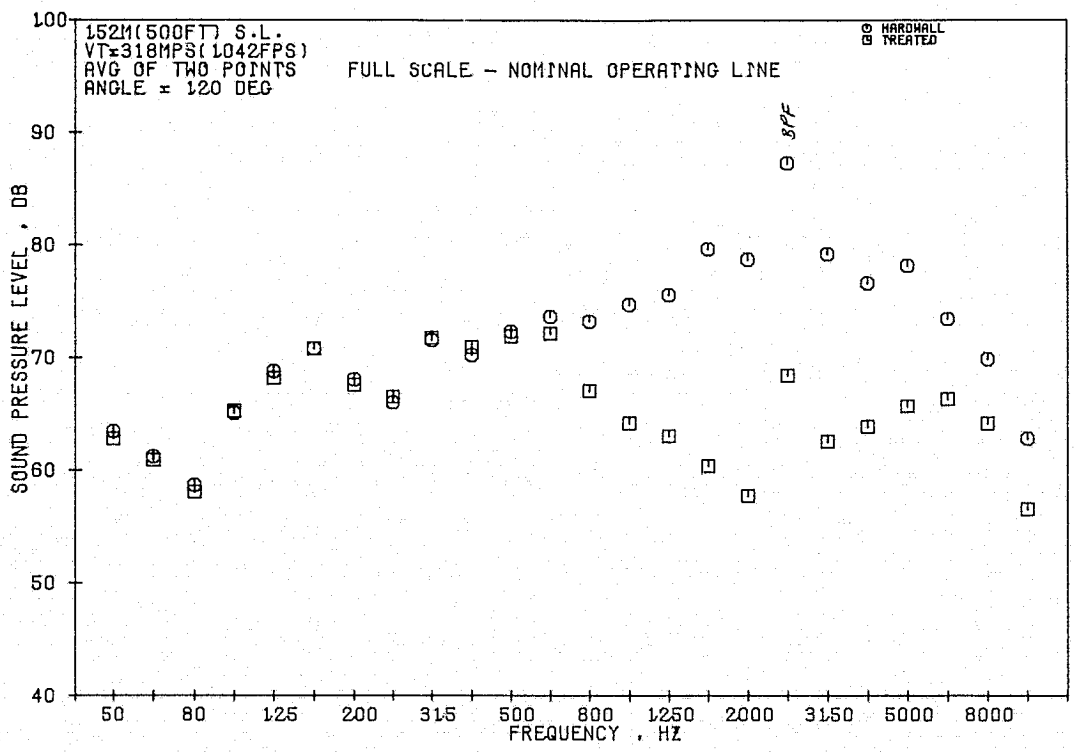

Figure 176. 1/3-Octave Spectra Comparisons at Approach, 120° Angle (Front-Drive Test).

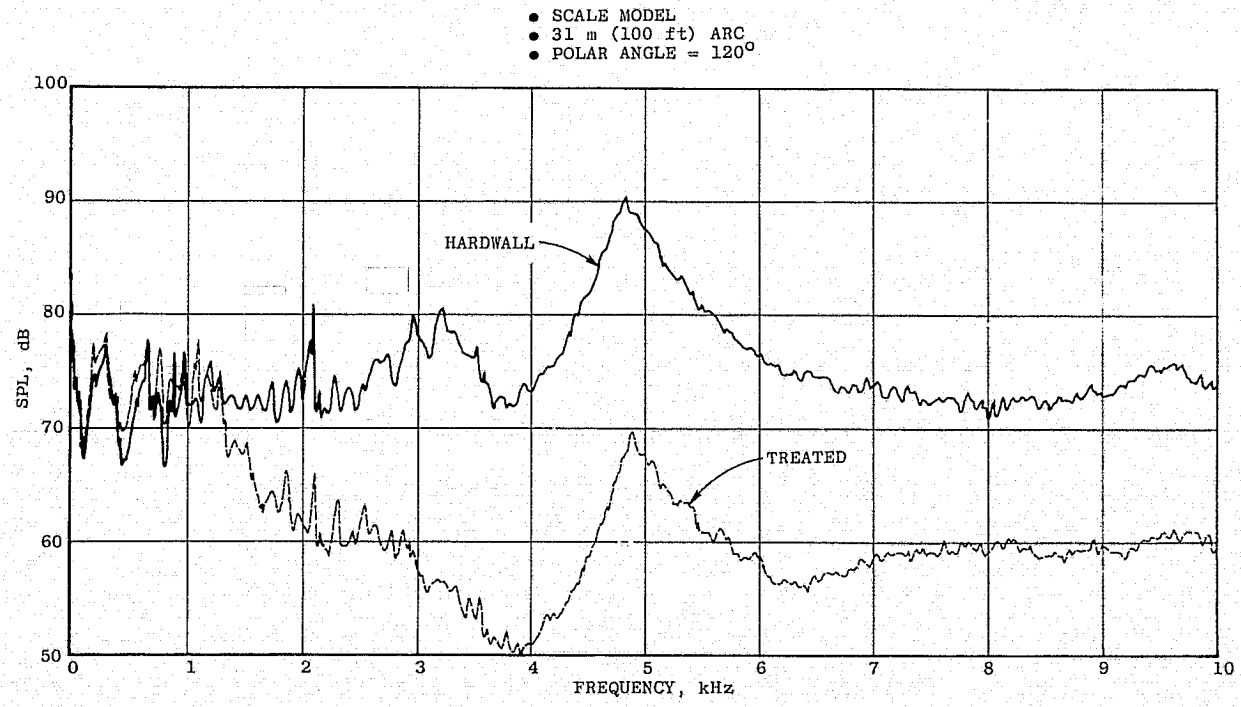

Figure 177. Farfield Narrowband Comparison for the Treated and the Hardwall Configurations at Approach (Front-Drive Test).

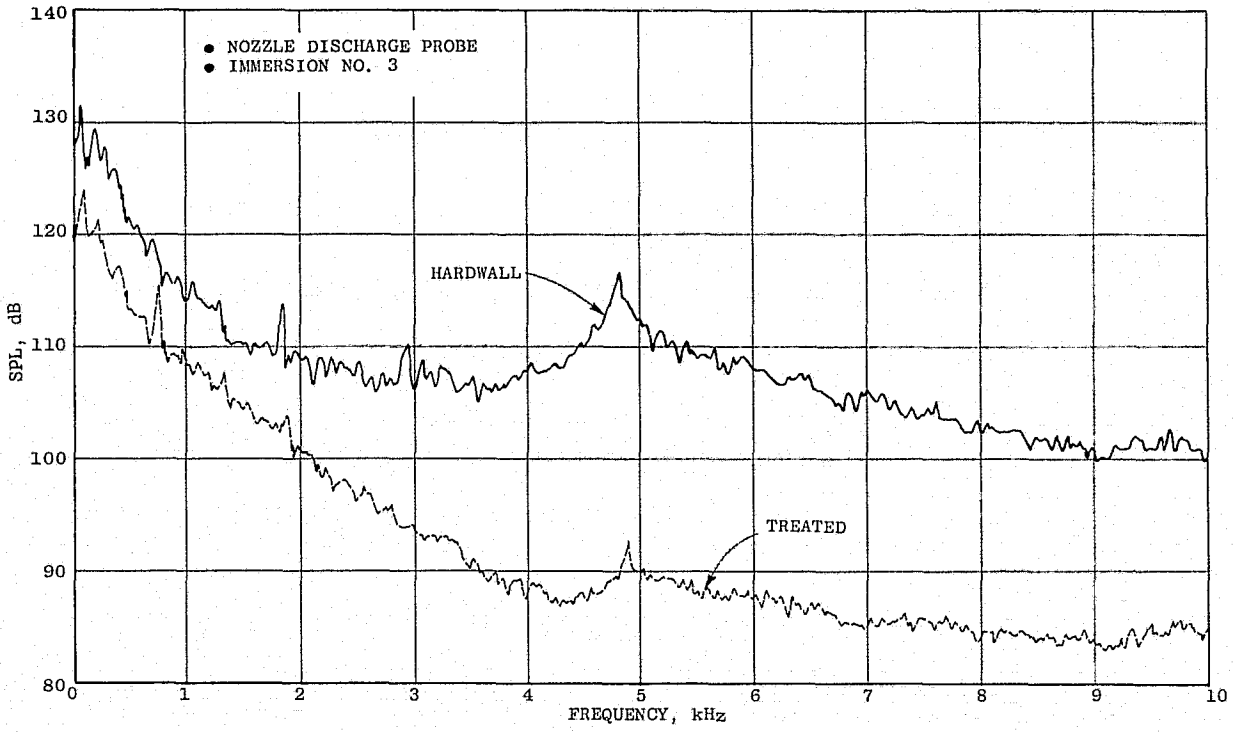

Figure 178. Probe Data Comparison at Approach (Front-Drive Test).

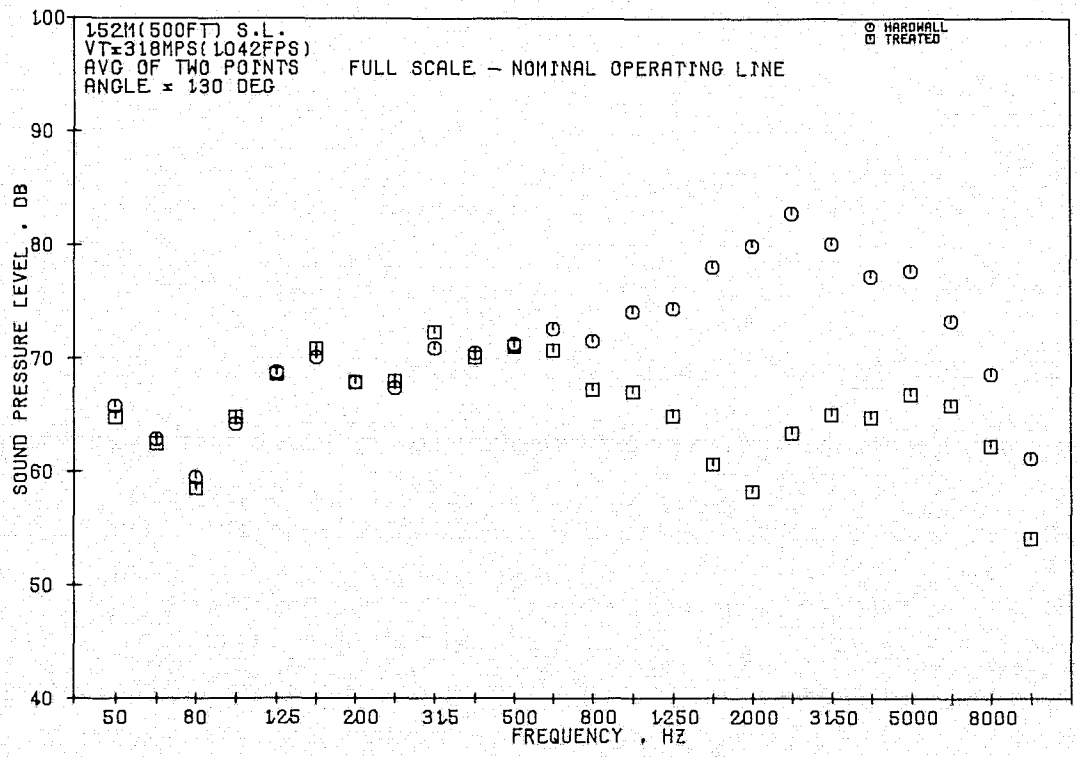

Figure 179. 1/3-Octave Spectra Comparisons at Approach, 130° Angle (Front-Drive Test).

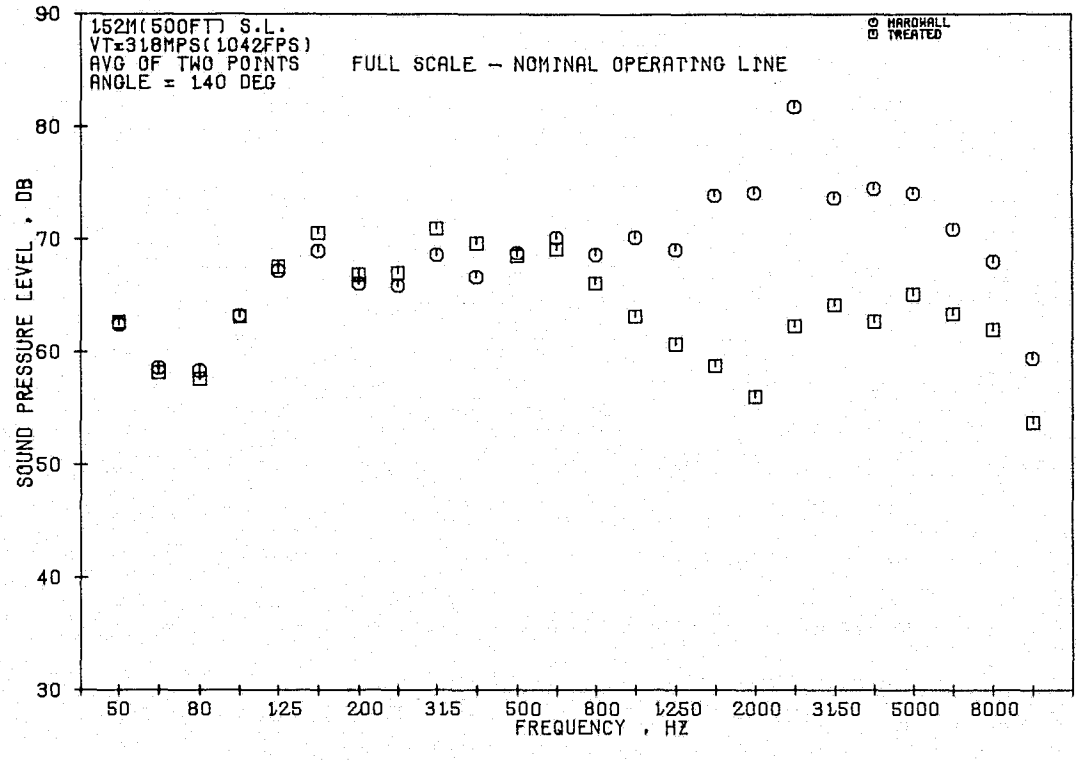

Figure 180. 1/3-Octave Spectra Comparisons at Approach, 140° Angle (Front-Drive Test).

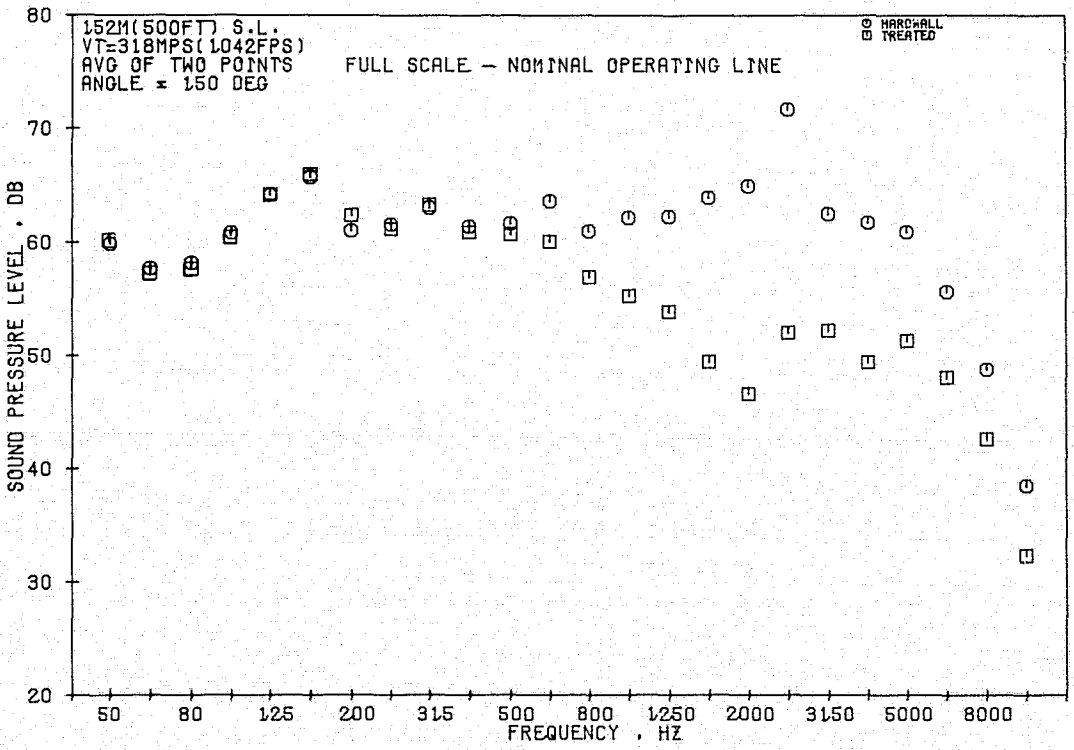

Figure 181. 1/3-Octave Spectra Comparisons at Approach, 150° Angle (Front-Drive Test).

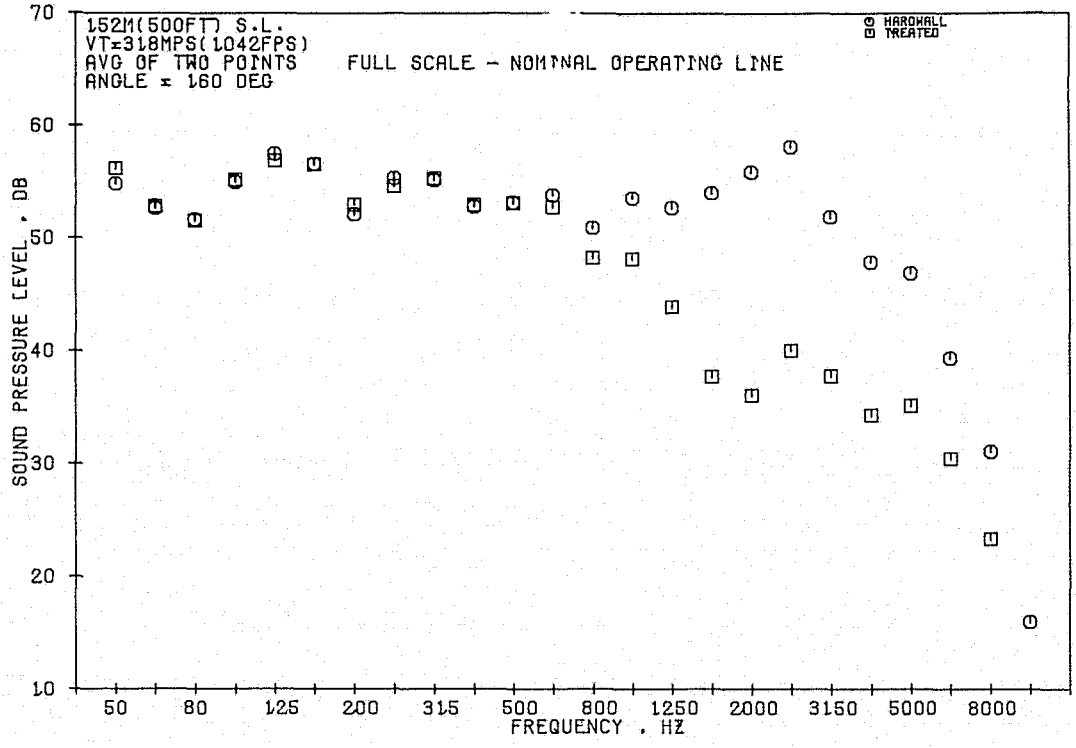

Figure 182. 1/3-Octave Spectra Comparisons at Approach, 160° Angle (Front-Drive Test).

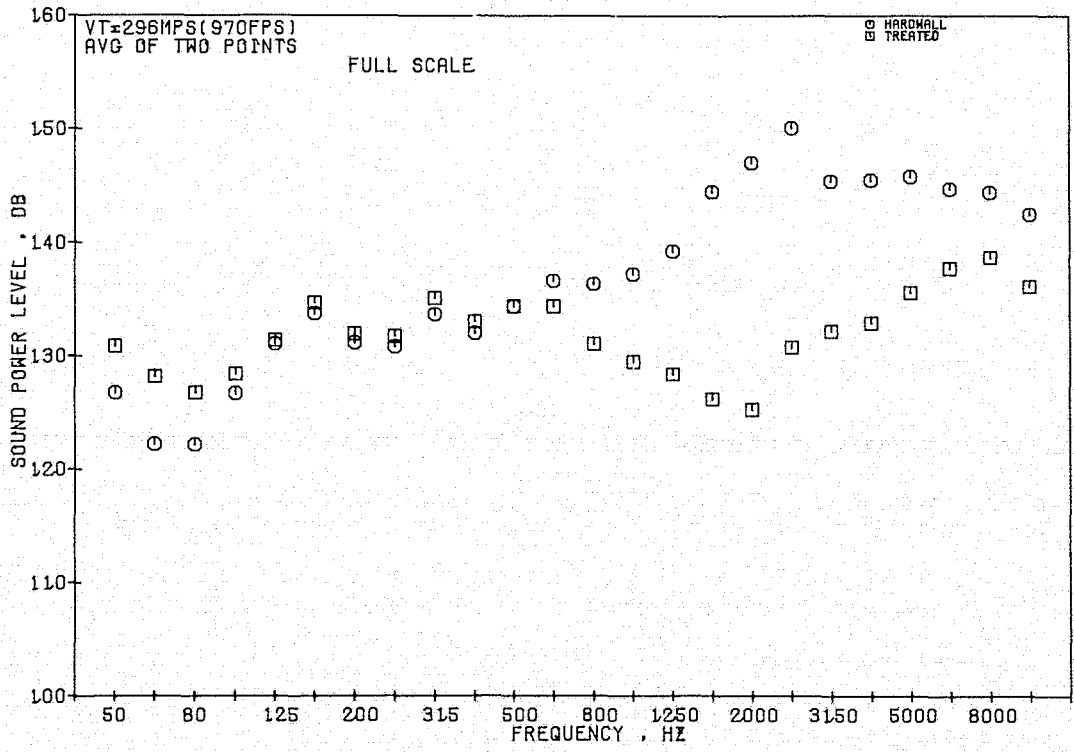

Figure 183. 1/3-Octave PWL Comparisons at Approach, V_T = 296 m/sec (Front-Drive Test).

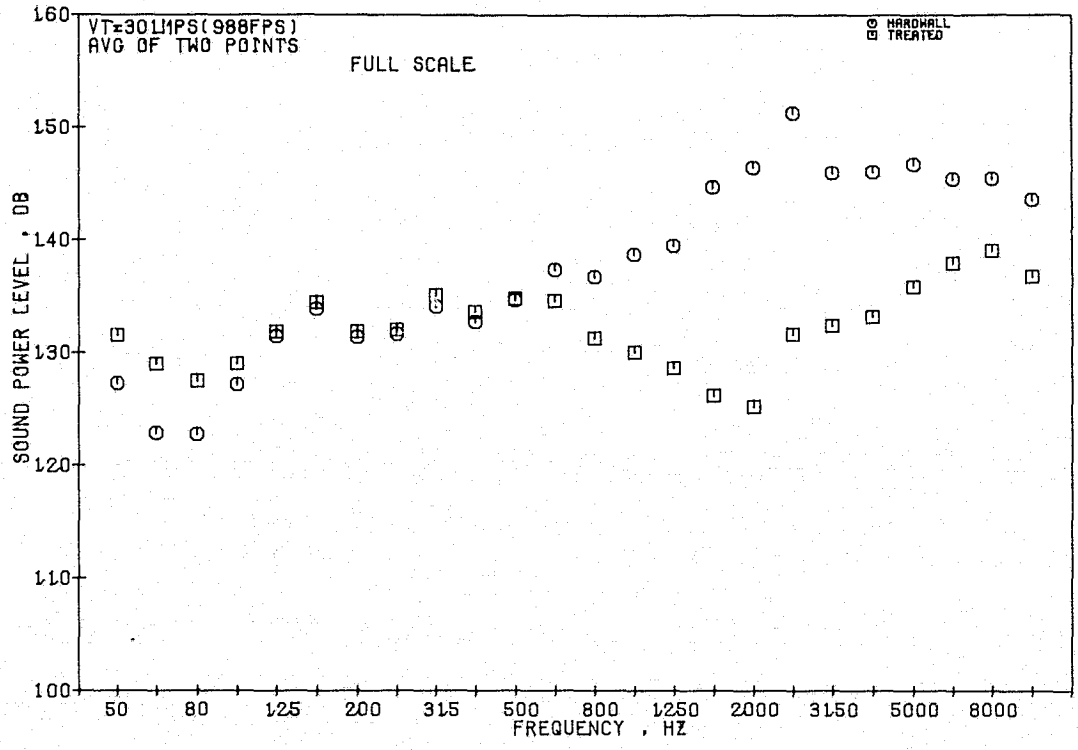

Figure 184. 1/3-Octave PWL Comparisons at Approach, V_T = 301 m/sec (Front-Drive Test).

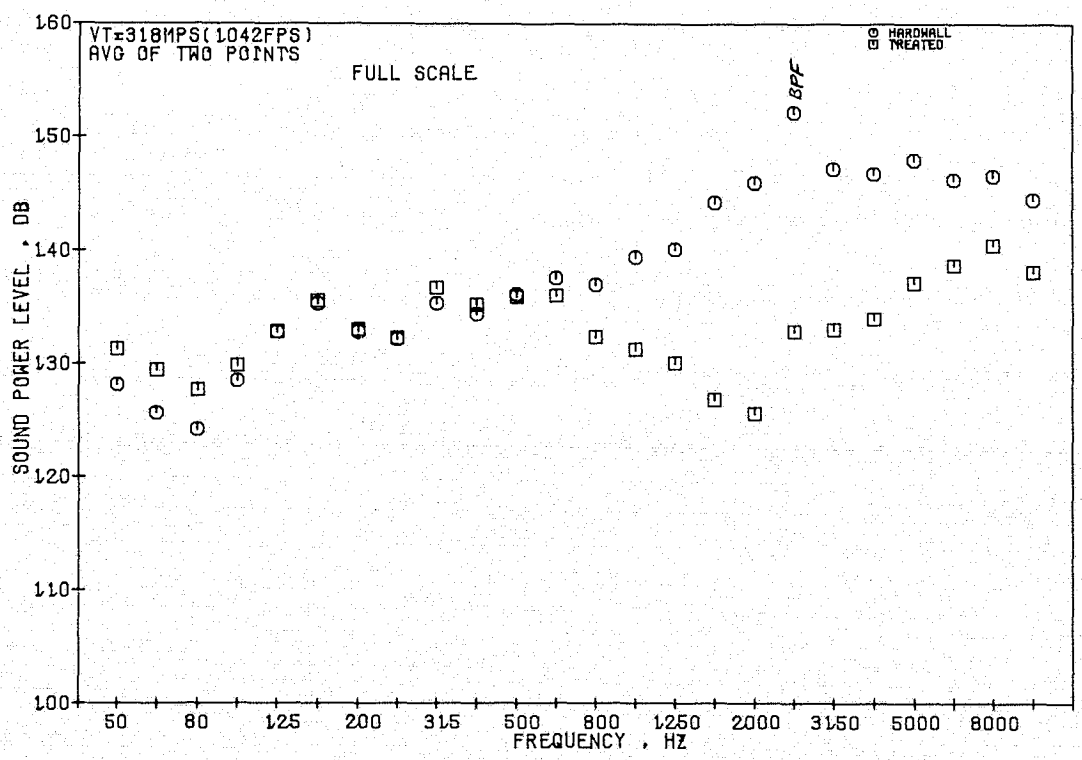

Figure 185. 1/3-Octave PWL Comparisons at Approach, V_T = 318 m/sec (Front-Drive Test).

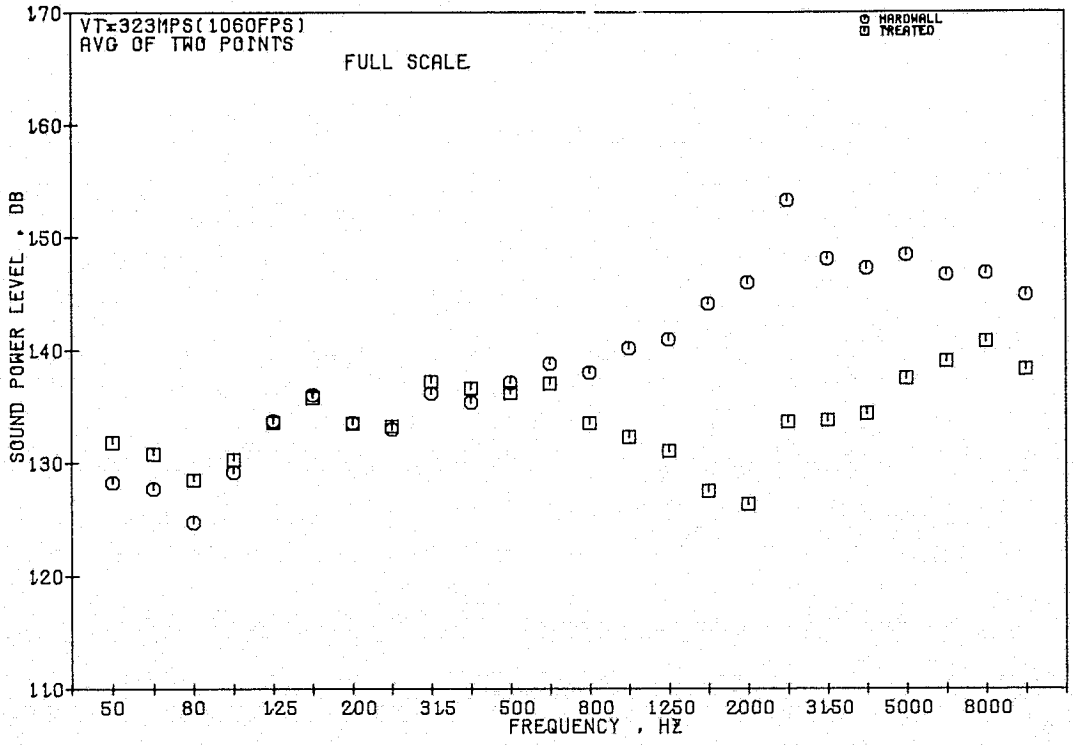

Figure 186. 1/3-Octave PWL Comparisons at Approach, V_T = 323 m/sec (Front-Drive Test).

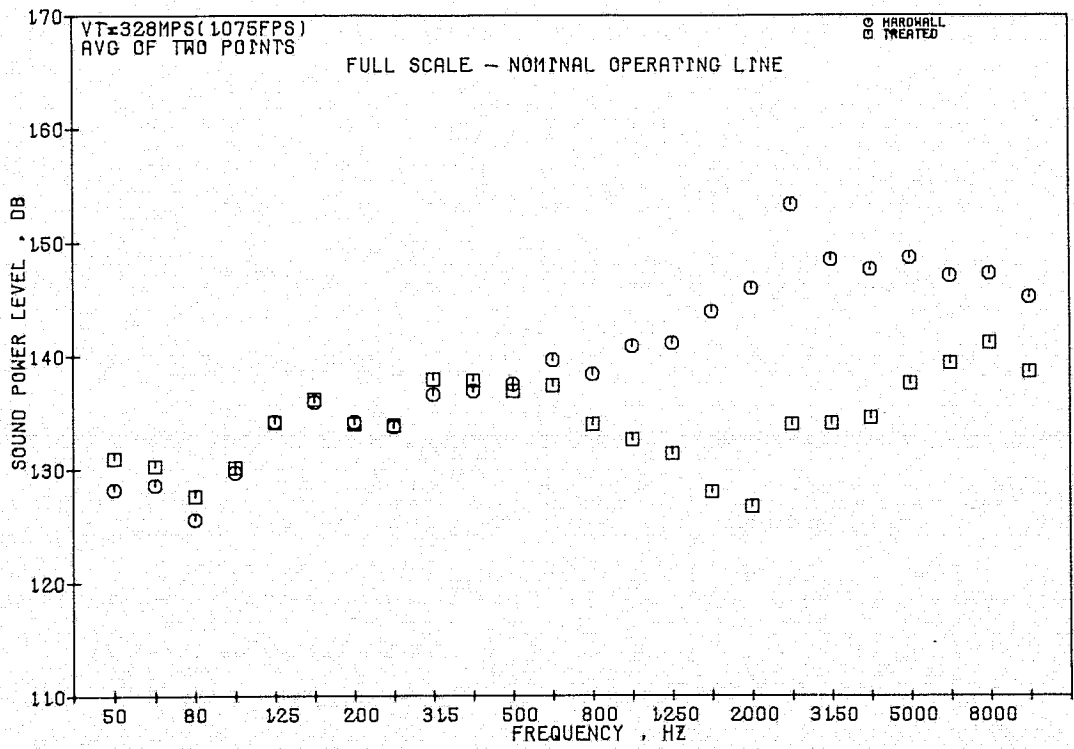

Figure 187. 1/3-Octave PWL Comparisons at Approach, V_T = 328 m/sec (Front-Drive Test).

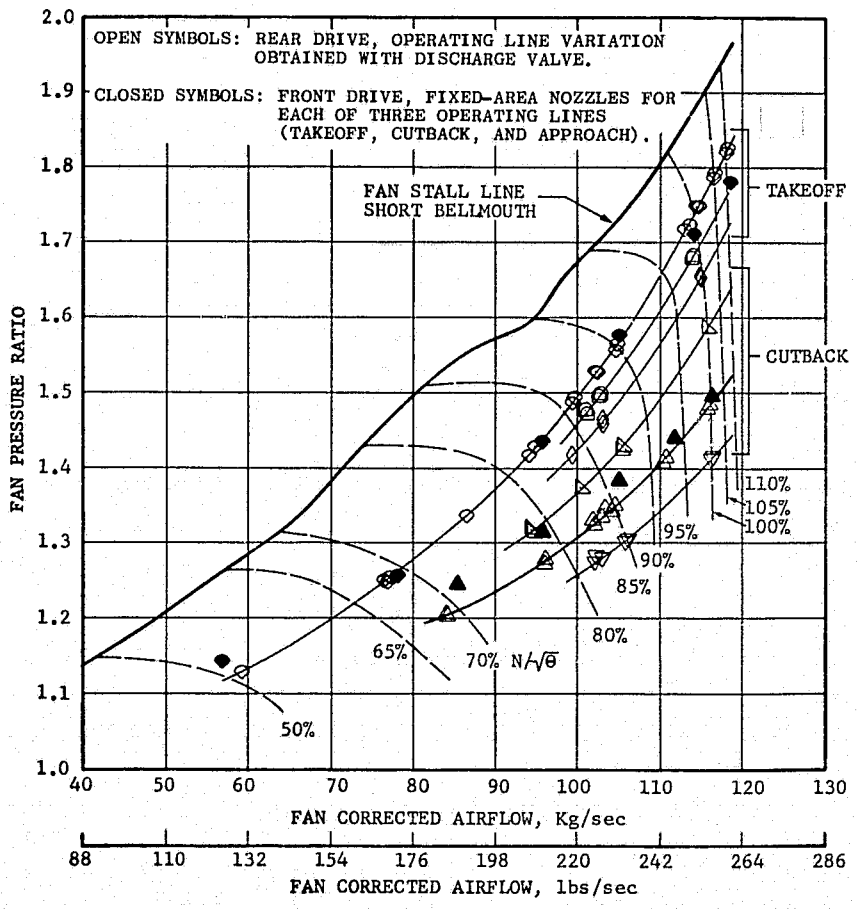

Figure 188. Aerodynamic Fan Performance Map - Baseline Inlet.

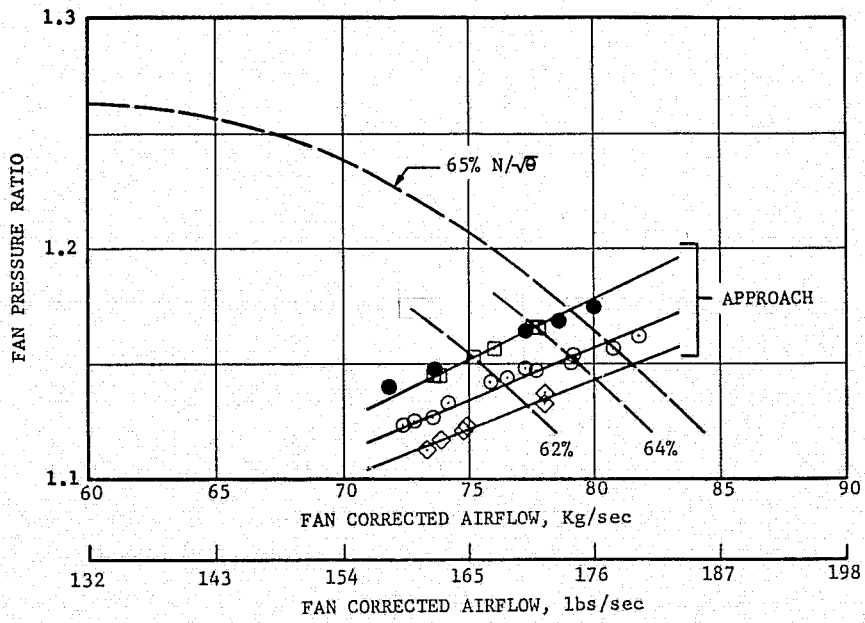

Figure 189. Aerodynamic Fan Performance Map - Baseline Inlet.

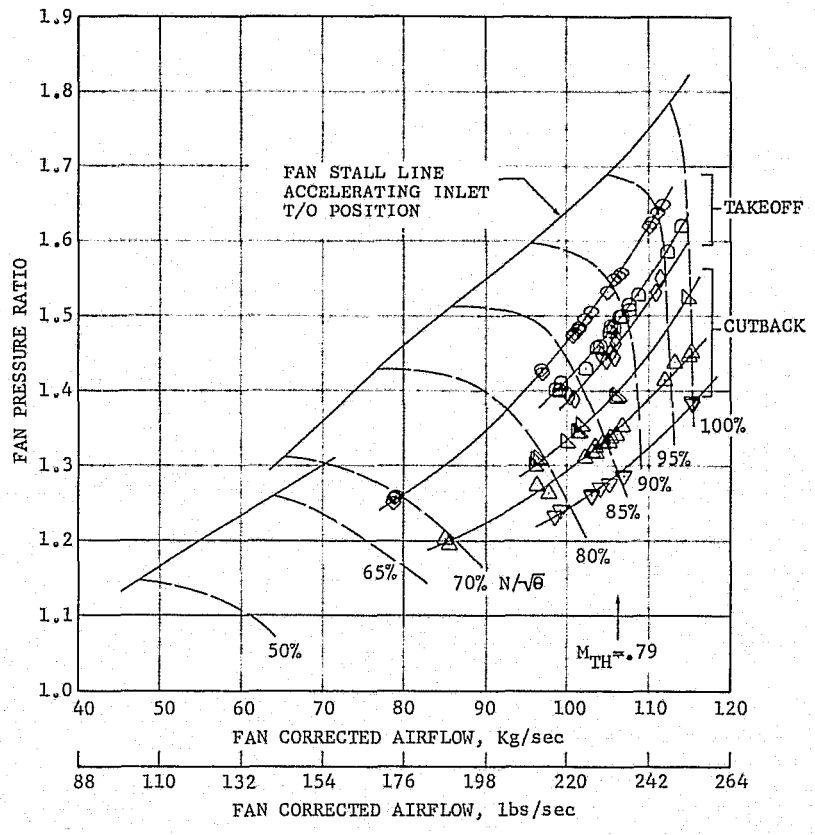

Figure 190. Aerodynamic Fan Performance Map - Accelerating Inlet, Takeoff Position.

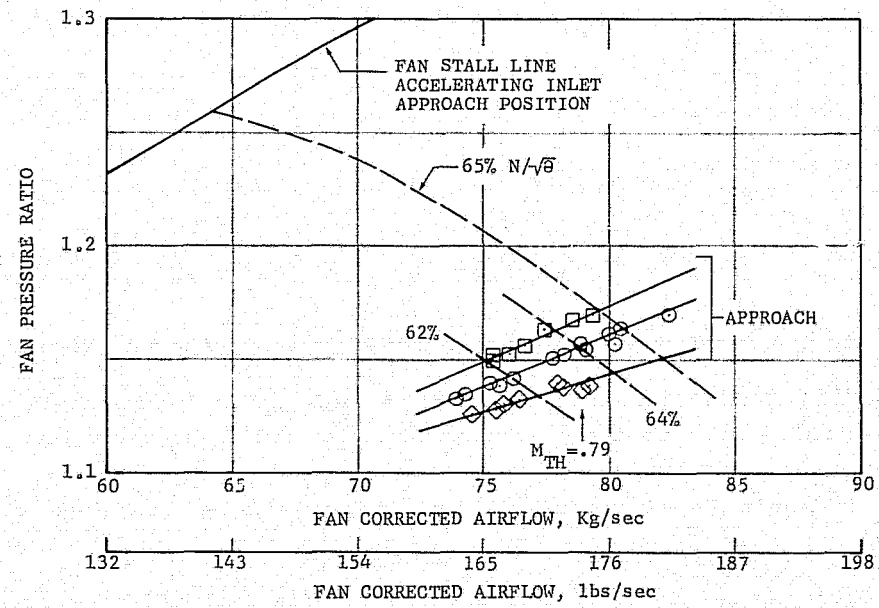

Figure 191. Aerodynamic Fan Performance Map - Accelerating Inlet, Approach Position.

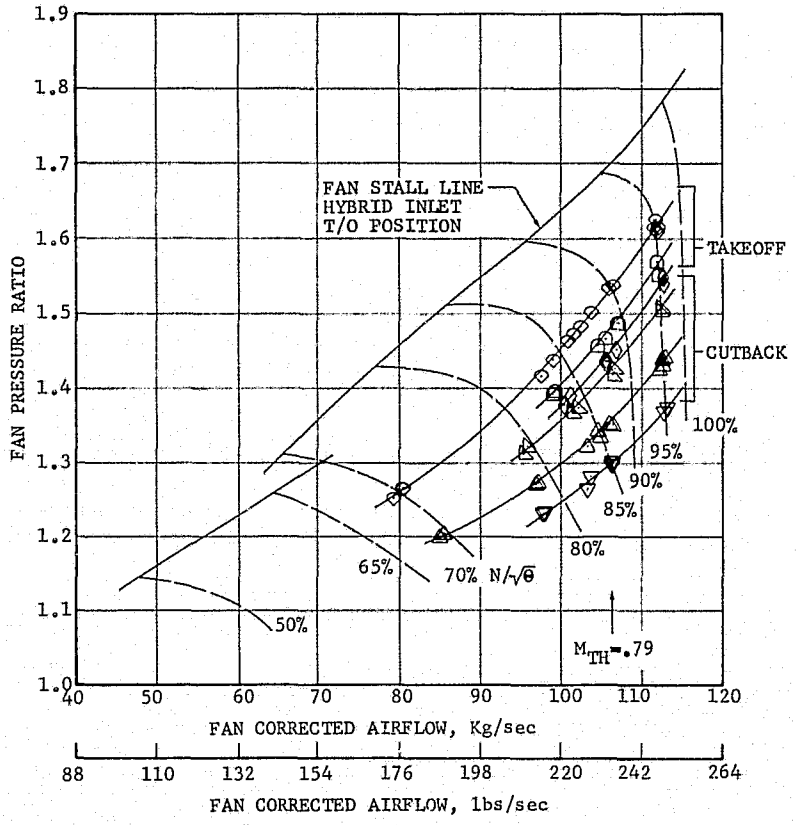

Figure 192. Aerodynamic Performance Map - Hybrid Inlet, Takeoff Position.

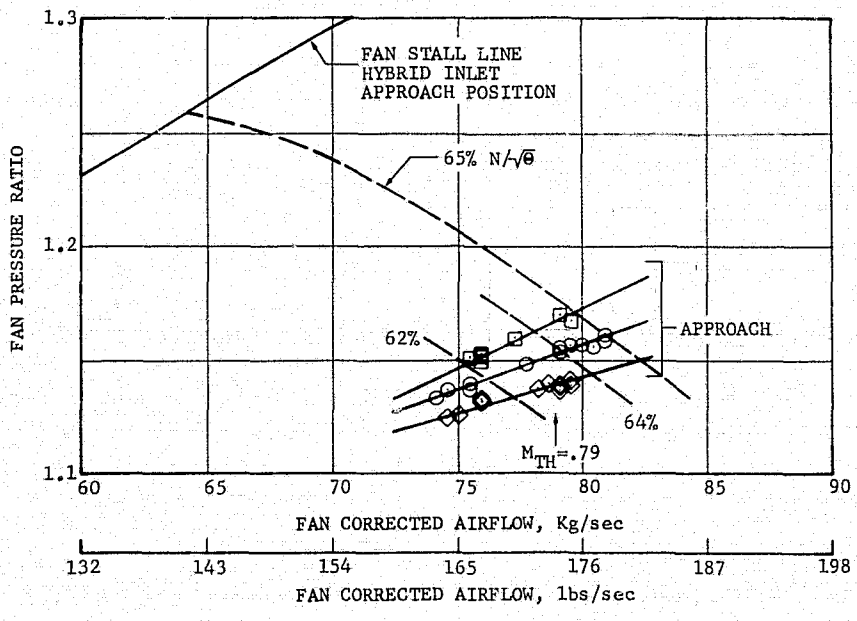

Figure 193. Aerodynamic Performance Map - Hybrid Inlet, Approach Position.

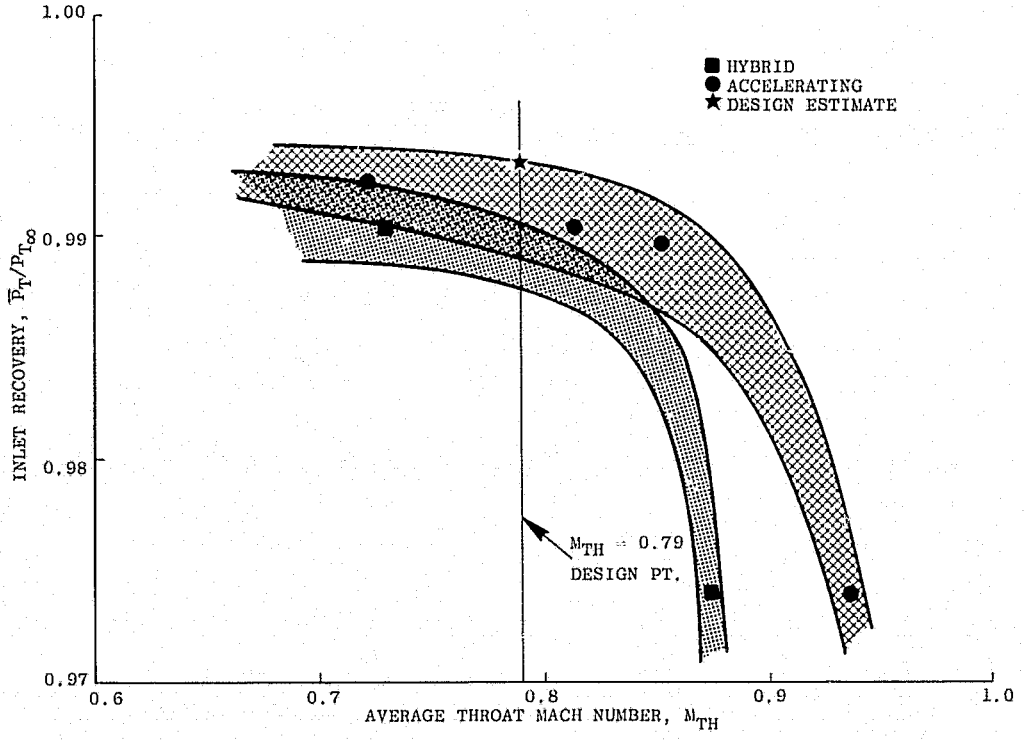

Figure 194. Takeoff Inlet Total Pressure Recovery.

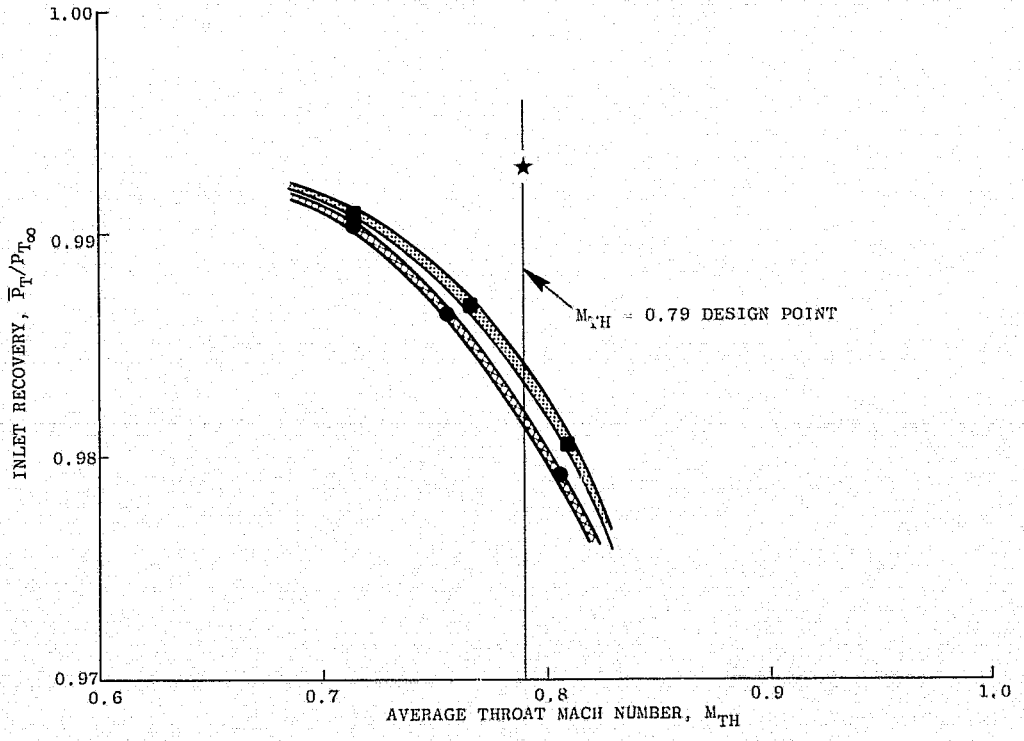

Figure 195. Approach Inlet Total Pressure Recovery.

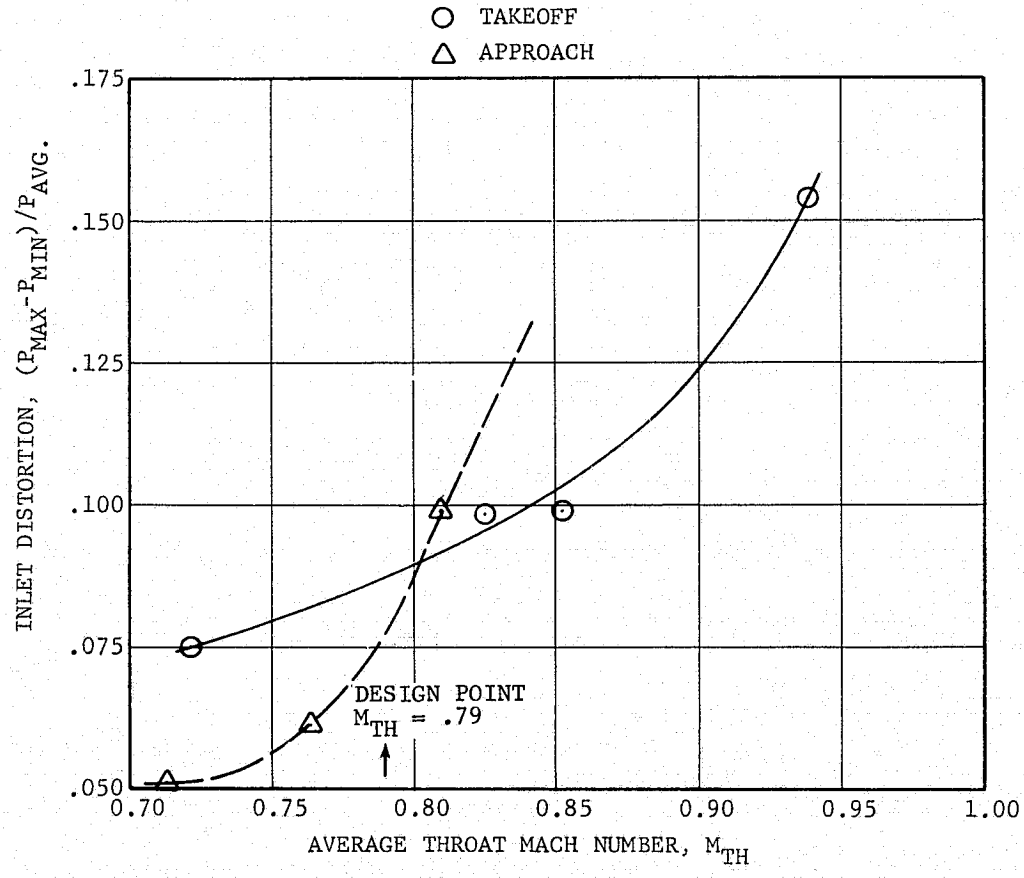

Figure 196. Inlet Distortion Vs. Average Throat Mach Number, Hybrid Inlet.

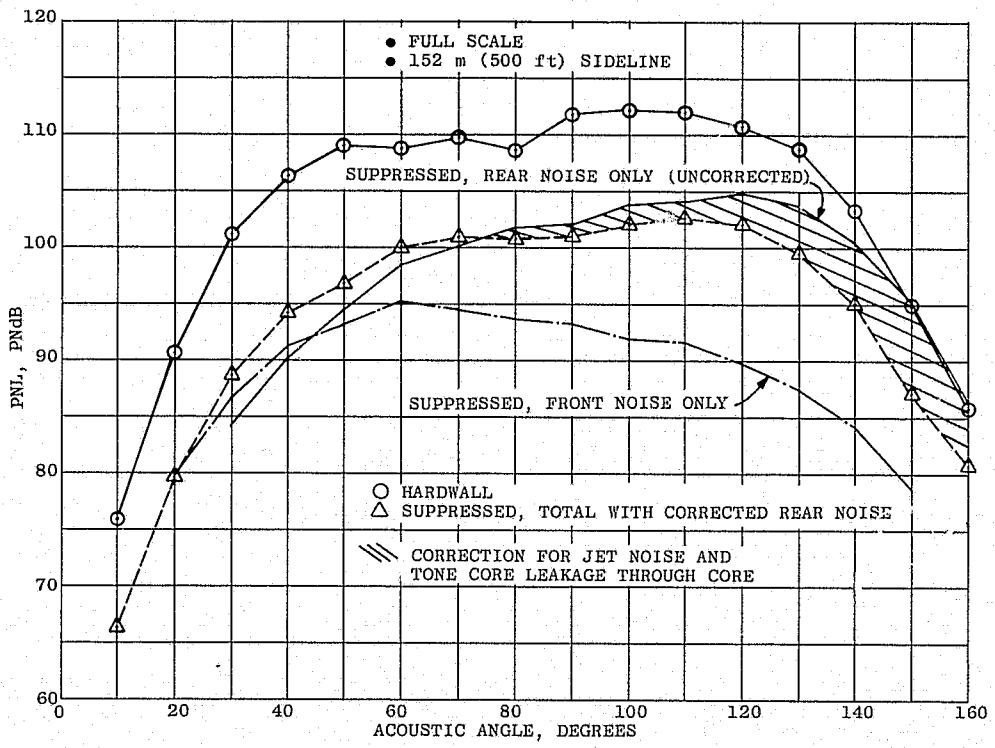

Figure 197. Combined Front- and Rear-Noise PNL Directivities, Takeoff.

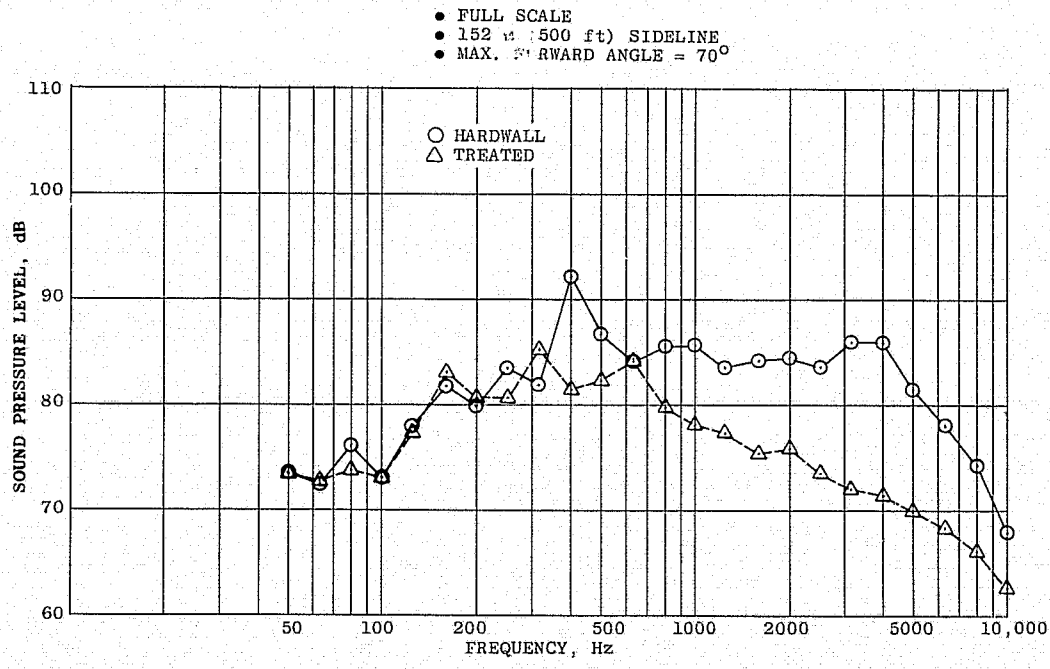

Figure 198. Combined Front- and Rear-Noise Spectra, Takeoff, 70° Max. Forward Angle.

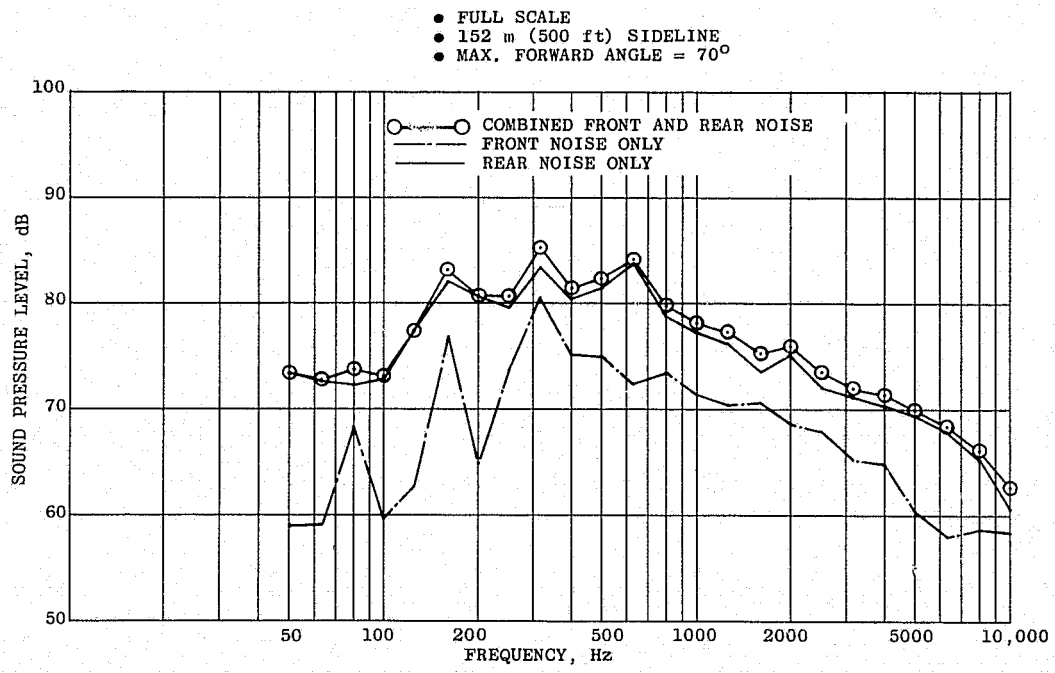

Figure 199. Combined Front- and Rear-Noise Suppressed Spectra and Components, Takeoff, 70° Max. Forward Angle.

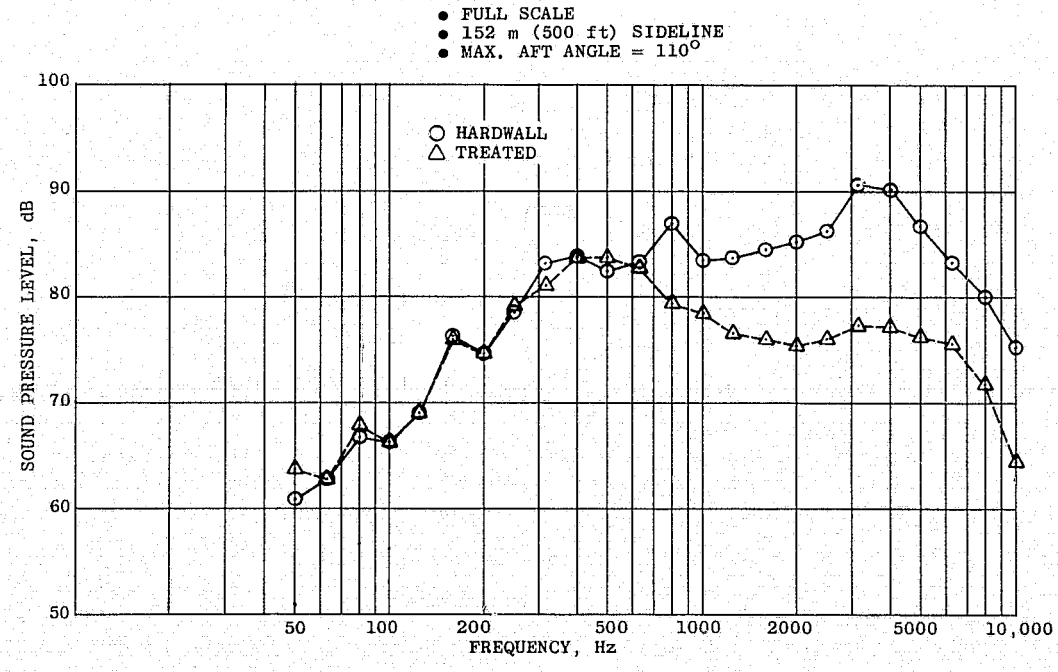

Figure 200. Combined Front- and Rear-Noise Spectra, Takeoff, 110° Max. Aft Angle.

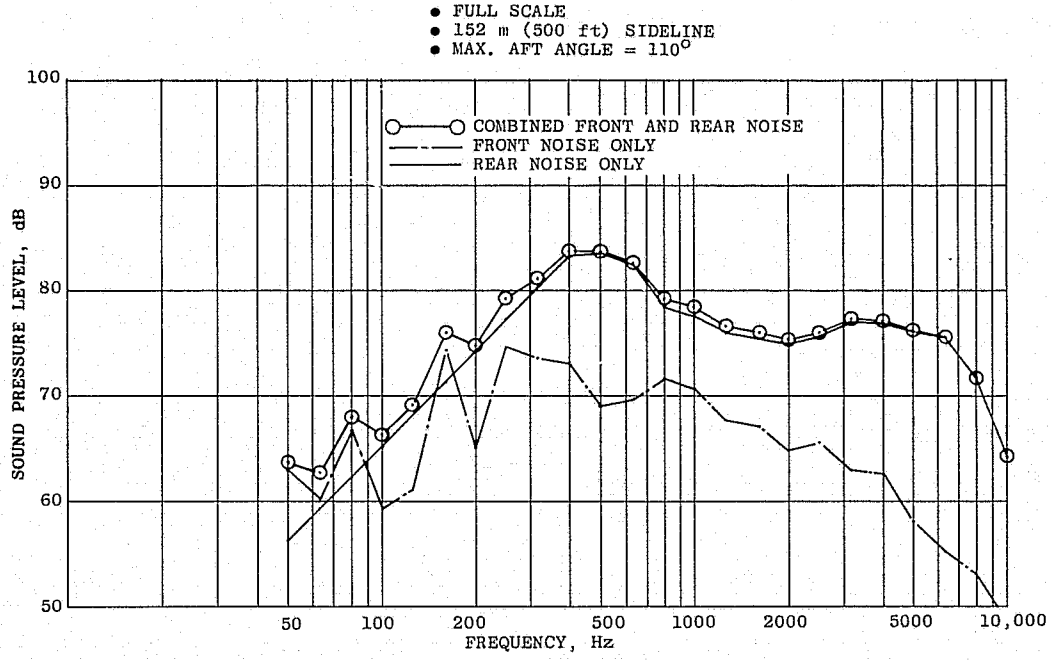

Figure 201. Combined Front- and Rear-Noise Suppressed Spectra and Components, Takeoff, 110° Max. Aft Angle.

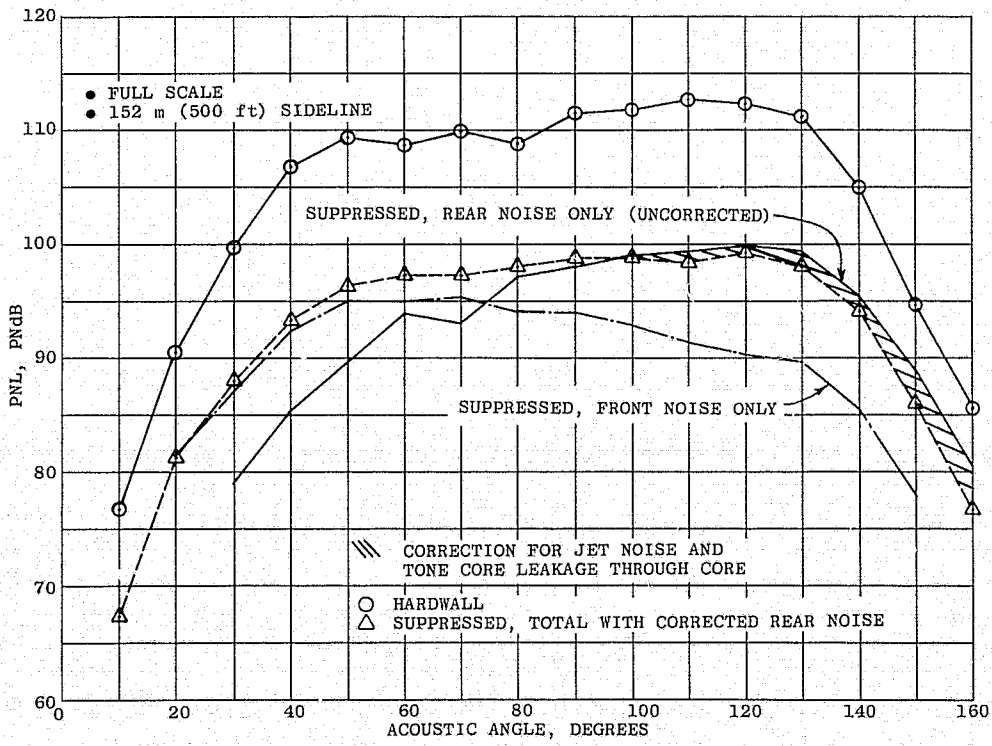

Figure 202. Combined Front- and Rear-Noise PNL Directivities, Cutback.

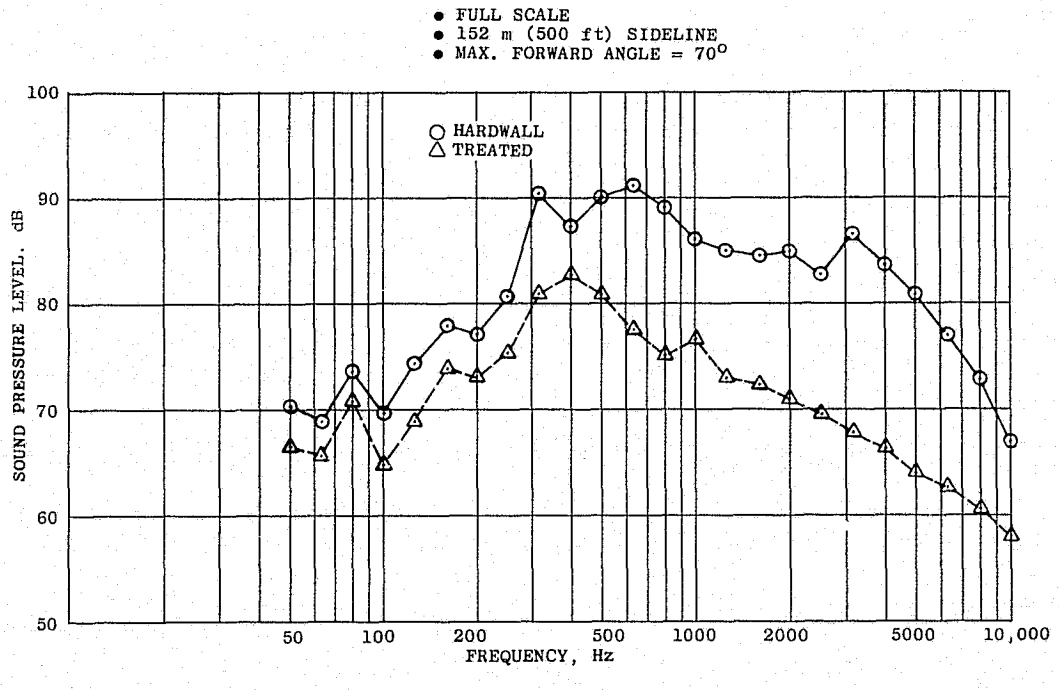

Figure 203. Combined Front- and Rear-Noise Spectra, Cutback, 70° Max. Forward Angle.

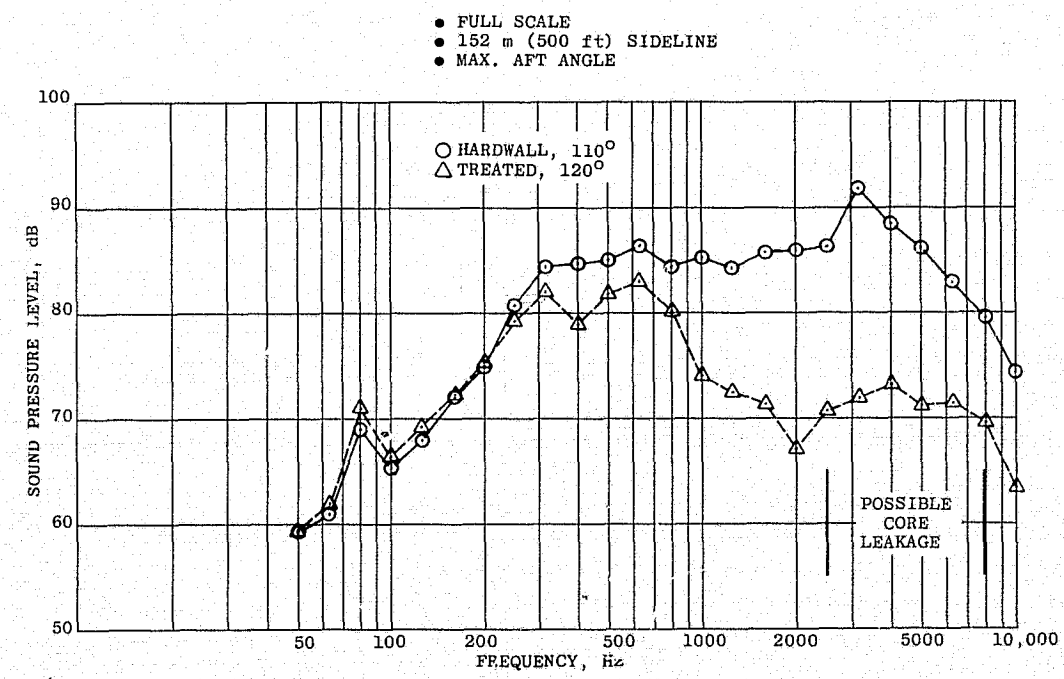

Figure 204. Combined Front- and Rear-Noise Spectra, Cutback, Max. Aft Angle.

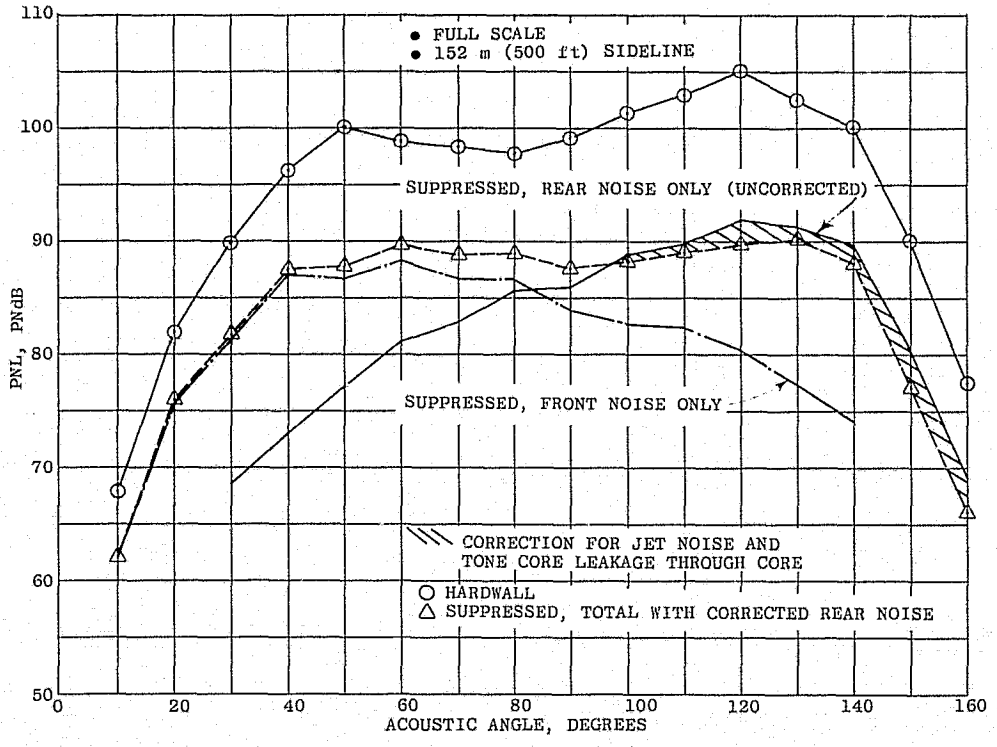

Figure 205. Combined Front- and Rear-Noise PNL Directivities, Approach.

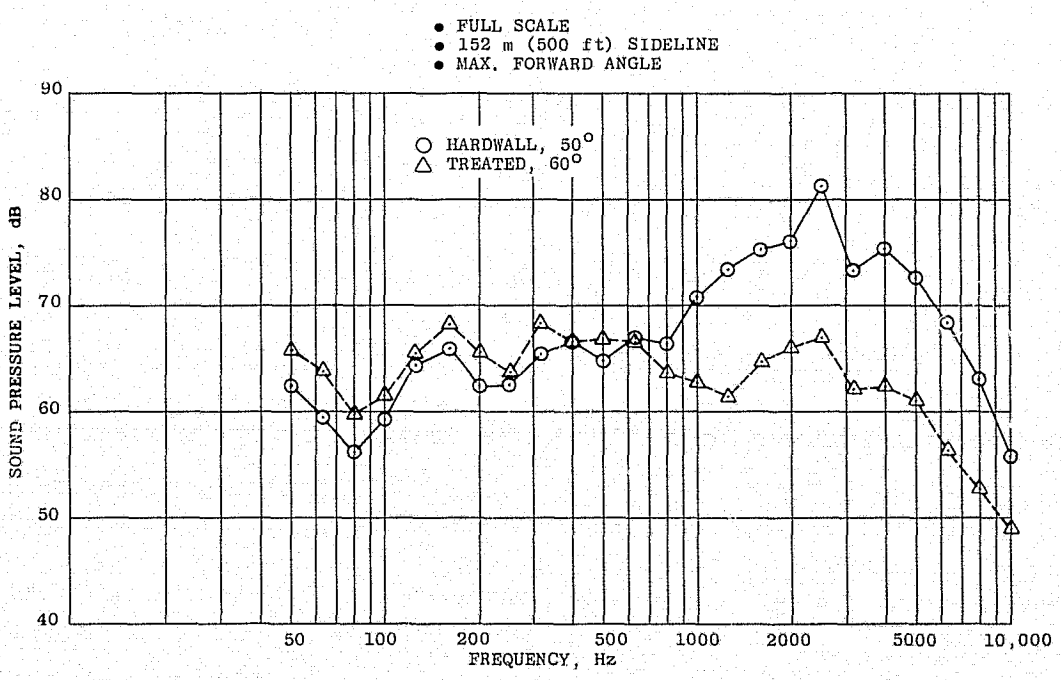

Figure 206. Combined Front- and Rear-Noise Spectra, Approach, Max. Forward Angle.

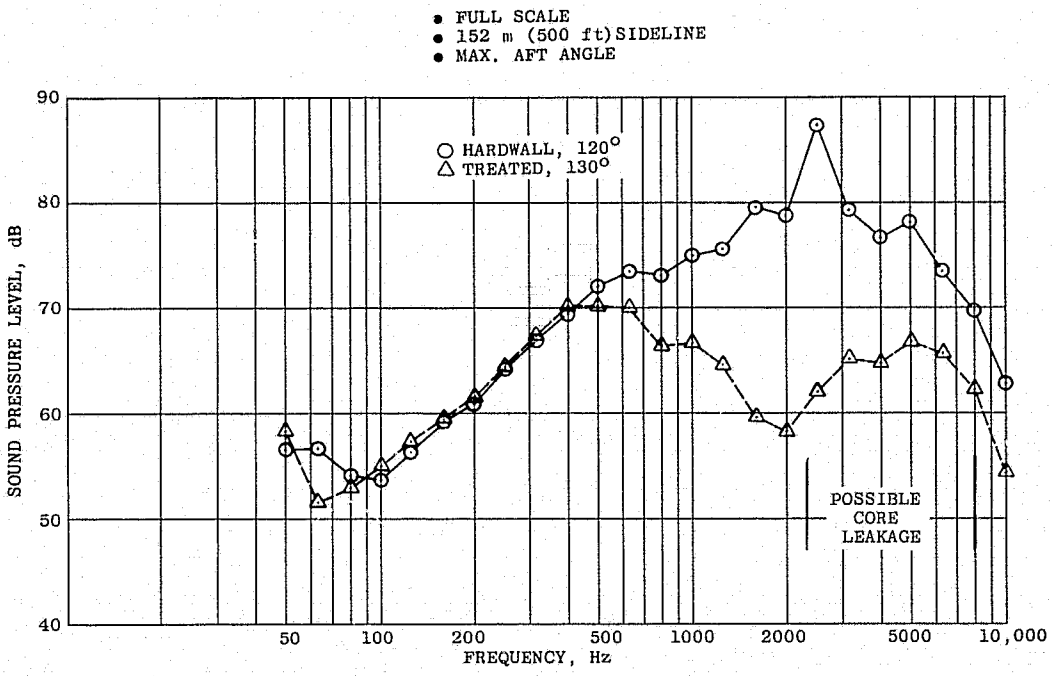

Figure 207. Combined Front- and Rear-Noise Spectra, Approach, Max. Aft Angle.

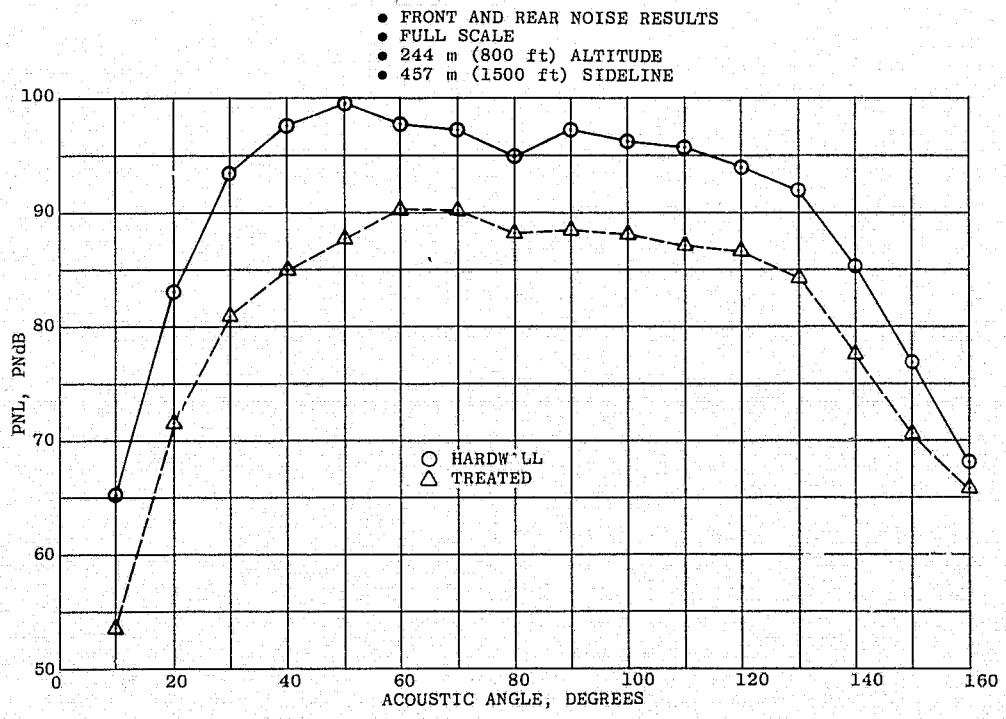

Figure 208. Flight PNL Directivity, Takeoff.

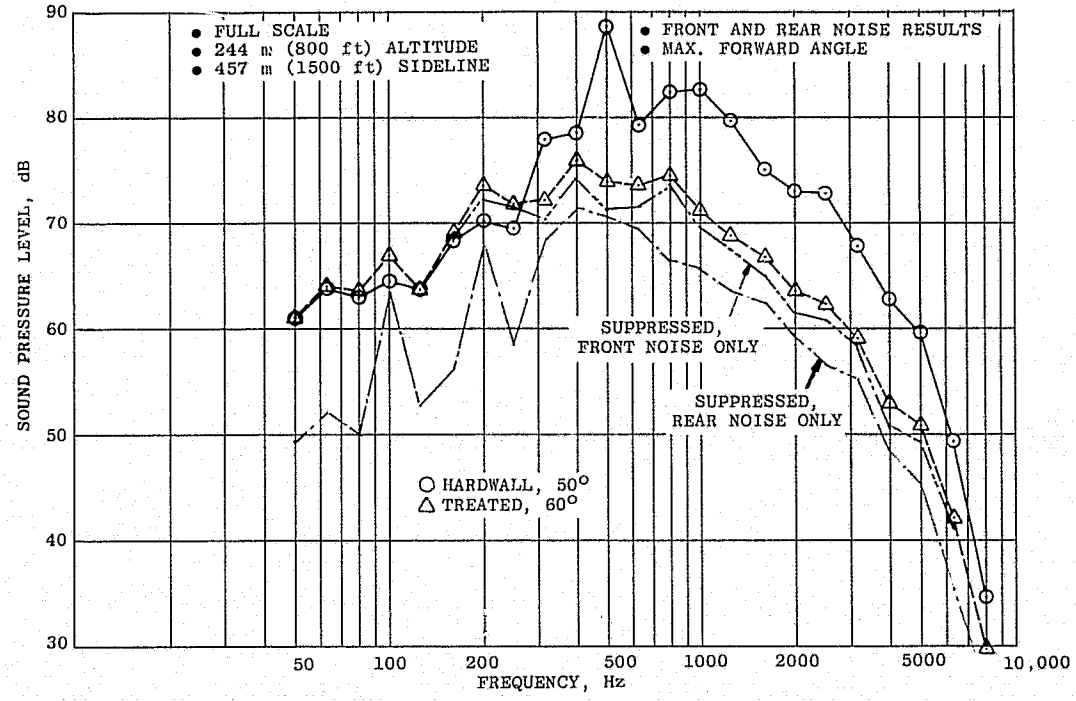

Figure 209. Flight Spectra, Takeoff, Max, Forward Angle.

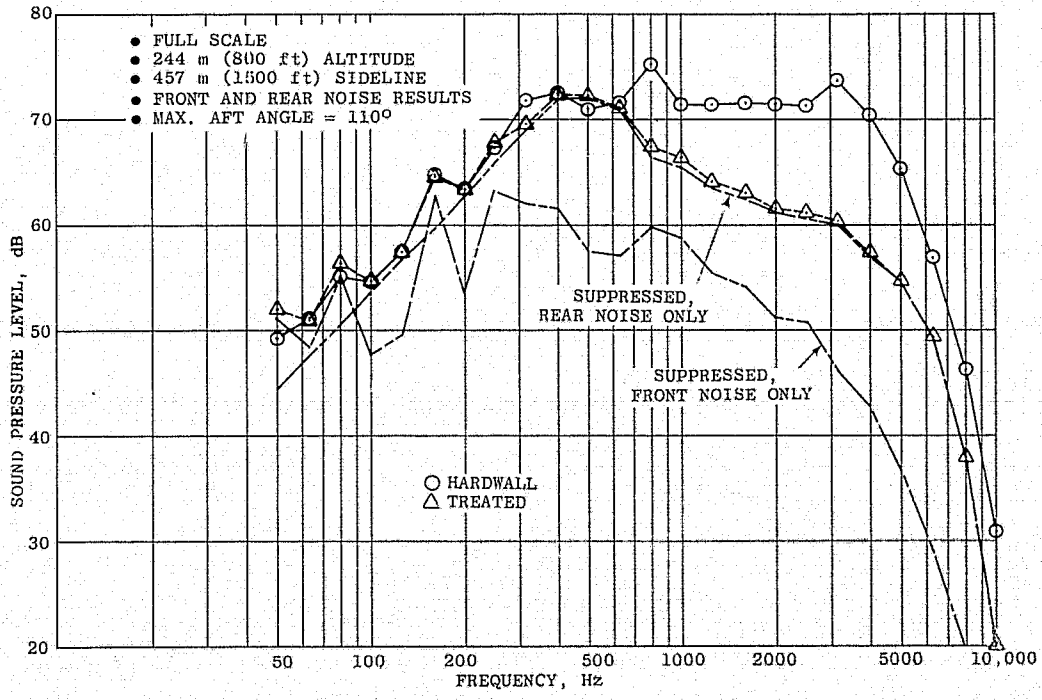

Figure 210. Flight Spectra, Takeoff, 110° Max. Aft Angle.

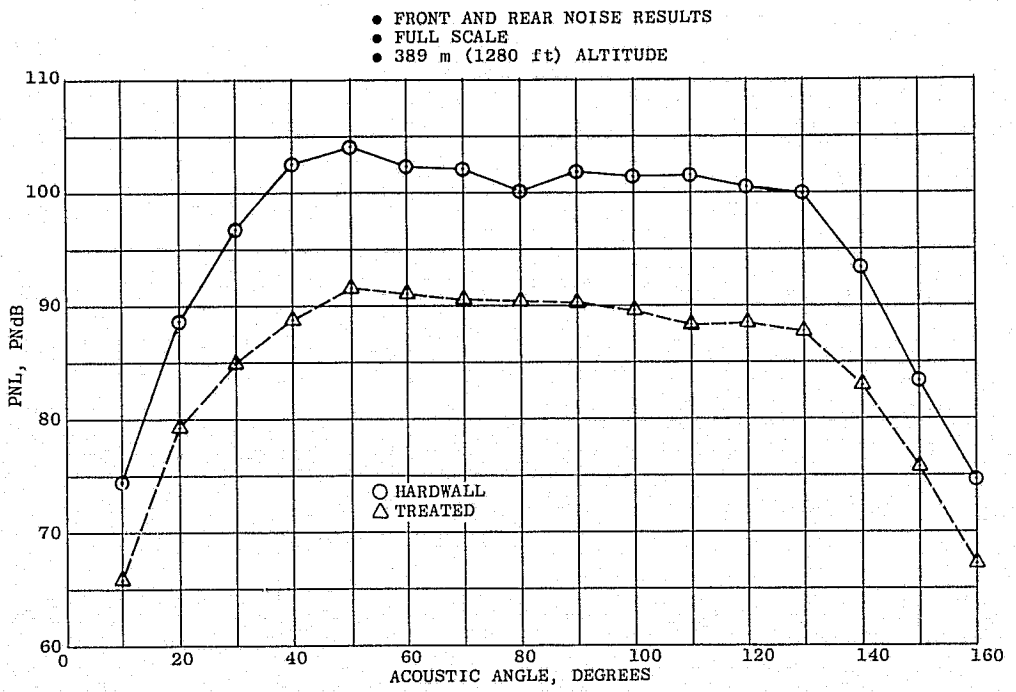

Figure 211. Flight PNL Directivity, Cutback.

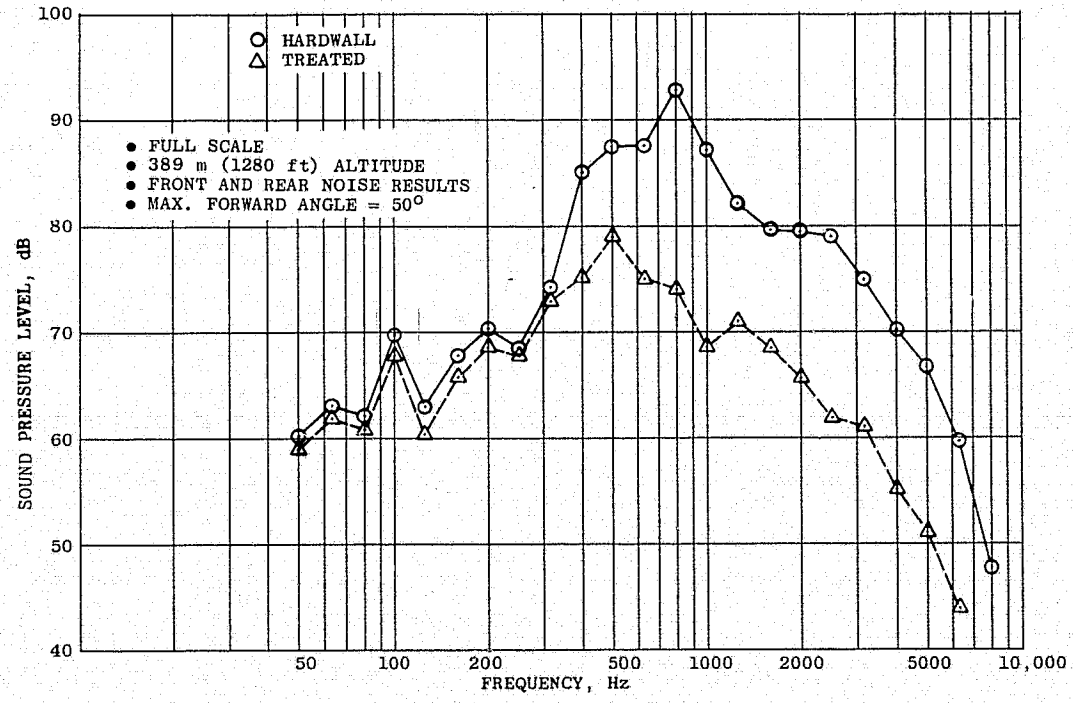

Figure 212. Flight Spectra, Cutback, 50° Max. Forward Angle.

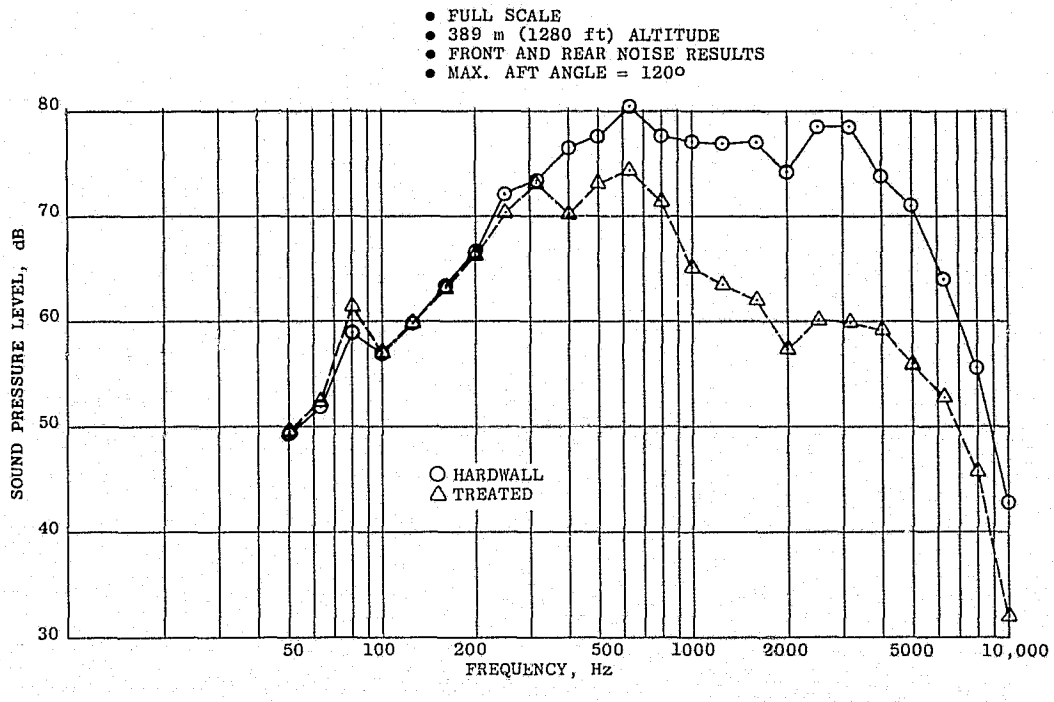

Figure 213. Flight Spectra, Cutback, 120° Max. Aft Angle.

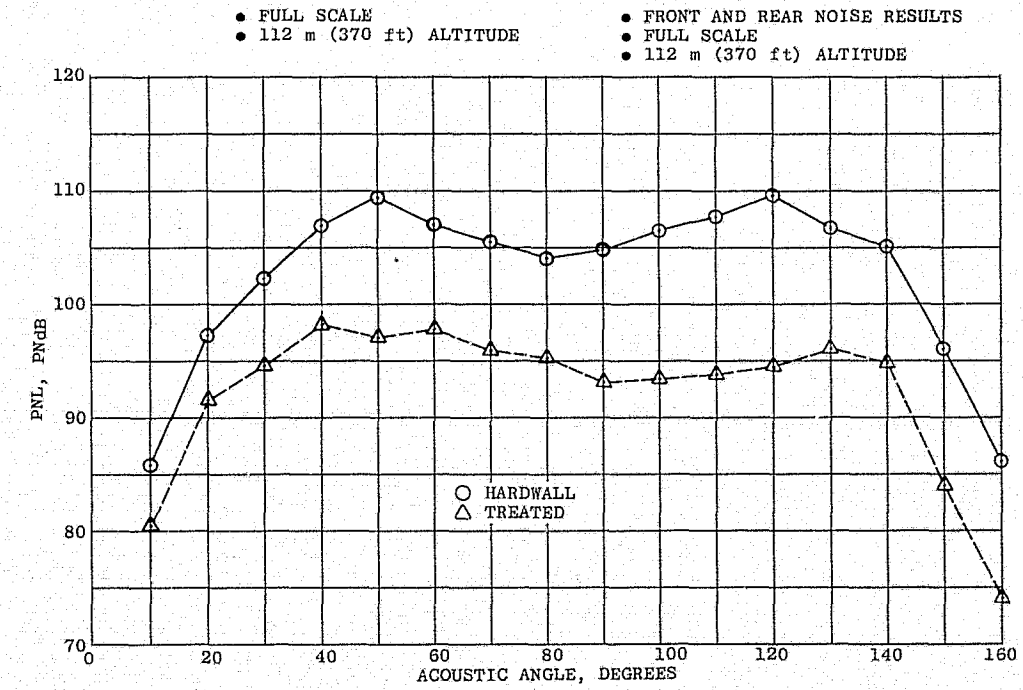

Figure 214. Flight PNL Directivity, Approach.

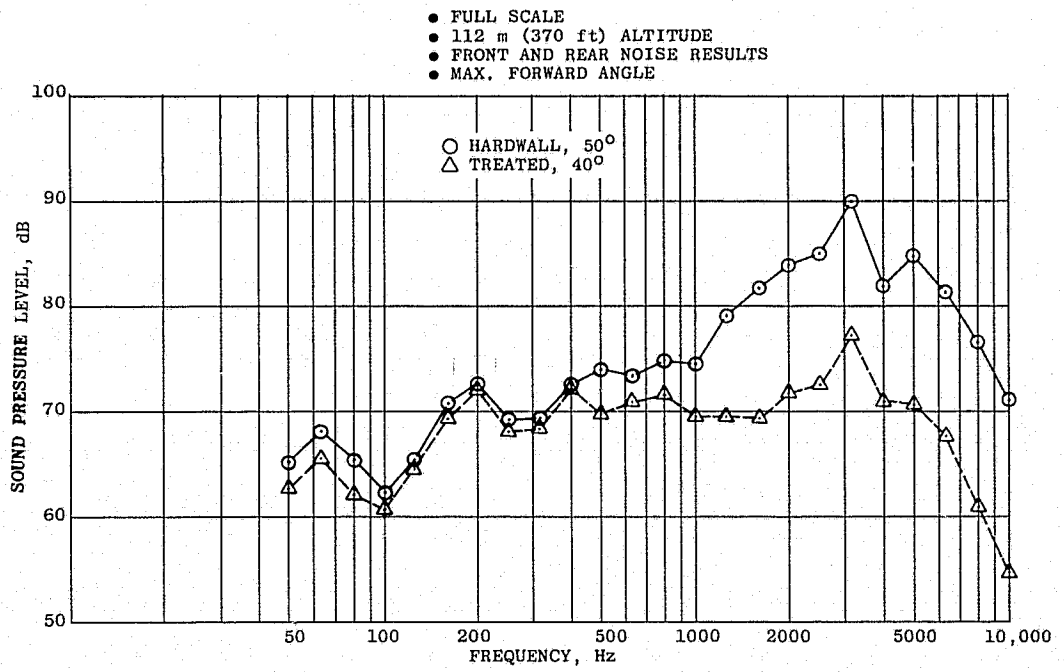

Figure 215. Flight Spectra, Approach, Max. Forward Angle.

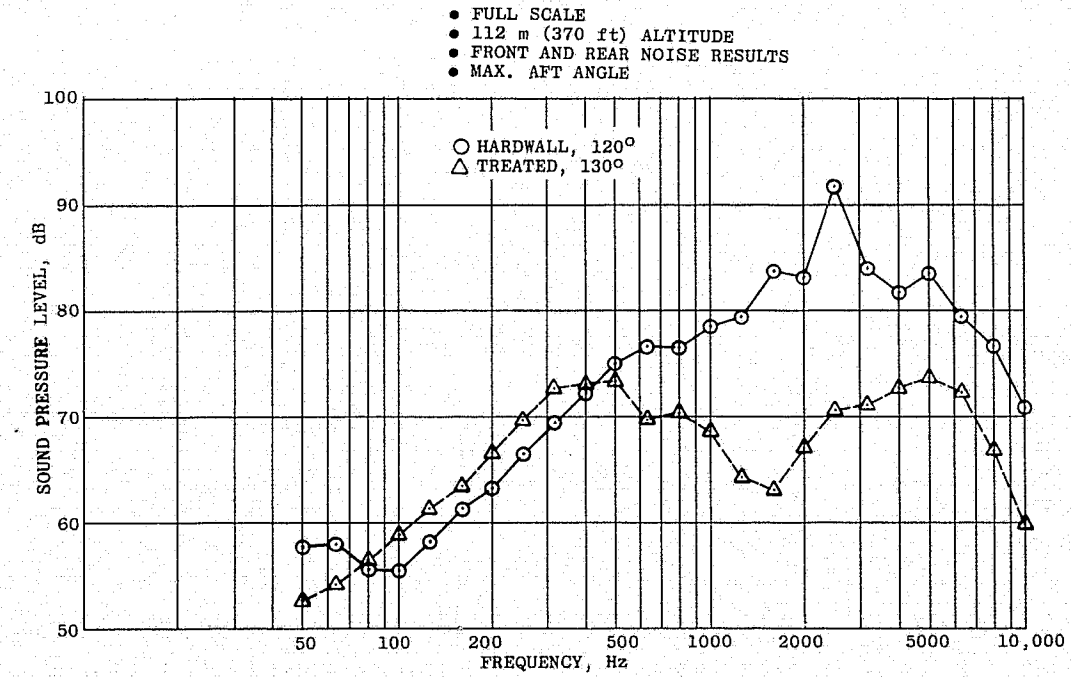

Figure 216. Flight Spectra, Approach, Max. Aft Angle.

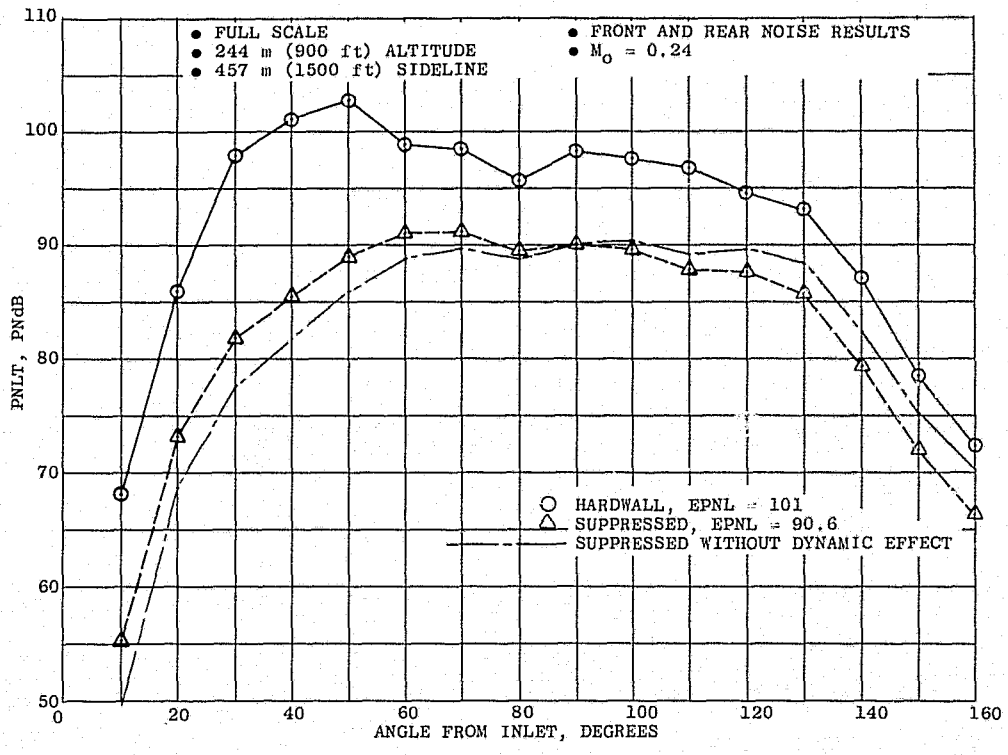

Figure 217. Flight PNLT Directivity, Takeoff.

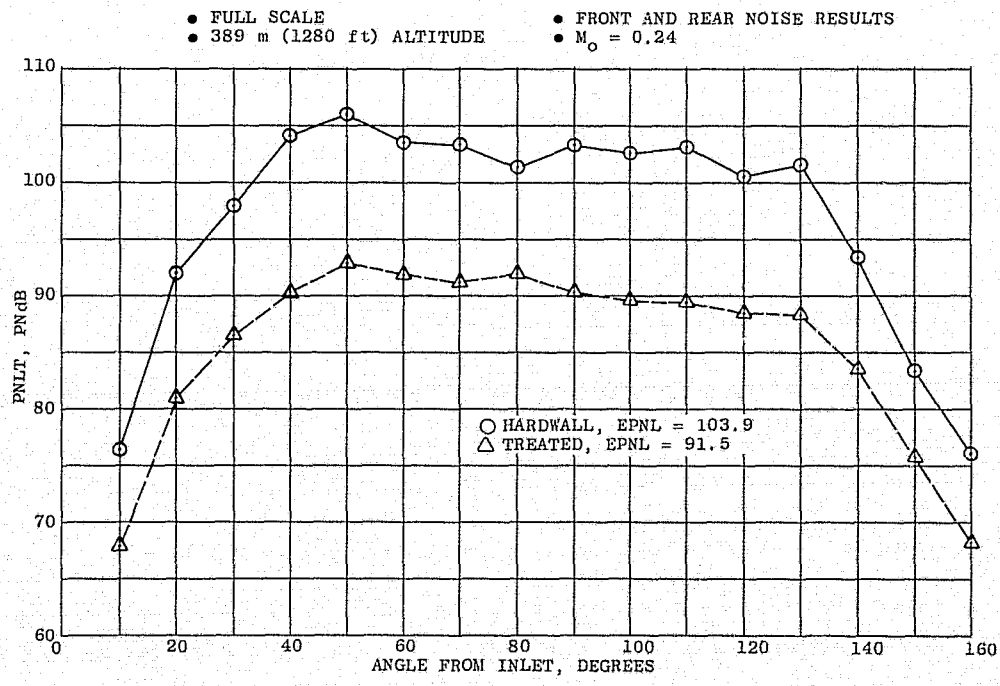

Figure 218. Flight PNLT Directivity, Cutback.

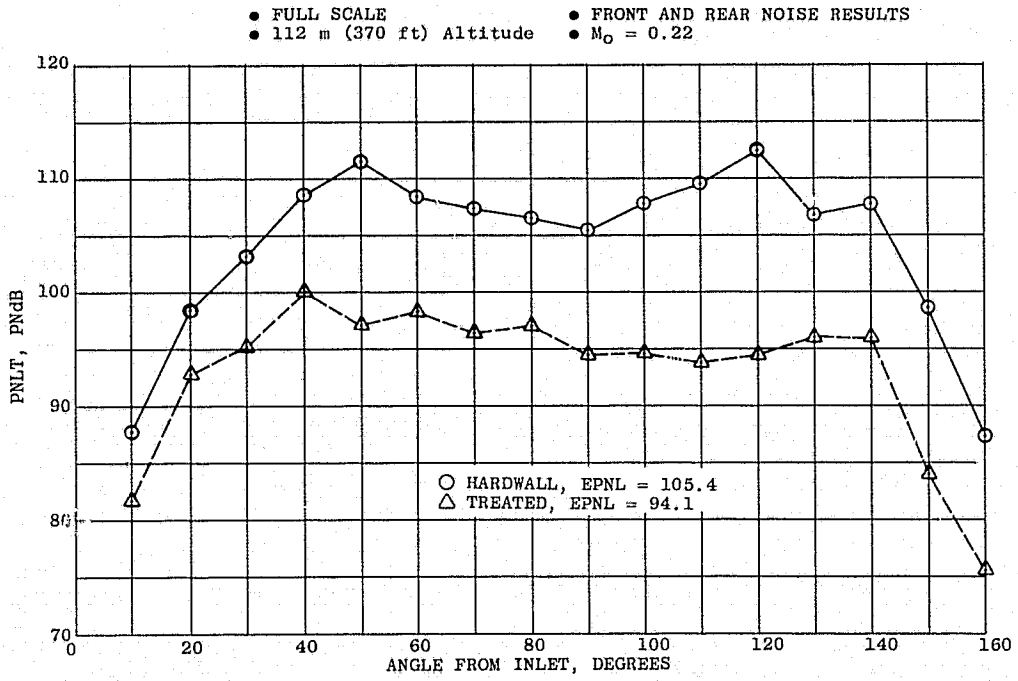

Figure 219. Flight PNLT Directivity, Approach.

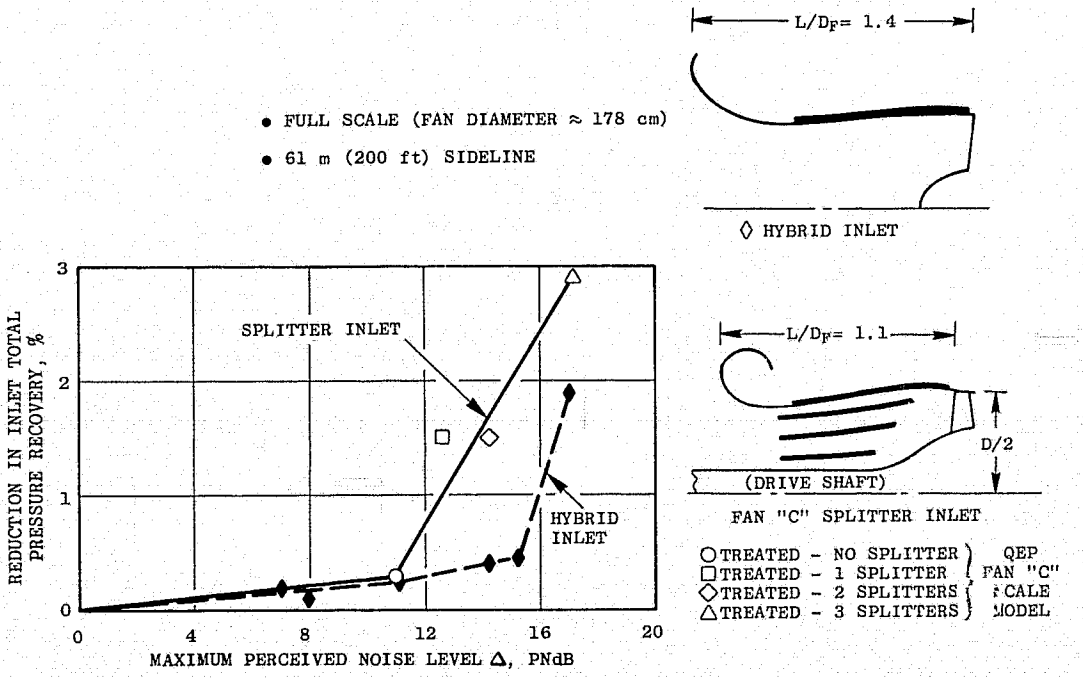

Figure 220. Comparison of Noise Suppression Efficiency Between Splitter and Hybrid Inlet.

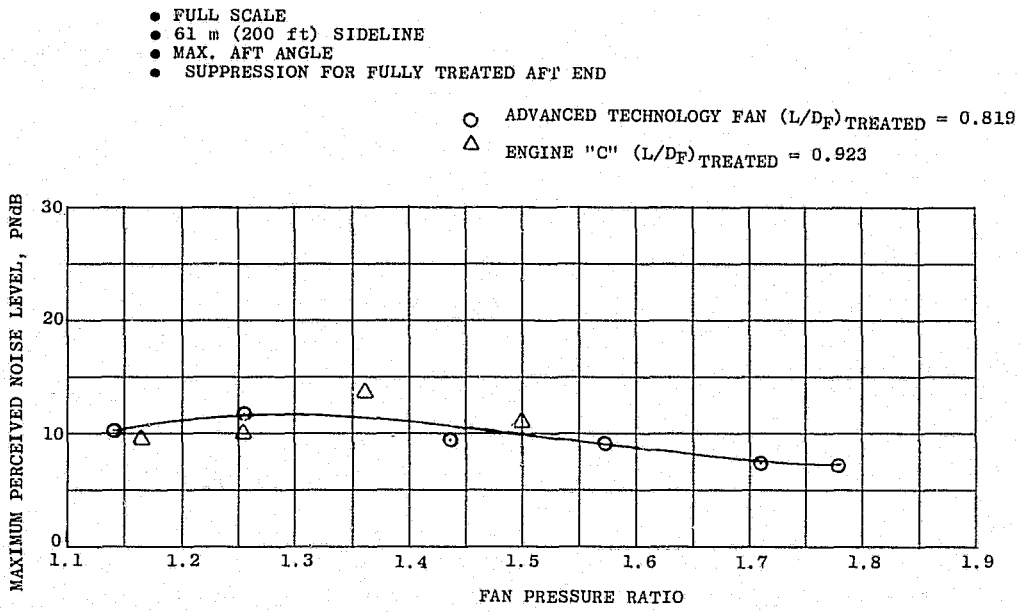

Figure 221. Suppressed Aft Fan Noise Comparison.

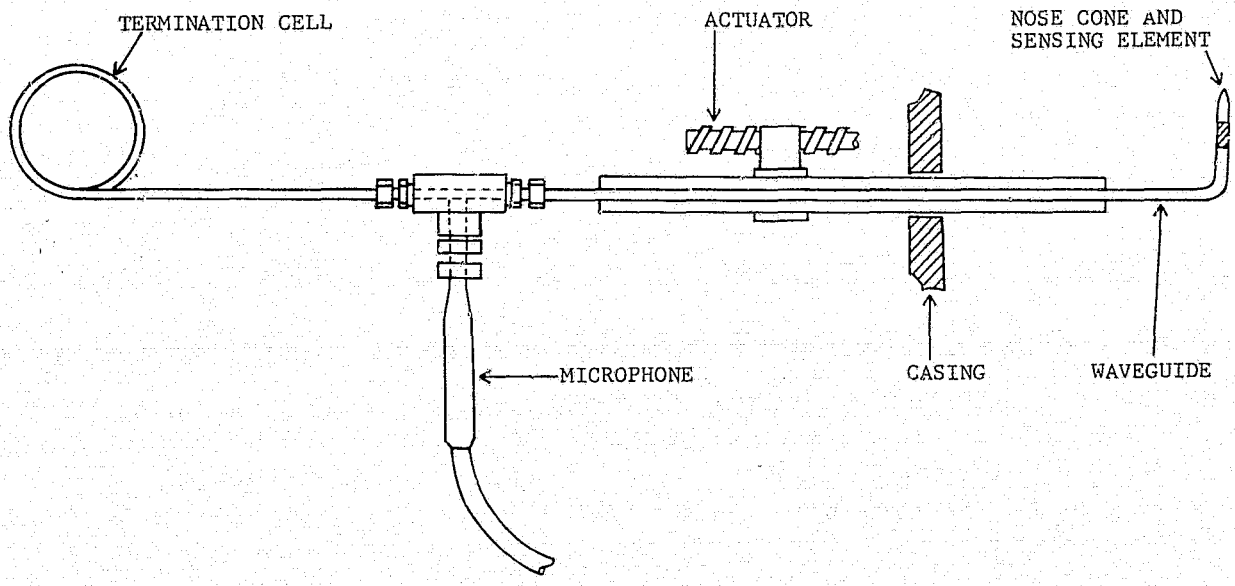

Figure A1. Typical Schematic of Acoustic Probe System.

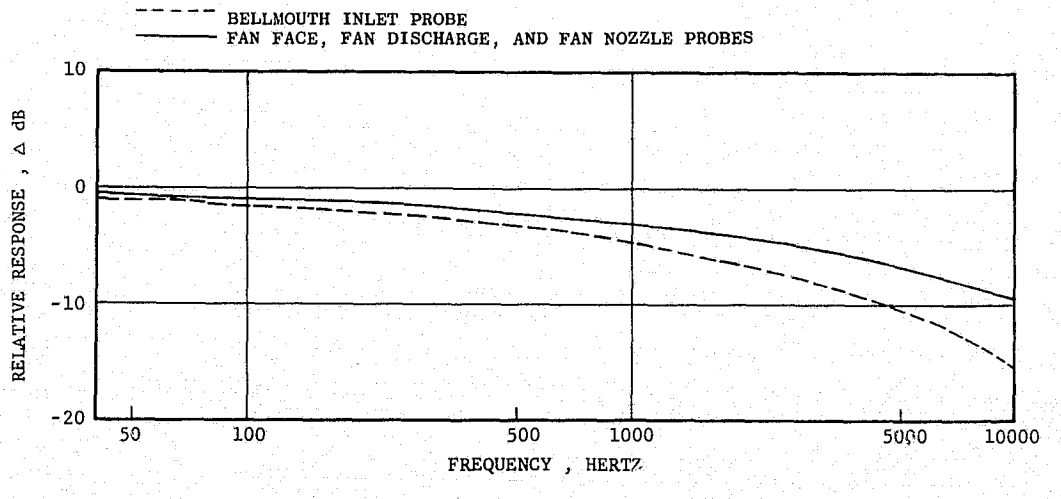

Figure A2. Acoustic Probe SPL Corrections for Viscous Losses (1/3-Octave Band).

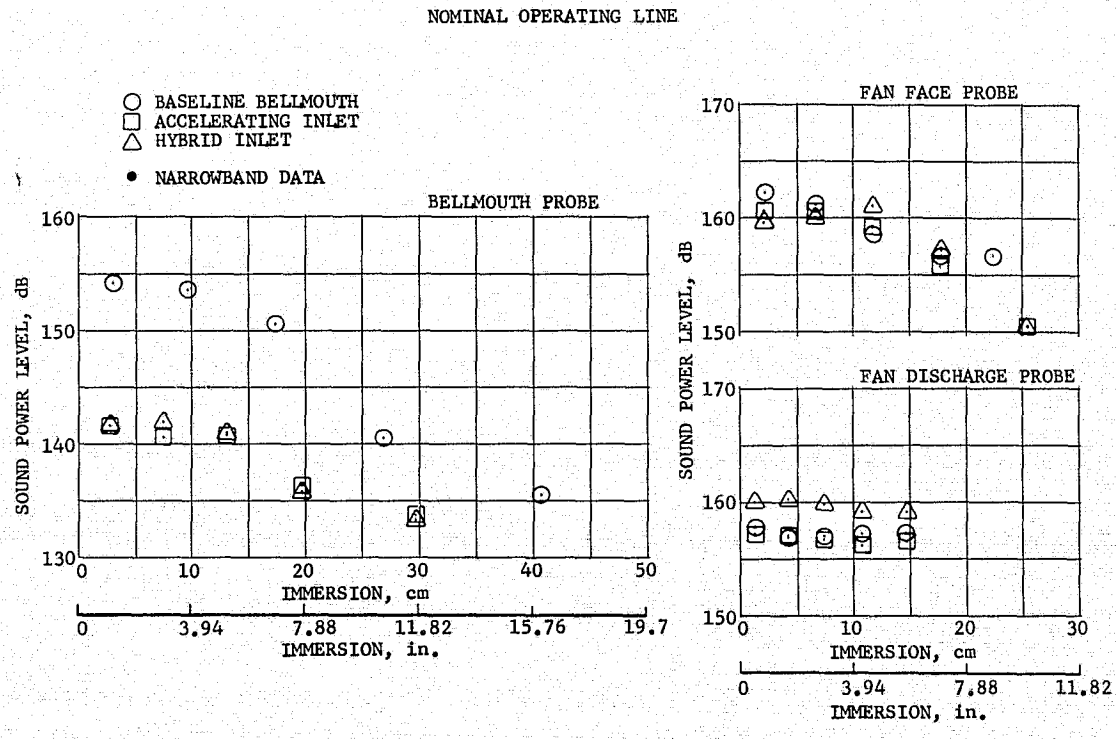

Figure A3. Total Sound Power Level Vs. Immersion, Takeoff (Rear-Drive Test).

C.3

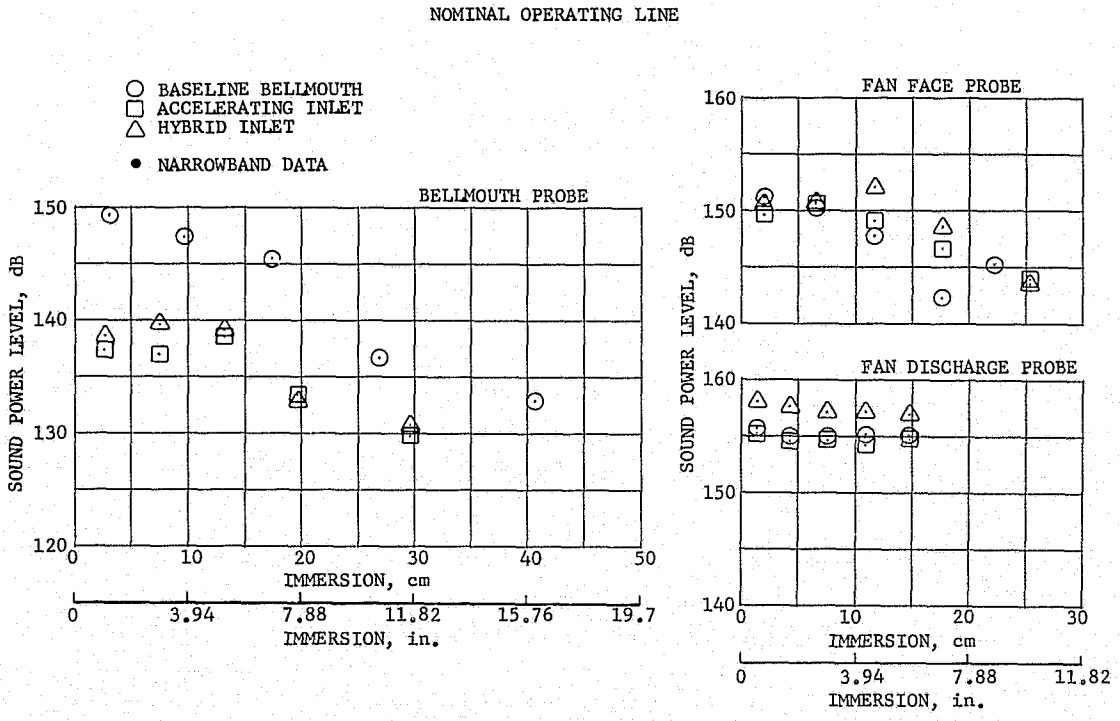

Figure A4. Broadband Sound Power Level Vs. Immersion, Takeoff (Rear-Drive Test).

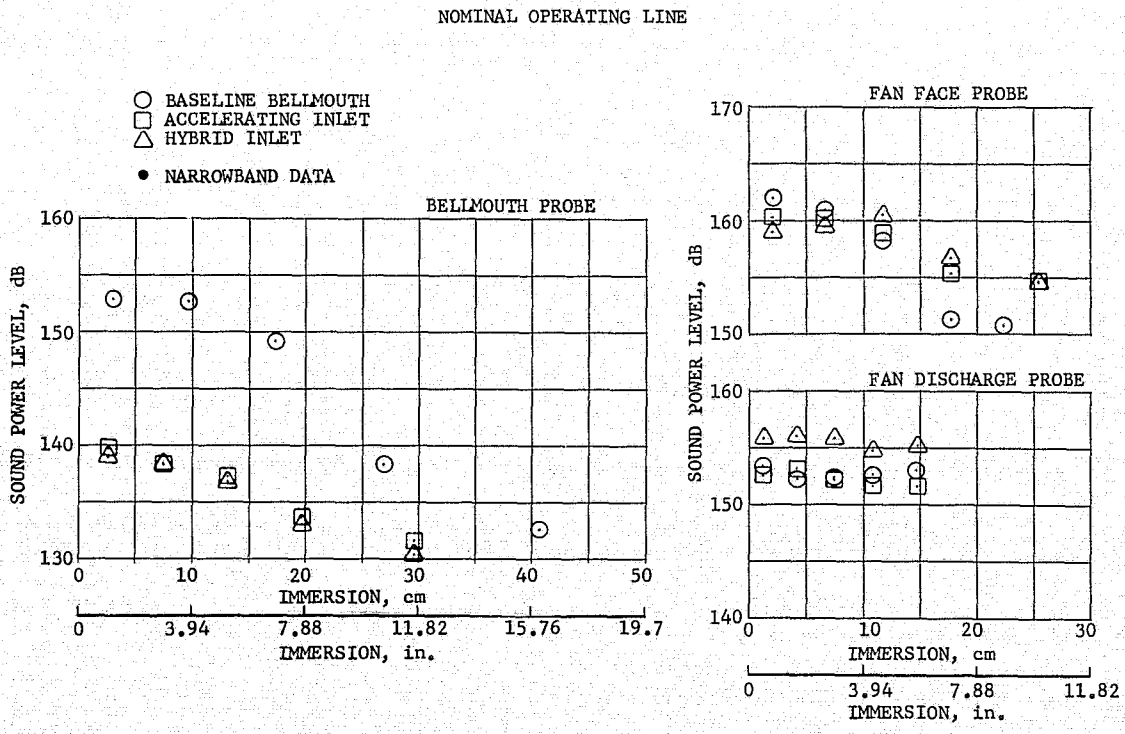

Figure A5. MPT Sound Power Level Vs. Immersion, Takeoff (Rear-Drive Test).

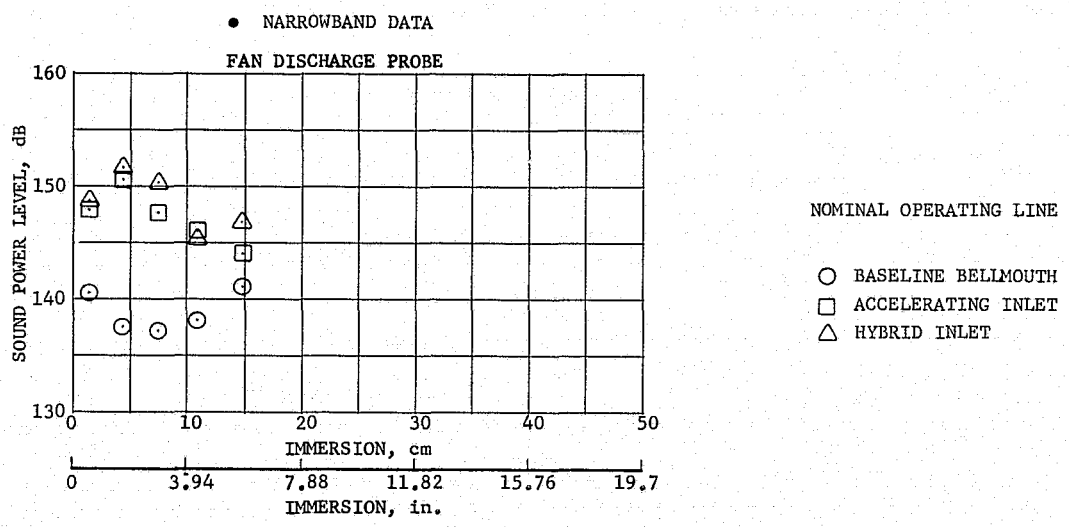

Figure A6. BPF Sound Power Level Vs. Immersion, Takeoff (Rear-Drive Test).

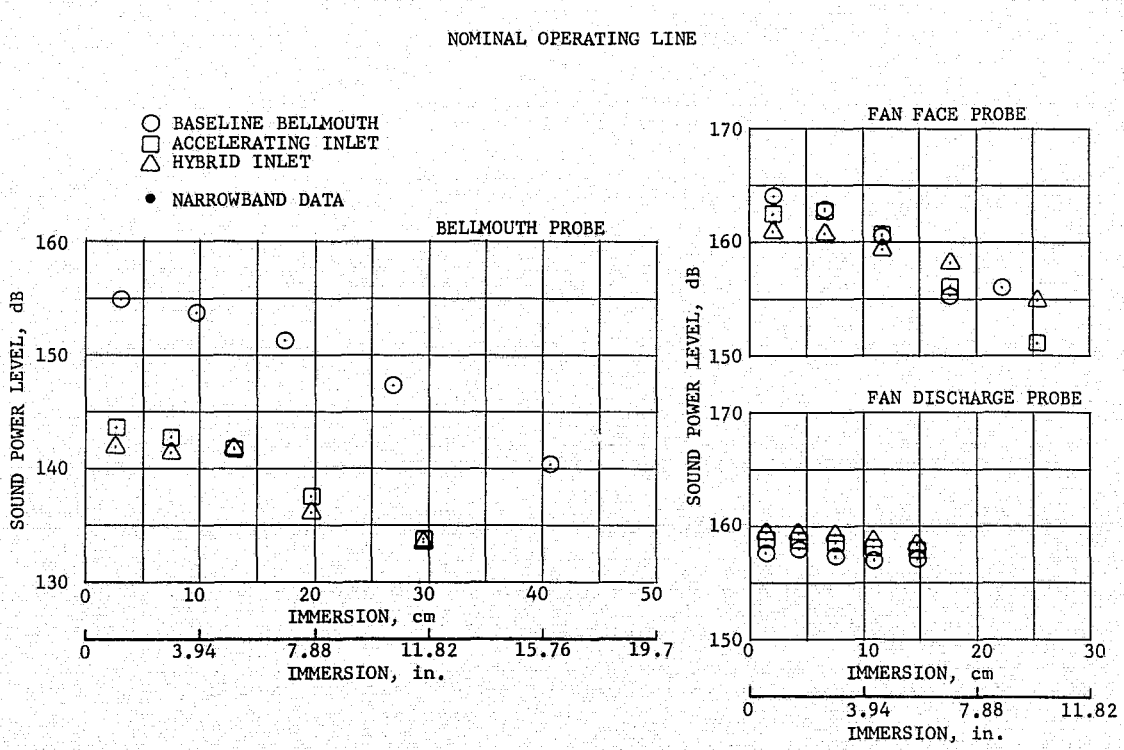

Figure A7. Total Sound Power Level Vs. Immersion, Cutback (Rear-Drive Test).

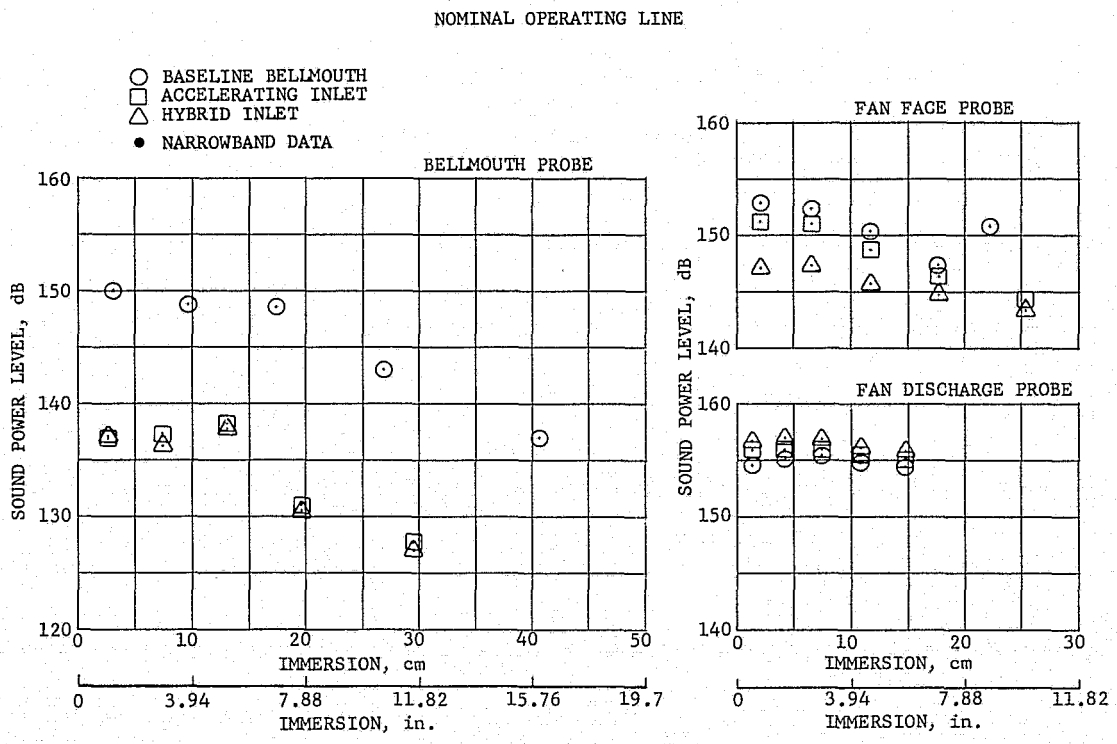

Figure A8. Broadband Sound Power Level Vs. Immersion, Cutback (Rear-Drive Test).

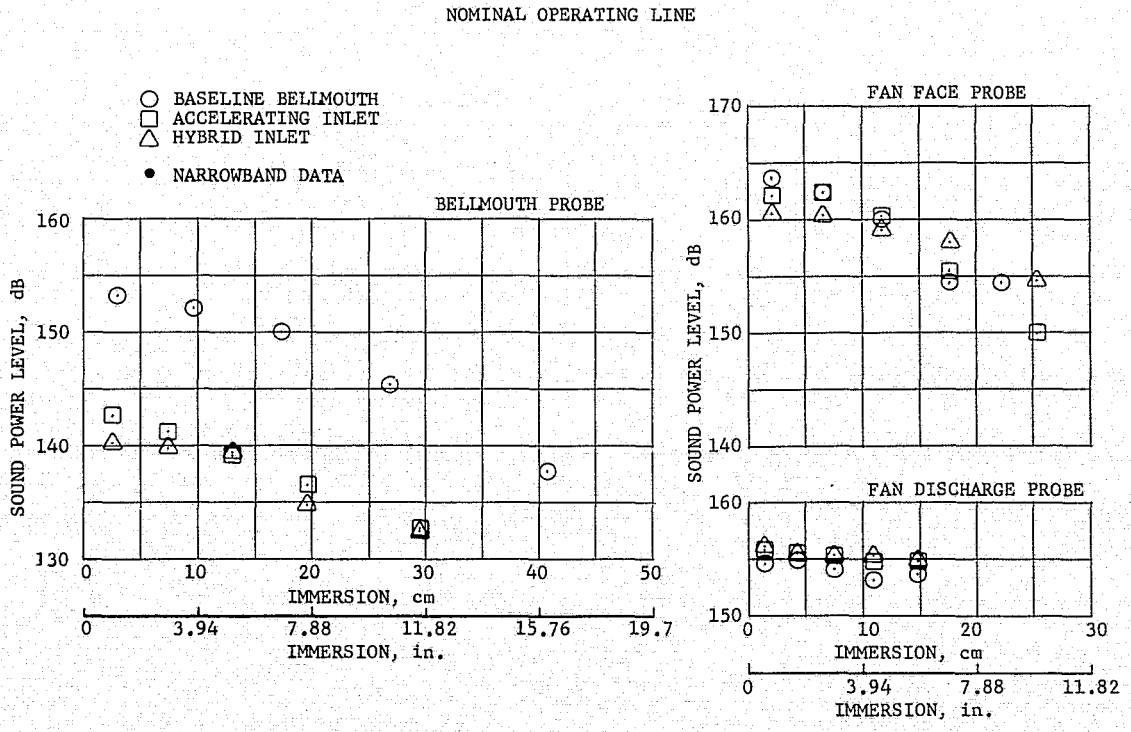

Figure A9. MPT Sound Power Level Vs. Immersion, Cutback (Rear-Drive Test).

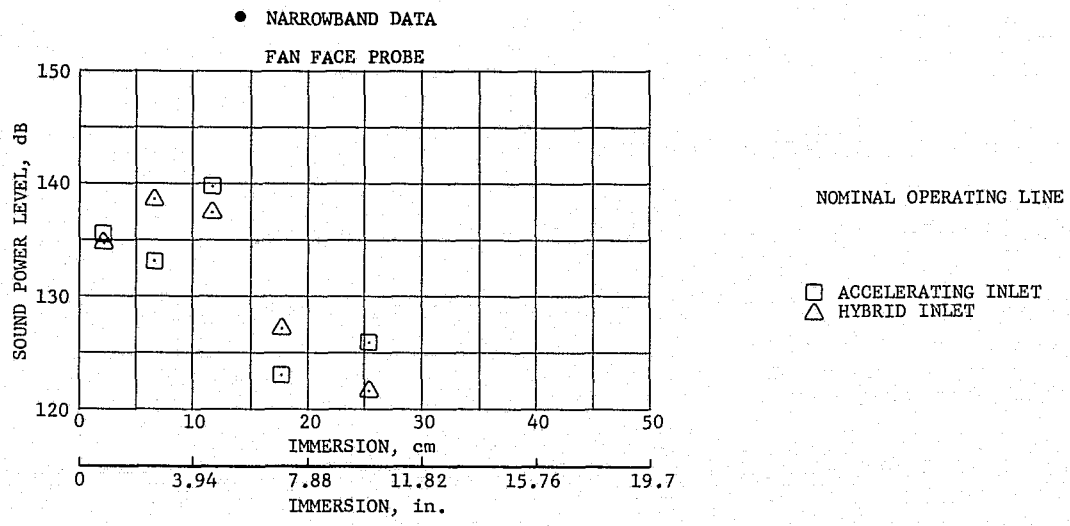

Figure A10. BPF Sound Power Level Vs. Immersion, Cutback (Rear-Drive Test).

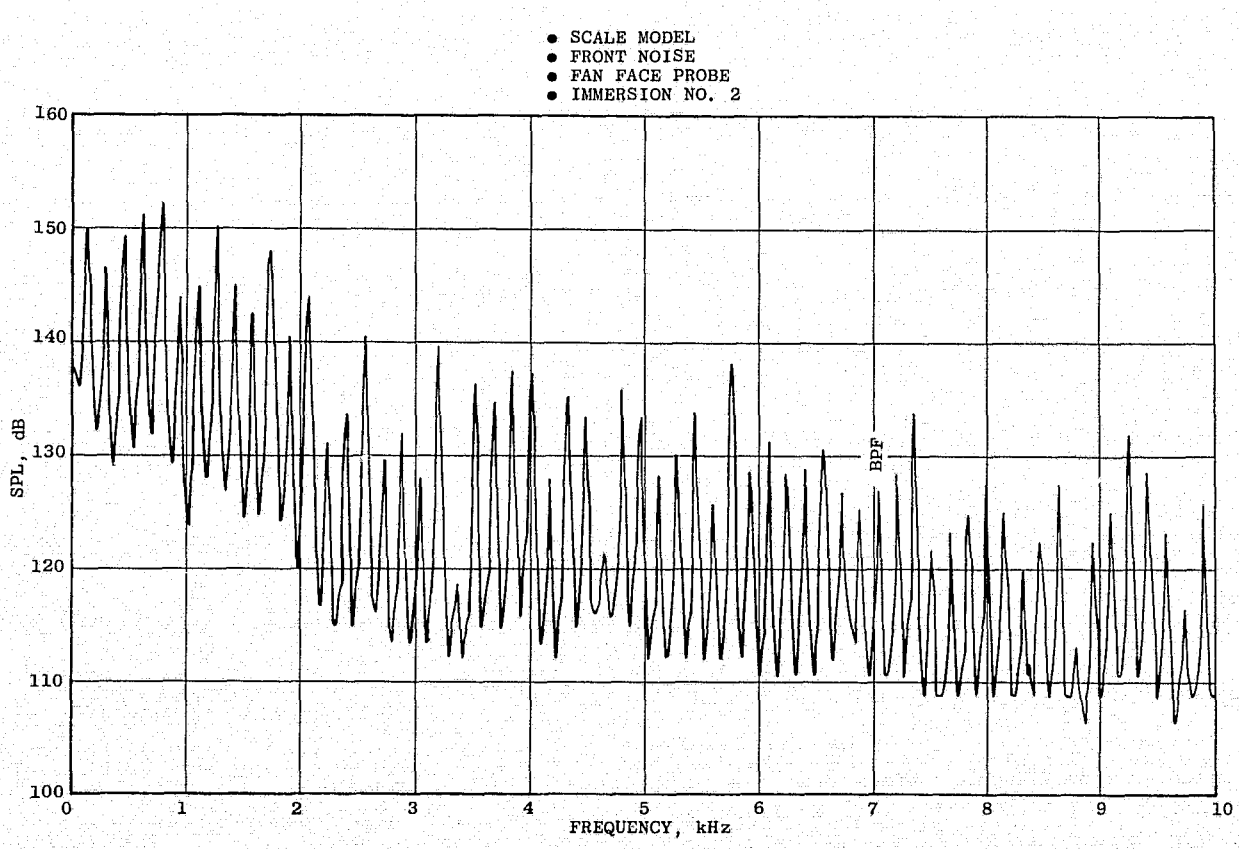

Figure A11. Probe Narrowband, Baseline Inlet at Cutback, Fan Face Probe (Rear-Drive Test).

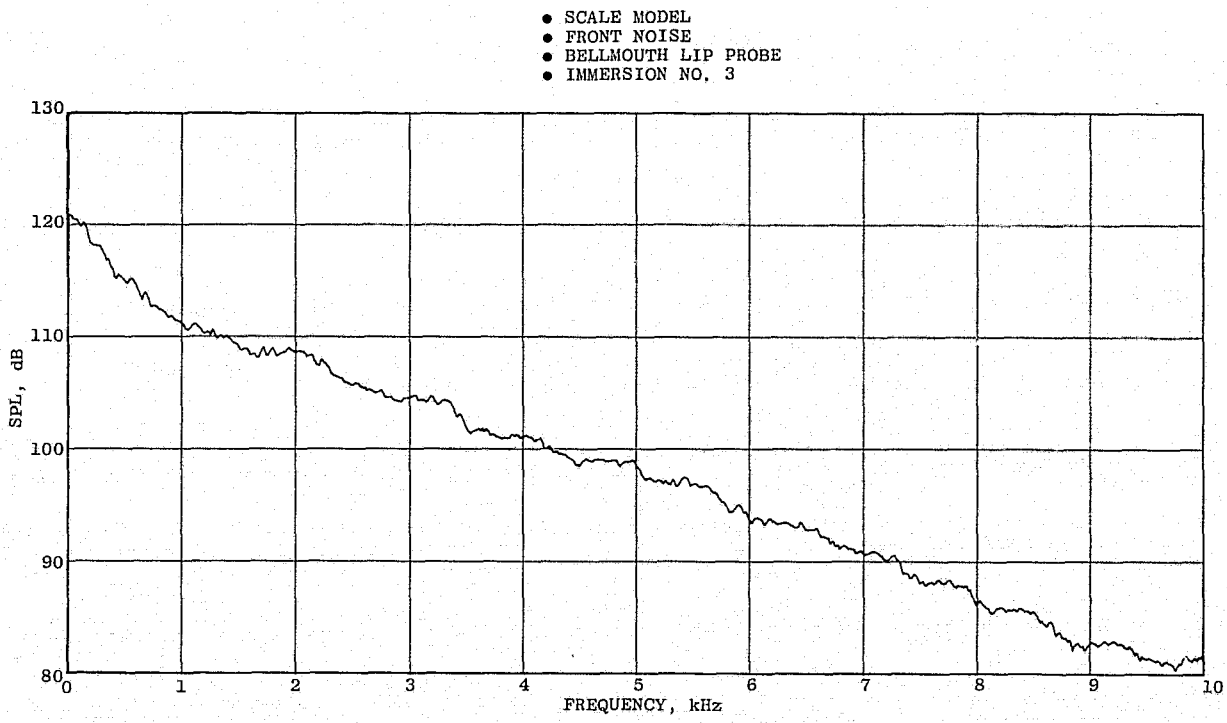

Figure A12. Probe Narrowband, Hybrid Inlet at Approach, Bellmouth Lip Probe (Rear-Drive Test).

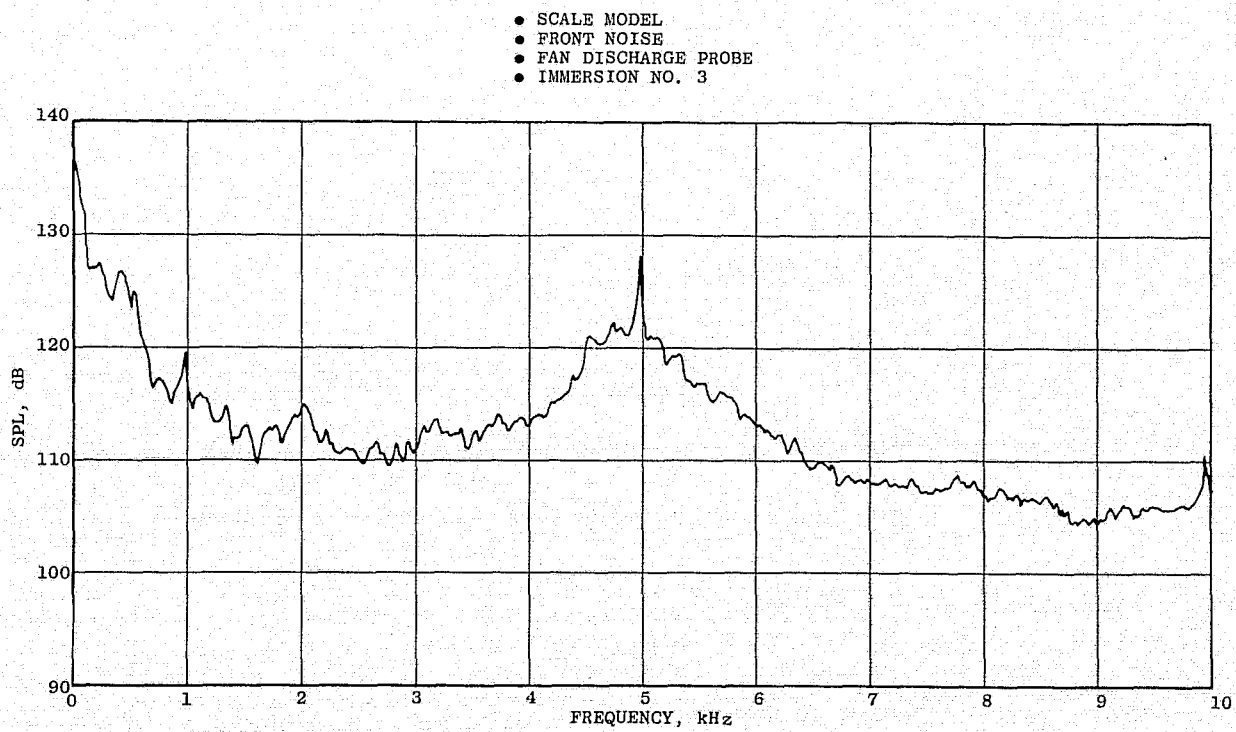

Figure A13. Probe Narrowband, Hybrid Inlet at Approach, Fan Discharge Probe (Rear-Drive Test).

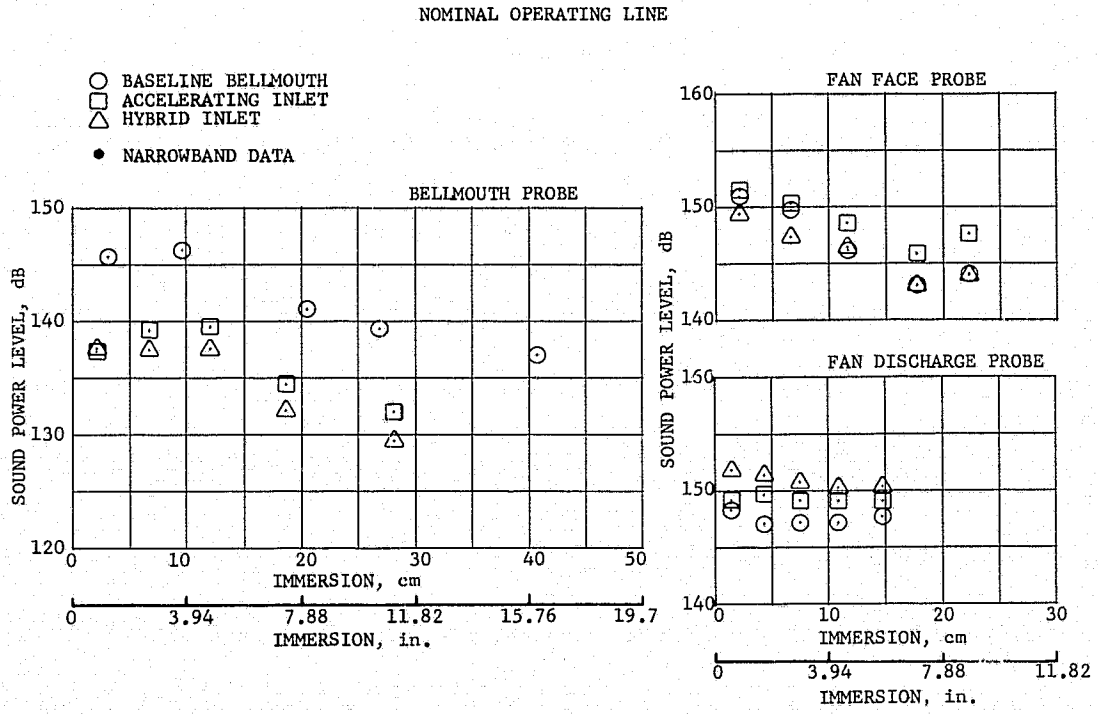

Figure A14. Total Sound Power Level Vs. Immersion, Approach (Rear-Drive Test).

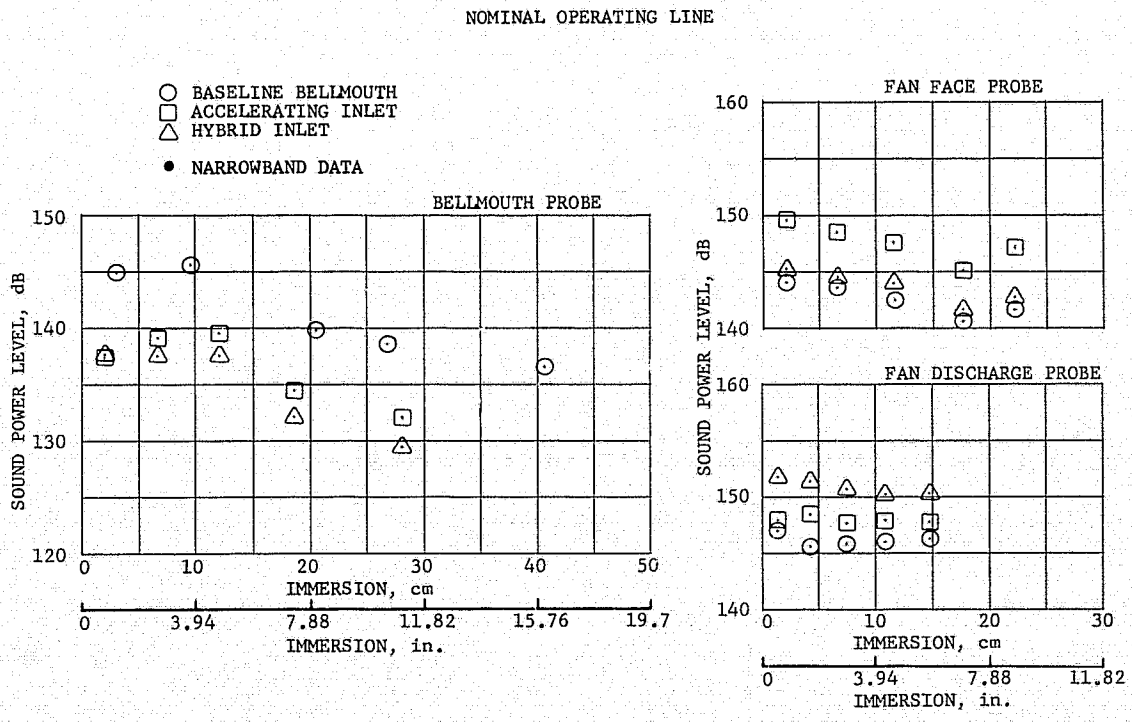

Figure A15. Broadband Sound Power Level Vs. Immersion, Approach (Rear-Drive Test).

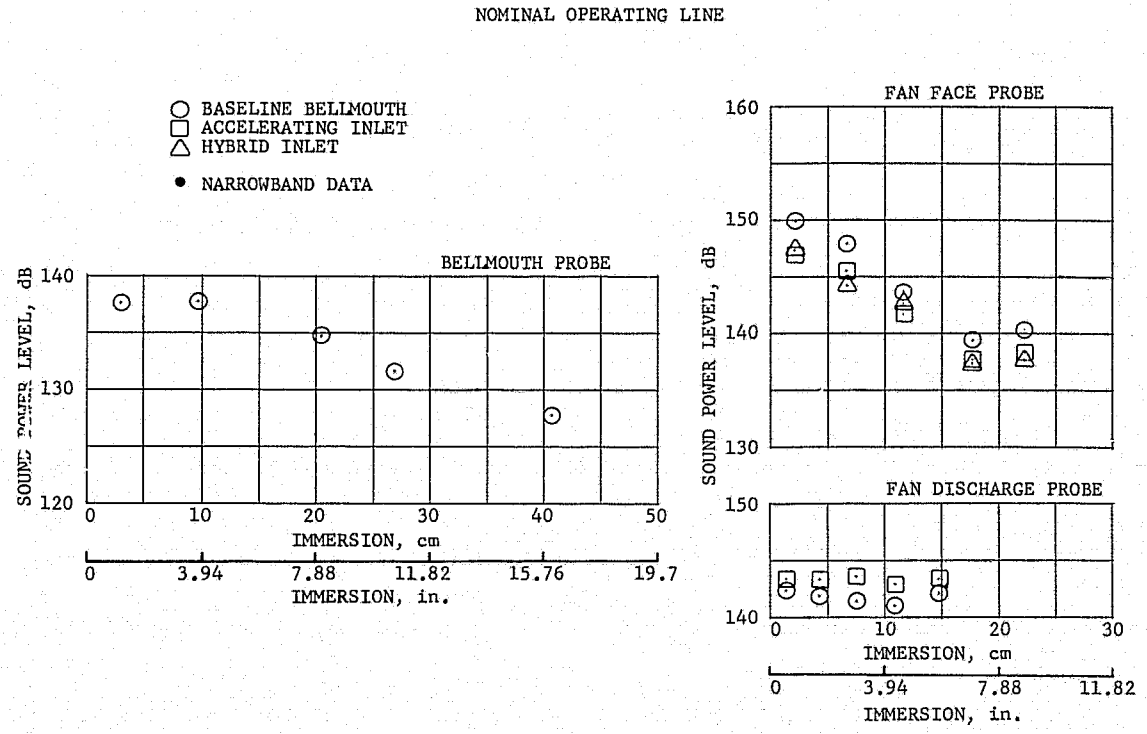

Figure A16. MPT Sound Power Level Vs. Immersion, Approach (Rear-Drive Test).

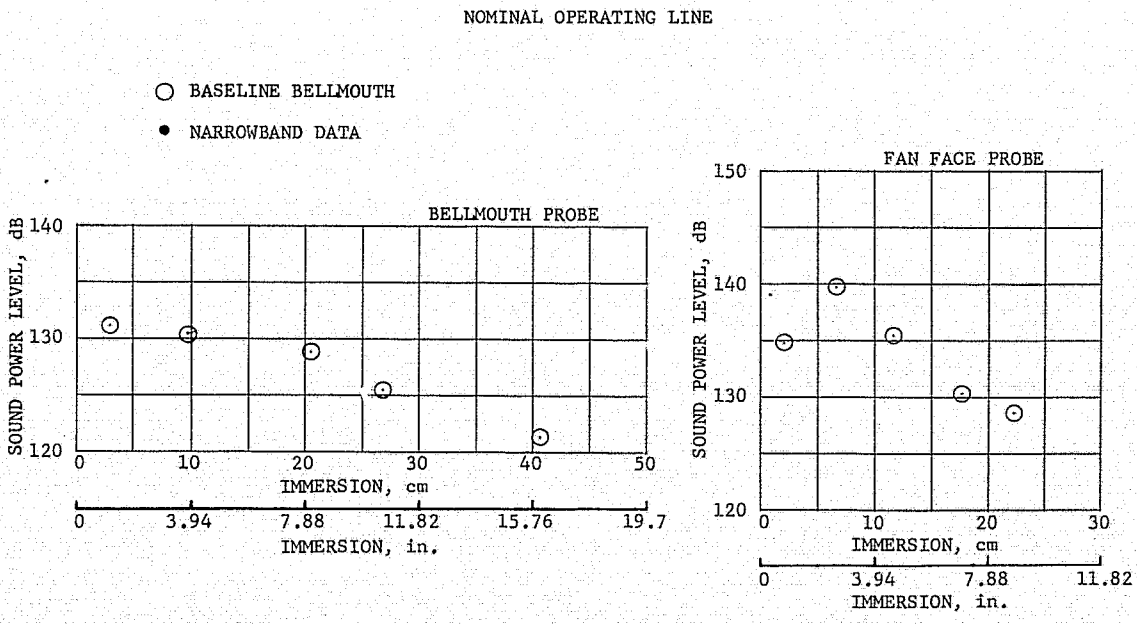

Figure A17. BPF Sound Power Level Vs. Immersion, Approach (Rear-Drive Test).

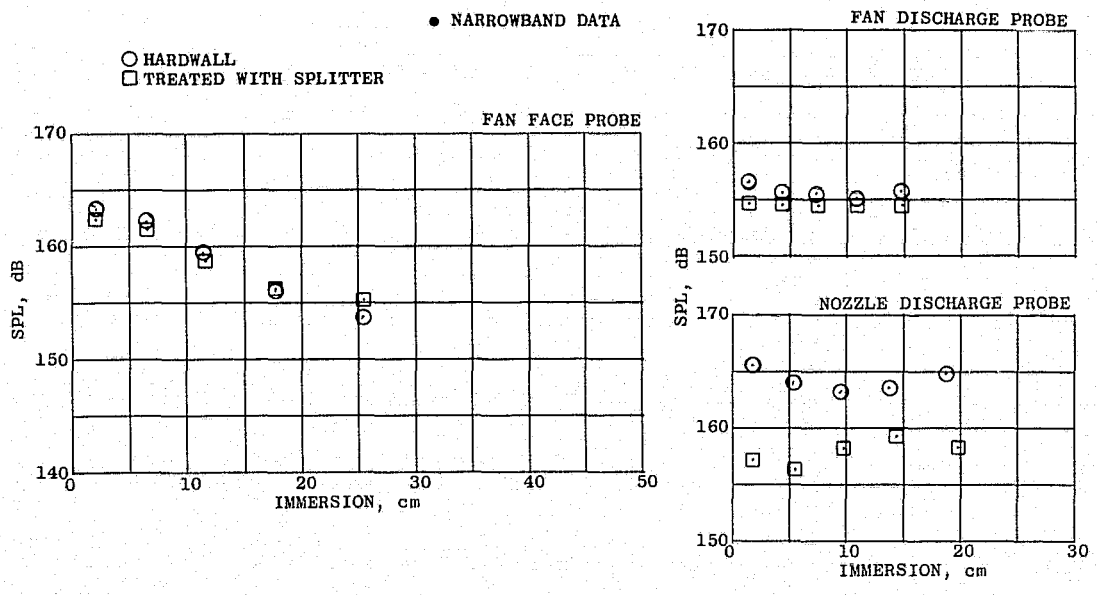

Figure A18. Total Sound Power Level Vs. Immersion, Takeoff (Front-Drive Test).

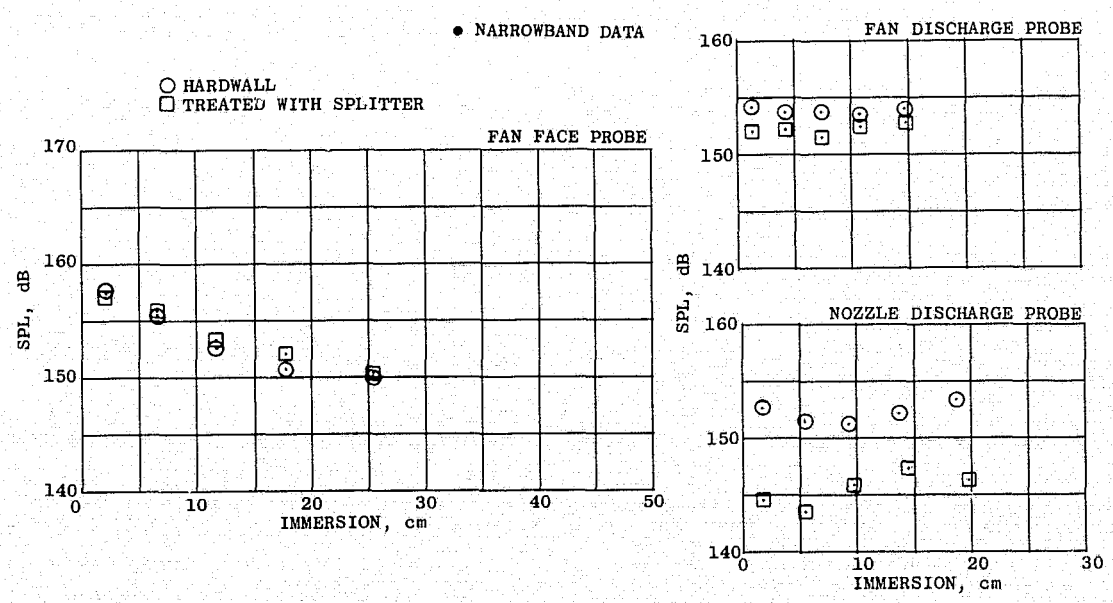

Figure A19. Broadband Sound Power Level Vs. Immersion, Takeoff (Front-Drive Test).

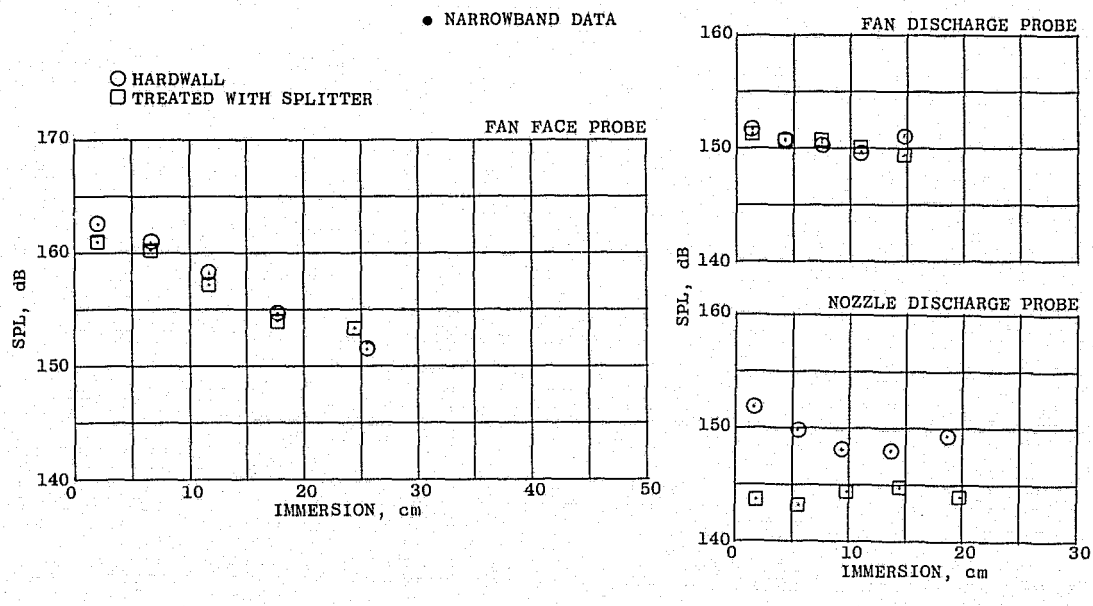

Figure A20. MPT Sound Power Level Vs. Immersion, Takeoff (Front-Drive Test).

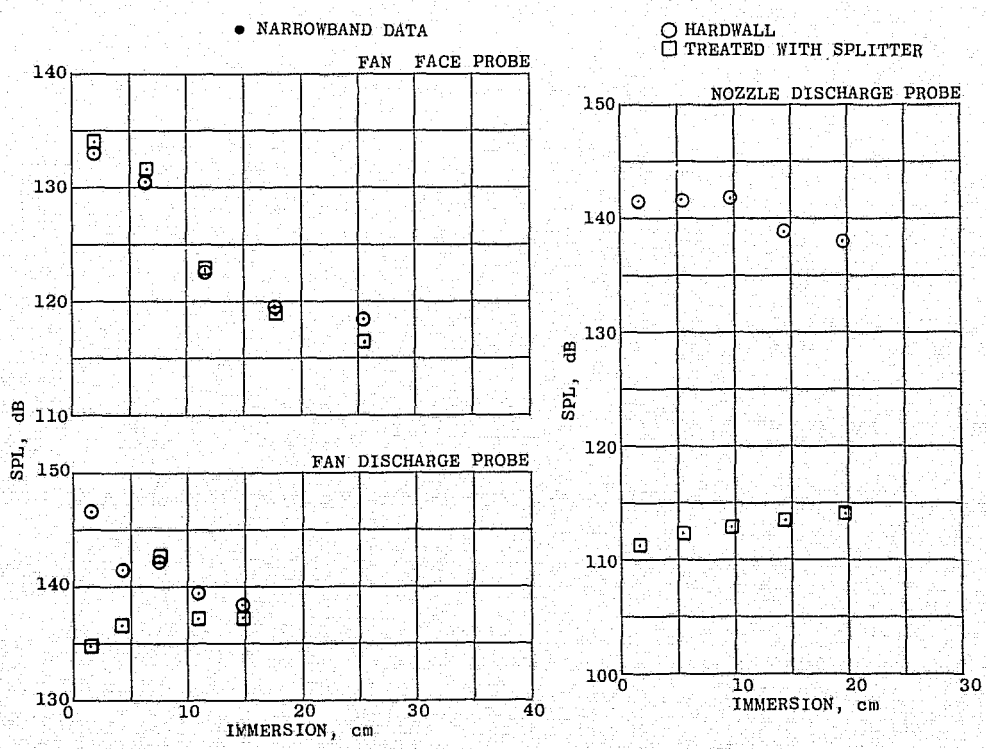

Figure A21. BPF Sound Power Level Vs. Immersion, Takeoff (Front-Drive Test).

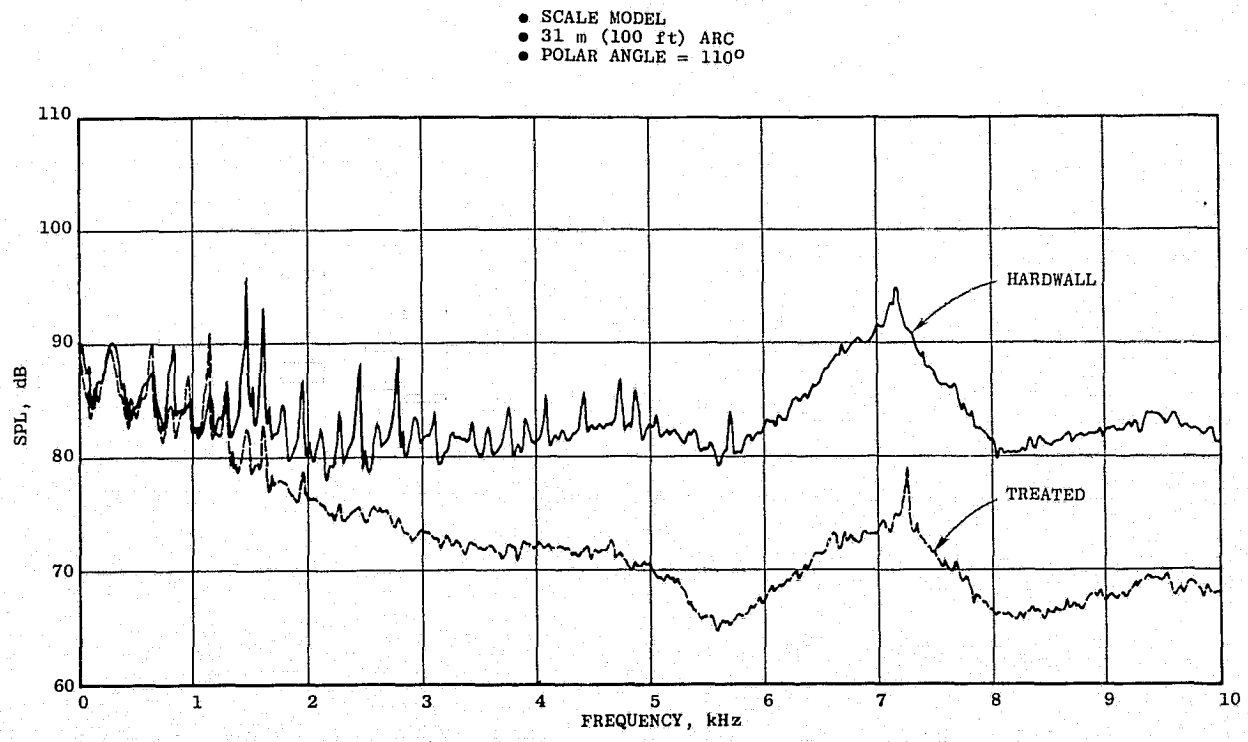

Figure A22. Farfield Narrowband Comparison, Takeoff (Front-Drive Test).

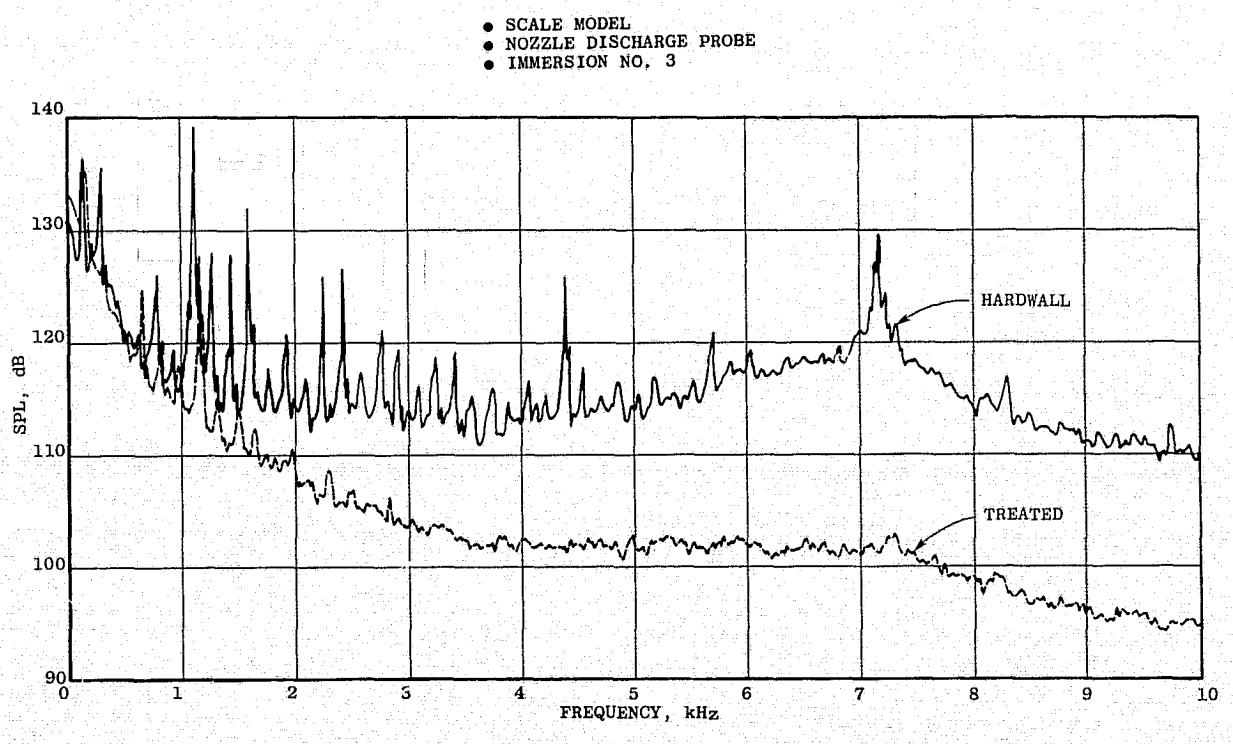

Figure A23. Probe Narrowband Comparison, Takeoff (Front-Drive Test).

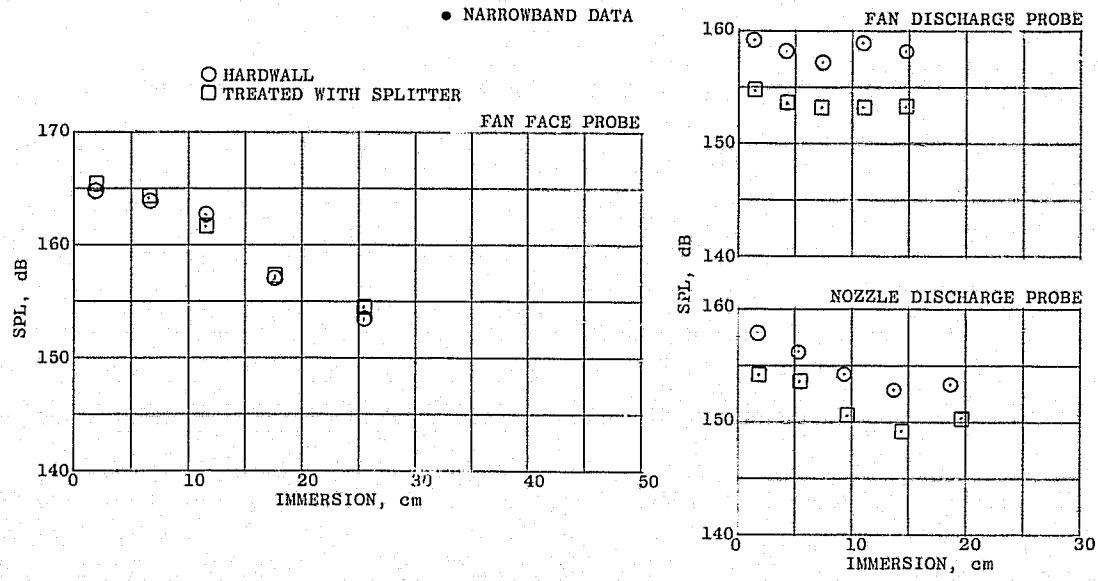

Figure A24. Total Sound Power Level Vs. Immersion, Cutback (Front-Drive Test).

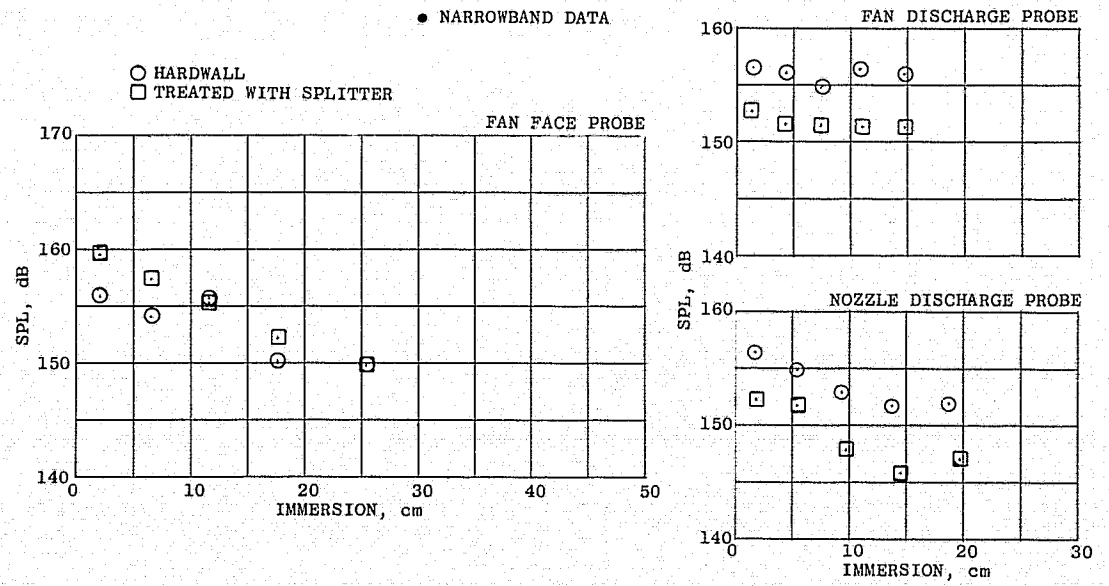

Figure A25. Broadband Sound Power Level Vs. Immersion, Cutback (Front-Drive Test).

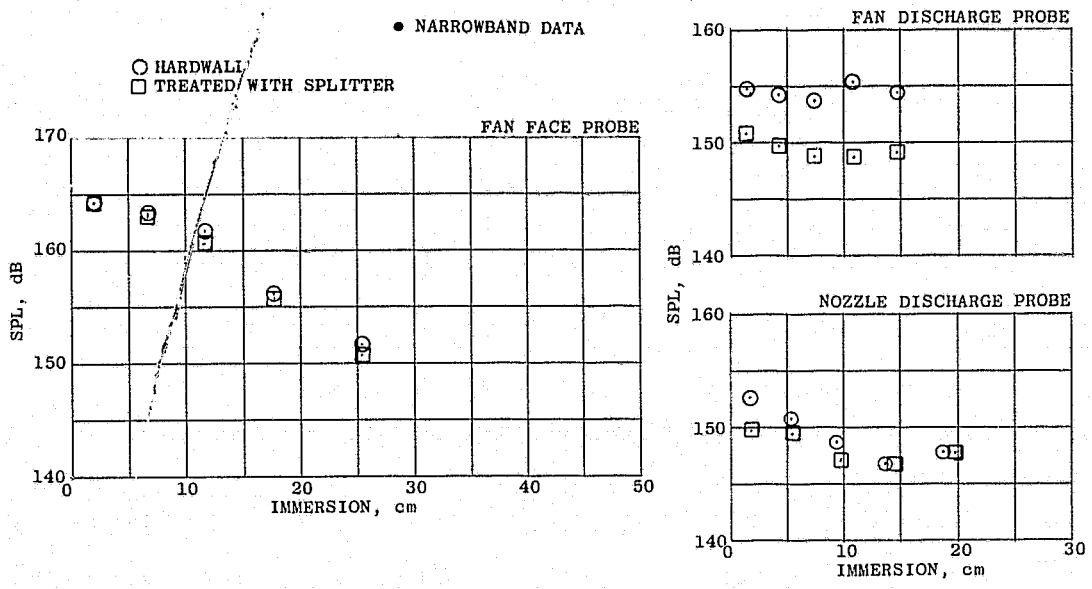

Figure A26. MPT Sound Power Level Vs. Immersion, Cutback (Front-Drive Test).

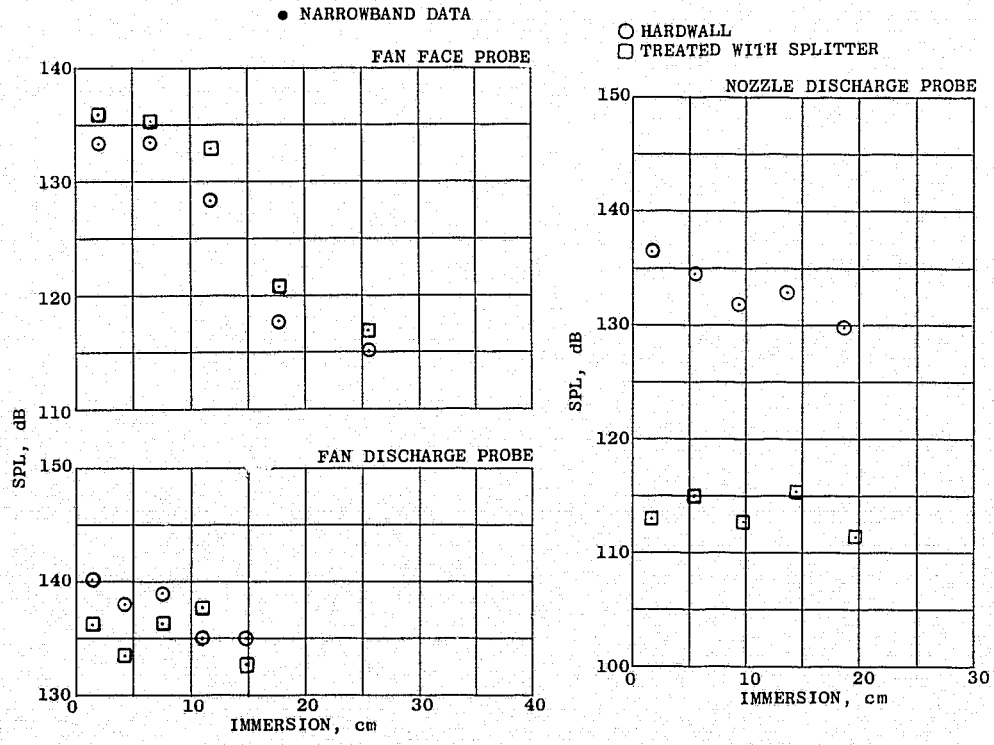

Figure A27. BPF Sound Power Level Vs. Immersion, Cutback (Front-Drive Test).

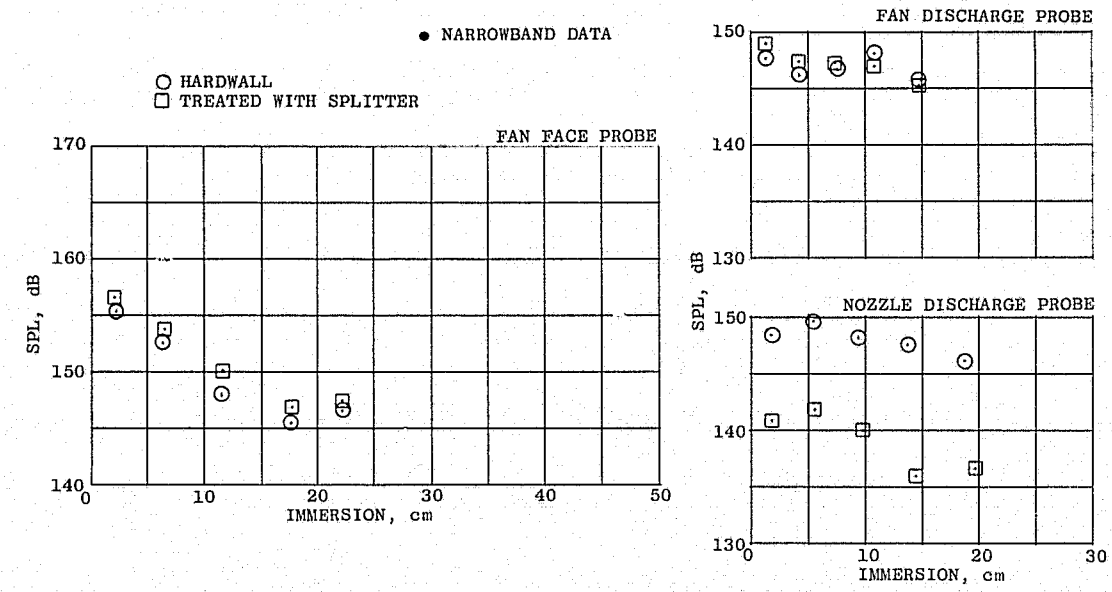

Figure A28. Total Sound Power Level Vs. Immersion, Approach (Front-Drive Test).

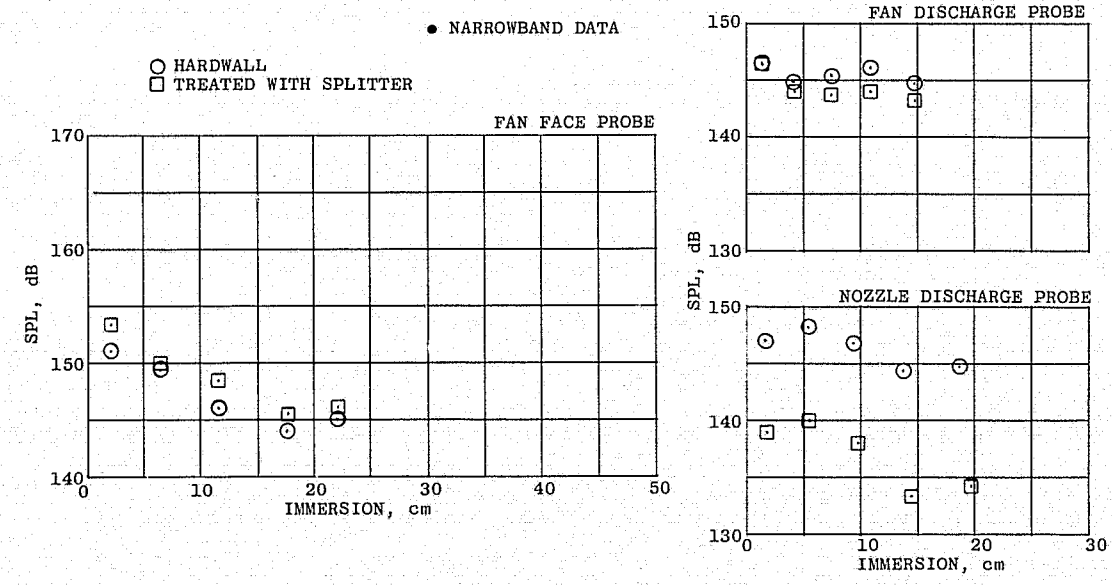

Figure A29. Broadband Sound Power Level Vs. Immersion, Approach (Front-Drive Test).

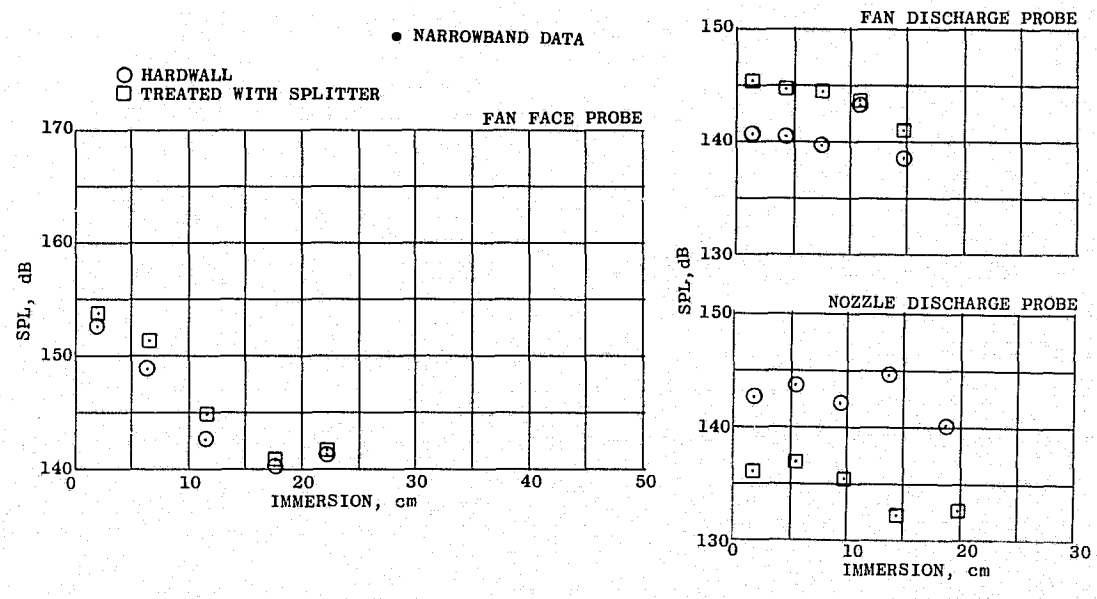

Figure A30. MPT Sound Power Level Vs. Immersion, Approach (Front-Drive Test).

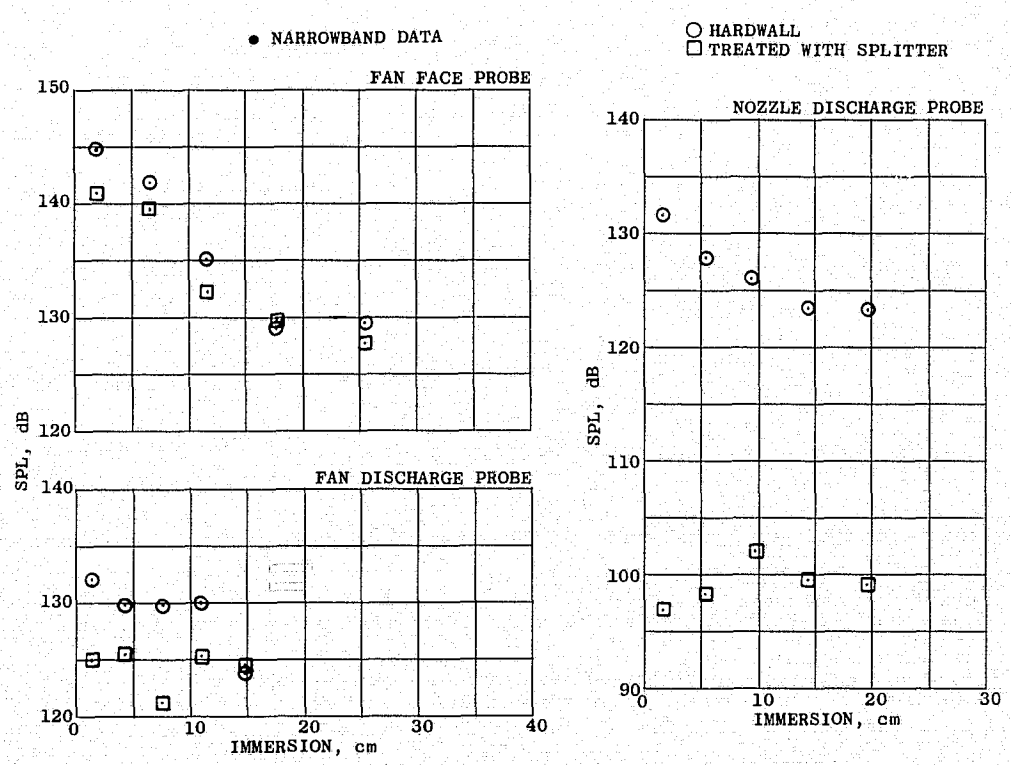

Figure A31. BPF Sound Power Level Vs. Immersion, Approach (Front-Drive Test).

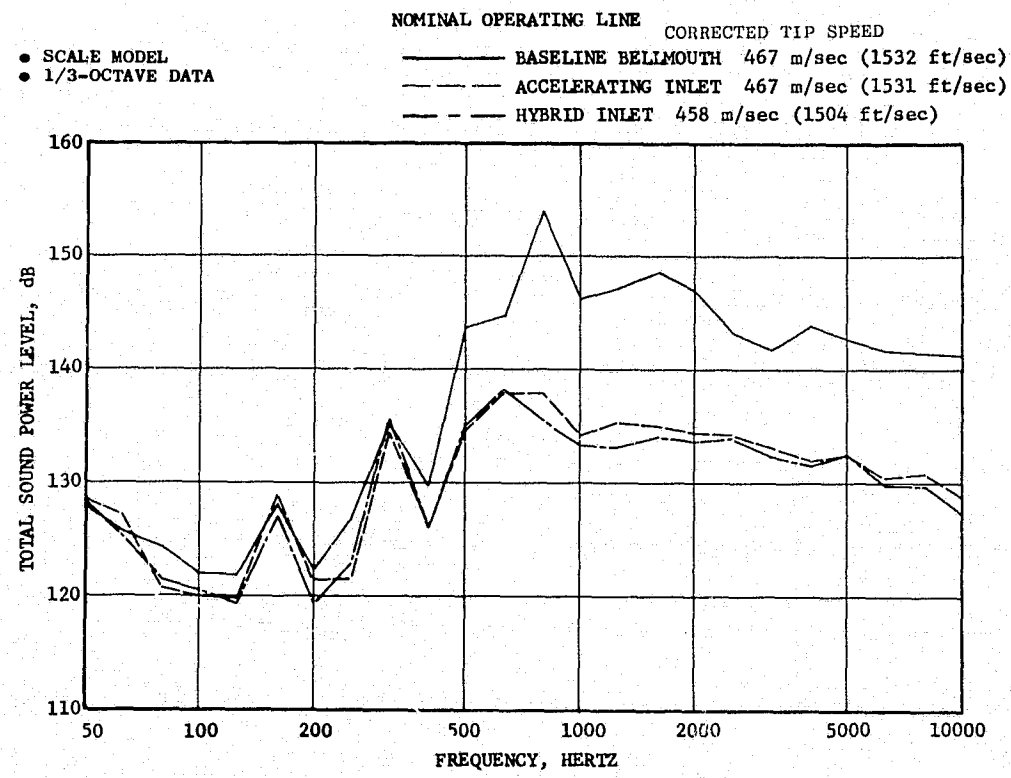

Figure B1. Total Sound Power Level Spectra, Takeoff M_{TH} = 0.79 (Rear-(Drive Test).

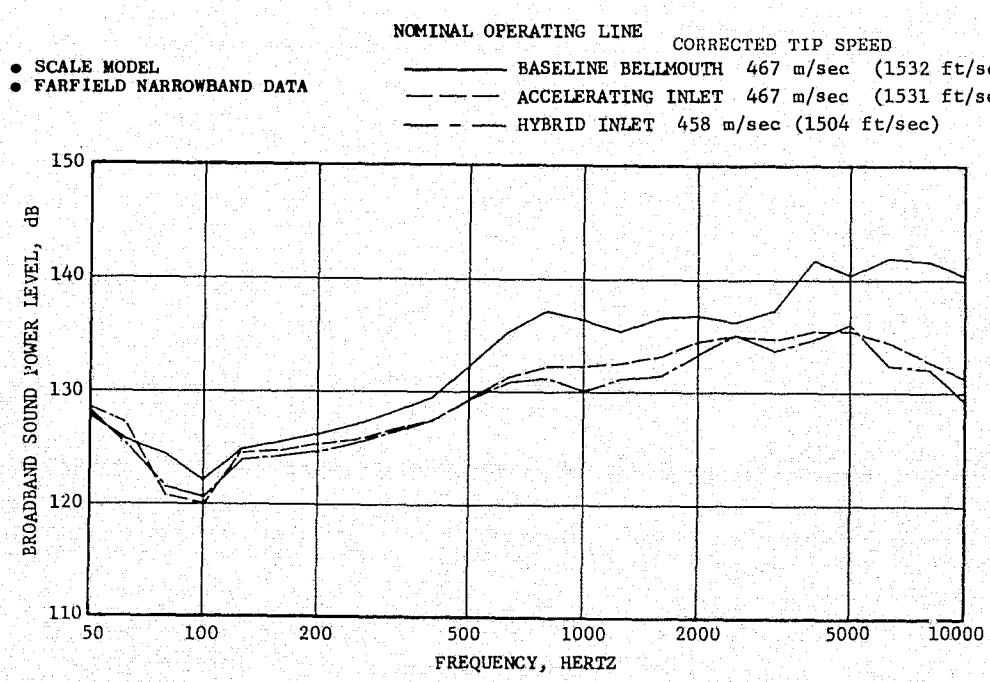

Figure B2. Broadband Sound Power Level Spectra, Takeoff M_{TH} = 0.79 (Rear-Drive Test).

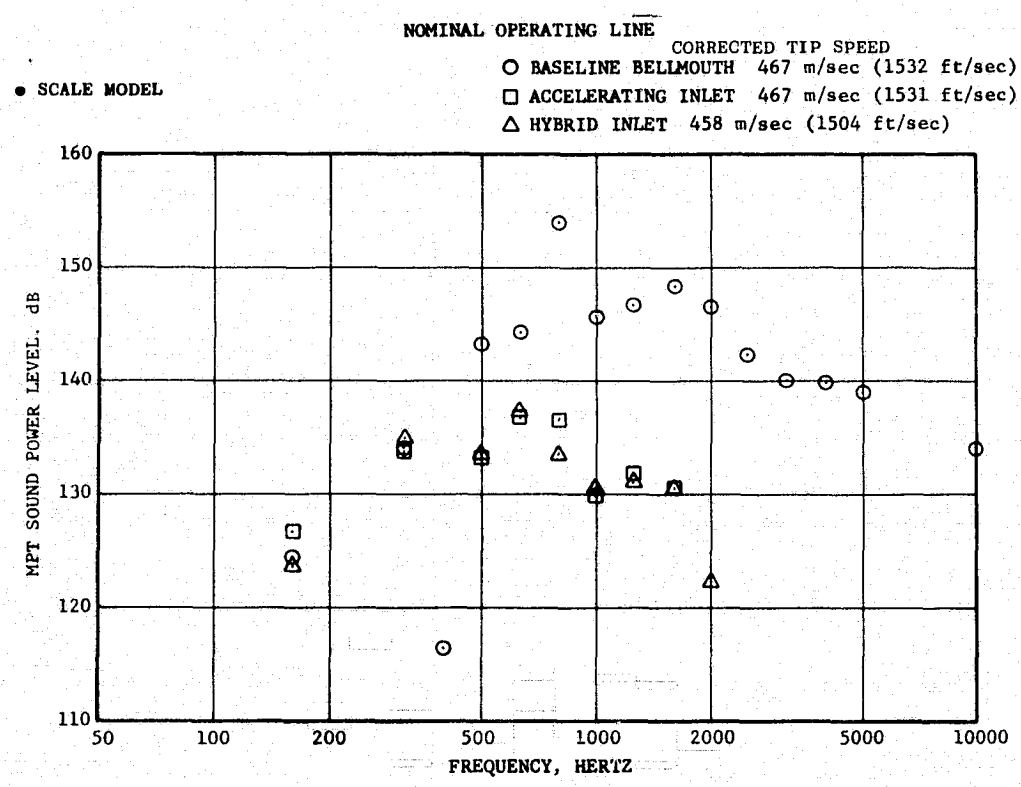

Figure B3. MPT Sound Power Level Spectra, Takeoff M_{TH} = 0.79 (Rear-Drive Test).

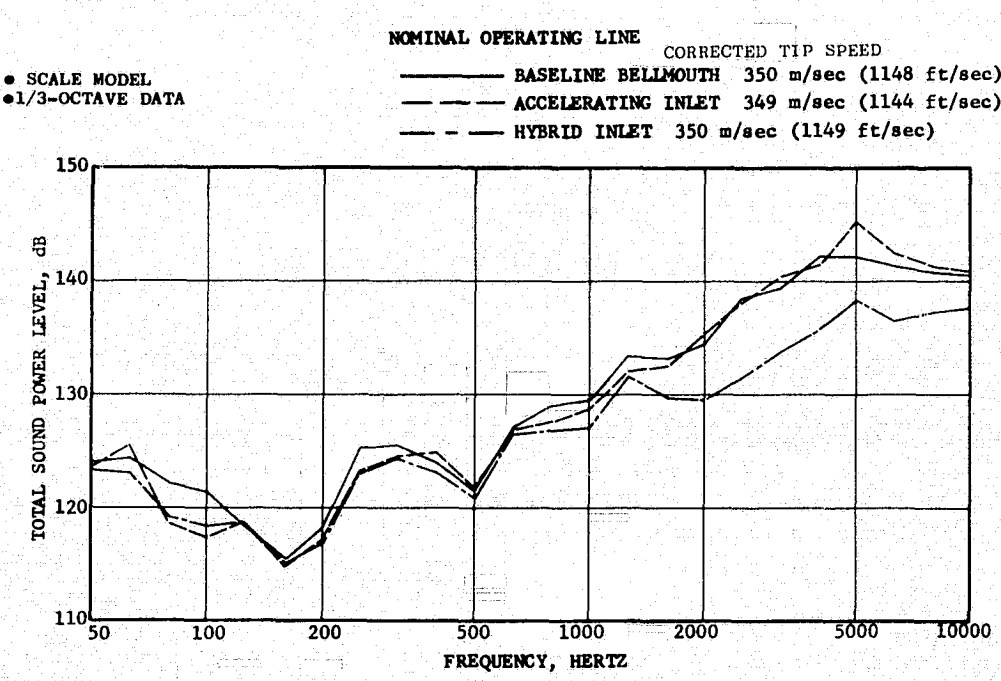

Figure B4. Total Sound Power Level Spectra, Takeoff M_{TH} = 0.47 (Rear-Drive Test).

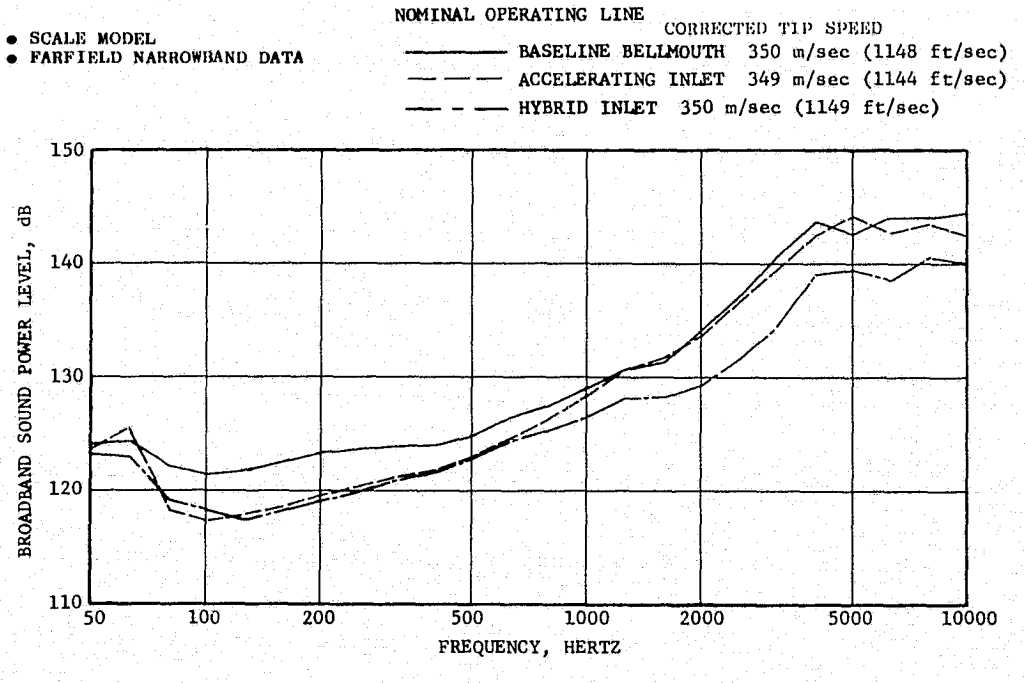

Figure B5. Broadband Sound Power Level Spectra, Takeoff M_{TH} = 0.47 (Rear-Drive Test).

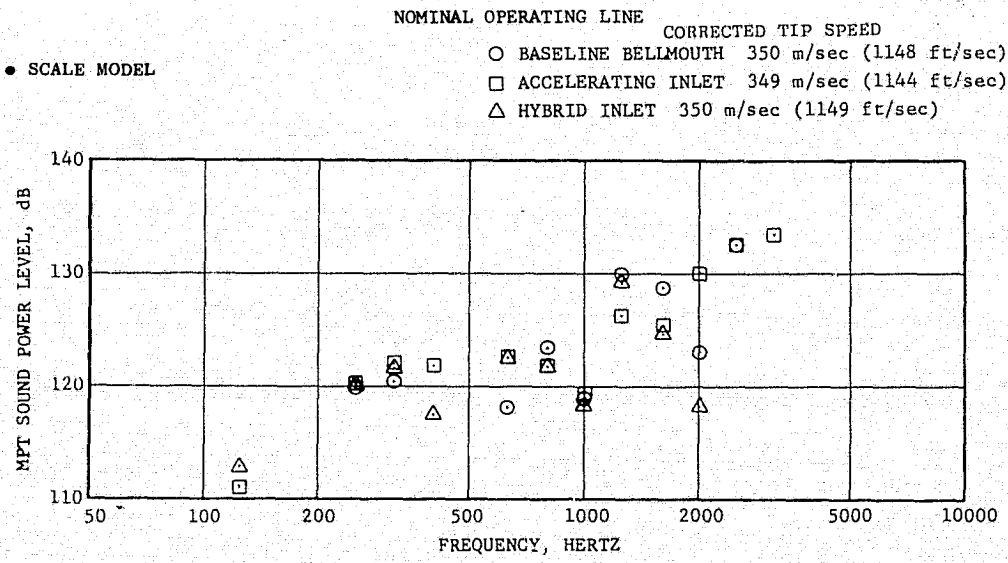

Figure B6. MPT Sound Power Level Spectra, Takeoff M_{TH} = 0.47 (Rear-Drive Test).

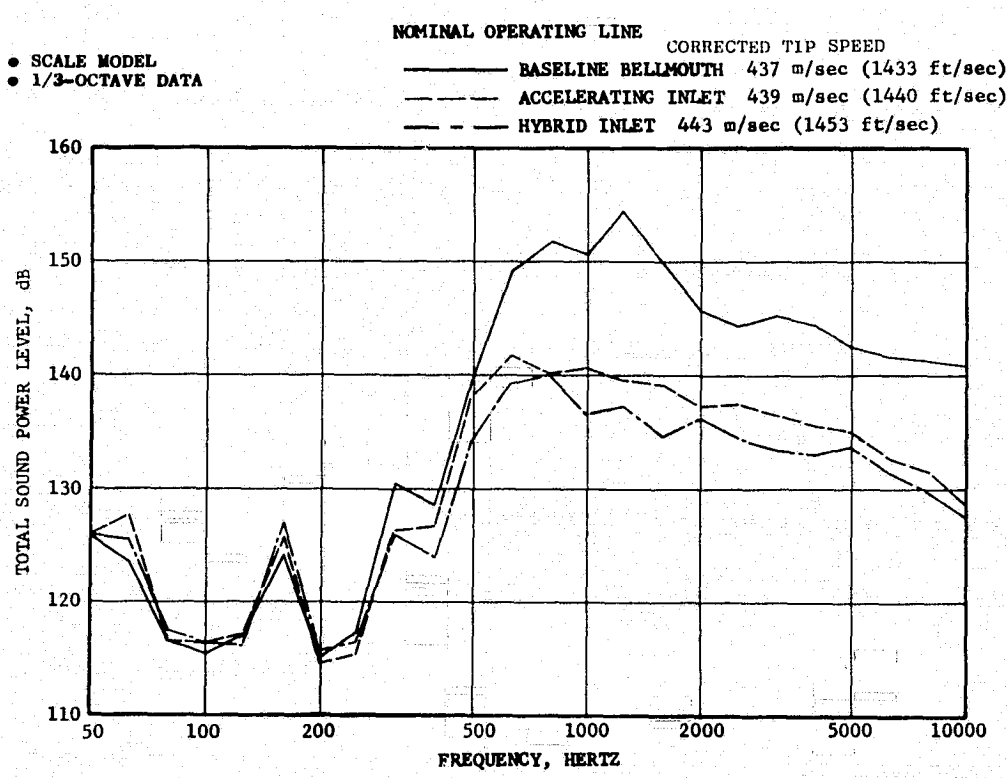

Figure B7. Total Sound Power Level Spectra, Cutback M_{TH} = 0.79 (Rear-Drive Test).

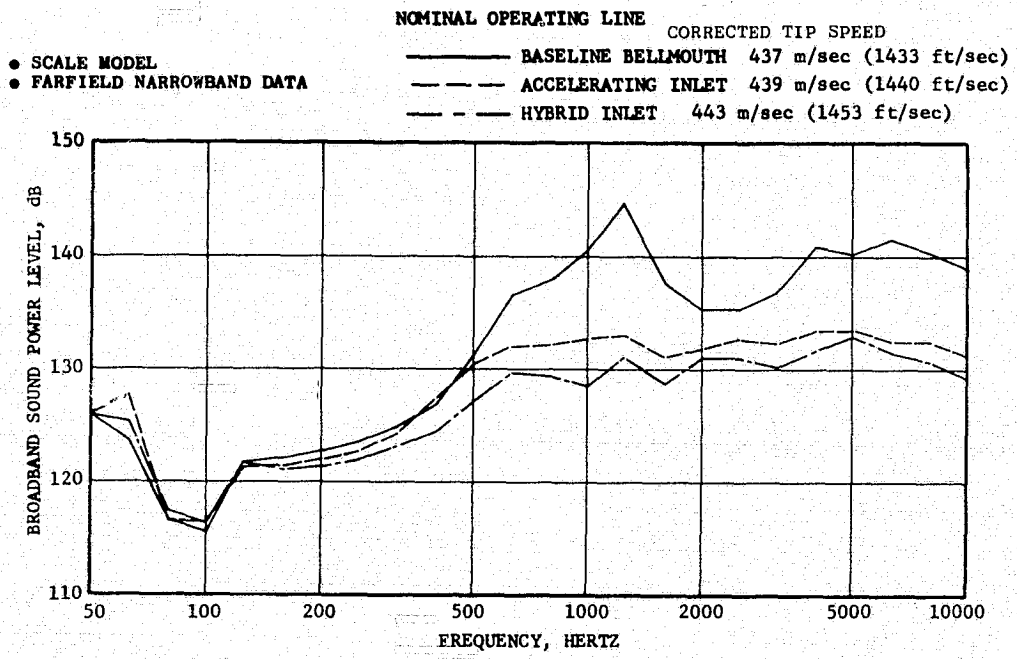

Figure B8. Broadband Sound Power Level Spectra, Cutback M_{TH} = 0.79 (Rear-Drive Test).

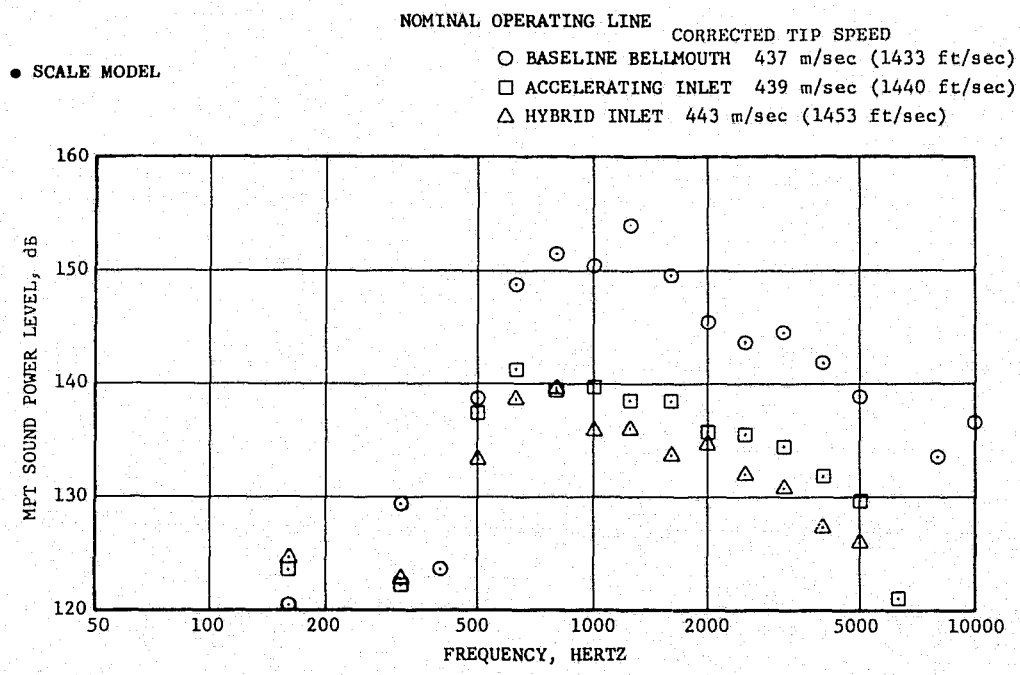

Figure B9. MPT Sound Power Level Spectra, Cutback M_{TH} = 0.79 (Rear-Drive Test).

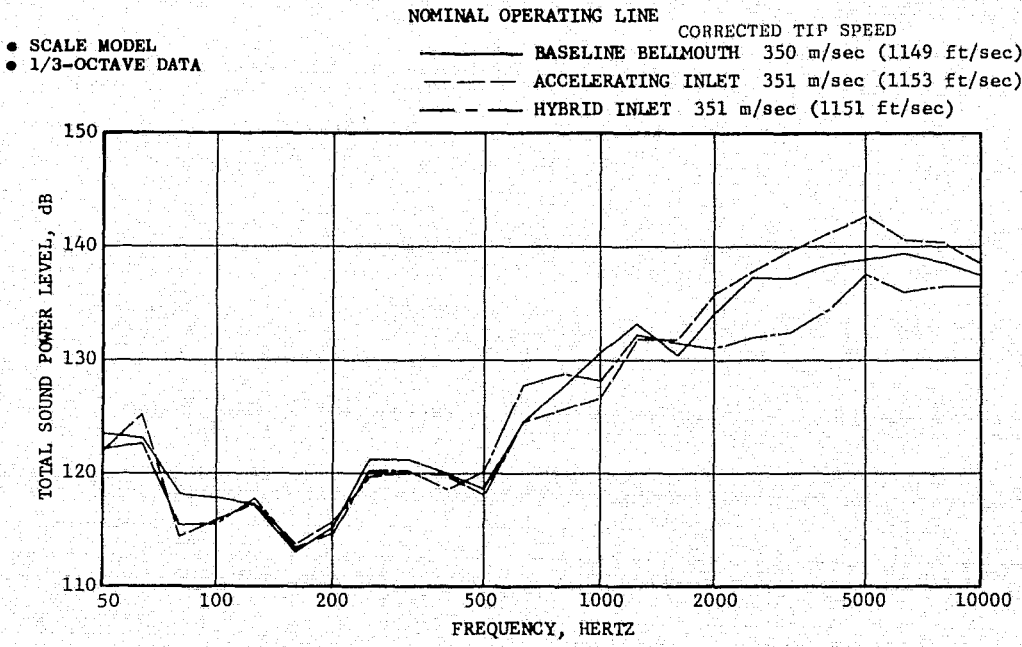

Figure B10. Total Sound Power Level Spectra, Cutback M_{TH} = 0.52 (Rear-Drive Test).

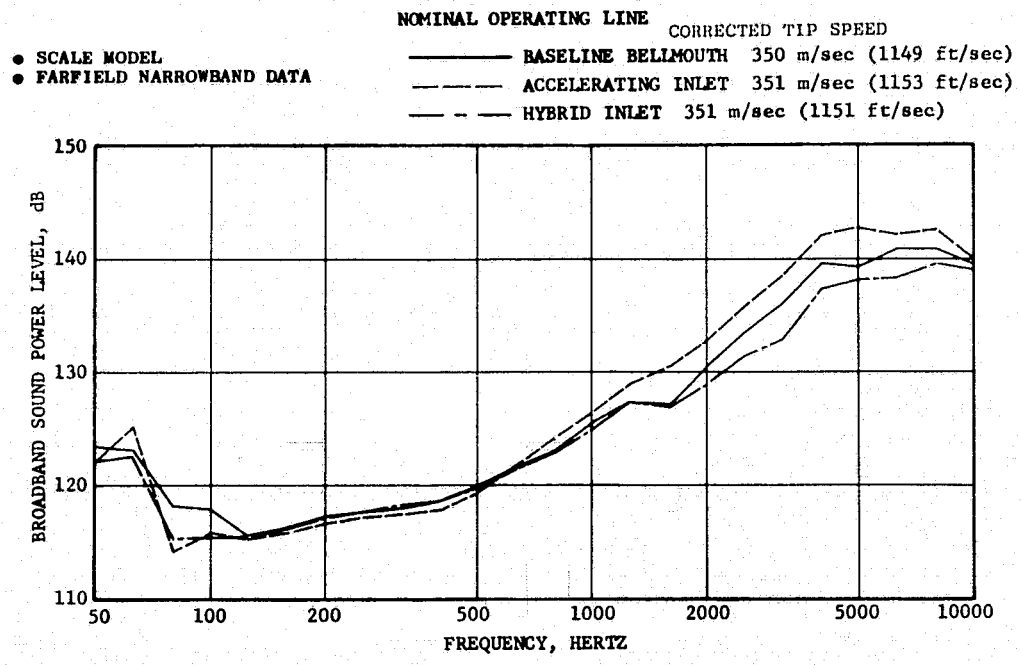

Figure B11. Broadband Sound Power Level Spectra, Cutback M_{TH} = 0.52 (Rear-Drive Test).

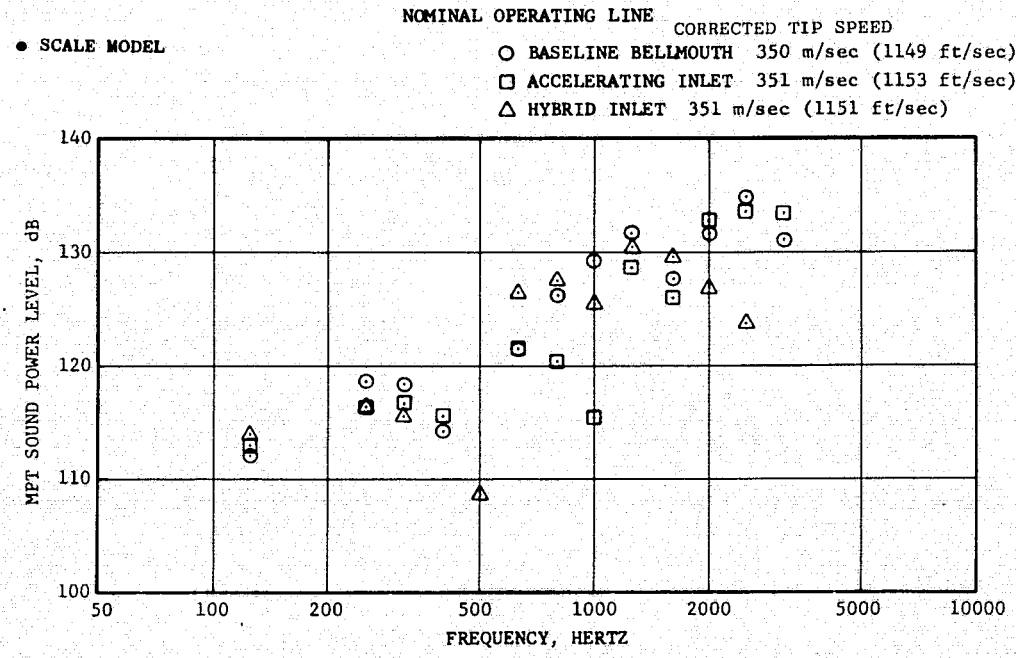

Figure B12. MPT Sound Power Level Spectra, Cutback M_{TH} = 0.52 (Rear-Drive Test).

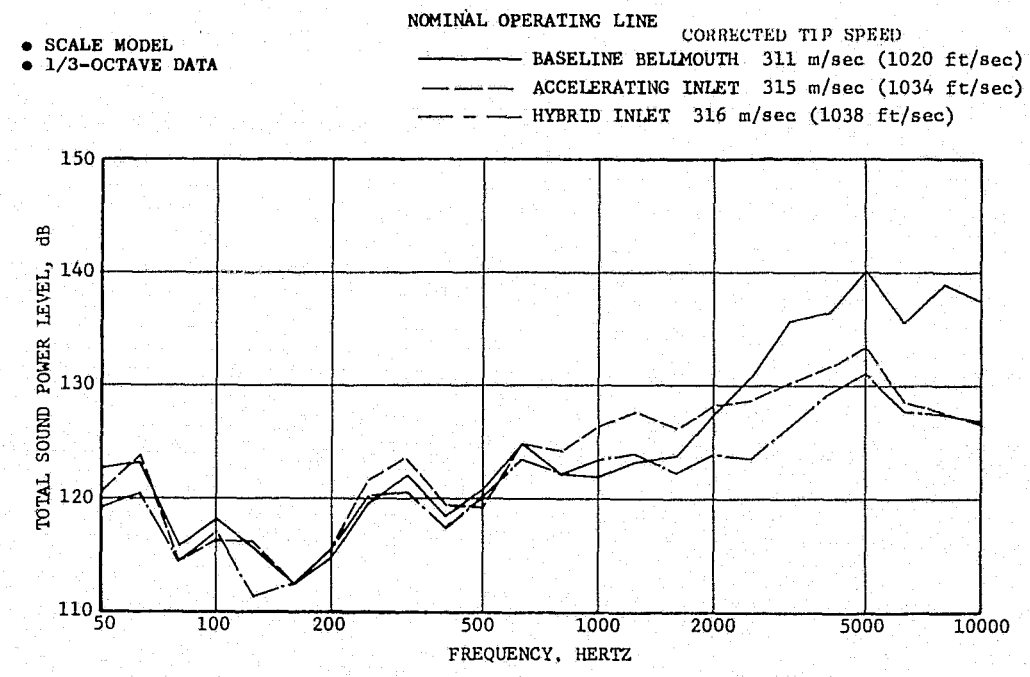

Figure B13. Total Sound Power Level Spectra, Approach M_{TH} = 0.79 (Rear-Drive Test).

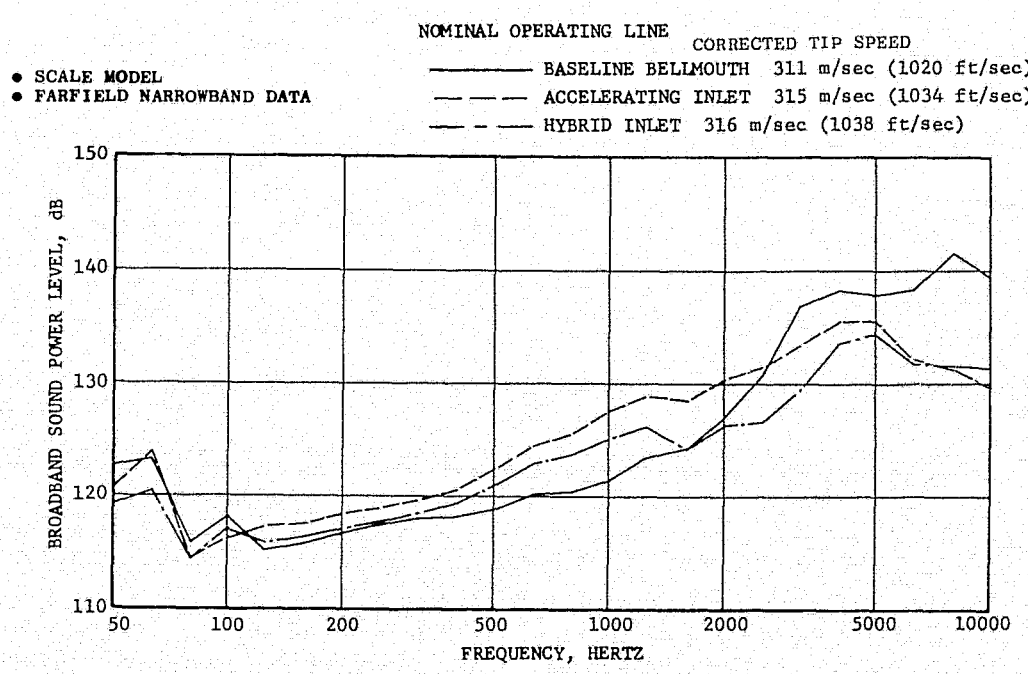

Figure B14. Broadband Sound Power Level Spectra, Approach M_{TH} = 0.79 (Rear-Drive Test).

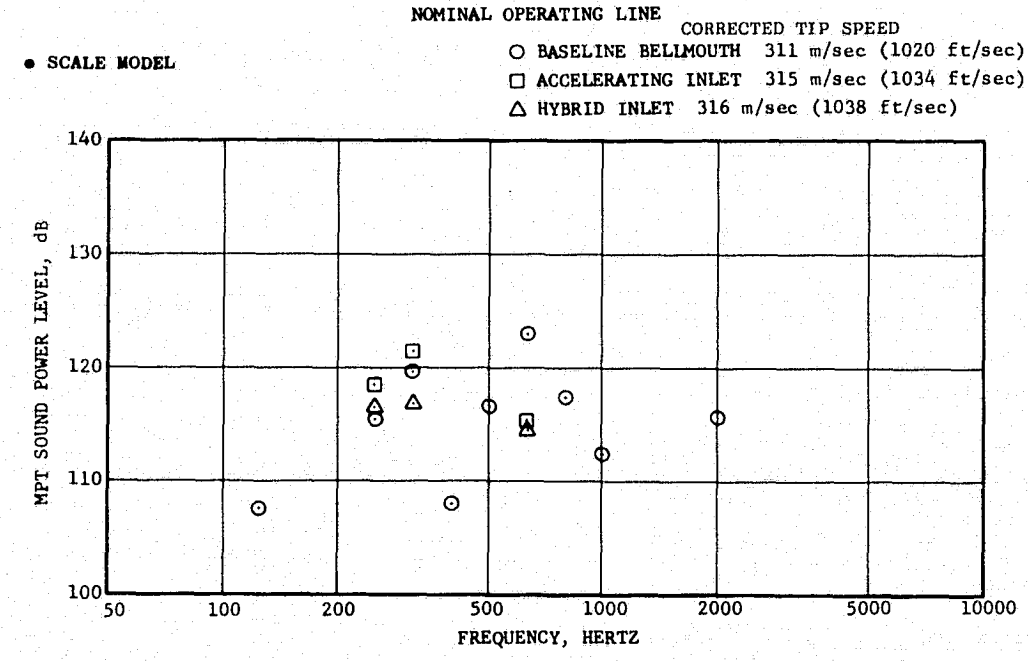

Figure B15. MPT Sound Power Level Spectra, Approach M_{TH} = 0.79 (Rear-Drive Test).

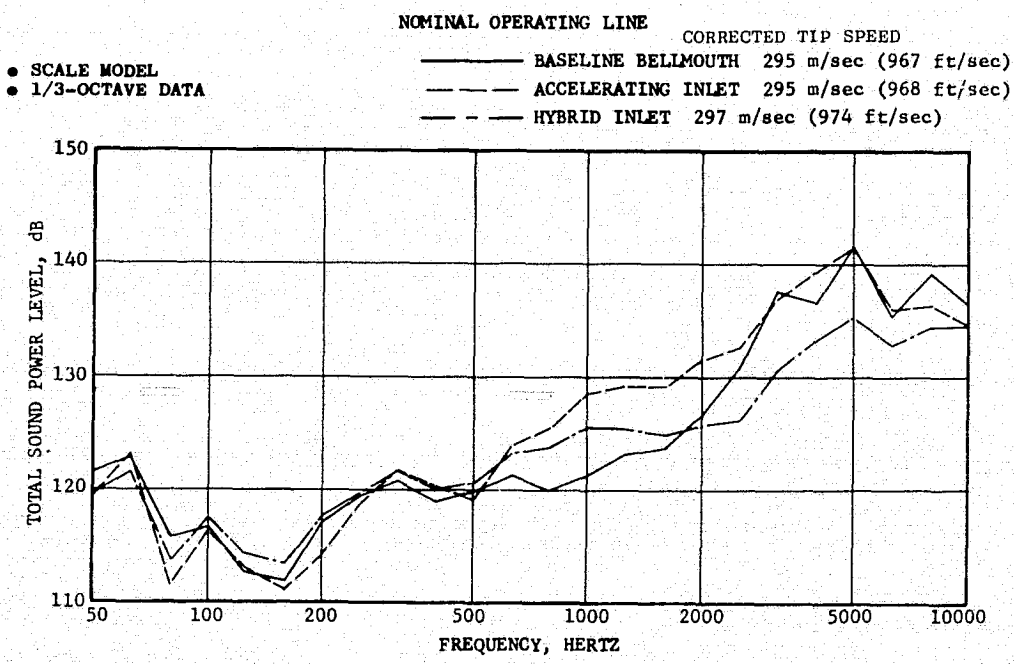

Figure B16. Total Sound Power Level Spectra, Approach M_{TH} = 0.68 (Rear-Drive Test).

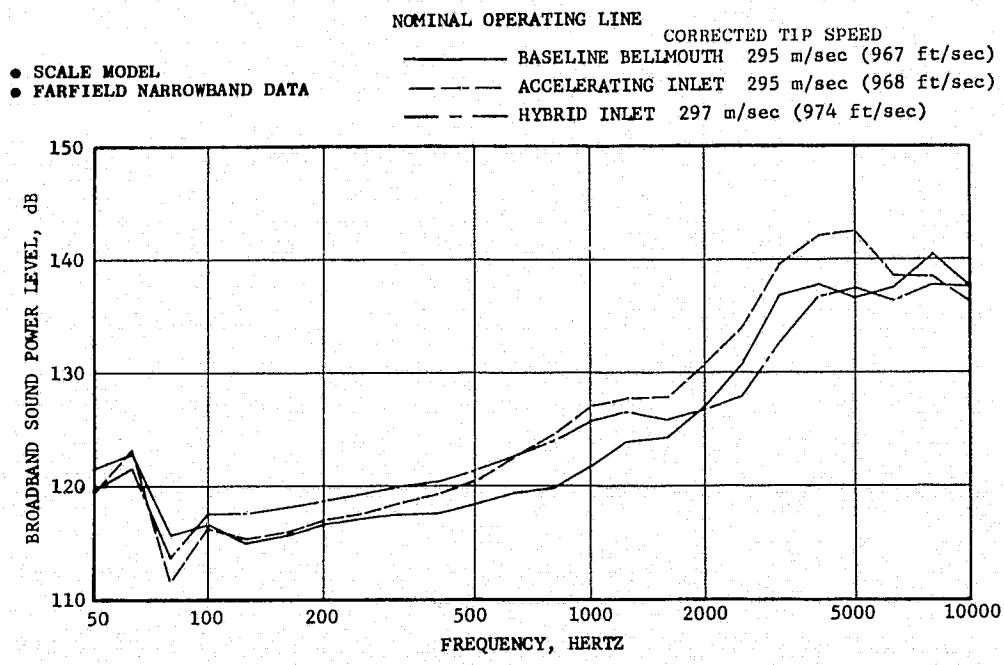

Figure B17. Broadband Sound Power Level Spectra, Approach M_{TH} = 0.68 (Rear-Drive Test).

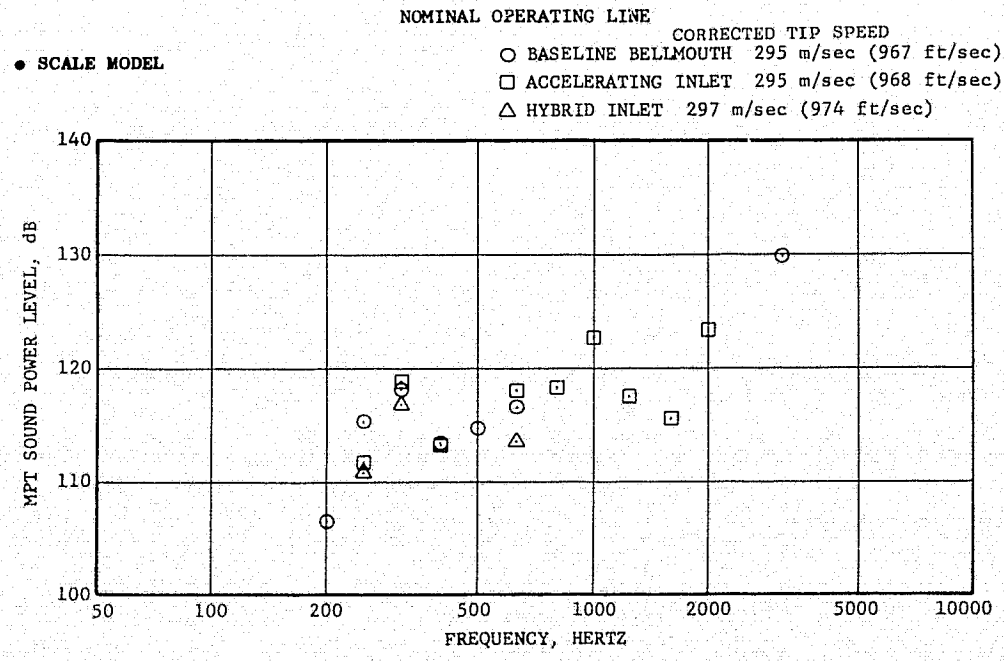

Figure B18. MPT Sound Power Level Spectra, Approach M_{TH} = 0.68 (Rear-Drive Test).

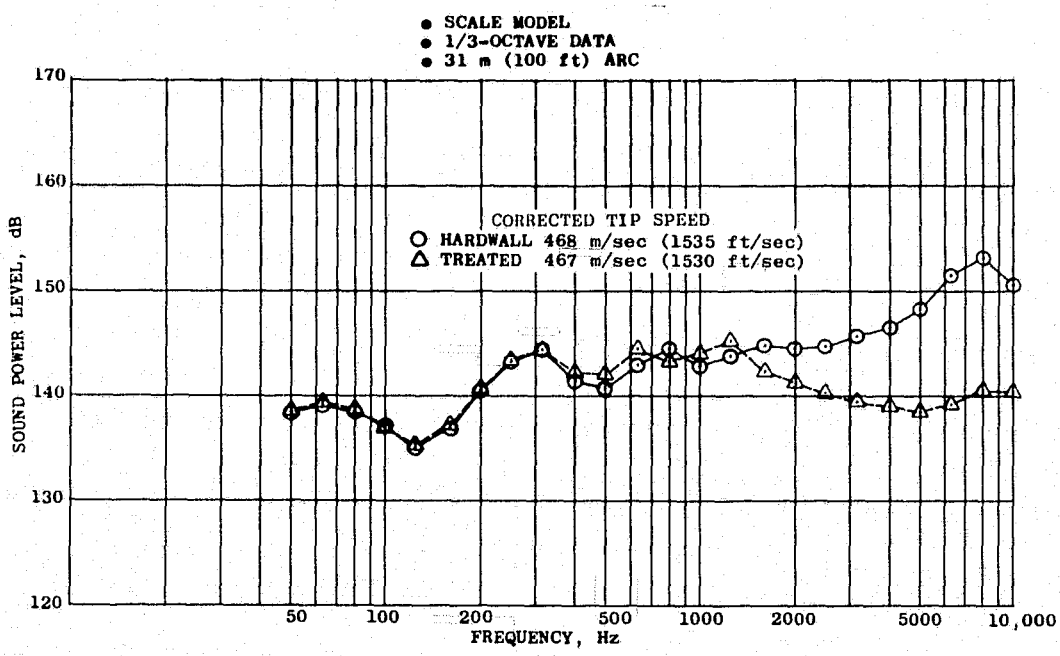

Figure B19. Total Sound Power Level Spectra, Takeoff (Front-Drive Test).

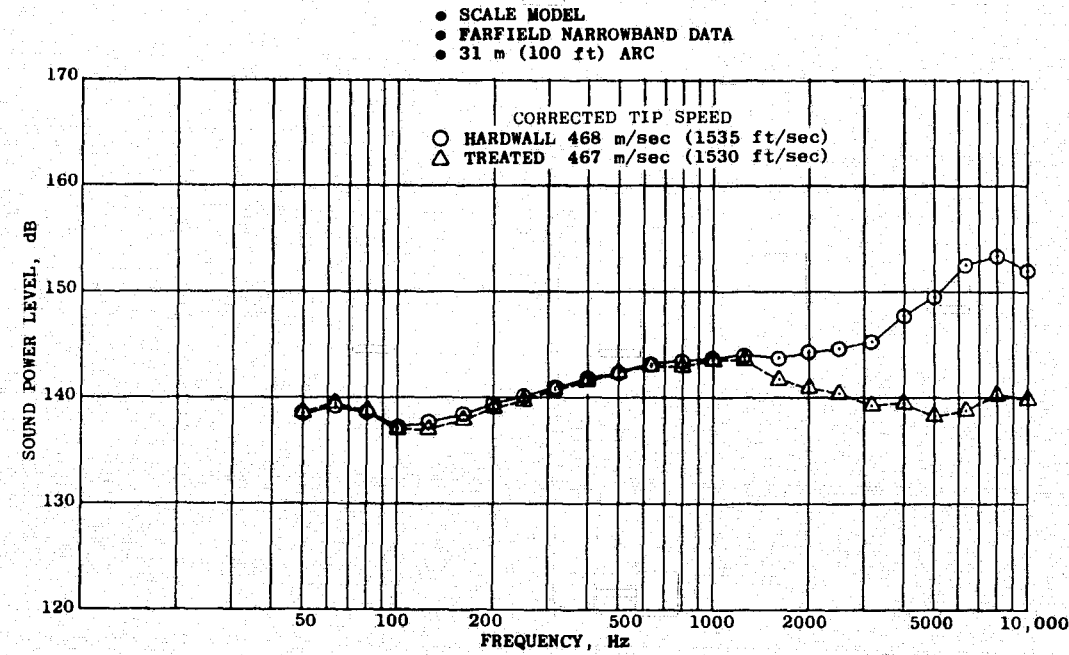

Figure B20. Broadband Sound Power Level Spectra, Takeoff (Front-Drive Test).

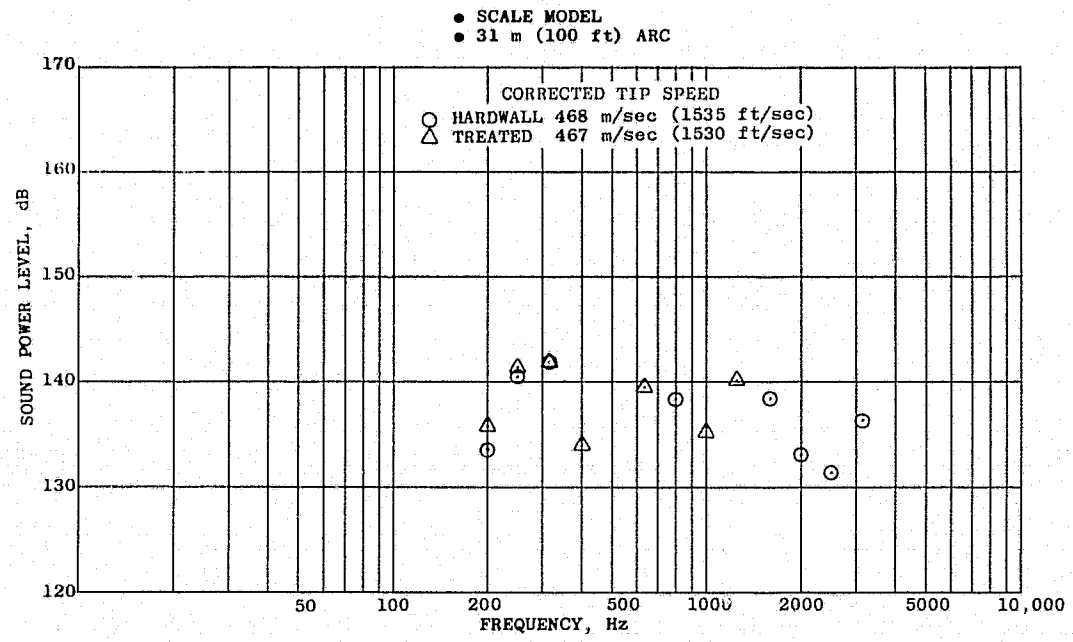

Figure B21. MPT Sound Power Level Spectra, Takeoff (Front-Drive Test).

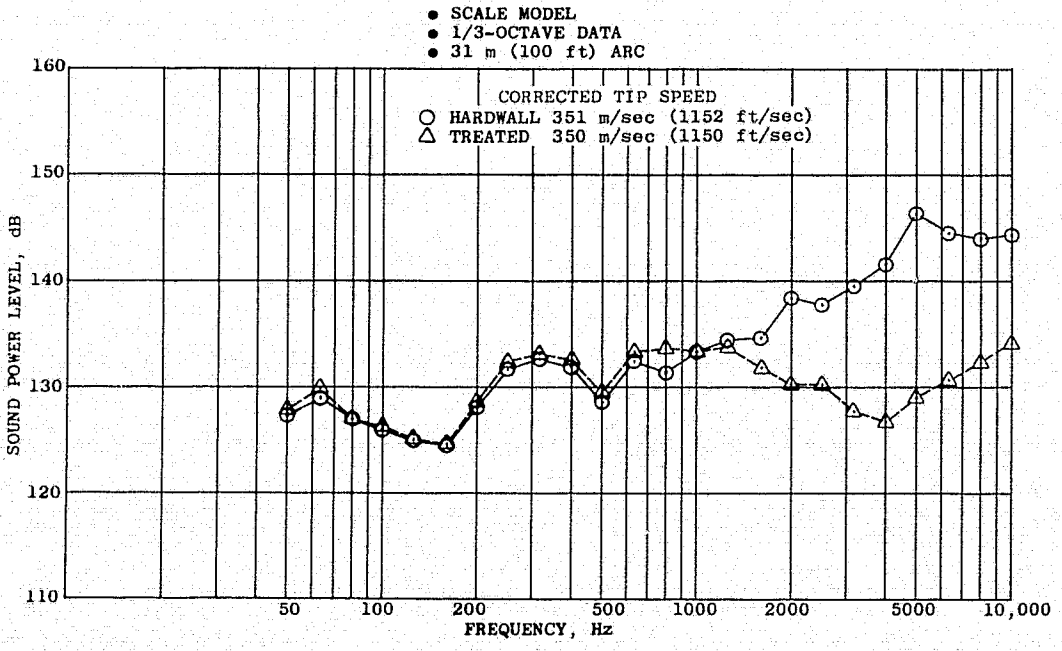

Figure B22. Total Sound Power Level Spectra, Takeoff (Front-Drive Test).

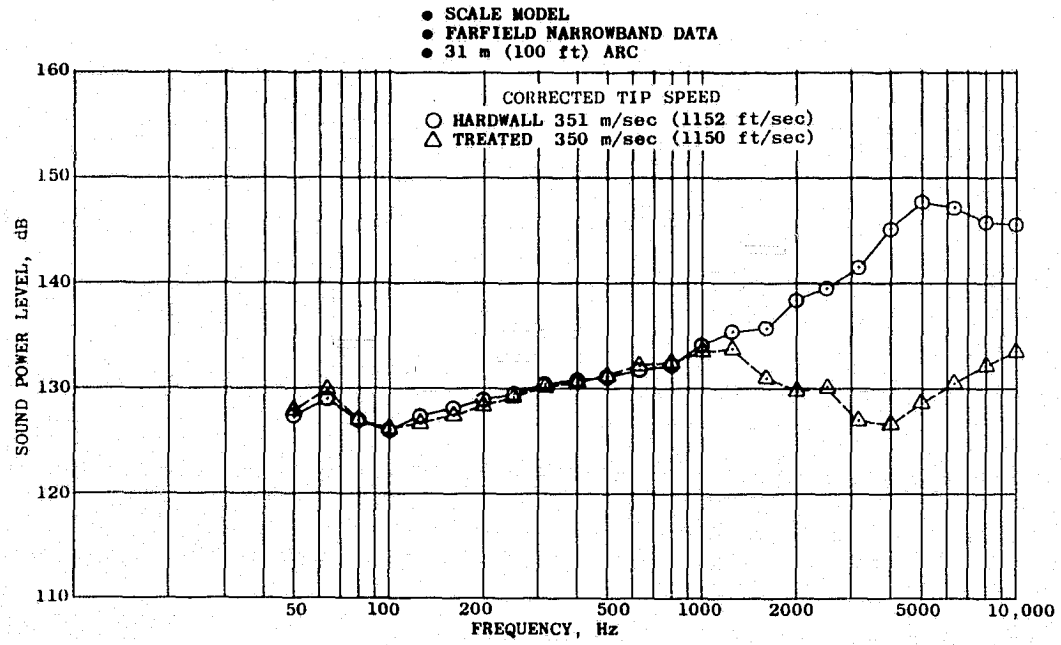

Figure B23. Broadband Sound Power Level Spectra, Takeoff (Front-Drive Test).

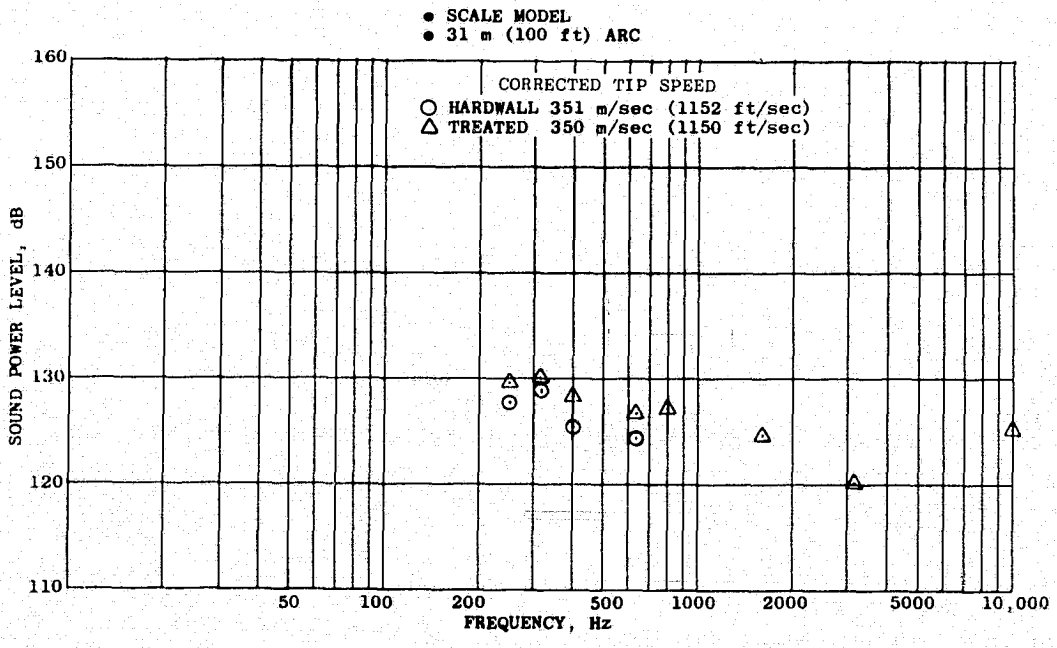

Figure B24. MPT Sound Power Level Spectra, Takeoff (Front-Drive Test).

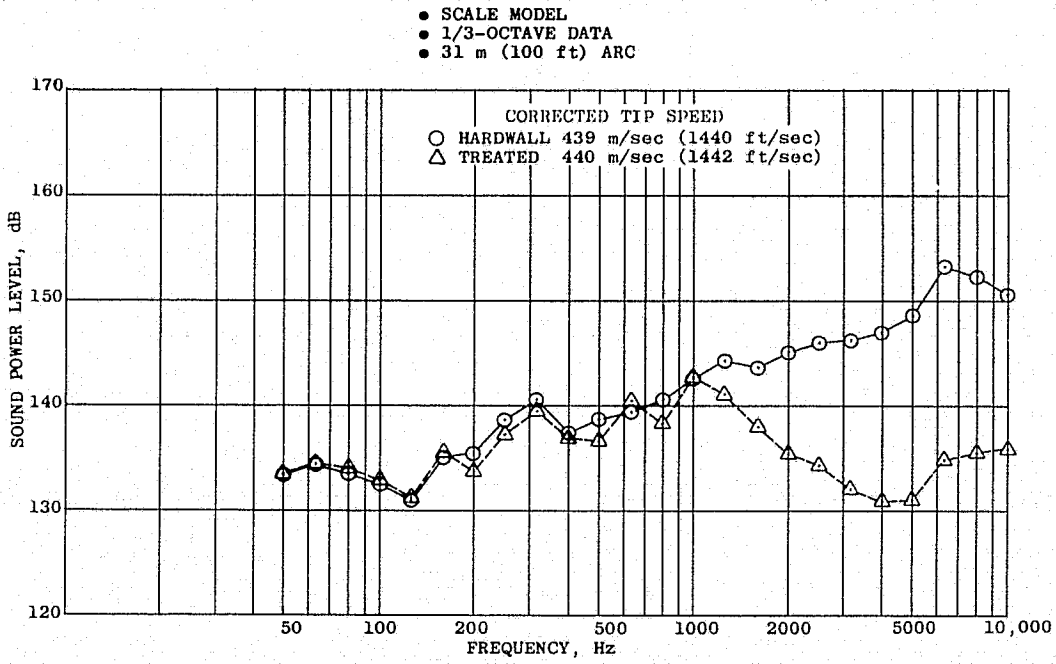

Figure B25. Total Sound Power Level Spectra, Cutback (Front-Drive Test).

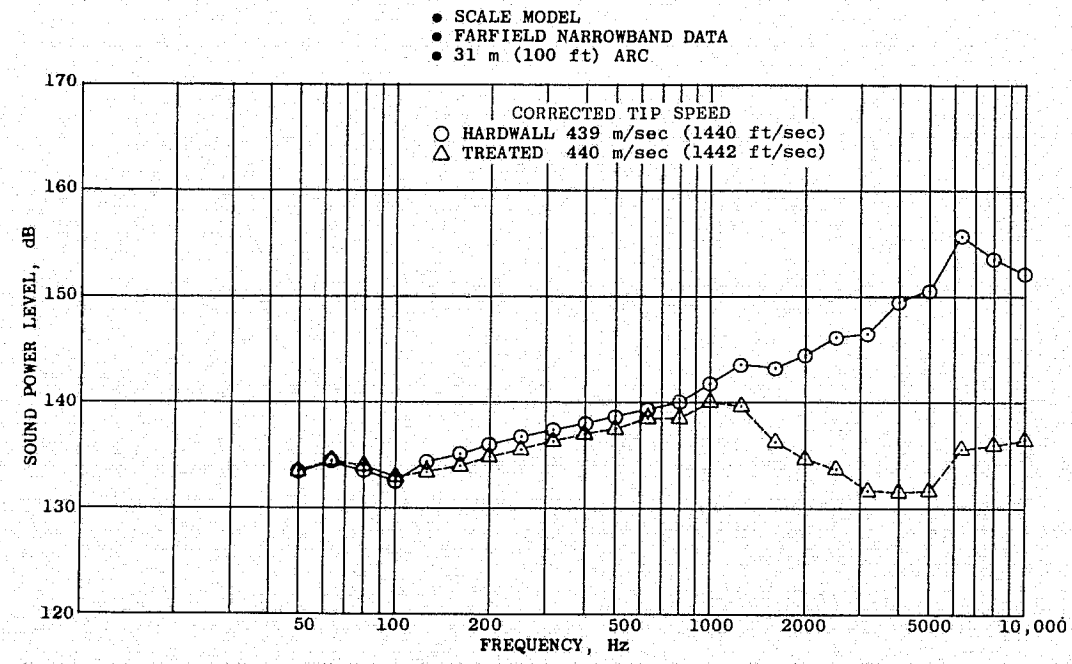

Figure B26. Broadband Sound Power Level Spectra, Cutback (Front-Drive Test).

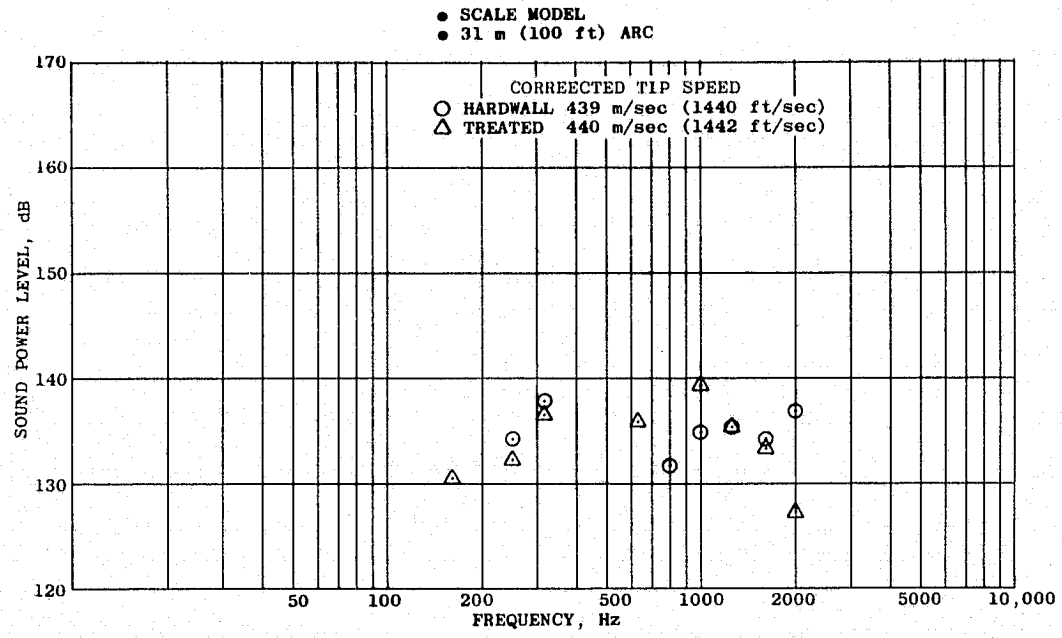

Figure B27. MPT Sound Power Level Spectra, Cutback (Front-Drive Test).

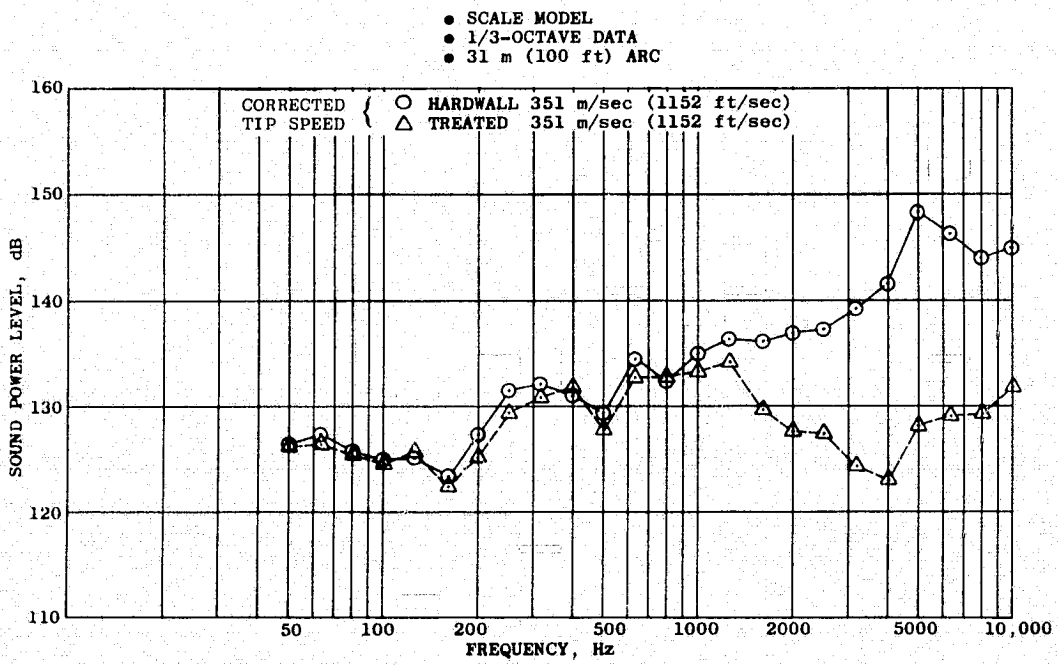

Figure B28. Total Sound Power Level Spectra, Cutback (Front-Drive Test).

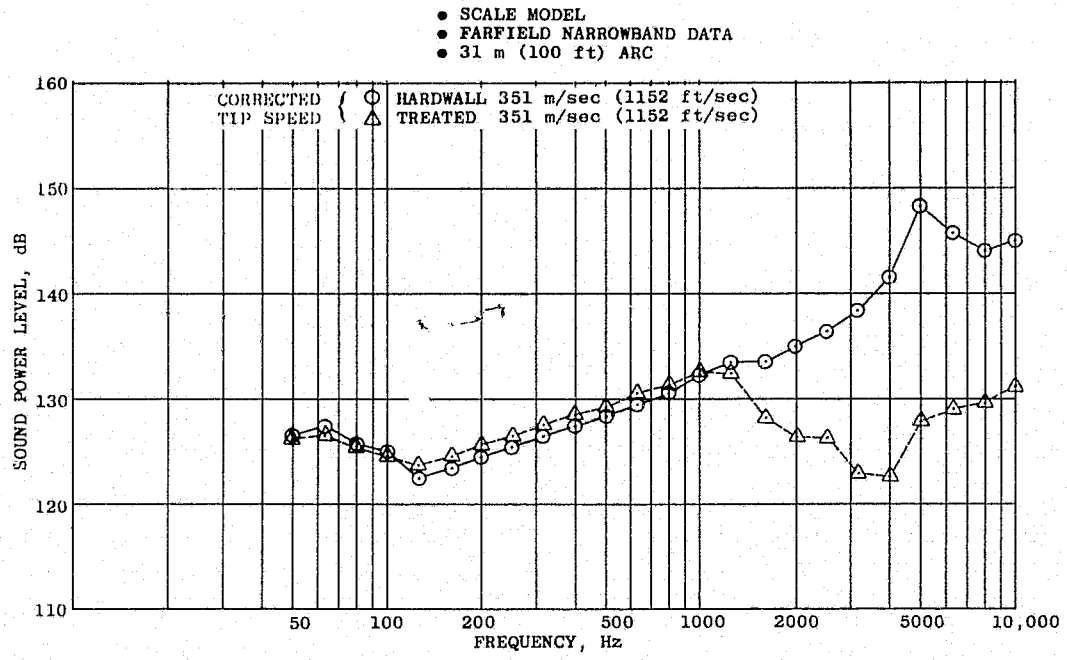

Figure B29. Broadband Sound Power Level Spectra, Cutback (Front-Drive Test).

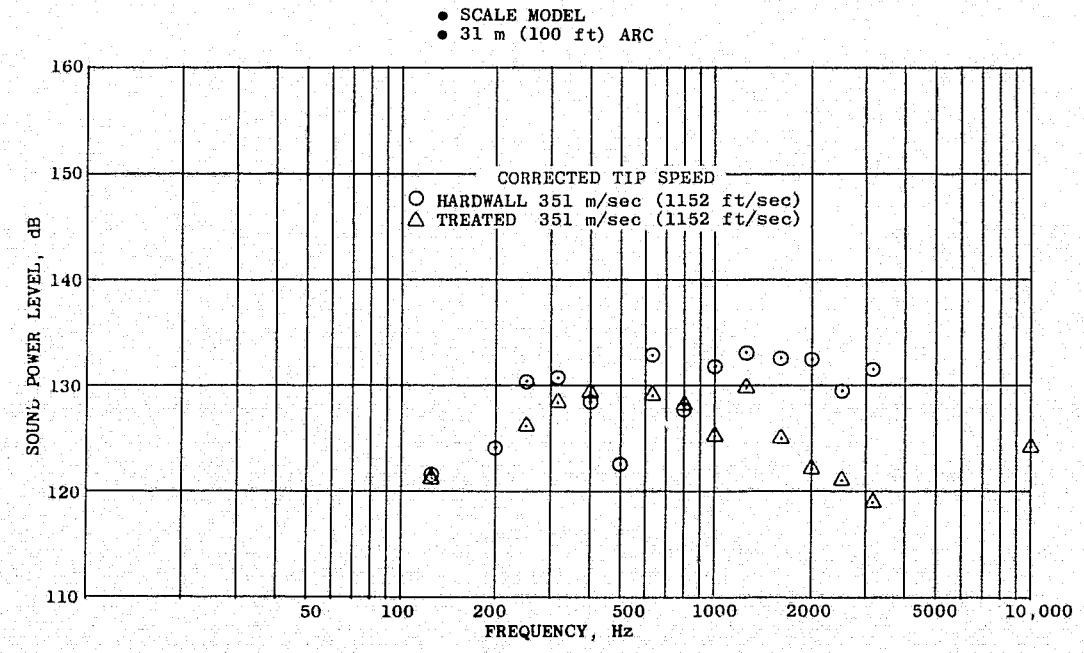

Figure B30. MPT Sound Power Level Spectra, Cutback (Front-Drive Test).

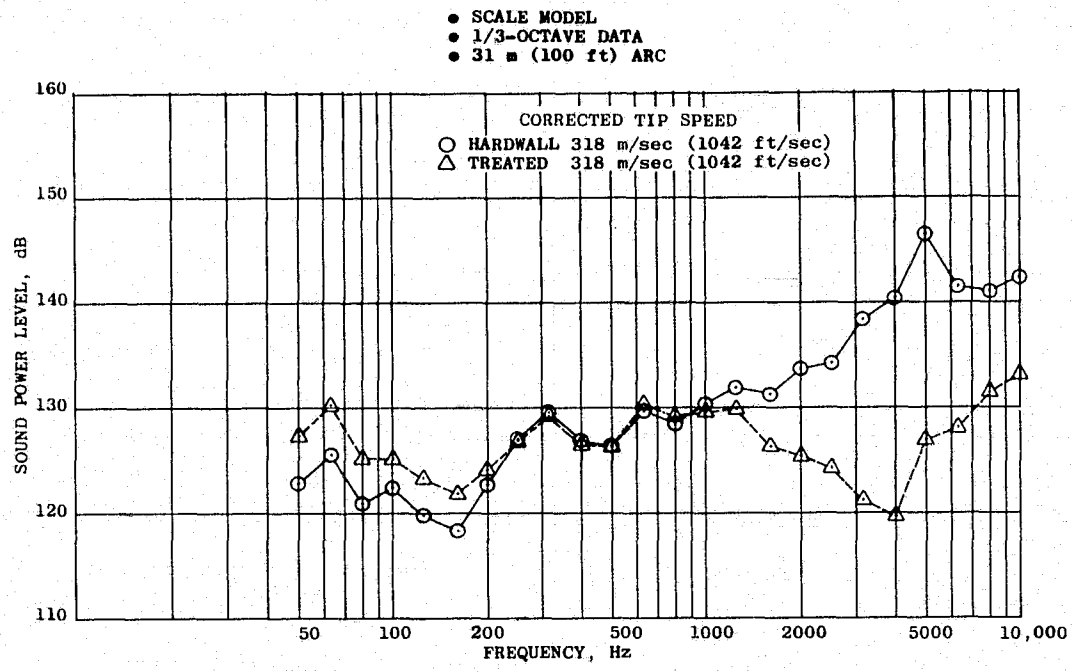

Figure B31. Total Sound Power Level Spectra, Approach (Front-Drive Test).

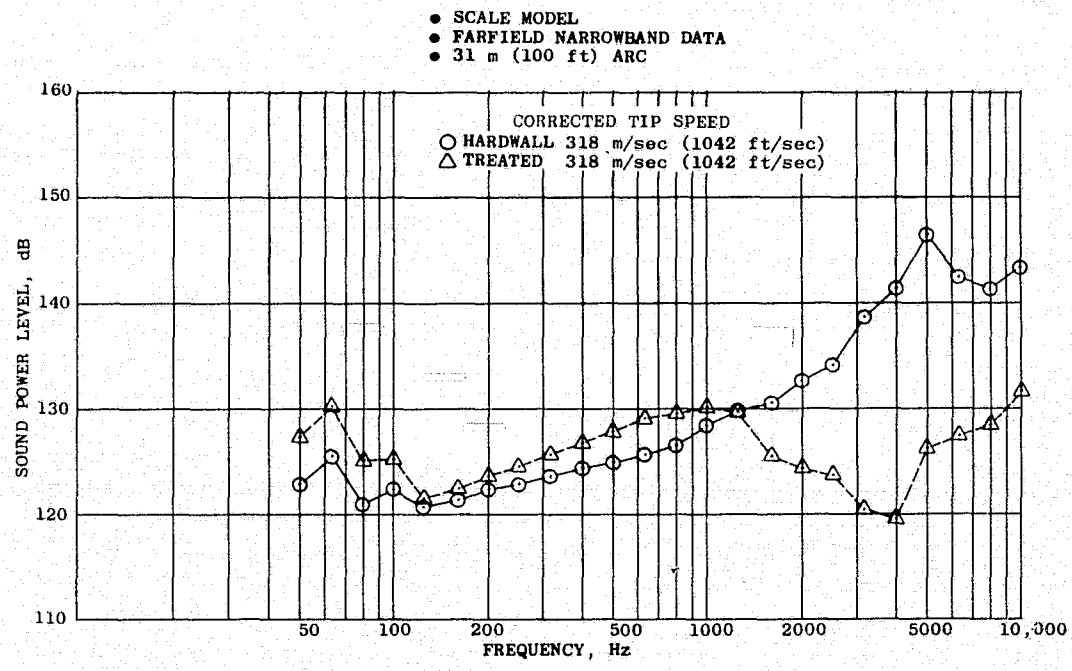

Figure B32. Broadband Sound Power Level Spectra, Approach (Front-Drive Test).

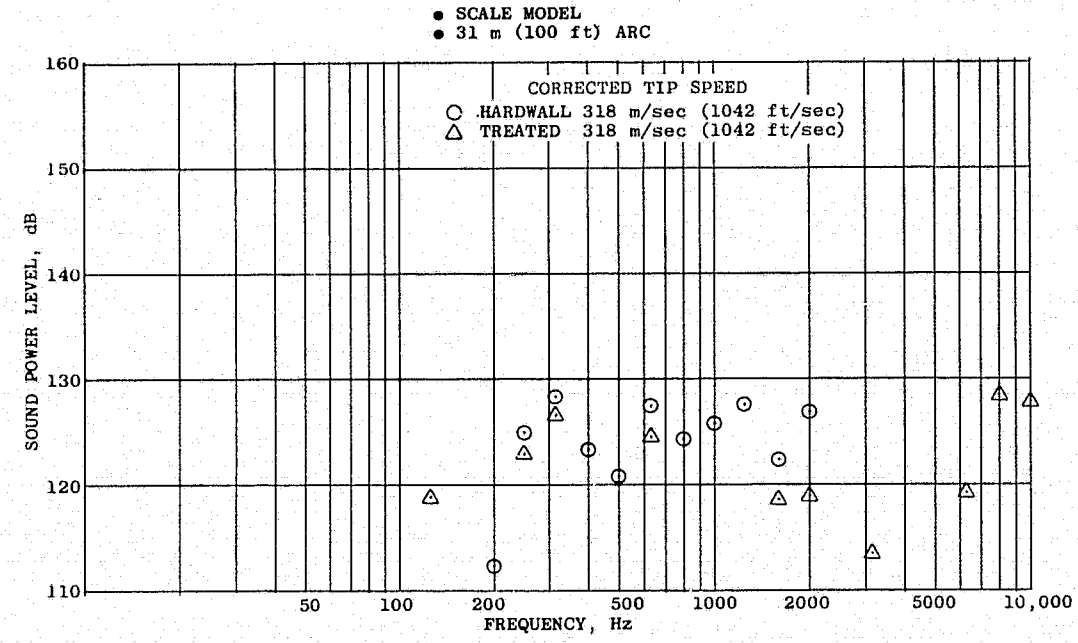

Figure B33. MPT Sound Power Level Spectra, Approach (Front-Drive Test).

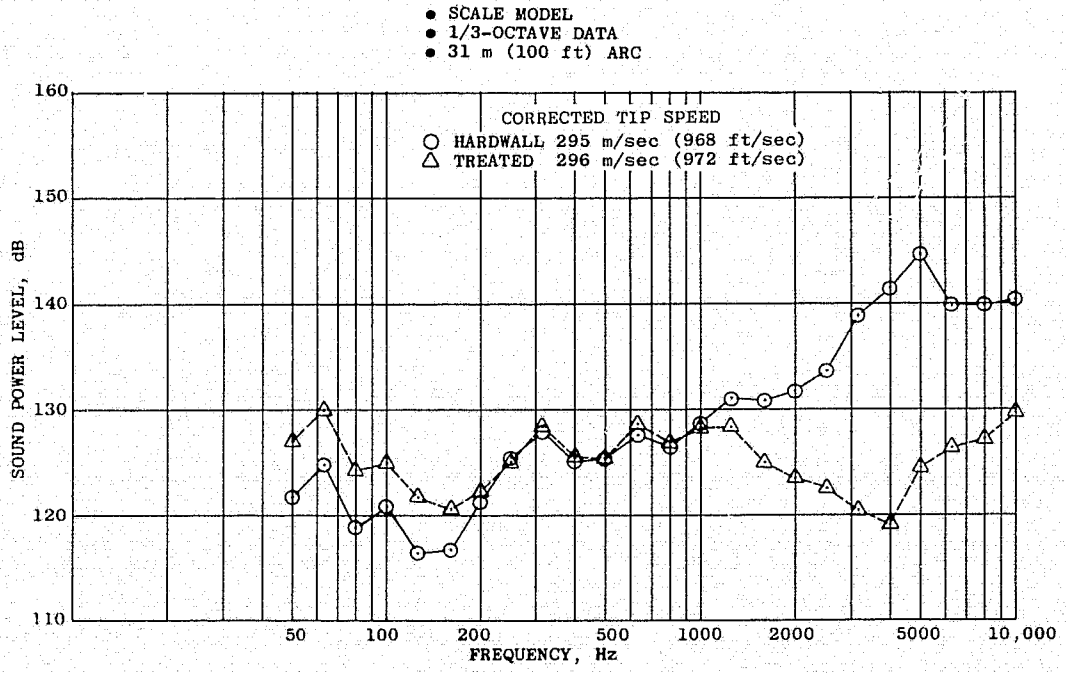

Figure B34. Total Sound Power Level Spectra, Approach (Front-Drive Test).

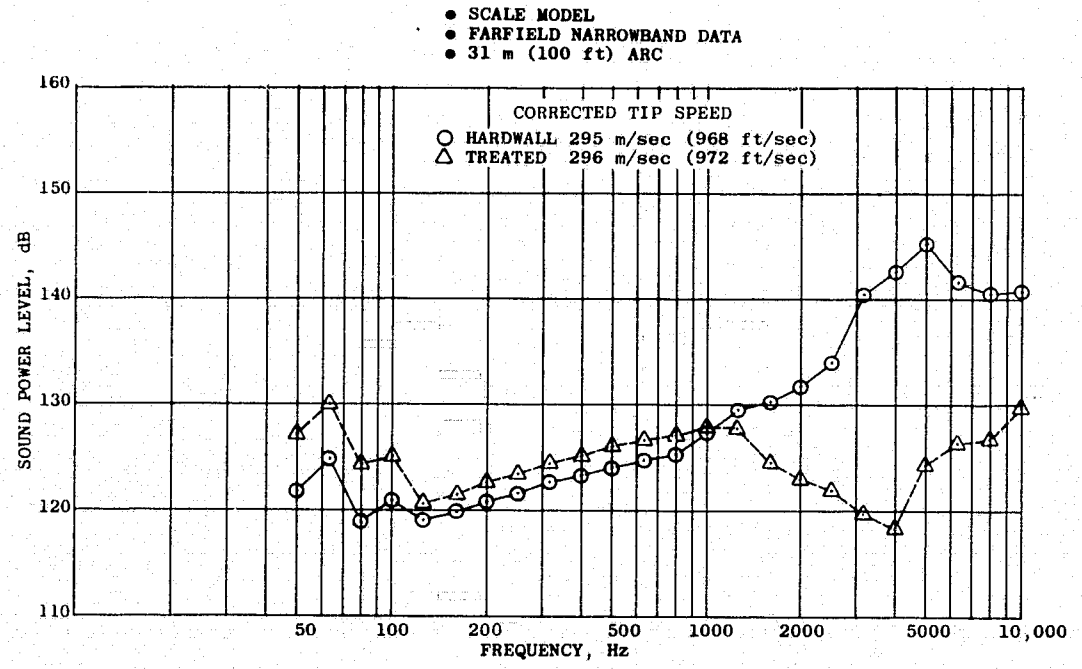

Figure B35. Broadband Sound Power Level Spectra, Approach (Front-Drive Test).

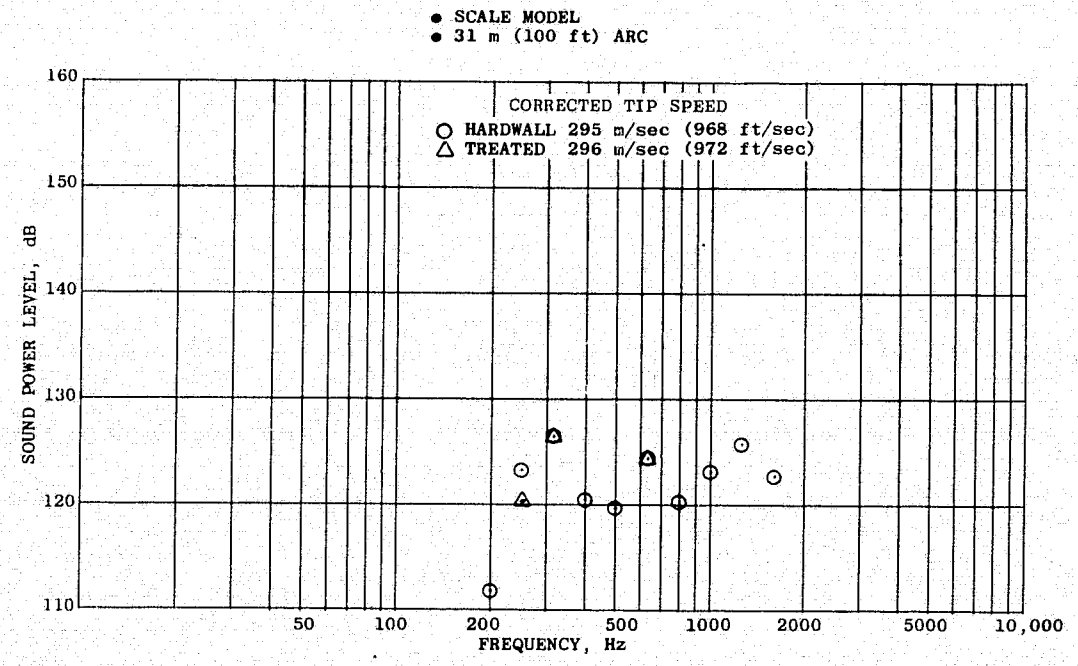

Figure B36. MPT Sound Power Level Spectra, Approach (Front-Drive Test).

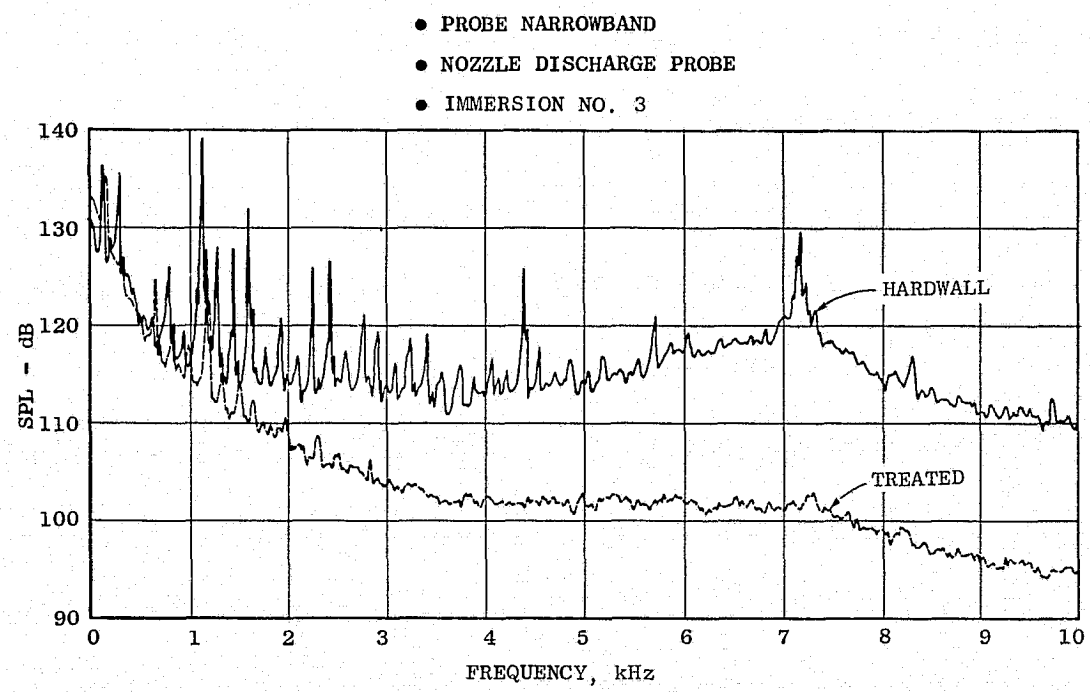

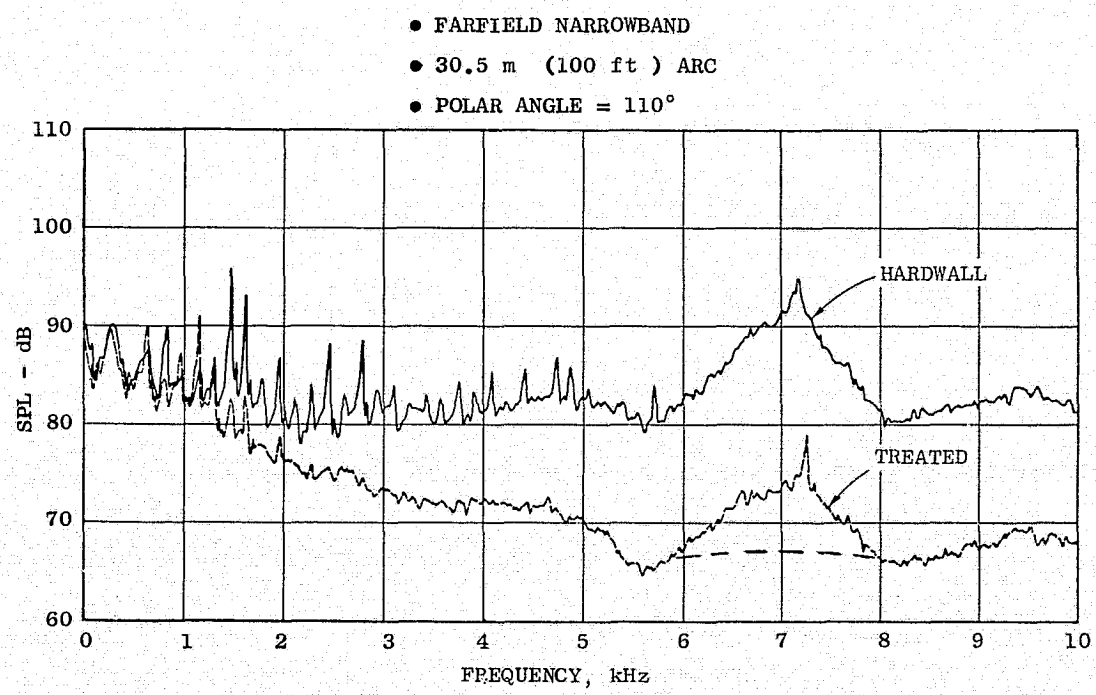

Figure C1. Probe and Farfield Narrowband Comparisons, Takeoff.

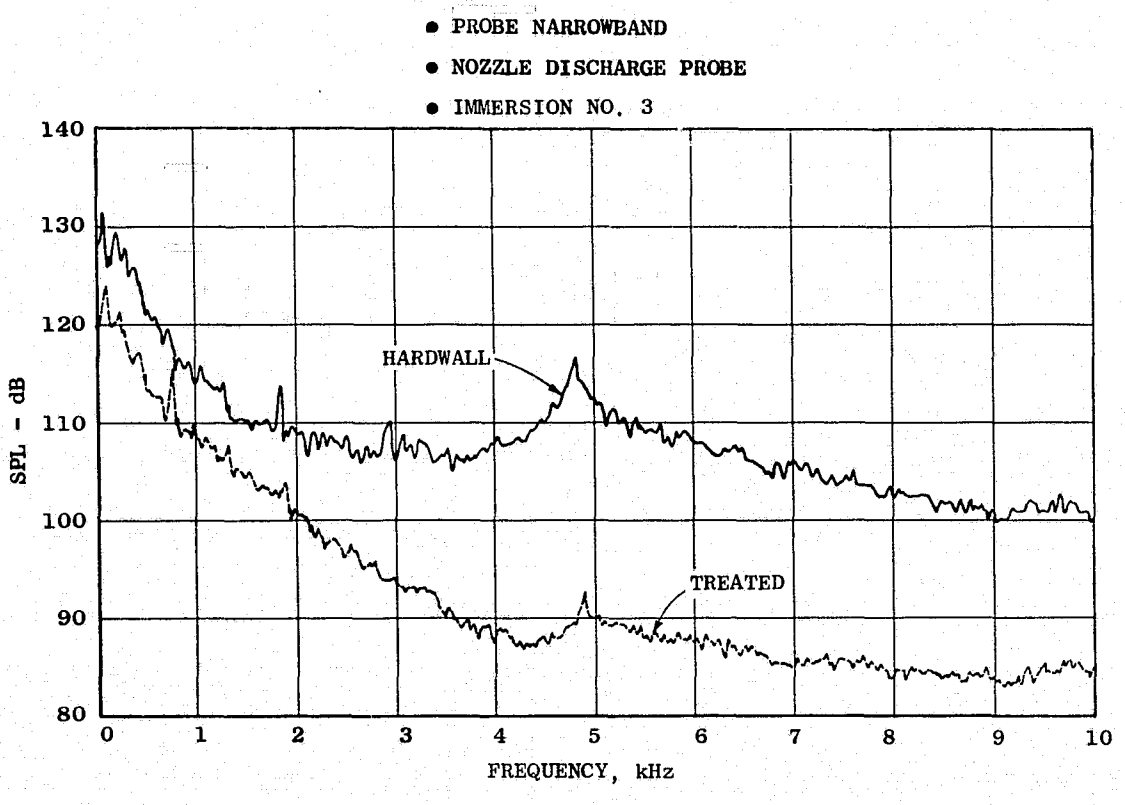

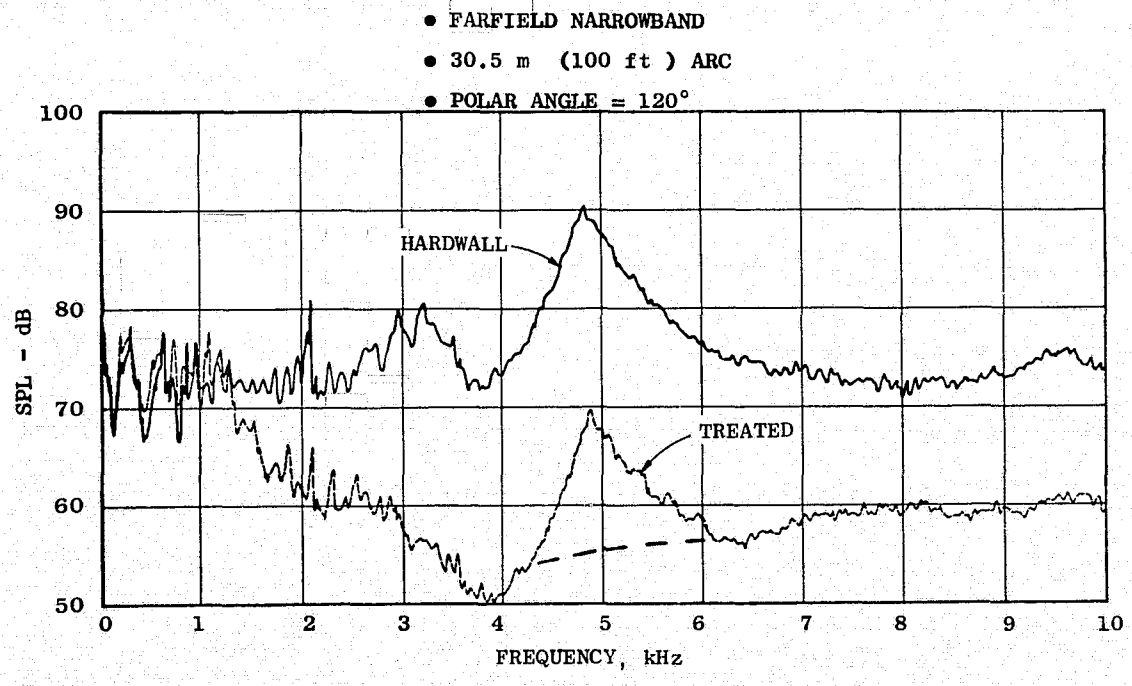

Figure C2. Probe and Farfield Narrowband Comparisons, Approach.

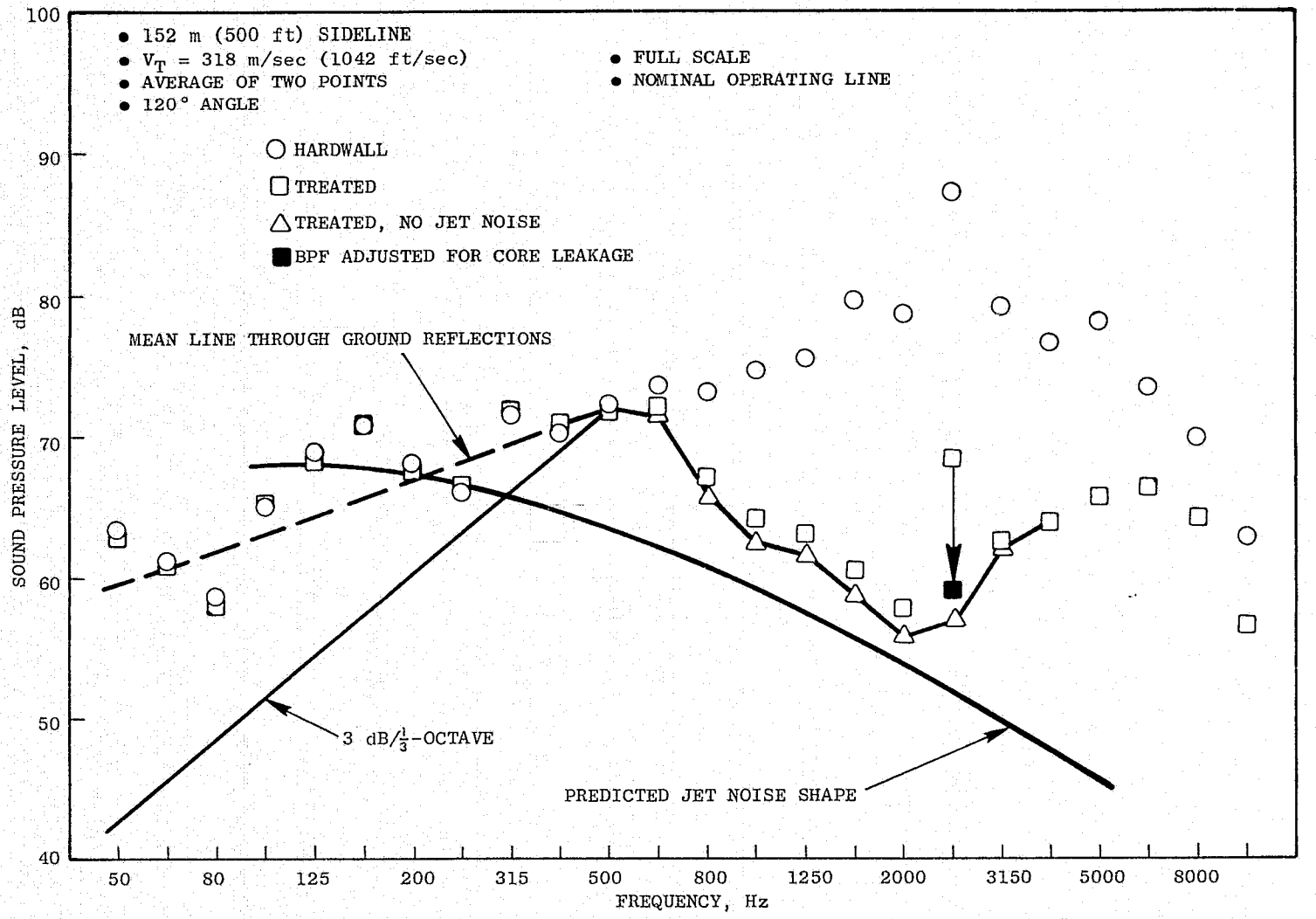

Figure C3. 1/3-Octave Spectral Comparison, Approach.